# Proceedings of the 38th International Manufacturing Conference (IMC38)

**August 30th, 2022, University College Dublin (UCD)**

**"ENGINEERING SUSTAINABILITY FOR THE FUTURE"**

Co-hosted by UCD and I-Form, the SFI Research Centre for Advanced Manufacturing


**Published by:** School of Mechanical and Materials Engineering
University College Dublin
Belfield, Dublin 4
Ireland


ISBN **978-1-910963-63-0**


**Editors:**
Dr Eamonn Ahearne,
Professor Denis Dowling,
School of Mechanical and Materials Engineering
University College Dublin
Belfield, Dublin 4
Co. Dublin
Ireland

## Foreword

The 38th International Manufacturing Conference, IMC38, showcases current research in the field of "manufacturing engineering" undertaken in Ireland by postgraduate students and experienced researchers. Indicative topics, in line with the contents of these proceedings, include; sustainable and energy efficient manufacturing, additive manufacturing, Industry 4.0 and digital manufacturing, machine tool, automation and manufacturing system design, surface engineering, forming and joining process research. The IMC community is also involved in research aimed at improving the learning experience of undergraduate and graduate engineers and developing high level skills for the manufacturing engineer of the future.

The theme for this year's conference is ***Sustainable Manufacturing,*** *with a particular emphasis on:*

a) Digitalisation of Manufacturing – its impact on sustainability
b) Addressing sustainability in Engineering Education, Industrial Training and CPD

This theme will be addressed in both keynote presentations and dedicated paper sessions. These proceedings present submitted papers on the main theme and on the aforementioned topics in manufacturing engineering research.

The conference provides a great opportunity for the dissemination and consolidation of new knowledge generated by research in these domains. We would like to thank all of the contributing authors and delegates for their input.

We hope you that you will find the conference intellectually stimulating, leading to new ideas, and welcoming, leading to new friendships and the beginnings of new collaborations.

**Dr Eamonn Ahearne,**

**Prof. Denis Dowling**

**University College Dublin**

# Contents

# Chapter 1: Engineering Education

# Re-thinking Entrepreneurship Education in Undergraduate Engineering Curricula

Morgan M., Joseph-Richard P., Cummins D. and McCartan A., Ulster University

***Abstract***

The importance of entrepreneurship teaching within engineering education is widely recognized by the engineering community and by government. There is however no consensus on how best to enthuse and engage engineering students in entrepreneurship studies and many of them struggle to see the relevance of the subject within the curriculum, particularly at the undergraduate study stage (Morgan and O'Gorman, 2017). Within existing engineering curricula, entrepreneurship teaching tends to be an 'add-on' activity, and is usually delivered within the subject discipline of 'Design' where engineering educators link it to the innovation and design of new products.

Preliminary findings of a study carried out at Ulster University to explore students' perceptions of entrepreneurship education identified that engineering students' understanding of the term 'entrepreneur' was beclouded with celebrity entrepreneurs which we argue may thwart the students' self-belief and desire to develop their entrepreneurial attitudes and skills during their undergraduate engineering studies.

Previous work (Cummins et al, 2021) identified that entrepreneurship teaching was most effective when 'embedded and not inserted' in curricula, and this current work examines an approach where engineering students are introduced to entrepreneurship in its broadest sense, that is, as a means of value creation (Voldsund et al, 2020) or as 'adding value'.

This paper proposes that entrepreneurship teaching could be more effectively embedded in engineering curricula by explicitly linking it to Lean Systems thinking (Womack and Jones, 1992). Lean Systems thinking is an important and well-recognized subject area within industrial engineering curricula and requires the value stream mapping of activities and processes to highlight all 'value-added' and 'non-value added' activities and processes within any system. A two-pronged plan of action can then be developed to eliminate wasteful (i.e. non-value added) activities, and to enhance value added activities. Whilst the identification and elimination of the non-value added activities and processes, commonly referred to as the 'seven deadly wastes', is taught mainly through modules in manufacturing systems or quality improvement, there is no clear consensus among engineering curriculum designers on how to 'design in' opportunities to add value. This work proposes that entrepreneurship studies should be embedded in Lean Systems modules to provide students with opportunities to develop their understanding of value creation, so that they can identify with and appreciate the relevance of it within their engineering programmes.

The presentation of entrepreneurship education to engineering students within the familiar pedagogic framework of Lean Systems thinking, provides educators with an established and accepted scaffold to use for the development of engineering students' entrepreneurial attitudes and skills throughout their curriculum.

*Key Words: Entrepreneurship education, Entrepreneurial skills development*

## 1. INTRODUCTION AND CONTEXT

The importance of entrepreneurship education within STEM disciplines (Science, Technology, Engineering and Maths) is widely accepted by the engineering community and by government (Wilson 2012), European Commission (2014), United Nations Conference on Trade and Development (2010), and World Economic Forum (2010). Despite this, engineering educators in the UK have been slow to develop effective pedagogic approaches that embed the subject area as a mainstream topic in undergraduate engineering curricula, with many considering entrepreneurship education as an optional 'add-on' or co-curricular activity (Shekhar and Huang-Saad, 2021) rather than as a core activity. This is understandable as undergraduate engineering curricula tend to be content-heavy, time intensive, and are already packed with the traditional topic areas described by the Engineering Council UK (and those professional engineering institutions that accredit higher education programmes in the

Email: Margaret Morgan
m.morgan@ulster.ac.uk

UK) namely: Science and Mathematics; Engineering Analysis; Design and Innovation; The Engineer and Society; and Engineering Practice. Previous work by Cummins et al (2021), argues that the most effective pedagogic framework for embedding entrepreneurship education across disciplines is to avoid the 'add-on' or 'inserted' approach and instead to 'integrate' entrepreneurship education into the curriculum with appropriate adaptation to suit specific disciplines. When entrepreneurship education is delivered in undergraduate engineering curricula it tends to be concentrated in the Design subject theme (a core theme across all engineering programmes) with educators usually linking it to the innovation and design of new products. Whilst this is a successful approach in the context that *entrepreneurship is concerned with noticing a market opportunity and exploiting it for wealth generation by the individual*, it does not prepare engineering students well for those graduate roles where engineers will be expected to display an entrepreneurial mindset in the creative solutions to problems and to capitalise on commercial opportunities that arise within their employing organisations. Antoncic and Hisrich (2003) describe 'intrapreneurship' as 'the ability to empower employees to innovate from within organisations'. Chang (2014) notes that "it is often a natural progression for a capable engineer to gain business experience working as an intrapreneur before starting down the path to become an entrepreneur".

Undergraduate engineering students often struggle to see the relevance of non-numerical subjects in their programmes and engineering educators are challenged to find ways to link the study of this important area in meaningful ways that will engage and enthuse their students and enable them to develop those entrepreneurial skills that employers and society need. From a pedagogic perspective, if engineering graduates are to develop a truly entrepreneurial mindset, it is desirable to find additional core engineering subject areas that could be used as scaffolds for the integration of entrepreneurship education.

This paper proposes that one such scaffold could be the teaching of Lean Systems thinking (Womack, 1992) which is an important, well-recognised and established subject area within industrial engineering. Lean Thinking in its broadest sense, is concerned with avoiding and eliminating waste, and being successful through a continuous and forced problem-solving approach. Jessop (1997) sets out the guiding principles as:

(i) the specification of value
(ii) the identification of the value stream
(iii) making value flow
(iv) allowing the customer to pull value
(v) the pursuit of perfection.

Lean systems teaching equips students to distinguish between those organisational activities that add value and those that do not add value, termed 'non-value-added' or wasteful activities.

## 2. UNDERGRADUTE ENGINEERING CURRICULA

There is much debate presently about what the engineers of tomorrow will look like and how their undergraduate education and training will prepare them to meet the big global challenges of the day. These challenges e.g. the net-zero carbon agenda, smart cities, health and well-being, inequality, etc. call for highly skilled, technically competent engineers who have the skill set to work in multi-disciplinary, multi-cultural teams to develop products and the cost effective solutions that society needs and wants. Clearly engineering graduates who have, not just the technical know-how, but also the entrepreneurial mindset to create new business opportunities in the solution of these so called 'wicked' problems will be well positioned for success in the jobs of tomorrow.

The opportunities for engineering students to develop an entrepreneurial mindset within undergraduate engineering programmes are generally restricted to those modules associated with the subject area of Design. Courses in Design include such topic areas, such as, market research, client discussion, problem definition, concept generation, idea presentation, business planning, and so on, all underpinned with a recognition of constraints around product functionality, cost and market opportunity; students typically study Design in all years of their programmes. Voldsund et al (2020) notes entrepreneurship education in undergraduate courses is about opportunity identification, business development, self-employment, venture creation and growth and in essence is about *becoming an entrepreneur*, and this applies to undergraduate engineering programmes.

The most recent accreditation standards set by the Engineering Council UK, in its publication Accreditation of Higher Education Programmes 4$^{th}$ Ed. the so-called AHEP4 standard, sets out what graduate engineers are

expected to be able to do at the output level (eg Masters or Bachelors) in the Design and Innovation space as, the "… the creation and development of an economically viable product, process or system to meet a defined need and involving significant technical and intellectual challenges commensurate with the level of study". The emphasis is clearly on the technical challenge but engineering employers and society more broadly expects the Higher Education community to provide graduates who have the skills to make them work-ready (Morgan and O'Gorman, 2010) which invariably means ready to 'add value' to their employing organisation as described by Trevelyan and Williams (2019).

Trevelyan and Williams argued that engineers did not recognise what 'value' meant in the context of their day-to-day engineering work as they understood value creation to be limited to purely technological innovations and in most organisations, engineers are employed in managing technology assets, technical sales, project management etc. They concluded that students should be helped to recognise value creation within the engineering curricula through:

*(i) Framing engineering analysis problems in ways that help students learn how engineering analysis can add value in an engineering enterprise*
*(ii) A case study for a design or mechanics course showing how engineering safe drinking water supplies can contribute social and economic value, and how a design can be configured to reduce the apparent risks for investors in the project.*
*(iii) Practice in solving routine mathematical problems enables engineers to make fast and approximate calculations to build confidence for investment in feasibility studies*
*(iv) Learning effective technical collaboration and due diligence skills through engineering practice in virtual worlds that simulate real-life engineering*

Whilst there is merit in the approach proposed by Trevelyan and Williams, a more natural scaffold for the teaching of value creation (in all its forms within the engineering context) and hence both entrepreneurship and intrapreneurship education would be for engineering educators to teach it within the manufacturing and/or quality improvement modules which are typical on industrial engineering programmes. These modules are usually well supported by industrialists and invariably cover the key subject area of Lean Systems thinking.

Lean Systems thinking is an important and well-recognized subject area within industrial engineering curricula and requires the value stream mapping of activities and processes to highlight all 'value-added' and 'non-value added' activities and processes within any system. It's a continuous improvement philosophy similar to Kaizen or the Toyota Production System, TPS, and is the manufacturing methodology of choice for many large organisations and SMEs. It is fully described elsewhere in earlier work by Morgan et al (2011).

The most widely recognised term associated with the lean implementation is *muda*. Sometimes referred to as the seven deadly wastes it's an interesting and engaging subject topic for engineering students. The seven visible wastes are summarised in the Table 1 and in our experience students tend to enjoy these topics, actively engage with the taught material and with real-life industry projects around waste reduction.

*Table 1. The seven 'deadly' visible wastes*

| Muda wastes | Description of waste |
|---|---|
| (i) Overproduction | Any part produced before it is needed for a customer order |
| (ii) Waiting | Materials queuing downstream because of upstream activity |
| (iii) Transport | Any unnecessary movement; work in progress intra-process |
| (iv) Over processing | Over-engineered part or process |
| (v) Inventory | All materials not currently being prepared for customer orders |
| (vi) Motion | Inefficient factory and/or storage layout |
| (vii) Defects | Any dis-satisfied customer |

.

More contemporary publications (Coleman, 2014) mainly driven by the engineering community have included an eighth waste, described as the 'wastefulness of under-utilized resource or talent' and it in this context, that entrepreneurship (and hence intrapreneurship) education could be embedded within the undergraduate engineering curricula. The creation of value at every stage of an organisation's processes (products and services) could be set as an overarching objective, such that students are educated that entrepreneurship is about *value creation* in its broadest sense. This would mean that engineering students would be introduced to entrepreneurship education in a meaningful way that contextualises their learning within an accepted core engineering subject area, and should help craft the entrepreneurial mindset that is so needed and valued by industry and society.

## 3. METHODOLOGY & PRELIMINARY FINDINGS

An exploratory scoping study was conducted on undergraduate engineering students at Ulster University using a simple, anonymous and online MS Forms questionnaire. The questionnaire was designed to establish a baseline around students' understanding of the term 'entrepreneurship' and to gauge students' views on whether or not they felt they considered themselves potential entrepreneurs.
The seven main questions (mainly open-ended) asked and the most commonly cited student responses are shown in Table 2. There was a wide variation in answers in all questions bar Q2.
The total number of responses was 123, with representation across all years of undergraduate study. 52% of respondents were female, 45% were male and 3% responded with 'prefer not to say'.

*Table 2. Questions asked and students' responses*

| Engineering students across all years | Most commonly cited responses |
|---|---|
| Q1. What does entrepreneurship mean to you? (Please describe your views on entrepreneurship) | Product creation<br>Starting one's own business<br>Someone who invents a product<br>Being one's own boss<br>Being creative and innovative<br>Making money |
| Q2. Can you name someone who you would consider to be an entrepreneur? (Identify a person) | Elon Musk<br>Alan Sugar<br>Bill Gates<br>Jeff Bezos<br>Mark Zuckerberg |
| Q3. Why have you selected his/her as your choice? | World famous<br>Successful<br>Business leader<br>Well known<br>Very driven |
| Q4. What characteristics/aspects make someone an entrepreneur? | Innovative and Creative<br>Hard-working and determined<br>Leadership<br>Risk-taker<br>Passion and Confidence |

| | |
|---|---|
| Q5. Do you consider yourself an entrepreneur? Yes/No | Yes 19.5%<br>No 80.5% |
| Q6. Explain why you consider[1]/did not consider[2] yourself an entrepreneur? | [1] Unique idea, Ambitious, Good at selling things, I want to own my own business<br>[2] Not able to risk failure, Want a good work-life balance, I feel I'm too young, I don't have enough money |
| Q7. What would persuade you to become an entrepreneur? | The chance to make a lot of money<br>If I was more confident in myself<br>Having a safety net<br>Lifestyle it offers<br>Job satisfaction |

---

***3.1. Student responses***

There was a wide variation in answers in all questions bar Q2, and Table 2 shows the most commonly cited response theme. It is clear from the student responses, that the teaching they have received in Design modules has made an impact and has presumably has helped shape their thinking in terms of creating/inventing a product, being innovative, owning one's own business, generating wealth, etc. There was a single response of entrepreneurship is '*taking risks to create a service or product that is of value to the world around you*' but no other responses mentioned creating 'value' or of working in organisations and being entrepreneurial in one's approach. We argue that this could be because students don't recognise corporate entrepreneurship or intrapreneurship as a sub set of the overall entrepreneurship subject area.

When students were asked to name an entrepreneur, the range of responses was surprisingly small. Students predominantly chose high-profile men in the tech sectors, who have an associated aura of success and celebrity. Only a few students named close family members or business owners in their local communities. Answers as to why students named a particular entrepreneur focused on global success and recognition, success and business leadership at the highest level. For students at Ulster University, which is widely recognised as a widening access university, it's reasonable to suggest that if the majority of engineering students see entrepreneurs as someone operating in the celebrity world or restricted to business owners only, they might see entrepreneurship education as something not relevant to them. We argue that the cult of the celebrity entrepreneur may indeed thwart students' self-belief in themselves and their potential to become entrepreneurs later in life.

Employment data from engineering students at Ulster University shows that around 90% of graduates will be in managerial or professional employment within six months of graduation. Students responses indicated that they had a good understanding of the entrepreneurial characteristics and that one in five considered themselves as potential entrepreneurs.

Responses to Q6 and Q7, indicate that engineering students perceptions of entrepreneurship are indeed restricted to the fairly narrow 'product creation, business start-up and individual business ownership' interpretation of entrepreneurship. Personal risk-taking and lack of business funds are cited as inhibitors of entrepreneurial activity. These inhibitors may not exist if students understood how an education in entrepreneurship equips them to act in entrepreneurial ways within employing organisations, effectively acting as an *intrapreneur*, highlighting to engineering educators at Ulster, that we should introduce the term as early as possible in degree programmes, and explain to students that the characteristics of both the entrepreneur and intrapreneur are indivisible, and that many intrapreneurs go on to become entrepreneurs later in their engineering careers.

## 4. CONCLUSIONS

Entrepreneurship education is a well-established discipline in most business and management schools and although engineering educators have long recognised the need for it to be taught at undergraduate engineering programmes there is no consensus on the best way to develop engineering students that have an entrepreneurial mindset. To date, most engineering departments in the UK provide entrepreneurship education using Design modules but students need additional educational opportunities to introduce them to entrepreneurship in its broadest context namely, value creation. This paper proposes that the ideal way to embed value creation within engineering curricula is to twin it with teaching on Lean Systems thinking. Further study will be required to see if the introduction of this pedagogic approach yields the anticipated outcomes and this will be reported at a future date.

## 5. REFERENCES

Antoncic, B. and Hisrich, R. (2001), Intrapreneurship: Construct refinement and cross-cultural validation. *Journal of Business Venturing*, 16(5), 77-86

Chang, M. (2014). From Engineer to Intrapreneur, to Entrepreneur: starting a Business Risk Free. IEEE Engineering Management Review, 42(4).

Coleman, L. (2014) Waste not, want not…In: ASQ Six sigma forum magazine, saqi.co.za. Accessed on 21 June 2022 at https://saqi.co.za/wp-content/uploads/2017/04/eQE-Issue-177-April-May-2014.pdf

Cummins, D., Joseph-Richard, P., Morgan, M., Harbs, S., and Kerber, F. (2021) Integrated, not inserted: a pedagogic framework for embedding entrepreneurship across disciplines. In H. Neck & Y. Liu (Eds), *Innovation in Global Entrepreneurship Education, Teaching Entrepreneurship in Practice* (pp 32-51) Cheltenham UK Northampton USA: Elgar

Engineering Council UK https://www.engc.org.uk/standards-guidance/standards/uk-spec/

European Commission (2014) *Entrepreneurship education: A guide for educators.* Accessed 5 July 2022 at https://op.europa.eu/en/publication-detail/-/publication/02bd63f7-291f-4665-b13a-24f9ad3d634b

Jessop, D.A. (1997). Lean Thinking. *European Journal of Purchasing &Supply Management* 3(4)

Morgan, M. and O'Gorman, P. (2010) *Developing industry-ready engineers: a regional university perspective* In: International Conference on Engineering Education, ICEE-2010, Poland.

Morgan. M., McKeag, D., O'Gorman, P. and Meehan, G. (2011) *A self-diagnostic approach for design and implementation of continuous improvement philosophy in an SME*. In: 27th International Manufacturing Conference, IMC27, Galway

Morgan, M. and O'Gorman, P. (2017) *Engaging with industry to improve student learning on undergraduate engineering programmes.* In: IEEE International Conference on Industrial Engineering and Engineering Management (IEEM) Singapore

Shekhar, P. and Huang-Saad, A. (2021) Examining engineering students' participation in entrepreneurship education programs: implications for practice. *International Journal of STEM Education* 8, 40. https://doi.org/10.1186/s40594-021-00298-9

Trevelyan, J and Williams, B. (2019) Value creation in the engineering enterprise: an educational perspective. *European Journal of Engineering Education*, 44(4),461-483.

United Nations Conference on Trade and Development (UNCTAD) (2010) *Entrepreneurship education, innovation and capacity-building in developing countries* TD/B/C.II/MEM.1/9 Geneva. Accessed on 6 July 2022 at https://unctad.org/system/files/official-document/ciimem1d9_en.pdf

Voldsund, K. H., Hasleberg, H. and Bragelien, J. J. (2020) Entrepreneurship Education Through Sustainable Value Creation. In: IEEE Global Engineering Education Conference (EDUCON)

Wilson, T. (2012), A review of business-university collaboration, Department for Business, Innovation & Skills, London.

Womack, J. P. and Jones, D. T. (1992) *The Machine That Changed the World* Australia: Simon & Schuster

World Economic Forum (2010) Educating the next wave of entrepreneurs: Unlocking entrepreneurial capabilities to meet the global challenges of the 21st Century. Accessed on 6 July 2022 at https://www.weforum.org/reports/educating-next-wave-entrepreneurs/

# Chapter 2: Sustainable and Energy Efficient Manufacturing

# Energy Efficient Manufacturing Scheduling : Challenges & Research Directions

Michele Garraffa[1] and Cemalettin Ozturk[2]

[1] Insight SFI Research Centre for Data Analytics, School of Computer Science and IT, University College Cork, Ireland*** 
[2] Process, Energy and Transport Engineering, Munster Technological University, Cork, Ireland†

**Abstract.** Energy-efficient production scheduling is a very active research area with more than 100 papers published in the last 5 years and a half. The reason for this interest is mostly due to the economical and environmental impact of considering energy in production scheduling. In this paper, we review recent papers in this area, provide a classification of the problems studied, and present an overview of the main aspects and methodologies considered as well as open research challenges.

## 1 Introduction

In 2021, manufacturing industry accounted for the 25.6% of the energy consumed within the EU [2]. Besides, European countries relies on imports to meet their energy needs, with an average energy dependency rate 60.7%. This aspect constitutes a major threat for energy security and can be mitigated by reducing the overall energy consumption. While there are substantial amount to reduce energy consumption of manufacturing equipment, research shows that the majority of the energy waste is observed during machine idle time and/or setup times. Hence, it is obvious that intelligent manufacturing scheduling methods have potential to help reducing energy consumption in manufacturing industry.

One direction to achieve this goal is exploiting Operations Research (OR) and Artificial Intelligence (AI) techniques to optimize the production schedules in industry. The basic idea of these methods is to reduce the energy cost of the system while still achieving a good level of productivity. An enormous amount of research has been recently conducted to propose the use of these techniques in a heterogeneous set of applications in production scheduling, arising in very different countries around the world. As an example; methods for energy-efficient production scheduling of flake ice units in Portoguese food retail stores is proposed in [28], while a case of study arising in a Chinese motor company is studied in [17], an Iranese extractor hood factory in [27], and a Belgian plastic bottle manufacturer in [8]. In this work, we review the recent research in the field of energy-efficient production scheduling, by analyzing and classifying 103 papers

*** michele.garraffa@ucc.ie
† cemalettin.ozturk@mtu.ie

published from 2017 till date. We focused on studies dealing with combinatorial problems arising in production scheduling, ignoring other contexts where energy efficient scheduling has been widely applied, such as domestic energy management systems [3], multi-core systems [13], cloud computing environments [5] and streaming applications [14].

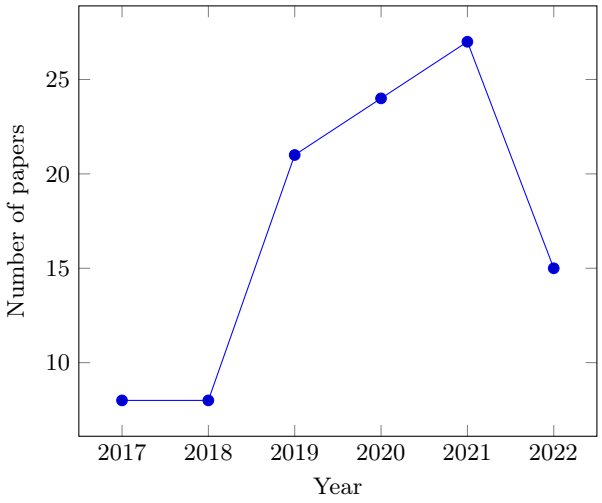


**Fig. 1.** Number of papers per year related to the area of energy efficient production scheduling and published from 2017 till date

Figure 1 shows how papers included in this review are spread in the different years from 2017 to 2022. Please note that only a half of the year 2022 is taken into account, hence the expected number of papers for the whole year is the double of the one reported (30). The key message is that the number of papers published in this area has been sharply increasing, in fact the value in 2021 is more than the triple of the value reached in 2017. The reason for that is surely linked to economical and political aspect as stated above, but we also believe that researchers have been attracted by this area because this type of production scheduling problems are very challenging and rewarding from a scientific perspective.

For this reason, we focus specifically on providing a generic framework for describing and classifying energy efficient scheduling problems. Similarly to the well known three fields notation for scheduling problems [9], we take into account the dimensions *machine environment* and *objectives*. In addition, we split the field related to the constraints into *energy-related aspects* and *other constraints*. In conclusion, an energy-efficient production scheduling problem can be written as follows:

Minimize/maximize $objective_1$

Minimize/maximize $objective_2$

.....

Minimize/maximize $objective_n$

subject to

*Machine environment*

*Energy-related aspects*

*Other constraints*

Section 2 describes in details the different dimensions we used to classify the studies and provides some statistics about the most studied scenarios. We also define four classes of problems, based on the number and type of objectives considered, and conclude that two of them are the most common by far. Section 3 provides a survey of the most frequently used techniques to solve energy-efficient production scheduling problems, including both exact and heuristic methodologies. Section 4 briefly describes directions for future studies in this area and provides some conclusions.

## 2 Problem characteristics

This section describes the main problem characteristics considered in this review.

### 2.1 Objectives

Numerous objective functions have been considered in energy-efficient production scheduling, however we identified three main categories that are considered in majority of the studies. These three categories are: system productivity objectives, energy-efficiency objectives and total cost objectives. The first category comprises all traditional objectives in scheduling, such as the makespan, the total tardiness, the total flowtime, etc. The second category is related to achieving energy efficiency in the system, which can be done by minimizing total energy consumption, total energy cost, total energy waste, etc. The third category can be expressed by a weighted sum or lexicographic order of multiple factors that

are taken into account and they can all be expressed in terms of cost. As an example, the energy cost can be combined with other costs, such as maintenance, transportation, setup,inventory and so on.

The first class of problems discussed in this review is indicated with $T_1$ and consists of problems where only one objective is considered, which represents a form of total cost [19,1,26,11,21,7]. The second class, indicated with $T_2$, consists of problems where only one productivity objective is optimized [7,23,24]. This is usually combined with a constraint limiting the overall amount or peak energy that can be used. Both $T_1$ and $T_2$ include single objective problems and they are formulated such that we strive for computing one optimal solution. The third category $T_3$ consists of a problem dealing simultaneously with two objectives: one productivity measure and an energy efficiency measure [17,6,29,34]. These two categories of objectives are in contrast with each other. This means that the most performing choices in terms of productivity require faster machines and hence a lot of energy. Therefore, the decision maker is looking for the best compromise between these two aspects. Finally, the last category $T_4$ includes all the problems where more than two objectives are considered, with at least one of them related to productivity and another one related to energy-efficiency [22,12,10]. Both $T_3$ and $T_4$ include multi-objective combinatorial optimization problems, whose goal is to compute the Pareto frontier, that is the set of efficient solutions, for which none of the objectives can be improved without sacrificing at least one of the other objectives.

Figure 2 depicts a bar chart showing the amount of papers tackling a problem belonging to each of the problem classes defined. The chart clearly shows that the most studied problems belongs to the classes $T_1$ and $T_3$. In other words, the most studied problems in the field of energy efficient production scheduling minimize a total cost function or dealing with two conflicting objectives, one related to productivity and another one related to energy efficiency. In particular, slightly less than 50% of the problems belong to the $T_3$ class, which is motivated by the fact that energy efficient scheduling is nowadays considered as a critical decision criteria where the goal is to find the right trade-off among two competing objectives.

### 2.2 Machine environment

Most of the machine environments classified in scheduling literature have been studied in terms of energy efficiency. In particular, the following machine environments have been considered in a good number of studies: single machine, parallel machines, jobshop, flowshop, distributed flowshop, hybrid flowshop. This is clearly shown by the bar chart in Figure 3. The most studied environment is the jobshop environment, which is probably the most common in the modern production facilities because of its high level of flexibility.

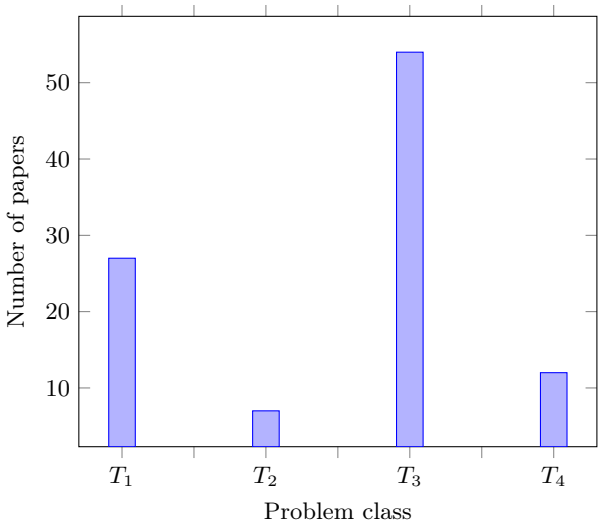


**Fig. 2.** Number of papers per problem class related to the area of energy efficient production scheduling and published from 2017 till date

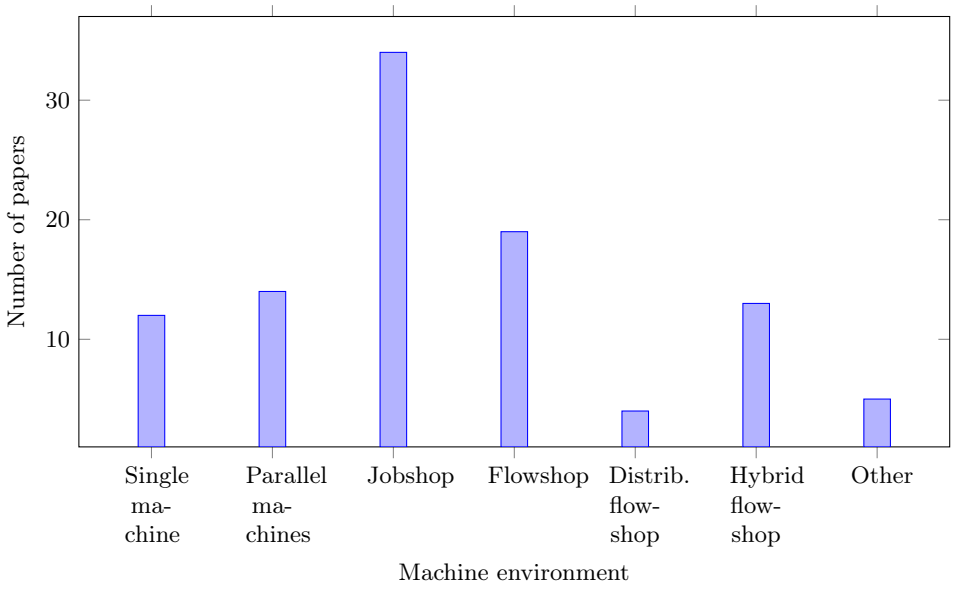


**Fig. 3.** Number of papers per machine environment related to the area of energy efficient production scheduling and published from 2017 till date

### 2.3 Energy-efficient aspects

Energy efficient scheduling can be performed by taking into account different aspects involving decisions about energy. One of the most common ways to minimize energy cost is to schedule jobs at a certain time of the day, when the energy price is lower [32,30]. This is valid in many countries, where time-of-use tariffs are defined in order to encourage customers to use energy when there is less demand. Another way to achieve energy efficiency is to use machines with different speeds [30,31,4]. Each speed allows to process a job with a certain processing time and a certain energy consumption, such that the shorter the processing time, the higher the energy consumption. A very similar scenario is the case where each machine has a different level of speed and energy consumption [20]. In this case, the choice of the machine where a job is processed has an impact on its processing time and the corresponding energy consumption. A very general case consists of optimizing different operating modes for the machines. These operating modes may be of different types, such as idle, standby, setup, or phases of a certain production process. A cost in terms of energy is associated to each of these modes and the time spent by a machine in a certain mode is taken into consideration in the computation of the total energy consumption. Transportation is also requiring energy in the production system, hence reducing transportation effort leads to improving energy efficiency [17,15]. Finally, we mention a typical energy-related constraint, that is the power peak constraint [19]. This is usually considered in problems of type $T_2$, where the single objective function is a productivity measure and the power peak constraint sets a limit on the amount of energy used in a certain time instant. Figure 4 shows that the first four aspects are the most studied since 2017. The inclusion of operating modes in the problem definition has attracted the most attention from researchers: strategies like the reduction of the machines' idle time are a focal point to reduce energy waste.

### 2.4 Other constraints

As for the machine environments, we can replicate any scheduling constraints in a study about energy efficient production scheduling. Here follows a non exhaustive list of constraints considered since 2017. First, a common constraint for flow shop environment is to impose that all the jobs have to be processed by all the machines in the same order (permutation constraint). Another important constraint is to consider sequence-dependent setup time for the machines [27]. The authors in [33] consider the no-wait constraint, meaning that the jobs' waiting time is equal to zero which is essential for process industries. Machine downtime is taken into account in [25]. A variety of process-dependent operational constraints have been also studied in multiple occasions.

## 3 Methodology

As for all combinatorial problems, energy-efficient scheduling problems can be addressed by both exact and heuristic methods. Single-objective methods are

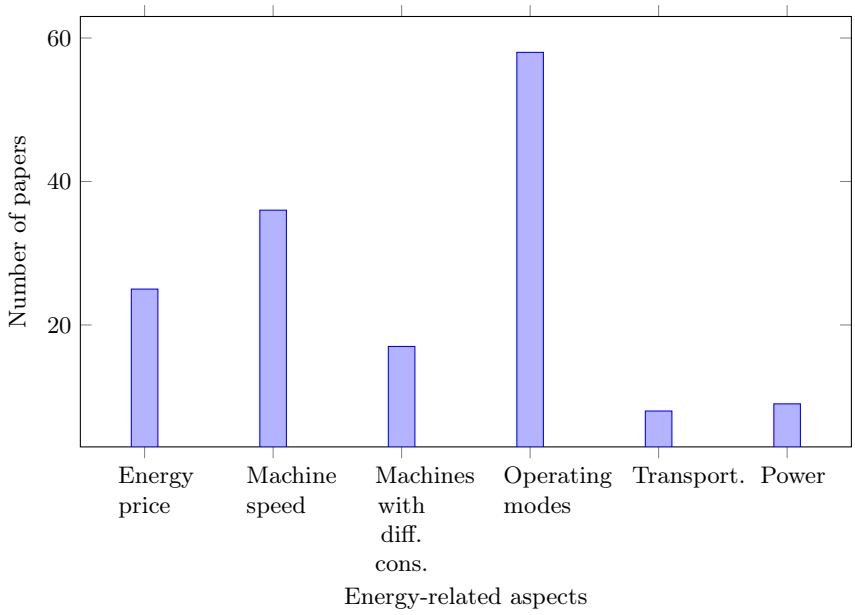


**Fig. 4.** Number of papers per energy-related aspect in the area of energy efficient production scheduling and published from 2017 till date

designed for solving the problems in the classes $T_1$ and $T_2$, while multi-objective methods are suitable for the problems in $T_3$ and $T_4$. Figure 5 shows the number of papers per methodology used. We considered Mixed Integer Programming (MIP), metaheuristics, matheuristics and exact decompositions. MIP and metaheuristics are predominantly used as exact and heuristic methods, respectively. The combination of both methods, matheuristics [18], implement a fix-and-optimize paradigm where some of the variables of a MIP model are fixed and the remaining problem is solved by means of a MIP solver [16]. The research about matheuristics for energy-efficient scheduling seems to be limited according to our investigation. Finally, exact decompositions such as Benders' decomposition have been used in a few research works to handle complicated constraints and solve energy-efficient scheduling problems to optimality [11].

## 4 Future work and conclusions

Energy-efficient scheduling has been a very active research area in the last few years. We analyzed 103 recent papers and proposed a classification for this type of problems. The recent trend is to formulate energy efficient scheduling problems in terms of bi-objective problems (class $T_3$) and the development of advanced bi-objective approaches seems to be attracting more and more interest from researchers in this field. Most likely, future studies will involve more problems with 3 or or more objectives (class $T_4$).

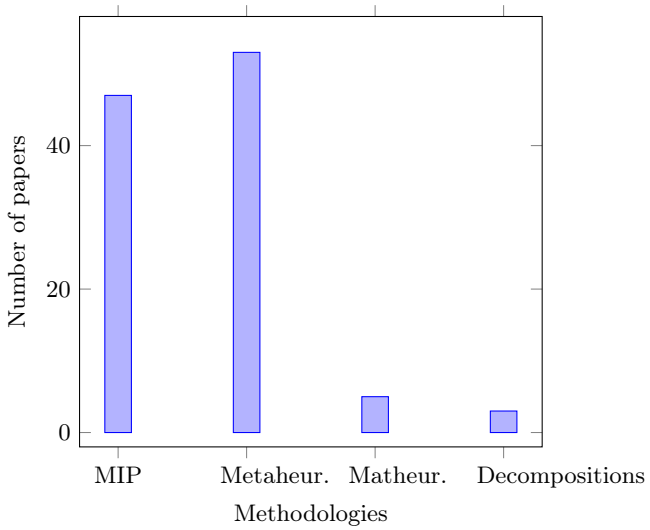


**Fig. 5.** Number of papers per type of solution methodology in the area of energy efficient production scheduling and published from 2017 till date

This study will be extended in order to include all the papers ever published in this research area. We are aiming at refining our classification, in order to provide a useful research framework for future studies.

## 5 Acknowledgements

This work was supported by Science Foundation Ireland (SFI) under grant number 12/RC/2289-P2 (Insight),and co-funded under the European Regional Development Fund.

## References

1. Mohammad Mohsen Aghelinejad, Yassine Ouazene, and Alice Yalaoui. Production scheduling optimisation with machine state and time-dependent energy costs. *International Journal of Production Research*, 56, 2018.
2. European Commission and Eurostat. *Key figures on Europe : 2021 edition*. Publications Office, 2021.
3. Federico Della Croce, Michele Garraffa, Fabio Salassa, Claudio Borean, Giuseppe Di Bella, and Ennio Grasso. Heuristic approaches for a domestic energy management system. *Computers and Industrial Engineering*, 109:169–178, 7 2017.
4. En da Jiang and Ling Wang. An improved multi-objective evolutionary algorithm based on decomposition for energy-efficient permutation flow shop scheduling problem with sequence-dependent setup time. *International Journal of Production Research*, 57, 2019.

5. A. Francis Saviour Devaraj, Mohamed Elhoseny, S. Dhanasekaran, E. Laxmi Lydia, and K. Shankar. Hybridization of firefly and improved multi-objective particle swarm optimization algorithm for energy efficient load balancing in cloud computing environments. *Journal of Parallel and Distributed Computing*, 142:36–45, 8 2020.
6. Junwen Ding, Sven Schulz, Liji Shen, Udo Buscher, and Zhipeng Lü. Energy aware scheduling in flexible flow shops with hybrid particle swarm optimization. *Computers and Operations Research*, 125, 2021.
7. Davide Giglio, Massimo Paolucci, and Abdolreza Roshani. Integrated lot sizing and energy-efficient job shop scheduling problem in manufacturing/remanufacturing systems. *Journal of Cleaner Production*, 148, 2017.
8. Xu Gong, Marlies Van der Wee, Toon De Pessemier, Sofie Verbrugge, Didier Colle, Luc Martens, and Wout Joseph. Integrating labor awareness to energy-efficient production scheduling under real-time electricity pricing: An empirical study. *Journal of Cleaner Production*, 168, 2017.
9. Ronald Graham, Eugene Lawler, Jan Karel Lenstra, and Alexander H.G. Rinnooy Kan. Optimization and approximation in deterministic sequencing and scheduling: a survey. *Annals of Discrete Mathematics*, 5:287–326, 1979.
10. Lijun He, Raymond Chiong, Wenfeng Li, Gregorius Satia Budhi, and Yu Zhang. A multiobjective evolutionary algorithm for achieving energy efficiency in production environments integrated with multiple automated guided vehicles. *Knowledge-Based Systems*, 243, 2022.
11. Minh Hung Ho, Faicel Hnaien, and Frederic Dugardin. Exact method to optimize the total electricity cost in two-machine permutation flow shop scheduling problem under time-of-use tariff. *Computers and Operations Research*, 144, 8 2022.
12. D. X. Huo, X. J. Xiao, and Y. J. Pan. Multi-objective energy-saving job-shop scheduling based on improved nsga-ii. *International Journal of Simulation Modelling*, 19, 2020.
13. Neetesh Kumar and Deo Prakash Vidyarthi. A novel energy-efficient scheduling model for multi-core systems. *Cluster Computing*, 24:643–666, 6 2021.
14. Hongjian Li, Hongxi Dai, Zengyan Liu, Hao Fu, and Yang Zou. Dynamic energy-efficient scheduling for streaming applications in storm. *Computing*, 104, 2022.
15. Ming Li and Deming Lei. An imperialist competitive algorithm with feedback for energy-efficient flexible job shop scheduling with transportation and sequence-dependent setup times. *Engineering Applications of Artificial Intelligence*, 103, 2021.
16. Jingran Liang, Yuyan Wang, Zhi Hai Zhang, and Yiqi Sun. Energy efficient production planning and scheduling problem with processing technology selection. *Computers and Industrial Engineering*, 132, 2019.
17. Chao Lu, Liang Gao, Xinyu Li, Quanke Pan, and Qi Wang. Energy-efficient permutation flow shop scheduling problem using a hybrid multi-objective backtracking search algorithm. *Journal of Cleaner Production*, 144, 2017.
18. Vittorio Maniezzo, Thomas Stützle, and Stefan Voß, editors. *Matheuristics - Hybridizing Metaheuristics and Mathematical Programming*, volume 10 of *Annals of Information Systems*. Springer, 2010.
19. Oussama Masmoudi, Xavier Delorme, and Paolo Gianessi. Job-shop scheduling problem with energy consideration. *International Journal of Production Economics*, 216:12–22, 10 2019.

20. Leilei Meng, Chaoyong Zhang, Xinyu Shao, and Yaping Ren. Milp models for energy-aware flexible job shop scheduling problem. *Journal of Cleaner Production*, 210:710–723, 2 2019.
21. Shamik Misra, Mangesh Kapadi, Ravindra D. Gudi, and R. Srihari. Energy-efficient production scheduling of a cryogenic air separation plant. *Industrial and Engineering Chemistry Research*, 56, 2017.
22. Hadi Mokhtari and Aliakbar Hasani. An energy-efficient multi-objective optimization for flexible job-shop scheduling problem. *Computers and Chemical Engineering*, 104, 2017.
23. István Módos, Přemysl Šůcha, and Zdeněk Hanzálek. Algorithms for robust production scheduling with energy consumption limits. *Computers and Industrial Engineering*, 112, 2017.
24. Amar Oukil, Ahmed El-Bouri, and Ali Emrouznejad. Energy-aware job scheduling in a multi-objective production environment – an integrated dea-owa model. *Computers and Industrial Engineering*, 168, 2022.
25. Myoung Ju Park and Andy Ham. Energy-aware flexible job shop scheduling under time-of-use pricing. *International Journal of Production Economics*, 248, 6 2022.
26. Michal Penn and Tal Raviv. Complexity and algorithms for min cost and max profit scheduling under time-of-use electricity tariffs. *Journal of Scheduling*, 24:83–102, 2 2021.
27. Reza Ramezanian, Mohammad Mahdi Vali-Siar, and Mahdi Jalalian. Green permutation flowshop scheduling problem with sequence-dependent setup times: a case study. *International Journal of Production Research*, 57:3311–3333, 5 2019.
28. António G. Ramos and José Leal. Ilp model for energy-efficient production scheduling of flake ice units in food retail stores. *Journal of Cleaner Production*, 156, 2017.
29. Weibo Ren, Jingqian Wen, Yan Yan, Yaoguang Hu, Yu Guan, and Jinliang Li. Multi-objective optimisation for energy-aware flexible job-shop scheduling problem with assembly operations. *International Journal of Production Research*, 59, 2021.
30. Sven Schulz, Udo Buscher, and Liji Shen. Multi-objective hybrid flow shop scheduling with variable discrete production speed levels and time-of-use energy prices. *Journal of Business Economics*, 90, 2020.
31. Zhenzhen Wei, Wenzhu Liao, and Liuyang Zhang. Hybrid energy-efficient scheduling measures for flexible job-shop problem with variable machining speeds. *Expert Systems with Applications*, 197, 2022.
32. Matthias Gerhard Wichmann, Christoph Johannes, and Thomas Stefan Spengler. An extension of the general lot-sizing and scheduling problem (glsp) with time-dependent energy prices. *Journal of Business Economics*, 89:481–514, 7 2019.
33. Xueqi Wu and Ada Che. Energy-efficient no-wait permutation flow shop scheduling by adaptive multi-objective variable neighborhood search. *Omega (United Kingdom)*, 94, 7 2020.
34. Like Zhang, Qianwang Deng, Yan Zhao, Qing Fan, Xiaoyan Liu, and Guiliang Gong. Joint optimization of demand-side operational utility and manufacture-side energy consumption in a distributed parallel machine environment. *Computers and Industrial Engineering*, 164, 2022.

# End-of-Waste Criteria: Helper or Hindrance for the Circular Economy in Ireland?

Cherrelle Johnson, Mechanical Engineering, School of Engineering, College of Science and Engineering, NUI Galway, Ireland; Ryan Institute for Environmental, Marine and Energy Research, NUI Galway, Ireland
Sinéad Mitchell, Mechanical Engineering, School of Engineering, College of Science and Engineering, NUI Galway, Ireland; I-Form, the SFI Research Centre for Advanced Manufacturing, Ireland; Ryan Institute for Environmental, Marine and Energy Research, NUI Galway, Ireland

***Abstract***

It is imperative that societies identify and implement mitigation measures to reduce the impact of the climate crisis on the environment, the economy, and human health. A circular economy provides an opportunity to shift away from the current 'take-make-waste' linear paradigm to a circular, regenerative-based model. Preliminary research into the Irish transition to a circular economy identified End-of-Waste criteria as a potential barrier to circularity. This study aims to better understand Ireland's progress in transitioning to a more circular economy and assess if the current End-of-Waste criteria is a regulatory barrier to achieving circularity within Ireland. Research for this study focuses on the circular economy in Ireland, End-of-Waste criteria, and company experiences with the End-of-Waste application process. For the purposes of identifying and understanding the current obstacles, a series of interviews were conducted with primarily Irish circular industry leaders, as well as an extensive review of the relevant literature. The interviews allowed for industry insight into perceived barriers to achieving circularity specific to the Irish context, and how those can be overcome. Gaps in the literature were also identified through the study, particularly a shortage of research into the practical transition from 'waste' to 'non-waste' classification and its effect on developing a circular economy in Ireland. The findings of this study conclude that Ireland has failed to make substantial progress towards circularity when compared to other European Union Member States as a result of unclear guidance at a European Union level, specifically the End-of-Waste criteria. It is recommended that EU-wide criteria be established for more waste streams, such as plastic or digestate. This would allow Member States to adapt to the circular economy approach expeditiously. This study will add to the limited knowledge base of the circular economy in Ireland, regulatory barriers to the circular economy in Ireland, and potential solutions to overcome those barriers.

*Key Words: End-of-Waste, Circular economy, Sustainability, Linear economy, Policy*

## 1. INTRODUCTION

Transitioning to a regenerative-based approach, such as a circular economy (CE), has the potential to reduce exploitation of natural resources and reduce energy consumption (Technopolis, 2016) by conserving natural capital and returning waste to the economy (European Environmental Agency, 2016). The Ellen MacArthur Foundation (2019) estimates that a CE has the potential to eliminate 3.7 billion tons (40%) of $CO_2$ emissions from the steel, plastic, cement, and aluminium industries in 2050, bringing the world closer to net-zero emissions. Similar research undertaken by Material Economics (2018) estimates that a CE could cut reductions in the same industries by up to 56% by 2050.

The United Nations Sustainable Development Goal (SDG) 12: Sustainable Consumption and Production Patterns, recognises that the current economic model has led to environmental degradation and is an endangerment to the world's future development and survival (United Nations, 2015). Therefore, reducing waste and consumption should be a priority, while still implementing solutions for unavoidable waste. Within a circular model, waste should be viewed as an economic resource that has economic value and must therefore be managed in a profitable, sustainable fashion (Scarpellini et al, 2019; EMF & McKinsey Center, 2015). If not utilised as a secondary raw material or managed sustainably, waste then becomes a heavy burden on the environment. Strict End-of-Waste (EoW) criterion is creating unnecessary obstacles for industry, making it difficult for circular business models to be adopted by some enterprises. The lack of research on the EoW criteria framework serves as one of the main

Email: Cherrelle Johnson
c.johnson8@nuigalway.ie

drivers of this study and contributed to one of the main limitations of the study as there was only a small sample size of EoW-approved companies from which to conduct industry interviews.

Additionally, there is a general lack of research on the CE at regional levels (Scarpellini et al, 2019). This serves as a secondary driver to the study as the CE in an Irish context has not been a primary source of research. Findings from this research aim to contribute to the EoW criteria knowledge and the current state of the CE in Ireland. It aims to provide insight to those seeking additional knowledge on Ireland's EoW application process as well as those searching for current knowledge on Ireland's transition towards a more CE. Both areas are relevant to the current economic and environmental situation.

This research aims to:

- Contribute to the empirical EoW criteria knowledge in Ireland
- Provide insight to practitioners on Ireland's EoW regulatory process in a transition towards a CE.

The objectives of this study are to:

- Assess Ireland's current position in shifting towards circularity
- Assess the EoW criteria regulation
- Identify ways in which barriers can be overcome to achieve circularity.

This study will focus on the CE in Ireland, EoW criteria, and company experiences with the EoW criteria application process.

## 2. LITERATURE REVIEW

### *2.1 Circular Economy in Ireland*

The current linear economic model is no longer sustainable nor ideal for the future of the environment. With only an estimated 9% of the world operating under a CE model (Circle Economy, 2019), there is still a considerable distance to go to close the circular gap. As part of the European Commission's (EC) 2019 Green Deal, a Circular Economy Action Plan was developed to 'close the loop'. The ambitious plan intends to encourage sustainable activity and unlock the potential of a circular economy (EC, 2020). However, the Action Plan set forth is to be implemented on an EU level, leaving participation voluntary for Member States (MS) on a national level. As research has indicated, for a CE paradigm to be most effective, large-scale, international buy-in is fundamental (GoN, 2016).

Ireland has only recently begun to explore the idea of transitioning to a more CE and has made minimal progress in adopting circular practices. In 2020, Ireland's circular material use rate (CMUR) was 2.0%, which is lower than the EU average of 12.8% (Eurostat, 2022), making Ireland one of the worst EU MS for circularity. However, in general, circular business models have yet to become prominent in our economies (VTT, 2020). The CE approach is still considered 'embryotic' both nationally and internationally (DBEI, 2019) and Ireland currently only has a handful of companies leading the pathway to a CE. Surveys conducted by Ibec and the Environmental Protection Agency (EPA) (2019) revealed that only 51% of businesses in Ireland understand the term "circular economy" and only 39% were aware of the EU's sustainability goals. The results highlight an opportunity to inform and educate Irish businesses on CE initiatives.

In 2017, a report on the CE in Ireland was published by the National Economic & Social Council (NESC) titled, *Moving Towards a Circular Economy in Ireland*. NESC set out to identify cases of CE practices in Ireland as well as enablers and barriers to their further development (NESC, 2017). The report concluded that several CE practices are underway in Ireland, however, there are numerous constraints, such as financial and regulatory barriers, hindering forward progress and preventing Ireland from reaching its full CE potential (NESC, 2017).

### *2.2 Barriers to the Circular Economy*

A full transition to a CE comes with several barriers and obstacles, making the transition complicated. One such barrier is product design. When designing new products or materials, it is essential that the products be designed in a way to ensure they can be kept in use or do not go to waste (EMF, 2019; VTT, 2020; Ibec, 2019). This becomes difficult when the materials used to create a product contain hazardous additives or substances. An example of this is in the production of plastics. Harmful substances such as flame retardants, pigments, and UV blockers pose significant health risks and make recycling challenging (VTT, 2020; Plastics Recyclers Europe, 2019). This design flaw means many plastics are less likely to be recycled (Technopolis, 2016; Plastics Recyclers Europe, 2019) and will either go to landfills, be incinerated, or escape into the environment (EMF, 2019). A solution to this problem lies within eco-design. Eco-design incorporates environmental aspects into every stage of the development process with the goal of having the lowest possible environmental impact throughout the product's entire life cycle (European Environment Agency, 2001).

Another significant barrier to the CE is legislation and regulation at EU and national levels. The literature argues that for a transition to a CE to take place, changes to the current regulatory framework are necessary (VTT, 2020; Technopolis, 2016). Recent case studies undertaken by Belgian consultancy firm, Technopolis Group (2016), sought to identify current regulatory barriers to achieving circularity within the EU. The Group concluded that the Waste Framework Directive was especially problematic. The Directive itself results in different and conflicting national implementations of the legislation, unclear definitions of targets, and incomplete or lagging enforcement of legislation (Technopolis, 2016).

### *2.3 End-of-Waste Criteria*

One such regulation that can be considered a regulatory barrier is the EU EoW criteria. Transposed from Article 6 of the revised EU Waste Framework Directive 2008/98/EC, the European Commission (EC) put forth a set of criteria, known as End-of-Waste criteria, that specifies when certain waste is no longer considered waste, but instead, it obtains the status as a product or secondary raw material (European Commission, 2019; Joint Research Centre, 2009). The goal of establishing EoW criteria was to "provide a high level of environmental protection and an environmental and economic benefit" (European Commission, 2019), making EoW an important element in the transition to a more CE.

It is the responsibility of the applicant to ensure all criteria are satisfied. Once a material has achieved EoW status, it is then seen to have intrinsic value (Joint Research Centre, 2009). EoW criteria are not applicable to all waste streams – only those for which criteria can be created, agreed upon, and implemented within the Waste Framework Directive provisions (Joint Research Centre, 2009).

EoW criteria in Ireland are regulated under Article 28 of the European Communities Waste Directive Regulations of 2011. Currently, the EC has set in place EoW criteria for priority waste streams of iron, steel, aluminium scrap, glass, and copper scrap. However, the Joint Research Centre has proposed criteria for additional waste streams such as paper, compost, and digestate (Joint Research Centre, 2020; Johansson & Forsgren, 2020). Article 28 allows for EU MS to decide on a case-by-case basis whether waste has ceased to be waste where criteria are absent on an EU level (EPA, 2020). Yet, the case-by-case decisions only apply to the MS in which they were decided unless another MS adopts the same EoW criteria for that waste stream. Nevertheless, there are arguably additional waste streams for which EoW criteria should be established on an EU level, such as food waste, manure, and plastic.

With MS having difficulty agreeing on set criteria, many EoW criteria proposals have been halted (Johasson & Forsgren, 2020), leading to a decentralisation of the legislation. EoW criteria were introduced by the EC in 2008, but research indicates the first approval of an EoW application in Ireland did not occur until 2018. Since then, ten additional applications have been approved. According to the EPA (2020), for most materials, the making of an EoW proposal will be complex for several reasons. These include the variety of sources, presence of hazardous contaminants, intended end uses of the material, quality control and the possibility that the end material will have to comply with REACH regulations (EPA, 2020). The complexities and difficulties associated with the EoW criteria and process are also highlighted in recently published case studies. Steel, specifically, has unyielding EoW criteria and administrative hurdles to overcome to achieve EoW status (Technopolis, 2016). There is a

disconnect between the EoW criteria and the steel industry, meaning the criteria have been found to be unjustifiable and disagreeable with current industry standards thus making the recycling of steel scrap unsuccessful (Technopolis, 2016). Furthermore, a case study from the copper recycling industry also identified EoW criteria as a significant regulatory barrier to the CE (Technopolis, 2016). It is the legal uncertainties that make the EoW criteria less enticing and easier for the industry to continue to focus on input from primary raw materials (Technopolis, 2016), leading to an unintended opposite effect.

### *2.4 Gaps in Literature*

At the time of this study, minimal literature existed on the CE in the Irish context. Furthermore, current studies lack focus on Irish enterprises that have taken steps towards and encouraged circularity. This area should be explored more to facilitate and promote CE practices throughout businesses and communities. Additionally, EoW is still an area largely unexplored in Ireland.

## 3. METHODOLOGY

This paper presents the views of people working towards EoW in Ireland to identify and understand the current CE and EoW practices more comprehensively. It is an exploratory study to elicit knowledge on aspects related to the EoW application criteria process in Ireland. It asks open-ended questions on the challenges faced and motivations towards a CE.

### *3.1 Approach*

This study seeks insights into practices and experiences of companies with EoW to identify potential obstacles and opportunities to Ireland transitioning to a CE. A qualitative inductive empirical approach was used for the industry interviews conducted for the study. The observable events serve as data, and the steps taken within the study can be replicated (Fischer, 2006). The methods of analysis used were a focused literature review followed by semi-structured interviews. The research is cross-disciplinary as it relates to both scientific and business disciplines. Furthermore, the interviews were cross-sectional as respondents all had experience with EoW, but all were not employed within the same sectors.

The semi-structured interviews allowed for a candid insight into the perceived barriers to achieving circularity within business models in the Irish context. Industry representatives were also asked to make recommendations on how to overcome the identified barriers.

The interviews are primarily representative of circular industry leaders in Ireland that have had direct EoW experience. Interview questions were specific to the EoW criteria application process.

### *3.2 Industry Interviews*

Using information published on the Irish EPA website, companies that had successfully obtained EoW status in Ireland were contacted to solicit an interview. Additional industry experts were identified and contacted to solicit interviews using a snowball data collection method. Thirteen pre-determined, relevant questions were asked, but also left room for deviation within the interview based on participant responses. The same interview format was followed for each interview. All interviews were recorded and transcribed. To reduce participant bias, interview questions were framed to be open-ended. Non-response bias was reduced by ensuring the confidentiality of responses to the interview and confirming participation using electronic communication.

### *3.3 Data Analysis*

Coding was the selected method of data analysis for participant interviews to allow for a ‘compare and contrast’ of participant responses. Transcription documents were coded using a word processing program. The codes were then transferred to tables and categorized into themes (thematic coding) to better interpret the data and formulate a conclusion.

### *3.4 Limitations of the Study*

There was only a small number of EoW-approved companies in Ireland from which to conduct industry interviews, so the results may not be generalisable to a broad range of enterprises.

## 4. RESULTS

Industry interviews were conducted virtually between June and August 2020. Companies were assigned pseudonyms in the form of alphabetical letters for anonymity and individuals are referred to as "they" to further ensure discretion.

### *4.1 Respondent Profiles*

Six interviews were conducted with three respondents (50%) having directly applied and received EoW status in Ireland, two having consulted on EoW applications in Ireland, and one respondent having consulted on EoW applications in Belgium. Three of the six respondents were employed in the waste collection/management sector, two respondents worked in the waste prevention/reuse and recycling field, and the remaining respondent worked in environmental consultancy. Additionally, five out of six (83%) of respondents worked in small to medium enterprises (SMEs).

### *4.2 Barriers to End-of-Waste Criteria*

Respondents were asked to state what they believe are barriers to achieving EoW criteria status. Using these responses, a list of perceived barriers to meeting EoW criteria was formed. The responses are presented in Table 1 below.

*Table 1. Respondent Perceived Barriers to End-of-Waste Criteria*

| Company | Barriers | Comments |
|---|---|---|
| A | Cost | Financial cost of administrative paperwork to process; Difficult to justify a budget for time consumed |
| | Time | Time to complete risk assessments and certifications is significant |
| | Regulations | Inconsistency in regulations; Lack of enforcement of regulations; Ambiguity and contradictions in the regulations; More incentive to extract virgin materials than using secondary materials |
| | EPA | EPA not collaborative or helpful throughout the process; EPA lacking the knowledge to adequately assess risk assessments associated with EoW application; Lacks staff to process applications in a timely manner |
| | Market | Irish market not up to speed on use of secondary materials from waste |
| B | Time | Application was not processed for 3+ years |
| | EPA | Staff evaluating may not be knowledgeable on the process from waste to non-waste |
| | Lack of Resources | Lack of EoW documents from other MS to reference for guidance |
| C | Cost | SMEs do not have the capacity to deal with complex EoW applications |
| | Applicability | EoW criteria should be developed for items being re-used/re-introduced to the market |
| | Cost | Consulting fees; risk analysis costs; time spent preparing for the application |
| | Time | Application/decision timeframe unclear |

| | | |
|---|---|---|
| D | Lack of Resources | Make more resources available within the EPA for applicants; EPA lacks resources to streamline EoW process - decisions might be different if the EPA had adequate resources |
| E | Cost | Testing requirements are expensive |
| | Time | Application process is complicated; takes several years to go through the process |
| | Applicability | SMEs unable to produce the volume of material necessary to be economically viable |
| | EPA | Companies afraid EPA will classify product as waste or by-product; EPA deemed unhelpful or difficult to work with during process |
| F | Cost | Cost of collecting enough waste is high |
| | Applicability | EoW not applicable to re-use sector, Re-use items cannot meet current EoW criteria |
| | Regulations | Meeting criteria differs between Member States |

### *4.3 Recommendations for End-of-Waste Application Process*

Respondents were also asked for recommendations for improving the EoW application process. Responses can be seen in Table 2 below.

*Table 2. Respondent Recommendations for Improvement of the End-of-Waste Application Process*

| Company | Recommendations | Comments |
|---|---|---|
| A | Become familiar with the end product | - |
| B | Website with all EoW decisions | - |
| | Separate entity to process EoW applications or collaboration from EPA | Companies are worried they will get prosecuted by EPA since they regulate their licenses and EoW applications; EPA cannot collaborate and regulate simultaneously |
| C | Review Austria's EoW criteria for reuse | Austrian EoW uses a unique approach to reuse items |
| | Include goods/reuse | EoW criteria language should be changed to include goods as well as materials |
| | Maintain strict criteria | EoW regime should be strict to avoid hazardous waste being inaccurately classified as EoW |
| D | Clear timeframe | EPA should provide a clear and definite timeframe of when application decisions will be made |
| | Make EoW inclusive | Criteria seem to be geared towards private companies, excluding the public sector |
| | Blanket approval | EoW products and by-products should receive a "blanket" approval as EoW instead of separate classifications |
| E | Make EoW applicable to SMEs | Most SMEs do not generate enough waste for the current EoW criteria to be applicable |
| | Research | Complete significant research before starting EoW application process |

| | | |
|---|---|---|
| | Simplification of guidance | Member States should have harmonisation of the criteria |
| F | EoW website | A website with applications and documentation relevant to EoW |
| | Faster decisions | Declare EoW ASAP, especially for re-use products |

## 5. DISCUSSION

The most prominent theme throughout the responses was the barrier of *cost* as the EoW criteria application process comes with several incurred costs. The financial cost of consultant fees, risk assessments, certifications, time commitment, and administrative personnel were cited costs, and therefore barriers. In addition to the above, there are often hidden costs such as time commitment and human capital that must be considered when changing business models. This echoes what research into CE transitions has also stated – that the costs associated with transitioning to a circular business model are frequently cited as a significant barrier to enterprises adopting sustainable practices (DBEI, 2019; Rizos et al, 2015; Ibec, 2019).

Furthermore, the Irish *EPA* is cited as an obstacle during the EoW process. Overall, the lack of adequate personnel on staff to process the complex EoW applications creates a trickle-down effect, leading to prolonged application processing times. Additionally, several participants mentioned a lack of EPA knowledge in the area as a factor in the EPA being perceived as a hindrance. This could potentially explain companies having the opinion that the EPA was "unhelpful" or unwilling to collaborate on the EoW initiative.

Additionally, mirroring the results of the case studies completed in 2016 (Technopolis Group), the lack of harmonisation between EU *regulations* and national regulations was named as an obstacle. The ability of individual MS to create different, case-by-case EoW criteria for various waste streams creates confusion. This was also stated in the Dutch government's Circular Economy report (2016) and by steel recyclers in a 2016 study. Further barriers arise when the EoW criteria focus heavily on waste and not reuse or recycling, according to several interview participants. Materials considered to be of reuse or refurbish value are unable to meet the stringent EoW criteria as some simply do not apply.

SMEs are most affected by each of these perceived obstacles to achieving EoW, which could lead to further delay in transition to an Irish CE, as SMEs make up most Ireland's 250,000 businesses. SMEs regularly lack the financial resources, either to pay for consultants or expert staff who would have the necessary expertise to work through the extensive process.

Steps could be taken to quickly remove many of the experienced barriers. Collaboration between industry and research institutes should be encouraged and funded so that the required extensive testing and validation, which may otherwise be a barrier, can be undertaken. As discovered in the literature review, many Irish companies are not even aware of basic CE approaches, and those that are aware do not necessarily have the knowledge or expertise required for an extensive EoW application process. Furthermore, the problems encountered by each of the Irish companies interviewed consistently pointed toward a lack of understanding within the responsible body, the EPA. This is understandable given the diverse range of potential waste streams and the level of regulatory knowledge required for each individual stream.

## 6. CONCLUSION

This research examined the transition to a CE in Ireland, and the impediments thereof, with a particular focus on the requirements to achieve EoW criteria status. The main contributions of this study are further knowledge of EoW criteria and the current state of the CE in Ireland. These areas have been shown by the research to be both relevant and important to the current economic and environmental situation.

There is an argument made that EoW criteria were a failure and efforts should focus on alternatives (Johannson & Forsgren, 2020) to circularity, however, examples of successful implementation of EoW criteria do exist. A CE may not have the ability to entirely 'close the loop', however, it can aid in lessening the gap. For a transition to be successful, there needs to be an alignment of producers, consumers, and regulating bodies.

## 7. REFERENCES


Circle Economy. (2019). *Closing the circularity gap in a 9% world.* Amsterdam: Circle Economy.

DBEI. (2019). *Realising the opportunities for enterprise in the Bioeconomy and Circular Economy in Ireland* . Dublin: Department of Business, Enterprise and Innovation.

European Commission. (2020). *Closing the loop - An EU action plan for the Circular Economy.* Brussels: European Commission.

Ellen Macarthur Foundation & McKinsey Center. (2015). *Growth within: A circular economy vision for a competitive Europe.* Cowes: Ellen MacArthur Foundation.

Ellen Macarthur Foundation. (2019). *Completing the picture: How the Circular Economy tackles climate change.* Cowes: Ellen MacArthur Foundation.

EPA. (2020). *Article 28 (End of Waste)*. Retrieved July 17, 2020, from http://www.epa.ie/waste/wastereg/art28/

EPA. (2020, July 13). EoW Experience.

European Commission. (2019). *European Commission*. Retrieved May 30, 2020, from https://ec.europa.eu/environment/waste/framework/end_of_waste.htm

European Environment Agency. (2001). *Eco-design*. Retrieved August 1, 2020, from https://www.eea.europa.eu/help/glossary/eea-glossary/eco-design

European Environmental Agency. (2016). *Circular Economy in Europe, Developing the knowledge base.* Copenhagen: European Environmental Agency.

Eurostat. (2022). *Eurostat*. Retrieved July 21, 2022, from https://ec.europa.eu/eurostat/web/products-datasets/-/sdg_12_41#:~:text=The%20circular%20material%20use%20rate,to%20the%20overall%20material%20use.

Fischer, C. T. (2006). Qualitative research methods for psychologists : Introduction through empirical studies. Burlington: Academic Press.

GoN. (2016). *A Circular Economy in the Netherlands by 2050: Goverment-wide programme for a circular economy.* The Hague: The Ministry of Infrastructure and the Environment; the Ministry of Economic Affairs.

Ibec. (2019). *Is Irish business getting ready for the Circular Economy.* Dublin: Ibec.

Ibec. (2019, August 14). New Ibec survey shows just half of businesses understand the Circular Economy. *Ibec*.

Johansson, N. & Forsgren, C. (2020, April). Is this the end of end-of-waste? Uncovering the space between waste and products. *Resources, Conservation & Recycling*.

Joint Research Centre. (2009). *EoW Criteria Final Report.* Seville: European Communities.

Joint Research Centre. (2020). *European Commission*. Retrieved June 14, 2020, from https://ec.europa.eu/

Kuhn, G., & Snijder, A. (2018). *Report of the joint workshop Waste/End-of-waste in Treviso (Italy).* Treviso: IMPEL.

Material Economics. (2018). *The Circular Economy: A powerful force for climate mitigation.* Stockholm: Material Economics.

NESC. (2017). *Moving towards the Circular Economy in Ireland.* Dublin: National Economic & Social Council Development Office.

Plastics Recyclers Europe. (2019). *Flexible polyethylene recycling in Europe: Accelerating the transition towards Circular Economy.* Brussels: Plastics Recyclers Europe.

Rizos et al. (2015). *The Circular Economy: Barriers and opportunities for SMEs.* Brussels: CEPS.

Scarpellini et al. (2019). Definition and measurement of the Circular Economy's regional impact. *Journal of Environmental Planning and Management, 62*(13), 2211-2237.

Technopolis. (2016). *Regulatory barriers for the circular economy: lessons from ten case studies.* Amsterdam: Technopolis Group.

United Nations. (2015). *Sustainable Development Goals*. Retrieved 23 July, 2020, from https://www.un.org/sustainabledevelopment/sustainable-consumption-production/

VTT. (2020). A Circular Economy of plastics: A vision for redesigning plastics value chains. VTT Technical Research Centre of Finland Ltd.

# Design and Optimisation of a Liquid-Cooling Plate System for the Thermal Management of Lithium-ion Batteries in Electric Vehicles

Keith Hickey,

keith.hickey1998@gmail.com,

Munster Technological University, Cork.

***Abstract***

In recent years electric vehicles have emerged as a new and promising mode of transport as an alternative to the traditional internal combustion engine as seen in pure electric vehicles (EVs) and hybrid electric vehicles (HEVs). The power source of choice for these vehicles are lithium-ion batteries due to their high energy density, long lifecycle, low weight and ability to be recharged making them practical and less expensive to run than traditional vehicles. With the promise of being much more environmentally friendly than other vehicles due to their low carbon footprint, and the world being on the brink of an irreversible environmental crisis, the market for EVs has grown and is set to grow immensely. Governments are set to accelerate the pace of EV take-up among private and public transport to reach carbon agreements to make the transport industry a much more sustainable one.

A problem associated with lithium-ion batteries is the enormous heat they generate internally due to enthalpy changes, electrochemical polarization and resistive heating inside the cell due to the transmission of lithium ions between the anode and cathode. This internal heat generation can limit battery performance, reduce battery lifetime and in severe cases can affect the integrity and safety of the vehicle. The optimum battery operating conditions include its maximum temperature lying in the range of 15 to 35 °C and a maximum temperature difference of 5 °C across the battery. Due to the extreme heat generated by lithium-ion batteries, thermally controlling them has always been a challenge and has been an area of some focus with the rise of the EV industry.

In this study, a three-dimensional thermal investigation was conducted on a lithium-ion battery using a multi-scale multi-dimensional modelling approach. The commonly used Newman, Tiedemann, Gu and Kim (NTGK) battery model was used to develop the electrochemical model for heat generation of the chosen lithium-ion battery. Once developed a liquid cooling plate system was designed and underwent an optimisation process using the Taguchi design of experiments (DOE). ANSYS Fluent was used model the cooling plate and lithium-ion battery under 5C discharging conditions to monitor the cooling plate effectiveness in which the coolant used was water at 20°C. The optimized cooling plate resulted in in a maximum temperature of 22.45 °C and temperature difference of 2.43°C, with coolant entering the cooling plate at a velocity of 0.05 m/s. These values lie comfortably inside the optimum battery operating conditions and show that the novel design analysed can perform quite well. The range method was used to find that the number of channels in the cooling plate has the most influence on the cooling effectiveness of the plate, while the channel angle has the least influence.

An effective cooling system would be of huge benefit to the industry in hopes of making lithium-ion batteries a more sustainable, longer lasting means of energy for the transport industry. The manufacturing of these cooling plates also adds to the sustainability of the transport industry while increasing digitalisation of the manufacturing process due to the additive manufacturing methods needed to produce the complex, non-standard geometry. The cooling channels lie internally inside the plate and so cannot be manufactured using standard machining processes. 3D printing the cooling plates can significantly reduce waste and ensure a high degree of precision in manufacturing.

Key words: Liquid-cooling, NTGK, honeycomb, optimisation, turbulent kinetic energy.

## *1. INTRODUCTION*

The continuous development and use of internal combustion engines powered by fossil fuels has caused the onset of climate change. Electric vehicles (EV's) have quickly emerged as a promising environmentally friendly means of transport with benefits including lower running costs, lower carbon footprint and long driving range before needing to recharge. The power source of choice for EV's are lithium-ion batteries (LIB's) due to their high energy density, extended lifetime and ability to be recharged when their capacity has been reached [1]. The increase in popularity in the EV industry is significantly down to onset of climate change, grant schemes available for EV's and increasing fossil fuel prices. Variations of EV include the hybrid, plug-in hybrid and fully battery powered which are mainly used to migrate people away from strictly using internal combustion engine cars. With the projected EV uptake in Ireland increasing by up to 95% within the next 10 years, LIB's have become a relevant topic for research [2].

A problem associated with LIB's during the discharging process is there can be significant heat generated inside the battery structure which heavily impacts the battery performance. If left untreated, temperature will continue to increase leading to degradation in battery performance, lifetime and an increasing possibility of thermal runaway [3]. Thermal runaway is when heat generated by the LIB exceeds the amount that can be dissipated to ambient conditions, leading to further temperature increase which can eventually lead to spontaneous combustion of the LIB. Other conditions which affect the heat generated by the LIB include high ambient temperature, large battery discharge rates and aggressive driving [4]. The aim of this research is to develop and optimise a liquid cooling plate system to maintain LIB temperature within a safe operating temperature range while also keeping temperature variation across the LIB to a minimum using the principles of heat transfer. The optimum temperature for LIB's, however, is between 15 and 35°C while the recommended maximum temperature variation for the LIB is ideally less than 5°C [5].

Liquid cooling is the most popular method due to its higher thermal conductivity than air yet there are many different forms of cooling seen in previous literature. One study investigated the cooling effectiveness of a cooling plate with a bionic spider web channel structure in the plate which allowed for the flow of coolant. This study managed to control a LIB with a discharge rate of 12C to a maximum temperature of 37.89°C and temperature difference of 8.86°C. This study analysed the impact of changing the number of channels, width of the channels and the angle of the channels to find which had the most impact on the cooling effectiveness [6]. Another study followed a similar process of testing two models with slight geometrical differences to find the most effective method [7]. This is proven to be an effective method of optimising cooling systems which is adapted in this analysis.

The aim of this investigation is to utilise the orthogonal design of experiments (DOE) and factor of most influence analysis to develop an optimised liquid cooling plate based on results from models with different characteristics. It is therefore expected than the optimised model should perform better than the models from the DOE.

## *2. METHODOLOGY*

### *2.1. LIB Development*

The initial selection of a LIB for analysis was a substantial process due to the vast array available and previously studied. The selected prismatic LIB was tested to compare with literature which was selected based on the abundance of information available to model the LIB in the literature. The LIB was a 5 Ah with 3.2 V and similar to the literature, ANSYS Fluent was the modelling tool used to simulate LIB behaviour and environmental conditions [8]. The multi-scale multi-domain (MSMD) battery option in ANSYS Fluent is a useful tool which aids in simulating battery behaviour, inside which the Newman, Tiedemann, Gu, and Kim (NTGK) method was used, which is a semi-empirical electro thermal model. This model needs input parameters including capacity, depth of discharge, C-rate and data from polarisation equations developed through experimentation on the LIB. This information was taken from the literature to replicate results as close as possible and information about the LIB being tested is in table 1 below.

*Table 1; LIB characteristics.*

| **Characteristics** | **Value** |
|---|---|
| Nominal Capacity (Ah) | 5 |
| Nominal Voltage (V) | 3.2 |
| Length (mm) | 117.7 |
| Width (mm) | 70 |
| Thickness (mm) | 7 |

The length, width and thickness of the LIB active zones are given above in table 1 which define the size of the heat generating portion of the LIB. This is the important section of the LIB in this investigation as this is where the cooling will take place. The LIB discharge process is simulated using the NTGK battery model which will allow Fluent to replicate the changes in its thermal behaviour. Figure 1 below shows the LIB inventor drawing and all dimensions while figure 2 shows the discretisation process used before simulating in ANSYS Fluent. The meshing function used was the body sizing function, with the element size of 0.001 m. LIBs are typically made from layers of materials joined together, however, it is assumed that the LIB is a solid object with constant density for the modelling process. This is why the model below appears to be one solid object.

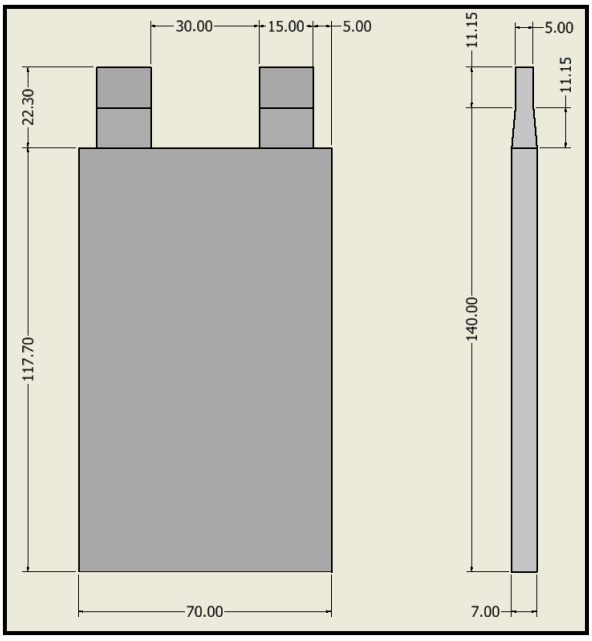


*Figure 1; LIB Inventor drawing.*

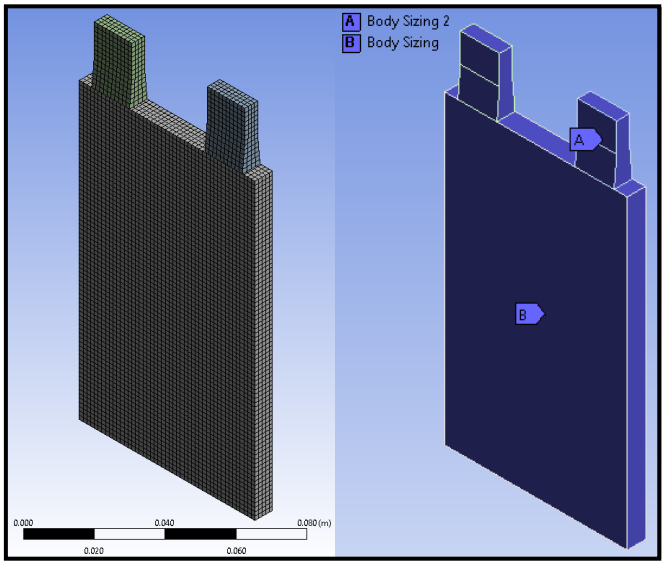


*Figure 2; LIB discretisation process.*

When discretisation of the model is complete, it is exported into ANSYS Fluent where it is analysed under particular conditions. Here the NTGK parameters, boundary conditions and solving time are also set. These boundary conditions include material properties, LIB properties and circuit continuity of the LIB. Equations 1 and 2 below are the U and Y polarisation equations needed for the NTGK battery model which have been obtained experimentally by plotting the current density vs electrode potential under different C-rates which has been validated through the simulation in the literature [8]. The numbers from equations 1 and 2 are transferred into U and Y coefficients boxes in the NTGK battery model as shown in figure 3 which allow ANSYS to simulate the real world thermal behaviour of the LIB as time passes.

$$U = 3.6 - 0.804(DoD) + 1.075(DoD)^2 - 1.177(DoD)^3 + 0.00095(T - T_{ref}) \quad (1)$$

$$Y = [1168.59 - 8928(DoD) + 52504.6(DoD)^2 - 136231(DoD)^3 + 158531.7(DoD)^4 - 67578.5(DoD)^5]\, exp\left[-1800\left(\frac{1}{T} - \frac{1}{T_{ref}}\right)\right] \quad (2)$$

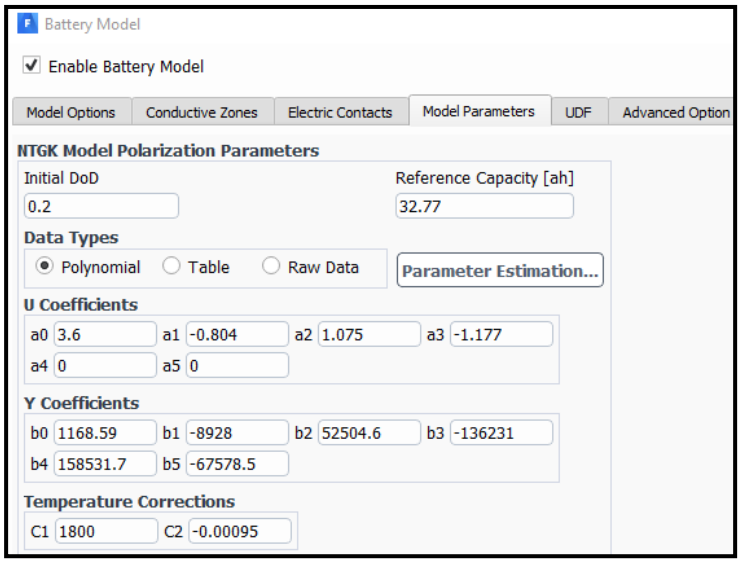


*Figure 3; NTGK battery model with polarisation parameters.*

Properties of the LIB for density, ρ, thermal capacity, Cp and thermal conductivity, k were found to be 2318.068 kg/m$^3$, 1056.082 J/kg°C and 55.66236 W/m·K respectively. These values were then input into Fluent as properties for the active zone of the LIB and the positive and negative tab properties were also set [8].

Other boundary conditions set included a discharging C-rate of 5, heat transfer coefficient of 5.5 W/(m2·K) and ambient temperature was set to 20°C. The analysis was set to transient with a setup of 56 time steps, 10 second time step size and maximum 50 iterations per time step. This resulted in 2800 timesteps and a 560 second flow time, the same as in the literature which should result in similar results. The factor of most importance to match for the purpose of validation of the model is the maximum LIB temperature. This is important as the aim of the cooling system is to manage temperature, so an accurate thermal behaviour is crucial to the accuracy of the results.

After simulation was complete, it was clear that the model had performed extremely well with a similar temperature contour seen in the literature as shown in figure 4. The contours are very similar with areas of most heat generation lying in the bottom third. The accuracy of the maximum and minimum LIB temperature is used to validate the results which have been found to be very accurate as given below.

Maximum temperature error: $\frac{43.61-43.55}{43.55}\, x\, 100 = 0.1378\,\%$

Minimum temperature error: $\frac{41.84-41.54}{41.84}\, x\, 100 = 0.717\,\%$

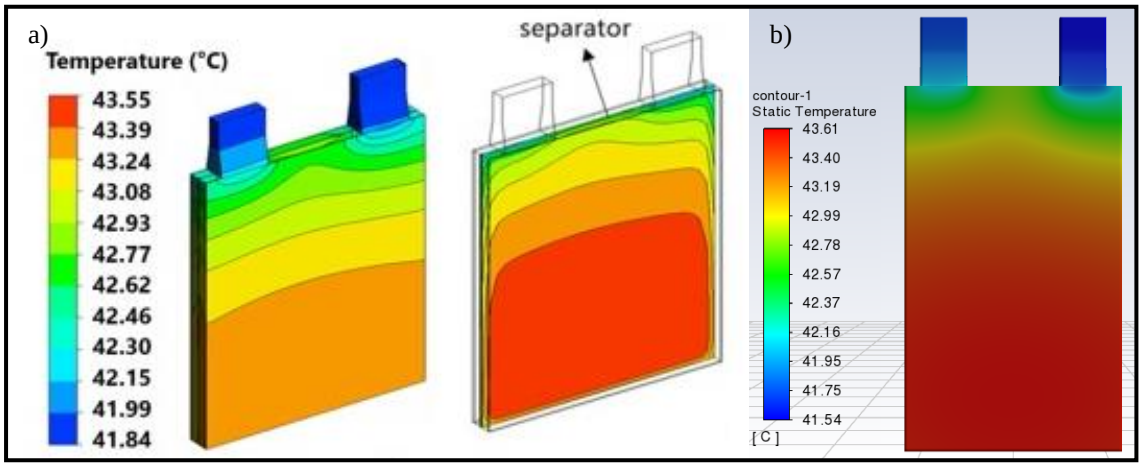


*Figure 4; a) LIB 3 literature and b) Simulated temperature results.*

The LIB analysis resulted in a very accurately behaving model with maximum and minimum LIB temperature error being below 1%. This extremely accurate model is also beneficial to the accuracy of the readings from the proposed cooling system to be modelled as it is known that the LIB thermal behaviour is correct. It should also be restated that the optimum operating temperature range for LIB's is 15 to 35°C which gives the LIB some scope for improvement through the use of a cooling system. Due to the high accuracy, ease of validation and abundance of information available, this LIB was chosen as the model for further research and cooling system investigation.

### *2.2. Model Quality Testing*

To further validate the behaviour of the model, a mesh independence study was completed. Its main purpose is to prove that with increasing elements, results become more accurate and converge to a point where a further increase in elements has no benefit to the accuracy of the model [9]. After modelling the LIB with the elements given in table 2, it was found that the results converged at approximately 50,000 elements. Using the 60,800 element density would ensure that a high accuracy would be obtained without excess solving time. LIB $T_{max}$, $T_{min}$ and anode potential were monitored for the convergence study with plots given below in figures 5, 6 and 7.

*Table 2; LIB mesh independence data.*

| Elements | Max Temp (°C) | Min Temp (°C) | Anode Potential (V) |
|---|---|---|---|
| 3465 | 43.60369 | 41.51553 | -0.00012327 |
| 6204 | 43.60381 | 41.51101 | -0.000121115 |
| 13856 | 43.60363 | 41.53274 | -0.000119662 |
| 26060 | 43.60372 | 41.53518 | -0.000118723 |
| 60800 | 43.60372 | 41.53985 | -0.000118028 |
| 116199 | 43.60372 | 41.54226 | -0.000117295 |
| 249236 | 43.60369 | 41.54409 | -0.000116721 |

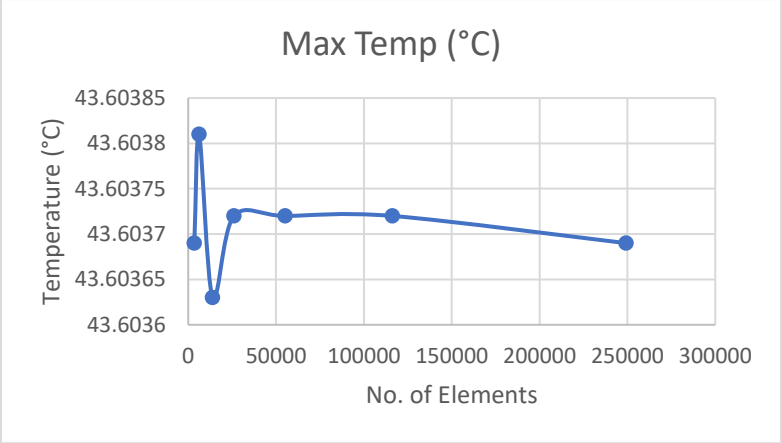


*Figure 5; Maximum LIB temperature mesh independence test.*

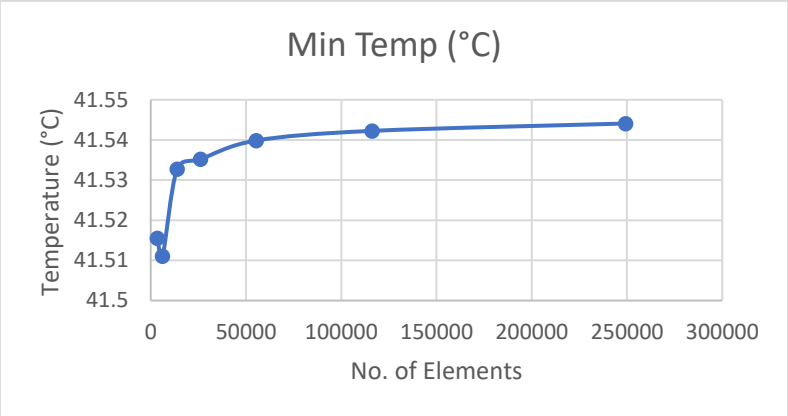


*Figure 6; Minimum LIB temperature mesh independence test.*

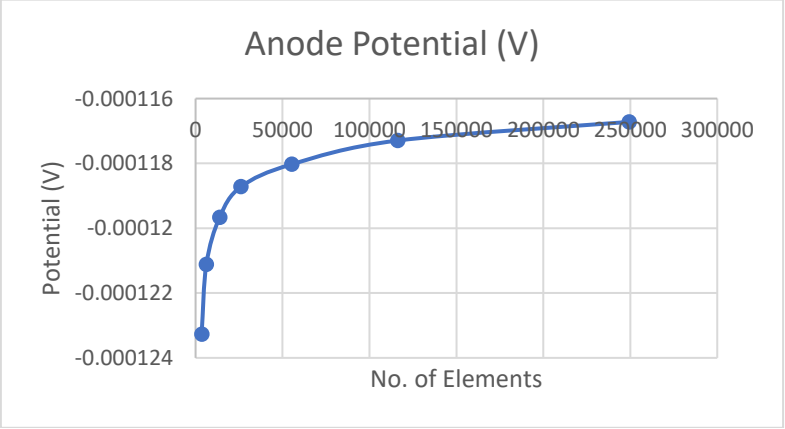


*Figure 7; LIB anode potential mesh independence test.*

### *2.3. Cooling Plate System Design*

A LIB liquid cooling plate employs the simple principles of heat transfer, conduction and convection between materials and fluids. Cold liquid will pass through channels or conjugates in a metal plate which will be in contact with the LIB. As the cold liquid passes through the plate, heat generated by the LIB will be transferred into the flowing liquid, due to heat flowing from hot to cold. Figure 8 below shows three cooling plates designed based on natural patterns in the form of a honeycomb, leaf and snake design. Since turbulence is a contributing factor in heat transfer, the designs were tested and solved for turbulent kinetic energy where it was found that turbulent kinetic energy was produced most frequently in the honeycomb channel [10]. Figure 9 shows that high turbulent kinetic energy occurs quite frequently in the honeycomb channel due to the diverging and converging nature of the honeycomb structure. This along with the other plates being over engineered and complex resulted in the honeycomb being selected to pursue further investigation on.

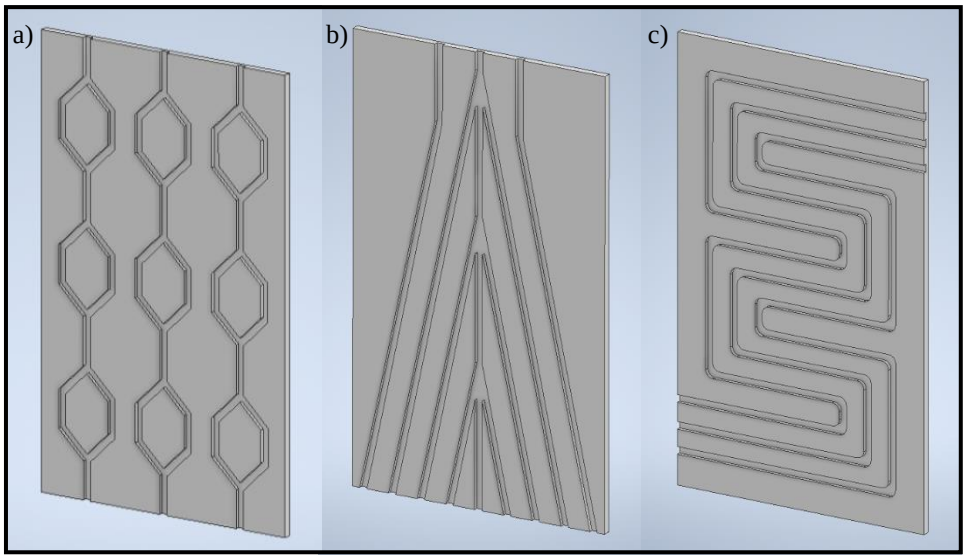


*Figure 8; a) Honeycomb, b) Leaf and c) Snake cooling plate structures*

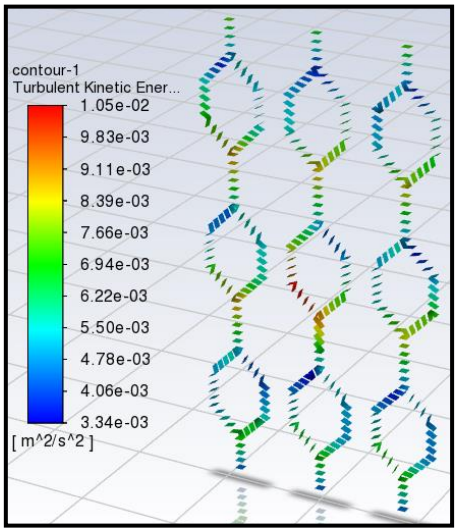


*Figure 9; Turbulent kinetic energy in honeycomb channel design with inlet velocity of 1 m/s.*

### *2.4. Design of Experiments (DOE)*

The cooling plate DOE process involves changing the model parameters slightly to produce a select number of models. Each of these models are tested to see which models perform the best and from this we can see what parameters have a major influence on the performance of the cooling plate. Many elements of the cooling plate design can be changed to develop the models, but they have to have a direct link to the cooling effectiveness of the plate. In this case, a 3 factor, 3 level experiment was chosen with factors being the number of inlet channels, channel width and channel diversion angle. The levels of each factor are given below in table 3. Some were picked based on previous literature and some based on space available on the dimensions of the cooling plate. It is assumed that the number of channels and channel width will have the greatest impact on LIB temperature with channel angle having the least impact but may have a greater impact on other results.

*Table 3; 3 factor 3 level experiment design.*

| **Factors** | **No. of channels, n** | **Channel width, l (mm)** | **Channel angle, α (°)** |
|---|---|---|---|
| **Level 1** | 1 | 2 | 35 |
| **Level 2** | 2 | 3 | 45 |
| **Level 3** | 3 | 4 | 55 |

Using the list of factors from table 3 above, different models had to be made that would capture the impact of changing the factors. In a typical DOE this would be calculated to be $3^3$ or 27 models due to the fact there are 3 factors and 3 levels displayed in figure 10, and this method can be seen in figure 11 showing all possible level combinations. Another option is the orthogonal DOE method where Minitab was used which reduced the number of models from 27 down to 9 shown in figure 12 below. This would save time both in developing models in Inventor and solving time in ANSYS Fluent. The orthogonal design also gives enough variety in the models that shows the impact of changing the parameters. To emphasise how the orthogonal DOE layout works, model one in figure 12 has one channel, with a channel width of 2 mm and the honeycomb is at an angle of 55°.

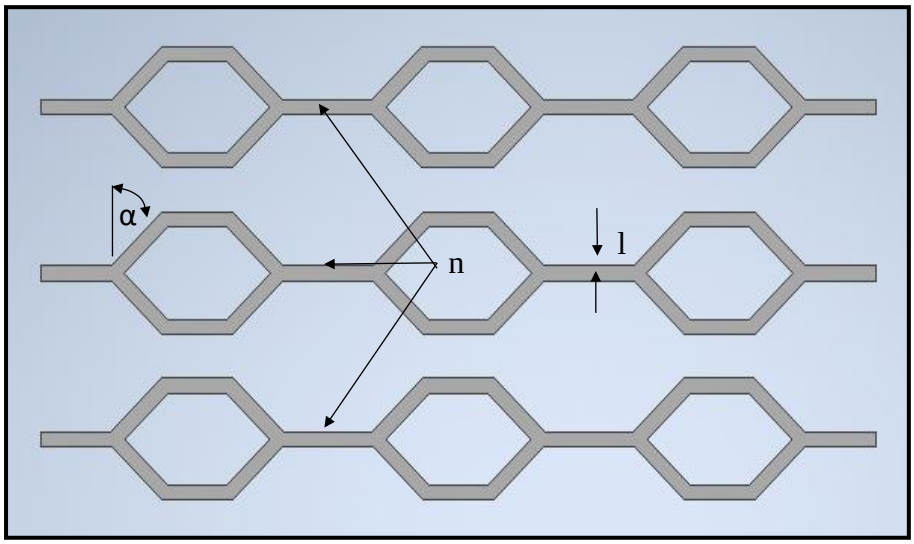


*Figure 10; Honeycomb factors for DOE.*

| | C1 | C2 | C3 |
|---|---|---|---|
| | No. Channels | Channel Width | Channel Angle |
| 1 | 1 | 4 | 75 |
| 2 | 3 | 2 | 55 |
| 3 | 3 | 2 | 75 |
| 4 | 3 | 4 | 55 |
| 5 | 3 | 3 | 65 |
| 6 | 2 | 2 | 65 |
| 7 | 2 | 3 | 75 |
| 8 | 3 | 4 | 75 |
| 9 | 2 | 2 | 55 |
| 10 | 3 | 2 | 65 |
| 11 | 2 | 4 | 75 |
| 12 | 1 | 3 | 75 |
| 13 | 2 | 3 | 55 |
| 14 | 2 | 2 | 75 |
| 15 | 2 | 3 | 65 |
| 16 | 2 | 4 | 65 |
| 17 | 1 | 3 | 55 |
| 18 | 1 | 3 | 65 |
| 19 | 3 | 3 | 75 |
| 20 | 1 | 2 | 75 |
| 21 | 1 | 2 | 65 |
| 22 | 1 | 4 | 65 |
| 23 | 3 | 4 | 65 |
| 24 | 1 | 2 | 55 |
| 25 | 2 | 4 | 55 |
| 26 | 1 | 4 | 55 |
| 27 | 3 | 3 | 55 |

*Figure 11; DOE using every possible factor combination.*

| | C1 | C2 | C3 |
|---|---|---|---|
| | No. Channels | Channel Width | Channel Angle |
| 1 | 1 | 2 | 55 |
| 2 | 1 | 3 | 45 |
| 3 | 1 | 4 | 35 |
| 4 | 2 | 2 | 45 |
| 5 | 2 | 3 | 35 |
| 6 | 2 | 4 | 55 |
| 7 | 3 | 2 | 35 |
| 8 | 3 | 3 | 55 |
| 9 | 3 | 4 | 45 |

*Figure 12; DOE using orthogonal design.*

## 3. RESULTS

### 3.1. DOE Results

ANSYS Fluent was used to simulate the effects of the cooling plate on the LIB $T_{max}$ under a range of inlet velocities including 0.05, 0.1, 0.5, 1 and 2 m/s. The nine models were analysed to find the best performer and it can be seen in figure 13 that model nine consistently performed the best. This model had three channels of 4 mm width which proved to be quite effective in managing the LIB $T_{max}$. Figure 14 below shows the LIB temperature contours under each inlet velocity which clearly shows how the cooling becomes more intense with increasing inlet velocity as heat transfer rate is reliant on mass flowrate shown in equation 3 below.

$$\dot{q} = \dot{m}\ x\ c_p\ x\ \Delta T \tag{3}$$

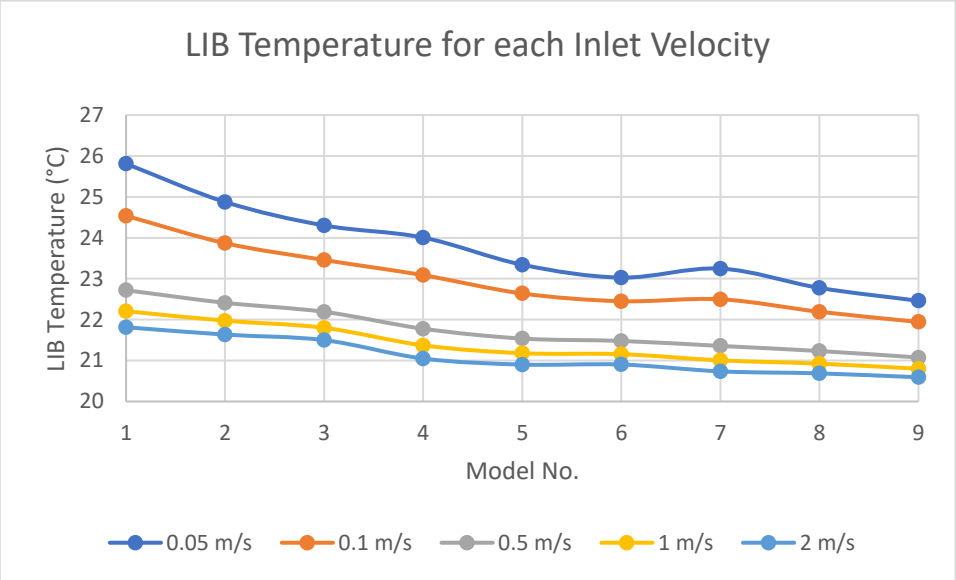


*Figure 13; Maximum LIB temperature results for each model and inlet velocity.*

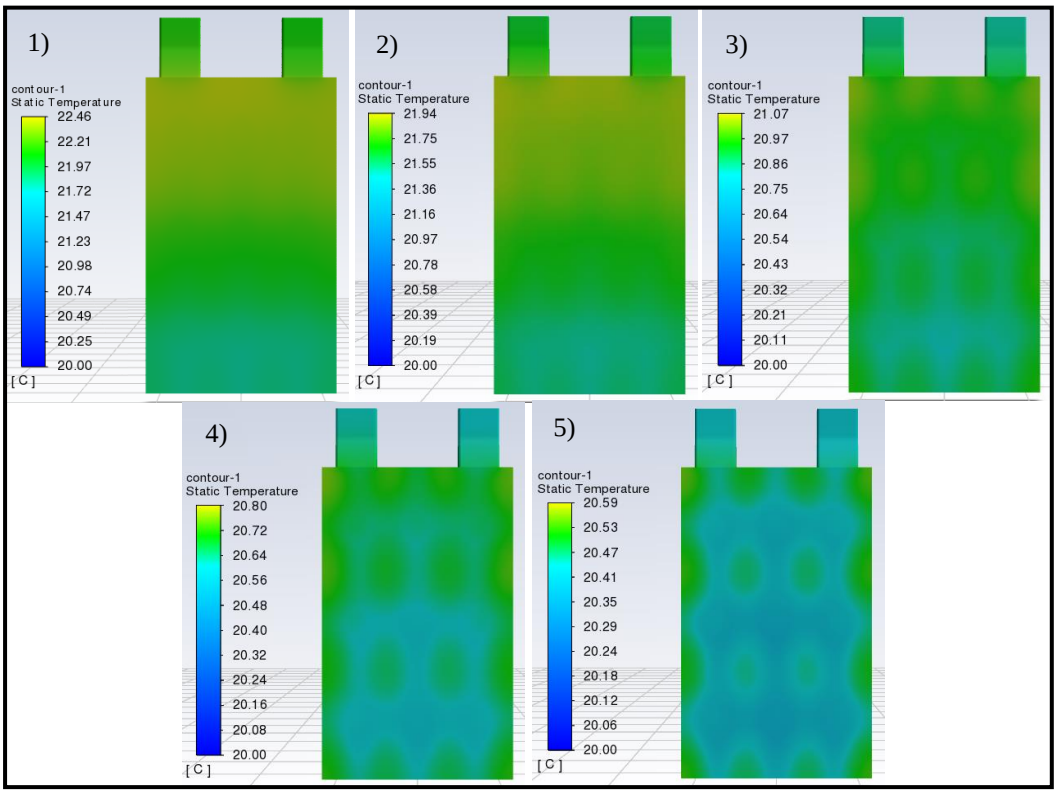


*Figure 14; Model 9 LIB surface temperature for each inlet velocity*

### *3.2. Optimisation Process*

To optimise the performance of the cooling plate, the most influential factors must be found in addition to finding the best performing level of each factor with respect to the maximum LIB temperature, as this is the critical result for this analysis. The factor of most influence analysis is based on the impact that changing each factor has on the cooling plates performance. For example, if the coolant channels are made wider, does this have a major effect on the LIB temperature and how does this compare with the effect seen if the number of channels is increased. The Range (R) method uses an evaluation index which reflects the degree of influence by a value where larger values represent a greater influence. The difference between the maximum and minimum average value of each level of a factor is used given in equation 4 below. $k_i$ is the average of the levels of each factor. To show the process behind this, the influence of the number of channels factor on $T_{max}$ is given. The analysis is completed on the 0.05 m/s trial.

$$R = \max(k_1, k_2, k_3) - \min(k_1, k_2, k_3) \quad (4)$$

For the number of channels, the levels are one, two and three channels where models one to three have one channel, models four to six have two channels and models seven to nine have three channels. The $T_{max}$ results for each level given previously in table 5 are used to find $k_1$, $k_2$ and $k_3$ as follows.

$$k_1 = \frac{25.80923 + 24.87484 + 24.30129}{3} = 24.99512$$

$$k_2 = \frac{24.00521 + 23.34173 + 23.02764}{3} = 23.45819$$

$$k_3 = \frac{23.24795 + 22.77557 + 22.45989}{3} = 22.8278$$

Once the $k_i$ values are found, equation 4 is used to find the range, this is the value which ranks the degree of influence of the factors.

$$R = \max(k_1, k_2, k_3) - \min(k_1, k_2, k_3)$$

$$R = \max(24.99512, 23.45819, 22.8278) - \min(24.99512, 23.45819, 22.8278)$$

$$R = 24.99512 - 22.8278$$

$$R = 2.16732$$

This R value for the number of channels, n, is compared with the R values for channel width, l, and channel angle, α, which will tell which factor has the most influence on $T_{max}$. Table 4 below gives the factor of most influence results for $T_{max}$, $\Delta T_{max}$ and $\Delta P$. It can be seen in table 4 that the number of channels had the most influence on $T_{max}$ meaning that increasing the number of channels had more influence on the cooling performance than increasing channel width or channel angle. For $T_{max}$, factor influence was in the order n > l > α. The $\Delta T_{max}$ factor of influence was the same as $T_{max}$, but $\Delta P$ came out as l > α > n with channel width having the most influence as pressure will be the same across each channel. The best performing levels of each factor are easily found by monitoring the $k_i$ values. For $T_{max}$ which is the result of most interest in this analysis, the lower the $k_i$ value the better it performed as it gave a lower $T_{max}$. Therefore, with respect to $T_{max}$, three is the optimum number of channels, 4 mm is the optimum channel width and 35° is the optimum channel diversion angle in the honeycomb structure.

*Table 4; Factor of influence, Range method results.*

| | $k_i$ | No. of Channels, n | Width of Channels, l | Channel Angle, α |
|---|---|---|---|---|
| **$T_{max}$ (°C)** | **$k_1$** | 24.99512 | 24.35413 | 23.63032 |
| | **$k_2$** | 23.45819 | 23.66405 | 23.77998 |
| | **$k_3$** | 22.8278 | 23.26294 | 23.87081 |
| | **R** | 2.167317 | 1.09119 | 0.24049 |
| **ΔT (°C)** | **$k_1$** | 4.96053 | 4.311953 | 3.608757 |
| | **$k_2$** | 3.436033 | 3.646923 | 3.755797 |
| | **$k_3$** | 2.81053 | 3.248217 | 3.84254 |
| | **R** | 2.15 | 1.063737 | 0.233783 |
| **ΔP (Pa)** | **$k_1$** | 17.30459 | 20.86785 | 19.53891 |
| | **$k_2$** | 17.6992 | 16.77889 | 17.58625 |
| | **$k_3$** | 17.72152 | 15.07857 | 15.60015 |
| | **R** | 0.416931 | 5.789278 | 3.938758 |

By finding the most influential factors and the best performing levels of each factor, it was possible to develop an optimised model aimed at providing the best cooling performance possible using the factors chosen. Figure 15 below shows the channel structure of the optimised cooling plate.

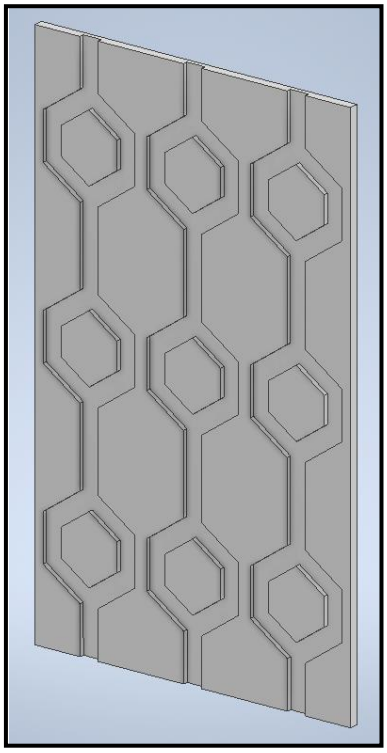

*Figure 15; Cross section of optimised cooling plate*

After developing the optimised cooling plate and testing in ANSYS Fluent, the results are given in table 5 below. Since the $T_{max}$ and $\Delta T_{max}$ are the factors of importance in this analysis, this is where the focus on improvement is. It can be seen that the $T_{max}$ is slightly lower across each inlet velocity for the optimised model proving that the combination of the best performing factors did result in an optimised model which performed better than models one to nine. Using the optimised model, the $T_{max}$ improved by up to 0.2507% while the $\Delta T_{max}$ improved by up to 8.15%.

*Table 5; Model 9 vs Optimised model results.*

| | **$T_{max}$ (°C)** | | **$\Delta T_{max}$ (°C)** | | **$\Delta P$ (Pa)** | |
|---|---|---|---|---|---|---|
| **Inlet Velocity (m/s)** | **Model 9** | **Optimised** | **Model 9** | **Optimised** | **Model 9** | **Optimised** |
| **0.05** | 22.45989 | 22.44576 | 2.44928 | 2.4353 | 15.018406 | 16.736324 |
| **0.1** | 21.9436 | 21.9194 | 1.93833 | 1.91422 | 36.323997 | 42.270446 |
| **0.5** | 21.07461 | 21.02639 | 1.07346 | 1.02527 | 551.70545 | 695.36801 |
| **1** | 20.79888 | 20.74673 | 0.79828 | 0.74616 | 2042.4445 | 2608.4815 |
| **2** | 20.59136 | 20.54318 | 0.59106 | 0.54288 | 7794.6371 | 10068.3894 |

Maximum $T_{max}$ improvement was at 1 m/s: $\frac{20.79888-20.74673}{20.79888}\ x\ 100 = 0.2507\ \%$

Maximum $\Delta T_{max}$ improvement was at 2 m/s: $\frac{0.59106-0.54288}{0.59106}\ x\ 100 = 8.15\ \%$

## *4. DISCUSSION*

The objective of developing an optimised cooling plate design based on the results from an orthogonal DOE and a factor of most influence analysis has been completed as it was found that the optimised cooling plate had performed better than the DOE models. It was found that the $T_{max}$ was improved by up to 0.2507% and the $\Delta T_{max}$ improved by up to 8.15% over the extent of the coolant inlet velocities used. Even though the $T_{max}$ improvement was not very big, any small improvement has a domino effect on the $\Delta T_{max}$ and thermal management of the LIB. It is however proof that the orthogonal DOE and factor of influence analysis was an effective method of developing an optimised model.

As well as developing an optimised model, the final LIB temperature results from the model showed that the cooling plate performed very well, with results lying well within the optimum operating conditions for LIBs which are a $T_{max}$ of 15 – 35°C and a $\Delta T_{max}$ of less than 5°C. The best results for $T_{max}$ and $\Delta T_{max}$ occurred at the highest inlet velocity of 2 m/s, which were 20.543°C and 0.543°C respectively. The $T_{max}$ and $\Delta T_{max}$ results for the lowest inlet velocity of 0.05 m/s were 22.446°C and 2.435°C respectively. This shows that the greater the coolant inlet velocity, the greater the cooling effectiveness of the cooling plate. It must be noted that increasing coolant inlet velocity converges to a point to where further increasing the inlet velocity would not result in improvement of results. This can be seen below in figure 17 as the LIB temperature converges towards the 2 m/s inlet velocity. The magnitude of the temperature improvement decreases as inlet velocity increases meaning that at some point, increasing inlet velocity will result in no improvement.

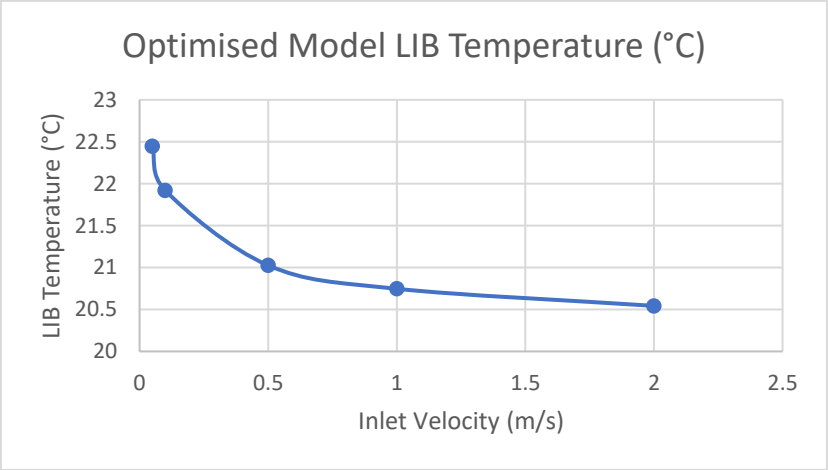


*Figure 16; Optimised model LIB temperature under each coolant inlet velocity.*

## *5. REFERENCES*


[1] V. G. Choudhari, D. A. S. Dhoble, and T. M. Sathe, "A review on effect of heat generation and various thermal management systems for lithium ion battery used for electric vehicle," *J. Energy Storage*, vol. 32, p. 101729, Dec. 2020, doi: 10.1016/J.EST.2020.101729.

[2] "New Climate Action Plan key to EV uptake – Energy Ireland." https://www.energyireland.ie/new-climate-action-plan-key-to-ev-uptake/ (accessed Apr. 25, 2022).

[3] D. Bernardi, E. Pawlikowski, and J. Newman, "GENERAL ENERGY BALANCE FOR BATTERY SYSTEMS.," *Electrochem. Soc. Ext. Abstr.*, vol. 84–2, no. 1, pp. 164–165, Jan. 1984, doi: 10.1149/1.2113792/XML.

[4] S. Ma *et al.*, "Temperature effect and thermal impact in lithium-ion batteries: A review," *Prog. Nat. Sci. Mater. Int.*, vol. 28, no. 6, pp. 653–666, Dec. 2018, doi: 10.1016/J.PNSC.2018.11.002.

[5] "(PDF) Review Of Comparative Battery Energy Storage Systems (Bess) For Energy Storage Applications In Tropical Enviroments." https://www.researchgate.net/publication/327966044_Review_Of_Comparative_Battery_Energy_Storage_Systems_Bess_For_Energy_Storage_Applications_In_Tropical_Enviroments (accessed Nov. 12, 2021).

[6] J. Wang, X. Liu, F. Liu, Y. Liu, F. Wang, and N. Yang, "Numerical optimization of the cooling effect of the bionic spider-web channel cold plate on a pouch lithium-ion battery," *Case Stud. Therm. Eng.*, vol. 26, p. 101124, Aug. 2021, doi: 10.1016/J.CSITE.2021.101124.

[7] "Optimization of liquid cooling and heat dissipation system of lithium-ion battery packs of automobile - ScienceDirect." https://www-sciencedirect-com.cit.idm.oclc.org/science/article/pii/S2214157X21001751 (accessed Oct. 06, 2021).

[8] H. Zhang, C. Li, R. Zhang, Y. Lin, and H. Fang, "Thermal analysis of a 6s4p Lithium-ion battery pack cooled by cold plates based on a multi-domain modeling framework," *Appl. Therm. Eng.*, vol. 173, p. 115216, Jun. 2020, doi: 10.1016/J.APPLTHERMALENG.2020.115216.

[9] "How to Perform a Mesh Convergence Study | Search | Autodesk Knowledge Network." https://knowledge.autodesk.com/search-result/caas/sfdcarticles/sfdcarticles/How-to-Perform-a-Mesh-Convergence-Study.html (accessed Apr. 25, 2022).

[10] P. M. Patil, A. P. Yadav, and P. A. Patil, "Comparative Study between Heat Transfer through Laminar Flow and Turbulent Flow," *Int. J. Innov. Res. Sci. Eng. Technol. (An ISO*, vol. 3297, 2007, doi: 10.15680/IJIRSET.2015.0404076.

# A Matheuristic Method for Sustainable Batching and Dyeing Planning in the Textile Industry

Ege Duran, Insight Centre for Data Analytics, University College Cork, Cork, Ireland
Cemalettin Ozturk, Department of Process, Energy and Transport Engineering, Munster Technological University, Cork, Ireland
M. Arslan Ornek, Department of Industrial Engineering, Yasar University, Izmir, Turkey

***Abstract***

Planning of yarn dyeing processes in the textile industry is a challenging engineering problem due to its modelling and computational complexity. Considering operational characteristics of the dyeing process such as weight, production quantity, and volume capacity of Dyeing Machines (DM) and auxiliary constraints like flotte, colour type, and chemical recipe of dye make formulating this planning problem a strenuous optimisation problem. Besides, the utilisation of chemical ingredients, as well as the usage of DMs, has a significant impact on the environmental and economic sustainability of the yarn dyeing process. Hence, there is a need for an intelligent method to batch customer orders so that environmental impact is minimised whilst scheduling them in a minimum number of machines to minimise energy and chemical waste during changeovers. Therefore, minimizing the number of DMs used and maximizing the number of orders processed add a multiobjective dimension and augment the complexity of the problem. Besides, the combinatorial nature of the problem makes it intractable for larger instances; hence, in this paper, we develop a matheuristic method to tackle this problem. Performances of the matheuristic method are compared with the results of an exact method published in the literature.

*Key Words Batching, Dyeing, Mixed Integer Programming, matheuristic, Sustainable Production Planning*

## *1. INTRODUCTION*

Textile is an essential component of both economic and social relations. It is vital for many aspects of life, from the use of clothing to the use of blankets and household items. Textile production consists of 6 main processes: yarn spinning and dyeing (yarn), warp making (unstarched warp), starching (starched warp), weaving (cloth), finishing, and dyeing (finished and dyed fabric), cutting and sewing (garment) [1].

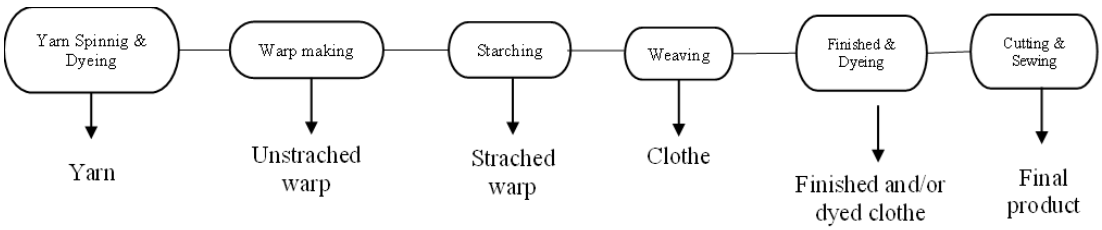


*Figure 1. The manufacturing process(Karacapilidis, N. I., & Pappis, C. P,1996)*

Yarn dyeing comes after the fibre has been spun into yarn. The dyestuff penetrates the strands to the centre of the yarn. Yarn dyeing differs slightly from woven or knit dyeing. Coloured yarns are used to make striped knit or woven textiles, solid dyed yarn fabrics, and sweaters.

This study focuses on scheduling the spinning and dyeing process, the first step of textile production. Yarn is coloured as packages, which are small reels fixed on hollow spindles. Package dyeing is one of the most widely used yarn dyeing procedures. The phrase package dyeing often refers to the dyeing of yarn coiled on perforated cores. With the aid of the tube package's designed perforations, the dye passes through to the yarn package. When the carrier of coloured yarn has reached complete exhaustion, it is withdrawn from the vessel.

Email: Ege Duran
ege.duran@outlook.com

Table 1 below summarizes decisions to be taken related to the problem where set of jobs needs to be assigned to one of the three batches of eligible machines while maximizing the number of jobs processed and minimizing the machines used.

*Table 1. Summary of the problem*

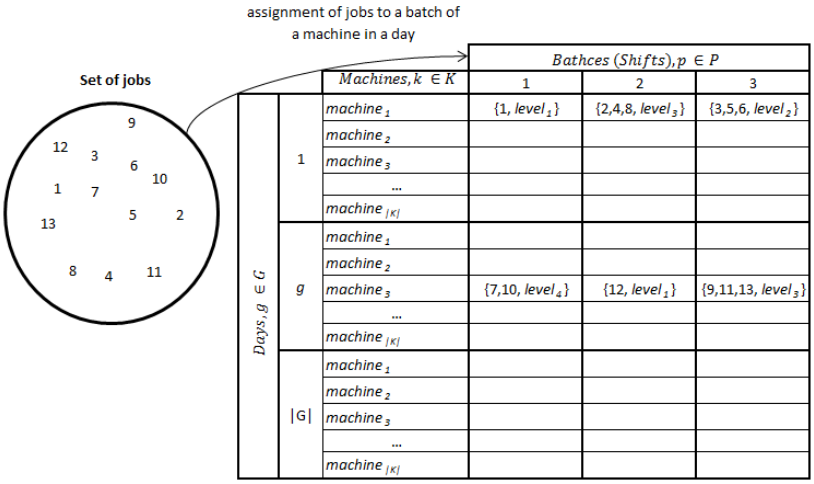


Jobs have different flotte values, recipe codes, and colour percentages. The flotte is calculated by dividing the capacity of the DM by the weight of the assigned jobs. The flottes' of the jobs assigned to a DM must be in the same range. In addition, each DM has more than one level, and the maximum and minimum weight capacities these levels can take are different. Furthermore, the number of spoons used also varies depending on the level of the DM and the weight of the jobs.

## *2. LITERATURE REVİEW*

Scheduling textile production is a tricky problem, as Dyeing Machines (DM) with different capacities and levels also involve planning multiple products and multi-phase manufacturing. Manufacturing management is exceedingly tough due to the mixed character of a textile production system that spans between the job shop and the flow shop. Additional sequence-dependent configurations exist for operations, as well as separate planning horizons and output characteristics for each process. As a result, each phase requires a new production planning algorithm. In recent years, scheduling problems have received widespread attention from practitioners and academics, mainly due to their wide application in the industry and challenging computational complexity (Li, S.,2017). Another reason why scheduling problems attract such attention is finding the most appropriate quantity and timing of production orders according to customer demands and resource capacities, which is the most critical activity for a manufacturing company (Öztürk, C., & Ornek, A. M.,2014). Therefore, much research has been done on multi-stage and complex scheduling. To solve these problems, researchers have suggested a variety of mathematical formulations, heuristic algorithms, and decomposition methods.

The yarn dyeing process is a parallel machine batch scheduling problem. When job families and setup needs exist between these families, Ghosh and Gupta (1997) address the single-machine batch scheduling problem; their goal is to minimise maximum lateness. Sáenz-Alanis et al.(2016) use the GRASP method to solve a parallel machine batch scheduling problem with sequence-dependent setup delays in the brewing industry. Shuguang Li (2017) investigated parallel batching machine scheduling with inclusive processing set constraints and non-identical machine capacities. Zhou et al.(2018) describe an MPSO approach for minimising maximum lateness in the single batch-processing machine problem.

Although a variety of research has been done on this subject, hardly any research has been done on textile production. Due to textile production's multi-stage and complex nature, software systems could not examine all aspects of textile production(1997). Some research on the programming of textile production is as follows:

Rui Zhang et al.(2017) researched a multiobjective ABC algorithm for solving the production scheduling problem in dyeing processes for fabrics. The scheduling strategy for producing yarn-dyed textiles is studied in Hsu et al. (2009). D. Li et al.(2021) investigate a parallel machine scheduling problem with numerous colour families, sequence-dependent setup times, and machine eligibility limits. An integer programming model is created to decrease overall latency.

Researchers have developed many exact and heuristic methods to solve problems with similar computationally expensive problems. The hybridisation of these two methods takes advantage of the exploration advantage of exact algorithms and exploration capability of heuristics and are called matheuristics (2009).

The main contribution of this paper is developing a mixed integer programming based matheuristic method to solve this computationally challenging problem and compare its performance with the ones published in literature from an exact method.

## *3. METHODOLOGY*

This study aims to minimise the number of DMs used to dye the yarns and arrange the order of dyeing the yarns, such as the minimum amount of chemicals used. Hence, the decision is the order of jobs and which jobs to assign to which DM. The first objective function maximizes the number of jobs completed by minimising the jobs assigned to the dummy DM. and the second objective function minimises the number of DMs used.

The MIP formulation is taken from C. Ozturk et al. [11] and is reformulated as a multiobjective model. However, the authors showed that solving this multiobjective model lexicographically is computationally expensive. Therefore, we exploit the problem structure and decompose it into smaller-scale ones, which are solved iteratively. Instead of solving the problem as a whole, we group the jobs that can be assigned together and solve the model for each group. DM availability and attributes (like color, flotte, etc.) are updated after each iteration. Steps of the decomposition method is shown in figure 2.

**Steps of the decomposition method**

Step 1. Group all jobs based on their colour percentages, flotte, Lyc, Reactive, and recipe.
Step 2. Sort groups by colour percentage in ascending order (light to dark).
Step 3. N:number of groups
Step 4. While i≤N
    Step 4.1. Minimise unassigned jobs in group *i* by using the MIP model and store the objective function value $O_1$
    Step 4.2. Minimise number of DMs used for group *i* by using the MIP model where the number of unassigned jobs, U, is less than or equal to $O_1$, $U \leq O_1$
    Step 4.3. Update DM availabilities and attributes
Step 5. End

*Figure 2. Steps of the decomposition method*

The comparison with the optimal solutions is shown in the results section.

## *4. RESULTS*

The heuristic for the initial solution is implemented on Python 3.7 using ASUS ZenBook 13 intel core i7 8$^{th}$ gen 16 GB RAM Computer by using CPLEX 12.8 optimization solver for MIP models. Random instances are generated first based on the number of jobs they have; 15, 40, 60, 80, and 100 jobs, respectively. And each group of jobs is furthermore used for generating 9 instances based on flotte values and colour percentages. In total, 45 instances are generated. Table 2 shows the number of different flotte values and colours for each group.

*Table 2. Number of different flotte and colour percentage for each group*

| # of different flotte | # of different colour |
|---|---|
| 1 | 3 |
| 2 | 3 |
| 3 | 3 |
| 1 | 7 |
| 2 | 7 |
| 3 | 7 |
| 1 | 10 |
| 2 | 10 |
| 3 | 10 |

A comparison of objective function values for MIP and decomposition-based matheuristic in Figure 3 shows the competitive advantages of our method.

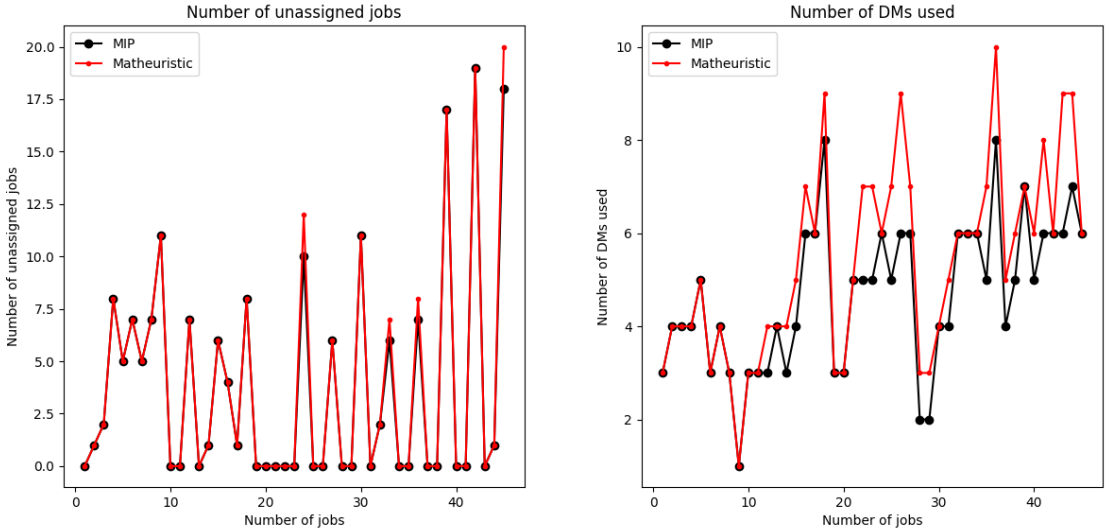


*Figure 3. Comparison of results*

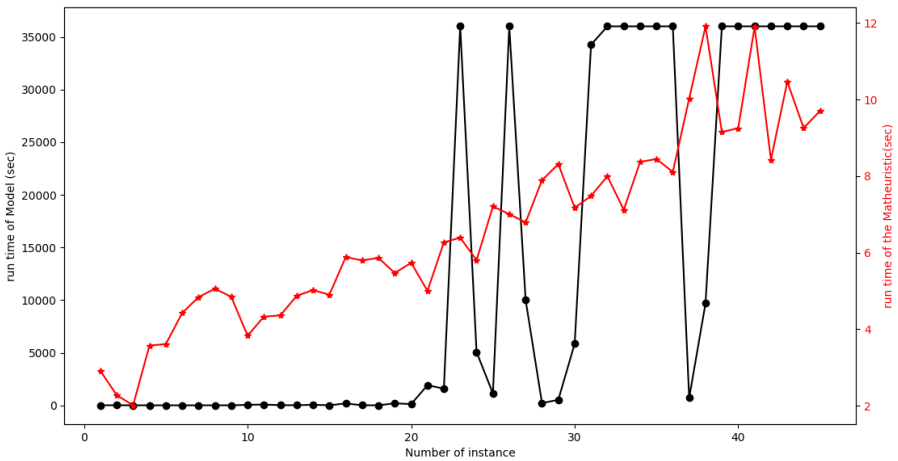


*Figure 4. Comparison of runtime*

The runtime of the matheuristic is shown with the red line and the runtime of MIP with the black line in Figure 3. The runtime performance of the matheuristic indicates a superior performance comparing the MIP model, particularly for larger size instances.

## *5. DISCUSSION*

This paper studies a real-life multi-period parallel machine batching problem in a yarn dyeing company. This study is novel in the sense that there exists no similar research in the literature about multi-period yarn dyeing and parallel batching problem. Small and medium-size examples with a different number of jobs ranging from 15 to 100 were solved with IBM ILOG CPLEX 12.8 software to check the validity of the model formulation. Results have shown that the runtimes of the mathematical models increase exponentially as the sizes and flotte values of the jobs increase. The matheuristic algorithm was solved using Python software. The performance of the proposed heuristic algorithms is evaluated against the optimal results obtained from the MIP models. The computational results show that while the heuristic does not guarantee the optimal result, the runtime of the heuristic is fast. However, this study can be extended in terms of the following perspectives:

- Developing different heuristics for an initial solution such as GA, Ant Colony Optimization(ACO)
- Application of adaptive multiobjective large neighborhood search algorithm [10] with different initial solutions, including the ones obtained by matheuristic in this paper.

## *6. REFERENCES*


Boschetti, M.A., Maniezzo, V., Roffilli, M., Bolufé Röhler, A. (2009). *Matheuristics: Optimization, Simulation and Control*. In: Blesa, M.J., Blum, C., Di Gaspero, L., Roli, A., Sampels, M., Schaerf, A. (eds) Hybrid Metaheuristics. HM 2009. Lecture Notes in Computer Science, vol 5818. Springer, Berlin, Heidelberg. https://doi.org/10.1007/978-3-642-04918-7_13

C. Ozturk, M. A. Ornek (2014). A Mixed Integer Programming Model For Multi-Period Dyeing And Batching Problem In A Yarn Plant. In C. Kubat, G. Çağıl,& Ö. Uygun (Eds.), *CIE44 & IMSS'14 Proceedings* (pp 175-189). Computers&Industrial Engineering https://www.computers-and-ie.org/conferences/44

Ghosh, J. B., & Gupta, J. N. (1997). Batch scheduling to minimize maximum lateness. *Operations Research Letters*, *21*(2), 77-80.

Hsu, H. M., Hsiung, Y., Chen, Y. Z., & Wu, M. C. (2009). A GA methodology for the scheduling of yarn-dyed textile production. *Expert Systems with Applications*, *36*(10), 12095–12103. https://doi.org/10.1016/j.eswa.2009.04.075

Karacapilidis, N. I., & Pappis, C. P. (1996). Production planning and control in textile industry: A case study. *Computers in Industry*, *30*(2), 127–144. https://doi.org/10.1016/0166-3615(96)00038-3

Li, D., Wang, J., Qiang, R., & Chiong, R. (2021). A hybrid differential evolution algorithm for parallel machine scheduling of lace dyeing considering colour families, sequence-dependent setup and machine eligibility. *International Journal of Production Research*, *59*(9), 2722–2738. https://doi.org/10.1080/00207543.2020.1740341

Li, S. (2017). Parallel batch scheduling with inclusive processing set restrictions and non-identical capacities to minimize makespan. *European Journal of Operational*

Öztürk, C., & Ornek, A. M. (2014). Operational extended model formulations for Advanced Planning and Scheduling systems. *Applied Mathematical Modelling*, *38*(1), 181–195. https://doi.org/10.1016/j.apm.2013.05.049

Sáenz-Alanís, C. A., Jobish, V. D., Salazar-Aguilar, M. A., & Boyer, V. (2016). A parallel machine batch scheduling problem in a brewing company. *International Journal of Advanced Manufacturing Technology*, *87*(1–4), 65–75. https://doi.org/10.1007/s00170-016-8477-8

Shaw, P. (1998, October). Using constraint programming and local search methods to solve vehicle routing problems. In *International conference on principles and practice of constraint programming* (pp. 417-431). Springer, Berlin, Heidelberg.

Zhang, H., Zhu, Y. and Ku, T., 2017, July. Multiobjective Job Shop Scheduling using a Modified Artificial Bee Colony Algorithm. In 2017 IEEE 7th Annual International Conference on CYBER Technology in Automation, Control, and Intelligent Systems (CYBER) (pp. 701-706). IEEE.

Zhou, H., Pang, J., Chen, P.K. and Chou, F.D., (2018). A modified particle swarm optimization algorithm for a batch-processing machine scheduling problem with arbitrary release times and non-identical job sizes. Computers & Industrial Engineering, 123, pp.67-81.

# Creating an Industry 4.0 Maturity Model for Wind Farm Asset Management

Heather Spain, University College Dublin
Eamonn Ahearne, University College Dublin

***Abstract***

Through an original review of the state-of-the-art, it was found that the concepts and technologies of Industry 4.0 potentially enable wind energy operations and maintenance companies to optimise asset performance, resulting in improved company revenues and more clean energy for society. However, since the application of Industry 4.0 to wind energy lags other sectors such as advanced manufacturing, the fundamental question of how to further adopt Industry 4.0 into wind farms is outstanding. Industry 4.0 maturity models can answer this question by assessing the current Industry 4.0 capability of the wind energy company, identifying high-potential technologies, and providing a roadmap for Industry 4.0 maturity. However, an extended literature review showed that no current Industry 4.0 maturity model is suitable for this sector. Hence, a multi-methodological approach was taken to create the WEAM Industry 4.0 Maturity Model. The model was built according to guidelines and the International Standard for the construction and verification of maturity models. It was deployed to industry after pilot testing and provided an overview of the current level of adoption while also enabling benchmarking of companies against a common standard. It was found that the average level of maturity in the sector was at level 3, where level 5 is defined as the highest level of maturity in Industry 4.0 technologies. The I4 technology where most respondents were found to be underdeveloped was in "Big Data and Advanced Algorithms". It is concluded that Wind Energy Asset Management (WEAM) Industry 4.0 Maturity Model can be usefully applied to support wind energy companies in Industry 4.0 adoption in a standardised, objective, and repeatable way.

*Key Words: Asset Management, Wind Energy, Industry 4.0, Maturity Model*

## 1. INTRODUCTION

A profound digital transformation is underway in the form of the fourth Industrial Revolution. This transformation promises higher productivity, reduced waste, more agile and flexible systems. These developments are collectively referred to under the term 'Industry 4.0'. It is estimated that global wind energy production could increase by 3 percent per annum with the resolution of wind energy performance issues, component faults and suboptimal operation, equivalent to $2bn of green energy every year (DNV, 2020). The Industry 4.0 technologies outlined in this paper can further these objectives by enabling operations and maintenance (O&M) teams to optimise their wind assets and increase global wind energy production.

For wind energy companies to realise the benefits of Industry 4.0, they must first assess their present level of Industry 4.0 adoption. Maturity models, which first appeared in the 1970s (Rafael et al., 2020) can be used to perform this assessment. They enable organisations to assess their current capabilities with reference to objective standards and to compare these capabilities with other companies in the industry thus identifying a roadmap for improvement. Industry 4.0 maturity models are therefore an essential tool for wind energy companies to realise the many benefits that Industry 4.0 offers such as reduced costs, increased safety and improved revenues.

## 2. LITERATURE REVIEW

An original state-of-the-art literature review of Industry 4.0 technologies for optimising wind farm O&M was undertaken. Table 1 summarises the reported technologies and ascribed benefits. Additionally, decision support tools utilise the Industry 4.0 concepts of big data and algorithms to enable O&M teams to make accurate and quick decisions and to increase the likelihood of making the decision that will minimise cost and maximise wind farm availability (Li et al., 2016). Practices such as advanced cybersecurity prevention, G-IoT, and green cloud computing are essential for wind energy companies to ensure a sustainable Industry 4.0 technological adoption (Adekanbi, 2021). Employee training and collaboration with external partners also ensure a smooth adoption of the above-mentioned Industry 4.0 technologies (Fettig et al., 2018; Smith, 2021).

Email: Heather Spain
hspainirl@gmail.com

*Table 1. Summary of Industry 4.0 technologies for wind energy O&M*

| Technology | Description |
|---|---|
| RFID | Technicians can easily and accurately identify parts which are not easily accessible or which would have otherwise required disassembly to access, reducing the time the turbine is down due to maintenance (Ferdous et al., 2016). |
| Sensors | Data captured from sensors help wind farm asset managers make maintenance decisions, monitor the health of the wind turbine, and enable maintenance strategies such as predictive and prescriptive maintenance which can reduce downtime. Additionally, sensors can be used by the turbine to perform independent tasks such as de-icing or turning the rotor away from the wind to minimise wake losses (Karad & Thakur, 2021; Nemitz, 2014; Fairley, 2019). |
| Digital Twin | Monitoring the wind turbine and its components over its entire life cycle and diagnosing faults virtually. Increased safety and reduced costs result from the use of digital twin (Pal, 2020). |
| Virtual Reality | Virtual training significantly reduces costs, increases training performance, and reduces the barrier to entry for aspiring wind turbine technicians (Wu, 2021). |
| Augmented Reality | Overlaying information using an AR headset reduces the time taken to complete a maintenance task, increasing wind turbine availability (Abraham & Annunziata, 2017). |
| Artificial Intelligence and Robots | Blade inspections can be performed more quickly and safely (Equinox, 2020). |

The fundamental question of how wind energy companies can adopt the above outlined Industry 4.0 technologies to realise the benefits presented in the state-of-the-art review is outstanding. Industry 4.0 maturity models help companies with this by assessing their relevant progression, providing them with a starting point for the effective realisation of Industry 4.0, and can be used to benchmark the Industry 4.0 maturity of an industry (Schumacher et al., 2016). A review of the most popular and well-regarded Industry 4.0 maturity models showed that there is a trend in recent Industry 4.0 maturity models to include both technological dimensions and organisational dimensions, as it is recognised that certain organisational influences can affect Industry 4.0 adoption (Schuh et al., 2020). It also showed that the majority of Industry 4.0 maturity models focus on specific industries such as manufacturing or IT and those models cannot be used by many industries due to overgeneralisation. Hence, it was concluded from this literature review that while Industry 4.0 technologies have many benefits for the wind energy industry, there is no suitable tool for wind energy companies to progress on a journey to realise these benefits.

## 3. METHODOLOGY

A multi-methodological approach to designing the maturity model was followed. This approach is based on international standards and guidelines and was inspired by the methodology presented by authors of existing Industry 4.0 maturity models such as Wagire et al. (2020) and Rafael et al. (2020). This approach to designing the maturity model follows the eight requirements outlined by Becker et al. (2009). Similar methodologies and approaches have been utilised in earlier studies (Schumacher et al., 2016; Caiado et al., 2020) for the development of maturity models.

### *3.1 Structure of the WEAM Industry 4.0 Maturity Model*

The name given to the proposed model is “Wind Energy Asset Management (WEAM) Industry 4.0 Maturity Model”, inspired by the well regarded SIMMI 4.0 model.

In accordance with the guidelines outlined by Becker et al. (2009), the WEAM Industry 4.0 Maturity Model was developed iteratively and was formed according to the ISO standard ISO-IEC 3304 which provides requirements for the construction of maturity models. It also follows the structure of highly cited models which have, in general, six principal elements; dimensions, maturity items, maturity levels, requirements for each dimension to reach a certain maturity level, assessment tools, and a method of quantifying maturity.

Five dimensions (specific capability areas structuring the field of interest) were chosen after the literature review comprising Industry 4.0 technologies which have the greatest potential to help wind energy O&M teams reduce maintenance costs, optimize overall performance and thus increase revenues and profits. These five dimensions are outlined in Table 2 along with their items. The Cybersecurity and Organisation dimension were deemed critical areas for Industry 4.0 implementation as they ensure the sustainable implementation of the Industry 4.0 technologies outlined by the Control Systems, Big Data and Advanced Algorithms, and Novel Technologies dimensions.

Eleven maturity items were chosen as the specific technologies within these dimensions which are important to the Industry 4.0 maturity of wind energy companies. It should be noted that every dimension was given two items, but Big Data and Advanced Algorithms was given three items since it forms the basis of many Industry 4.0 technologies.

*Table 2. Dimensions and their items*

| Dimension | Items |
|---|---|
| Control Systems | Perceived importance of computer-based monitoring systems to O&M, tasks completed by computer-based monitoring systems |
| Big Data and Advanced Algorithms | Method of component identification, Digital Twin, decision-support systems |
| Novel Technologies | Utilisation of novel technologies, e.g., AR, Automation of routine maintenance tasks |
| Cybersecurity | Implementation of cybersecurity measures, Aspiration to achieve a certain level of cybersecurity |
| Organisation | Employee training, collaboration with external partners such as academia, industry, suppliers, clients or customers |

The ISO-IEC 3304 standard requires that maturity models specify a continuous set of maturity levels representing increasing levels of organisational process maturity, starting at the basic maturity level. Hence, five maturity levels which represent increasing Industry 4.0 maturity were chosen to identify the Industry 4.0 maturity level of a company. According to the ISO standard ISO-IEC 3304, maturity levels shall be characterised by the demonstration of achievement of a set of process profiles. Specific requirements to achieve each maturity level were hence formed for all five dimensions.

A questionnaire was chosen as the most suitable assessment tool to gain information on the organisation in order to assess Industry 4.0 maturity. This was chosen because the most highly cited, well founded, and best regarded maturity models reviewed used a questionnaire as their assessment tool. Additionally, there is a wealth of research on how to optimise questionnaire design to obtain objective, impartial, consistent, repeatable, and comparable results in accordance with the ISO standard ISO-IEC 3304. A questionnaire was developed according to the recommendations outlined by the Krosnick and Presser (2009). The questionnaire consists of eleven closed-ended questions, or one question per item.

For each completed questionnaire, the Industry 4.0 maturity level was calculated. Scores were assigned on a Likert scale for each item-level question, and these scores were aggregated to provide both an overall company score and an overall dimension score. The scores were translated into maturity levels using Table 3. For each dimension, the minimum and maximum scores were determined and then divided to make five equal maturity levels. Note that since the Big Data and Advanced Algorithms dimension has one item more than the rest of the dimensions, it has a different maximum score and thus a different numerical translation from score to maturity level.

*Table 3. Conversion from score to maturity level*

| Level | Big Data and Advanced Algorithms score | All other dimensions score | Overall score |
|---|---|---|---|
| 1 | 0-3 | 0-2 | 0-11 |
| 2 | 4-6 | 3-4 | 12-22 |
| 3 | 7-9 | 5-6 | 23-33 |
| 4 | 10-12 | 7-8 | 34-44 |
| 5 | 13-15 | 9-10 | 45-55 |

### *3.2 Model Testing and Deployment*

As part of the fourth and fifth steps of the multi-methodological approach to building the WEAM Industry 4.0 Maturity Model, and in accordance with the recommendations made by Krosnick and Presser (2009), the questionnaire was subject to pilot testing and subsequently deployed to industry.

Pilot testing was completed by asking the Operations Team Leader of Company A to fill out the questionnaire, taking note of the time it took to complete, and recording any improvements or positive aspects of the questionnaire. Additionally, after the questionnaire was completed, the Operations Team Leader of Company A was asked if they understood each question and if they used the definitions outlined prior to the relevant questions. The feedback received was positive. They noted that the questionnaire was clear and easy to both understand and answer, that they understood the model structure and purpose, that the definitions of technologies were distinct and clear, and that the questionnaire took just over eleven minutes to complete. This feedback validates that the questionnaire follows the recommendations for questionnaire design made by Krosnick and Presser (2009).

Additionally, the questionnaire was pretested on a person who has no wind energy asset management industry experience but has industry experience in market research and hence is familiar with good questionnaire design. The benefits of testing the questionnaire in such a way was that this person was able to focus on the structure and length of the questionnaire, the question order, the ease of use of the questionnaire, and other factors which would affect the response rate of the questionnaire, instead of the content of the questions. Their feedback was implemented before deploying the WEAM Industry 4.0 Maturity Model to wider industry.

After pilot testing, the WEAM Industry 4.0 Maturity Model was deployed to industry. The questionnaire was sent to the wind energy operations and maintenance teams of thirteen wind energy companies via email. Five responses were received, including from some of Ireland and Europe's leading renewable energy companies, giving a survey response rate of 38.5%. Baruch and Holtom (2008) found that the average response rate for studies that utilised data collected from organisations was 35.7%. Hence, it can be concluded that the response rate of the proposed questionnaire is above average.

## 4. RESULTS

The questionnaire was completed by operations team leaders, managing directors, wind performance analysts, and operations engineers. It can be seen from this list that the respondents are experienced in wind farm O&M. A combination of the high level of O&M knowledge of the employees and the given explanations of Industry 4.0 concepts and technologies mean that respondents have adequate understanding of the implications of Industry 4.0 technologies for their assets, and thus accurate results can be expected from the model. Table 4 shows the scores and maturity levels of each respondent company, in order of descending maturity.

*Table 4. Maturity Levels of five respondents, in descending order*

| | Score | Maturity Level | Company |
|---|---|---|---|
| 1st | 39 | 4 | Company B |
| 2nd | 37 | 4 | Company D |
| 3rd | 32 | 3 | Company C |
| 4th | 32 | 3 | Company E |
| 5th | 29 | 3 | Company A |

Since the WEAM Industry 4.0 Maturity Model is the only suitable method of assessing Industry 4.0 maturity for wind energy O&M teams, the WEAM Industry 4.0 Maturity Model results of Company B represent a benchmark of Industry 4.0 maturity for wind energy O&M teams. Their Industry 4.0 maturity level is a standard by which all other companies can be measured since this is the highest Industry 4.0 maturity of any company ever measured.

From Table 4 we see that the average maturity level of the five companies is Level 3. Table 4 also shows that no company reached the highest level of maturity, Level 5, which indicates that every company in the wind energy industry has areas to improve upon for their Industry 4.0 adoption.

### *4.1 Demonstration of Model Use*

An example of the results presented to Company B follows. These results demonstrate how each company can use the model to their advantage. It can be seen from Table 4 that the Industry 4.0 adoption of Company B is at Level 4, which represents an advanced implementation of Industry 4.0 with a clear increase in availability and decrease in operating costs.

A radar chart is used to summarise their overall result. It is evident that the Big Data and Advanced Algorithms dimension is one to be improved upon the most, and the Control Systems and Cybersecurity dimensions are at the highest level of Industry 4.0 maturity for Company B.

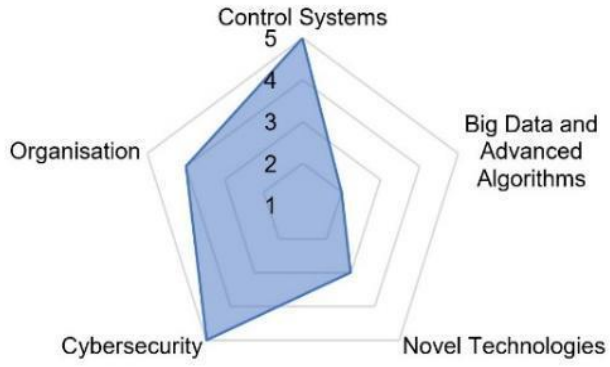


*Figure 1. Radar Chart showing the maturity level results for each dimension of Company B*

Table 5 shows a breakdown of the scores obtained for each question response and the actions needed to get to the next level of Industry 4.0 maturity for each item. These suggestions were made according to the requirements to reach a certain maturity level for each dimension. This table demonstrates how the WEAM Industry 4.0 Maturity Model can be successfully used to identify areas of improvement in Industry 4.0 adoption so that these companies can decide which suggested actions to take to realise the competitive advantages of Industry 4.0 and optimise the performance of their assets.

*Table 5. Suggested actions for Company B to take in order to reach a higher level of Industry 4.0 maturity*

| Dimension | Q# | Score | Suggested step to achieve the next level of Industry 4.0 maturity |
|---|---|---|---|
| Control Systems | Q1 | 5 | None. |
| | Q2 | 5 | None. |
| Big Data & Advanced Algorithms | Q3 | 1 | Upgrade from serial numbers to a more sophisticated method of wind turbine component identification |
| | Q4 | 2 | Capitalise on investigation into digital twins by putting resources into the development of a digital twin |
| | Q5 | 3 | Investigate the implementation of a decision support systems separate from computer-based monitoring systems |
| Novel Technologies | Q6 | 2 | Investigate the adoption of AR, VR, and/or autonomous robots |
| | Q7 | 4 | Automate remaining possible routine maintenance tasks |

| | | | |
|---|---|---|---|
| Cybersecurity | Q8 | 4 | Implement a mechanism that ensures security practices are proactively optimized |
| | Q9 | 5 | None |
| Organisation | Q10 | 4 | Become actively involved in one or more collaboration projects with external partners |
| | Q11 | 4 | Increase the frequency of employee training to once a month or more |

## 5. DISCUSSION

Five O&M employees completed the WEAM Industry 4.0 Maturity Model for Company A. This was done to perform a statistical analysis to evaluate the quality of the design of the model. A 95% confidence interval was calculated for the results of Company A. The analysis shows that that the confidence interval is smaller for the Control Systems, Big Data and Advanced Algorithms, and Novel Technologies dimensions but considerably wider for the Cybersecurity and Organisation dimensions. This validates the high-quality design of the questions in the Control Systems, Big Data and Advanced Algorithms, and Novel Technologies dimensions but shows that the question design in the Cybersecurity and Organisation dimension can be improved upon. This analysis also shows how as more employees complete the survey in each company, the confidence interval is reduced and thus the model becomes more accurate.

The WEAM Industry 4.0 Maturity Model is the only existing assessment of the Industry 4.0 maturity of wind energy O&M teams, and so the results of the deployment of this model to industry represent the Industry 4.0 maturity of the entire industry. These results show that the average Industry 4.0 maturity level is at Level 3 implying partial implementation with clear return on investment of new Industry 4.0 technologies being observed. Considering that the implementation of Industry 4.0 to wind energy is in its initial stages, this level of Industry 4.0 maturity shows the enthusiasm that wind energy O&M teams have for Industry 4.0. This further shows how the development of a standardised, repeatable tool for wind energy O&M teams to be able to prioritise I4 technologies is long overdue.

The Big Data and Advanced Algorithms dimension has the lowest maturity level across industry. This may be due to a lack of awareness of the benefits that these technologies bring to their wind farms including adaptive real-time analytics, proactive and predictive maintenance and self-optimisation of systems. Therefore, it can be suggested that wind energy companies perform a cost-benefit analysis of these Industry 4.0 technologies based on these potential benefits.

The WEAM Industry 4.0 Maturity Model can also be used to track a company's progress in their adoption of Industry 4.0 technologies. Companies can revisit the model as they implement the suggested actions and track their progress in achieving their corporate vision for Industry 4.0 maturity across their wind farm.

## 6. CONCLUSION

A review of Industry 4.0 technologies for wind farms identified high potential technologies to help O&M teams optimise overall plant performance. To manage Industry 4.0 adoption in wind farms, it is recognised that companies should analyse their current capabilities, identify gaps and systematically develop a roadmap towards Industry 4.0 maturity. A review of Industry 4.0 maturity models has shown that they are an effective tool to help companies in this process. However, this review also showed that no Industry 4.0 maturity models have been developed specifically for wind energy companies. Accordingly, a robust Industry 4.0 maturity model, named the Wind Energy Asset Management (WEAM) Industry 4.0 Maturity Model, was built based on best practice according to Becker et al. (2009), and with reference to the International Standard for the Construction and Verification of Maturity Models, ISO-IEC 3304. The proposed model consists of five dimensions, eleven items, and five maturity levels. Clear requirements for each maturity level are outlined.

The results of the deployment of the model to industry were reported and shown to identify high potential Industry 4.0 technologies for adoption. The results also enable as assessment of the level of adoption in the sector and

inter-company benchmarking. The further adoption of Industry 4.0 technologies is in the interest of both companies in the sector and in the interest of government striving to increase clean energy generation to meet clean energy targets. Since the WEAM Industry 4.0 Maturity Model is a useful tool and a systematic approach to realising both industry and government objectives, wind energy companies should be encouraged to apply this tool and develop a technology roadmap to holistically exploit the potential benefits of Industry 4.0 technologies.

Further work includes investigating the development of strategies which help wind energy companies implement the suggested actions given by the WEAM Industry 4.0 Maturity Model, encouraging as many people in the operations and maintenance team within each company to participate in the questionnaire in order to increase accuracy of the assessment tool, and gaining detailed feedback on the model by interviewing participants at different stages in their use of this model to improve their Industry 4.0 adoption.

## 7. REFERENCES


Adekanbi, M. L. (2021). Optimization and digitization of wind farms using internet of things : A review. *International Journal of Energy Research*, *45*(11), 15832–15838. https://doi.org/10.1002/er.6942

Abraham, M., & Annunziata, M. (2017). Augmented Reality Is Already Improving Worker Performance. Retrieved from https://hbr.org/2017/03/augmented-reality-is-already-improving-worker-performance

Baruch, Y., & Holtom, B. (2008). Survey response rate levels and trends in organizational research. *Human Relations*, *61*(8), 1139-1160. doi: 10.1177/0018726708094863

Becker, J., Knackstedt, R., & Pöppelbuß, J. (2009). Developing Maturity Models for IT Management. *Business &Amp; Information Systems Engineering*, *1*(3), 213-222. doi: 10.1007/s12599-009-0044-5

Caiado, R., Scavarda, L., Gavião, L., Ivson, P., Nascimento, D., & Garza-Reyes, J. (2021). A fuzzy rule-based industry 4.0 maturity model for operations and supply chain management. *International Journal Of Production Economics*, *231*, 107883. doi: 10.1016/j.ijpe.2020.107883

DNV. (2020). WindGEMINI - DNV. Retrieved 20 June 2022, from https://www.dnv.com/power-renewables/services/data-analytics/windgemini/

Equinox. (2020). Drones for Wind Turbine Blade Inspection |Equinox's Drones. Retrieved from https://www.equinoxsdrones.com/renewable-energy-wind

Fairley. (2019). Algorithms Help Turbines Share the Wind. Retrieved from https://spectrum.ieee.org/teaching-wind-turbines-wake-steering

Ferdous, R., Reza, A., & Siddiqui, M. (2016). Renewable energy harvesting for wireless sensors using passive RFID tag technology: A review. *Renewable And Sustainable Energy Reviews*, *58*, 1114-1128. doi: 10.1016/j.rser.2015.12.332

Fettig, K., Gacic, T., Koskal, A., Kuhn, A., & Stuber, F. (2018). Impact of industry 4.0 on organizational structures. *2018 IEEE International Conference on Engineering, Technology and Innovation (ICE/ITMC)*. https://doi.org/10.1109/ice.2018.8436284

International Organization for Standardization, International Electrotechnical Commission. (2015). *Requirements For Process Reference, Process Assessment And Maturity Models* (ISO/IEC 33004:2015)

Krosnick, J., & Presser, S. (2009). Question and Questionnaire Design. *Handbook of Survey Research, 2nd edition.*

Karad, S., & Thakur, R. (2021). Efficient monitoring and control of wind energy conversion systems using Internet of things (IoT): a comprehensive review. *Environment, Development And Sustainability*, *23*(10), 14197-14214. doi: 10.1007/s10668-021-01267-6

Li, X., Ouelhadj, D., Song, X., Jones, D., Wall, G., & Howell, K. et al. (2016). A decision support system for strategic maintenance planning in offshore wind farms. *Renewable Energy*, *99*, 784-799. doi: 10.1016/j.renene.2016.07.037

Nemitz. (2014). Smart anti-icing system for rotor blades. Retrieved from https://www.fraunhofer.de/en/press/research-news/2014/december/smart-anti-icing-system-for-rotor-blades.html?_cldee=ZWxpemFiZXRoLmJ1dHRuZXJAcG8uc3RhdGUuY3QudXM%3D&urlid=7

Pal, S. (2020). How digital twins could transform the wind energy industry. Retrieved from https://www.windpowerengineering.com/how-digital-twins-could-transform-the-wind-energy-industry/

Rafael, L., Jaione, G., Cristina, L., & Ibon, S. (2020). An Industry 4.0 maturity model for machine tool companies. *Technological Forecasting And Social Change*, *159*. doi: 10.1016/j.techfore.2020.120203

Schuh, G., Anderl, R., Dumitrescu, R., Krüger, A., Hompel, M., & Studie, acatech. (1970, January 1). *[PDF] Industrie 4.0 Maturity Index. managing the digital transformation of companies – update 2020 – (Acatech Study): Semantic scholar*. [PDF] Industrie 4.0 Maturity Index. Managing the Digital Transformation of Companies – UPDATE 2020 – (acatech STUDY) | Semantic Scholar. Retrieved June 28, 2022, from https://www.semanticscholar.org/paper/Industrie-4.0-Maturity-Index.-Managing-the-Digital-Schuh-Anderl/51f83380d584d5da2d6193a7e920c12e9b16782b

Schumacher, A., Erol, S., & Sihn, W. (2016). A Maturity Model for Assessing Industry 4.0 Readiness and Maturity of Manufacturing Enterprises. *Procedia CIRP*, *52*, 161-166. doi: 10.1016/j.procir.2016.07.040

Smith. (2021). Collaboration is key to addressing digital skills gap. Retrieved from https://luminate.prospects.ac.uk/collaboration-is-key-to-addressing-digital-skills-gap

Wagire, A., Joshi, R., Rathore, A., & Jain, R. (2020). Development of maturity model for assessing the implementation of Industry 4.0: learning from theory and practice. *Production Planning &Amp; Control*, *32*(8), 603-622. doi: 10.1080/09537287.2020.1744763

Wu, E. (2021). Virtual Reality is Bringing Wind Turbines to a Classroom Near You. Retrieved from https://www.masscec.com/blog/2021/04/02/virtual-reality-bringing-wind-turbines-classroom-near-you

# Chapter 3: Additive Manufacturing

# Additive manufacturing of titanium alloys for biomedical applications - Review and Trend

Surinder Pal, Atlantic Technological University (ATU), Sligo, Ireland
Waqas Saleem, Atlantic Technological University (ATU), Sligo, Ireland
Xavier Velay, Atlantic Technological University (ATU), Sligo, Ireland

***Abstract***

Titanium alloys have gained growing attention for their diverse applications in the biomedical sector due to their excellent properties. This article presents a concise review and an analysis of the contemporary trends focusing on the additive manufacturing (AM) of Ti-6Al-4V. Currently, numerous AM techniques are used to manufacture biomedical devices and implants. Additive Manufacturing has replaced traditional machining processes, such as turning, drilling, and milling. These processes make it hard to machine the Ti alloys due to their high hardness and low thermal conductivity. AM technologies have successfully overwhelmed the issues associated with the conventional machining operations of Ti alloys. This review addresses published articles from the last ten years and discusses the important developments of AM technologies for biomedical applications, especially the Ti-6Al-4V. Furthermore, the gaps in the current research and an evaluation of the future scope of AM for biomedical applications are presented.

***Key Words:*** *Titanium, Additive Manufacturing, Medical, Machining.*

## 1. INTRODUCTION

According to recent statistics, over 90% of patients above the age of 40 undergo joint disease [1]. Consequently, artificial implants and advanced arthritis are fabricated from biomedical materials to improve the patient's life [1]. The biomedical implants are designed and fabricated with the changing requirements of body parts. Therefore, titanium and Co-based alloys are widely used due to their excellent corrosion and wear resistance characteristics in the human body [2-3]. Furthermore, extensive research has been conducted on Ti alloys to evaluate their mechanical strength, biocompatibility, and lightweight properties [4-7]. Traditionally, titanium alloys are made through foaming and casting technology, which requires various intermediate stages and consumes higher energy resources [8-9]. During the last decade, the growth of AM technology has matured enough and applied for the improvement of biomedical implants [10–14]. Two representatives AM techniques are most common for biomedical applications, the electron beam and selective laser melting process [2, 11]. Thus, this review focuses on these AM technologies, especially using Ti-6Al-4V.

### *1.1. Development of AM Biomedical Ti Alloys*

For biomedical implants, Ti alloys are developed with the highest precision. Initially, the commercially pure titanium (CP Ti) was planned to substitute for the 316L SS (stainless steel), and Cobalt-chrome or cobalt-chromium (Co Cr) showed better corrosion resistance and biocompatibility [15-17]. Later, Co-Cr stainless steel alloys were considered that include various toxic elements, such as Co, Ni, and Cr. Despite this fact, Ti alloy satisfies the requirement of biomaterial application. The main application of Ti alloy is to restore the lost structure and replace the damaged and worn joints [18]. However, not all Ti alloys are biocompatible. The Ti-6Al-4V is widely used in biomedical industries due to its fracture toughness, high strength, and corrosion resistance [19-20]. However, Ti alloy is challenging due to its high reactivity, low thermal conductivity, and poor machinability [21]. For these reasons, it is necessary to use AM technologies which further reduce the fabrication cost and broaden the usage of this alloy.

#### *1.1.1 EBM Process*

Electron beam melting (EBM) is a promising metal additive manufacturing technology for producing metal parts directly from powder in layers, each layer carrying a thickness of approximately 100 µm [22]. It is performed in a vacuum atmosphere and can create dense parts precisely from a CAD model. The EBM is an appealing technology for manufacturing titanium alloy components with complex geometry [23]. The microstructure of components produced by the EBM techniques is ultrafine by micro-zone melting and crystallising of shapeless powder [24-25]. The vacuum device and electron beam are regulated by an electromagnetic lens [26]. A preheating process ensures reducing the effect of residual stress. The model developed in CAD is divided into thin layers, and then the bed powder is scanned by the EBM systems to create a complete part [27-28]. Several

Surinder Pal
Email: surinder.pal@mail.itsligo.ie

studies have revealed the control of EBM Process parameters for Ti alloys [29-31]. The outcomes showed that the mechanical properties of the EBM manufactured components can be enhanced by varying the processing parameters, building temperature, and scanning strategy. The factors that consistently affect the microstructure morphology and solidification processes include the melt pool size, thermal distribution, cooling rate, maximum temperatures, and thermal gyrations. The energy input density (E) for Ti alloy during the EBM process is [32].

$$E = \frac{P}{v.t.s} \qquad (1)$$

Where v is scan speed (in mm $s^{-1}$), P is electron beam (in W), s is scan spacing (in mm), and t is layer thickness (in mm). Equation 1 shows that the higher the E (energy input density), the more powder is melted at the bed which results in better product density. Multiple studies have investigated different parameters and scanning patterns that significantly influence the building process of the EBM part. However, EBM technology has become easy to use in the last few years. Lindhe and Harrysson (2003) stated some preliminary testing of the EBM process for several alloys. Their study focused on tensile strength, yield strength, modulus of elasticity, and elongation for Ti–6Al–4V. [33] Many studies have been reported on the EBM fabrication method, and a few of these are discussed in Table 1. Fig 1 (a) shows the numbers of an article published from 2010 to 2021 years.

*Table 1. Summary of Previous studies performed on Ti alloy by EBM Process*

| Author | Remarks |
|---|---|
| Parthasarathy et al., (2010) | This paper examined the mechanical evaluation of porous Ti6Al4V structures manufactured by the EBM process. It was found that the grain density is equal to the dense Ti6Al4V. It was also shown that the manufactured design meets the required mechanical strength necessary for craniofacial applications [34]. |
| Marin et al. (2010) | This study investigated the mechanical properties of the Trabecular Titanium (TT) to improve the biological fixation of the prosthetic implants that can accept the success of improved clinical outcomes. Also, the elastic modulus of TT has been proven to be close to the human spongy bone. As a result, it has been revealed that the EBM can be used effectively to get cellular solids in metallic biomaterials that can provide good mechanical properties [35]. |
| Koike et al. (2011) | This analysis compared and studied the grind ability, corrosion resistance, and mechanical properties of Ti–6Al–4V manufactured by the EBM method and cast/wrought samples. It was found that the grindability of the used model was significantly better than of cast or wrought samples. Also, the EBM manufactured samples were investigated having rippled rough surfaces [36]. |
| Weiwei et al. (2011) | The preheating of Ti powder particles in the EBM method was investigated. The results show the formation of powder aggregation at the preheating above 600 °C. Moreover, it was observed that the tiny particles were partly or entirely melted in cubic aggregation. These metal drops function as a binder to bond the bulk of large particles together and create the powder block, which further helps the particles to withstand the impact of electron beam force [37]. |
| Fukuda et al. (2012) | The effects of the electron beam of the EBM manufactured part (Ti–6Al–4V) at a different energy density were examined. The results revealed that the grain size and porosity could be manipulated by energy density varying on the electron current beam. Besides, the EBM-manufactured Ti alloy showed anisotropy in its deformation behaviour due to the cast defects' arrangement [38]. |
| Safdar et al. (2012) | This article studied the influence of sample thickness on the surface roughness of the EBM-manufactured Ti-6Al-4V metallic component. It was found that the surface roughness (Ra) rises with increasing beam current and sample thickness and reduces with a rise in scan speed and offset focus. The process was investigated for |

| | |
|---|---|
| | 1-20 μm for various samples, differing in the thickness and process parameter (such as beam current, probe size on powder, scan speed, etc.) [39]. |
| Hrabe et al. (2013) | The results exhibit a small effect of sample size on YS (2% change) and UTS (1% change). However, no significant impact of distance and sample size were found on mechanical properties and microstructure [40]. |
| Chan et al. (2013) | Chan et al. studied the fatigue life of Ti-6Al-4V alloys fabricated by the EBM and LBM (laser beam melting) under stress-controlled environments at 10 Hz (until fracture). The outcomes reveal that the LBM material shows a longer fatigue life than the EBM part [41]. |
| Springer et al. (2014) | Springer et al. evaluated the biocompatibility of EBM fabricated Ti6Al4V. As a result, it was figured out that EBM fabricated implant surfaces ($r_a$<0.5 μm) are acceptable with the contact of dermal fibroblasts, and the production was also enhanced [42]. |
| Liu et al. (2014) | This study's primary purpose is to find whether the EBM locking compression plate (LCB) printed Ti-6Al-4V implants suit clinical implants. The results show substantial advantages of EMB printed implants, such as bending strength (190.7% more), bending stiffness (87.67%), hardness (341.1 HV10 ± 1.93 and 27.9% greater), and bending structural stiffness (73.2% greater) and surface roughness of 0.49 ± 0.02 μm [43]. |
| Chan (2015) | The reported investigation focused on surface topography's effect on the fatigue life of EBM-processed Ti– 6Al–4V plates. The fatigue life of the EBM-produced part is controlled by the fatigue crack growth of big cracks. It was found that the EDM fabricated parts decrease fatigue life performance. Thus, the surface roughness is further improved by tumbling or polishing [44]. |
| Kok et al. (2015) | The EBM-built impeller of Ti-6Al-4V was studied with changing thickness. The results stated the common issues of near-spherical pores metallisation, and smoke during the EBM fabrication. Moreover, the microstructure turns finer with lowering build thickness [45]. |
| Sato et al. (2016) | In this study, the Ti-6Al-4V powder specimen was fabricated by EBM. It was found that the fatigue strength can be increased by 21% by shot peening or cavitation peening [46]. |
| Galarraga et al. (2016) | The influence of the porosity and microstructure on properties of Ti-6Al-4V alloy manufactured by EBM. Tensile properties such as yield strength, ultimate tensile strength, and elongation are more significant at the spot of lower porosity [47]. |
| Hrabe et al. (2017) | This study evaluated the effects of internal pores and residual stress on the fatigue properties of EBM fabricated Ti–6Al–4V. It was examined that most of the fatigue cracks were initiated from voids and reducing these initiation sites helps in improving fatigue strength. Moreover, the hot isostatic pressed (HIPed) reduced the void and pores [48]. |
| Galarraga et al. (2017) | The effect of different heat treatments was performed on the EBM-manufactured Ti alloy. The ductility and strength of the fabricated alloy can be transformed by changing the temperature and time of aging heat treatment. In case of high ductility, the aging time increased to 8 h and 550 °C. On the other hand, for high strength, the condition changes to 5 h and 500 °C [49]. |

| | |
|---|---|
| Rotella et al. (2018) | The surface integrity of machined AM Ti alloy was studied. The overall outcomes proved that even though AM components were manufactured from the same powder material, these showed distinct machinability behaviour at different methods (DSLM, EBM) [50]. |
| Priscot et al. (2019) | The effect of heat input rate concerning roughness and microstructure was studied on EBM-fabricated Ti-6Al-4V alloy. It was found that by raising the rate of heat, input tends to coarser the microstructure. Likewise, the increase in heat input decreases the roughness of the top surface of the manufactured part [51]. |
| Umer et al. (2019) | The study was performed to predict the deformation and stress due to the overhang structure of Ti alloy manufactured by EBM. The results show an error of 22% in the deformations of all cases. The FE evaluation found that the 2D plane strain models can predict variations and have good agreements with experimental results [52]. |
| Hojati et al. (2020) | The micro-milling of EBM manufactured Ti6Al4V was investigated concerning the specific cutting energy cutting forces, burr formation, and surface quality. The outcomes showed the better surface quality of the EBM manufactured part compared to the extruded component. The produced burr was continuous in extruded parts; however, discontinuity was noted in EBM parts because of the irregular surface. In addition, without a rough surface, the burr formation of EBM Ti6Al4V is higher in the EBM fabricated Ti6Al4V [53]. |
| Jin et al. (2020) | This study investigated the effect of laser shock peening on the fatigue behaviour of Ti alloy (Ti-6Al-4V) fabricated by the EBM technique. The results revealed the enhancement in fatigue strength with the LSP process [54]. |
| Gupta et al. (2021) | Gupta discussed the influence of strain rate, surface finish, temperature, and build orientation together along with tensile properties of EBM Ti-6Al-4V alloy. It was found that the inadequate surface finish of the samples lowered the ultimate tensile and yield strength. However, it was noted that variations in the orientation of voids and microstructure along with loading direction affect anisotropy in the mechanical strength of EBM fabricated alloy [55]. |
| Tamayo et al. (2021) | The results revealed that internal porosity and high surface roughness significantly lead to fatigue failure [56]. |

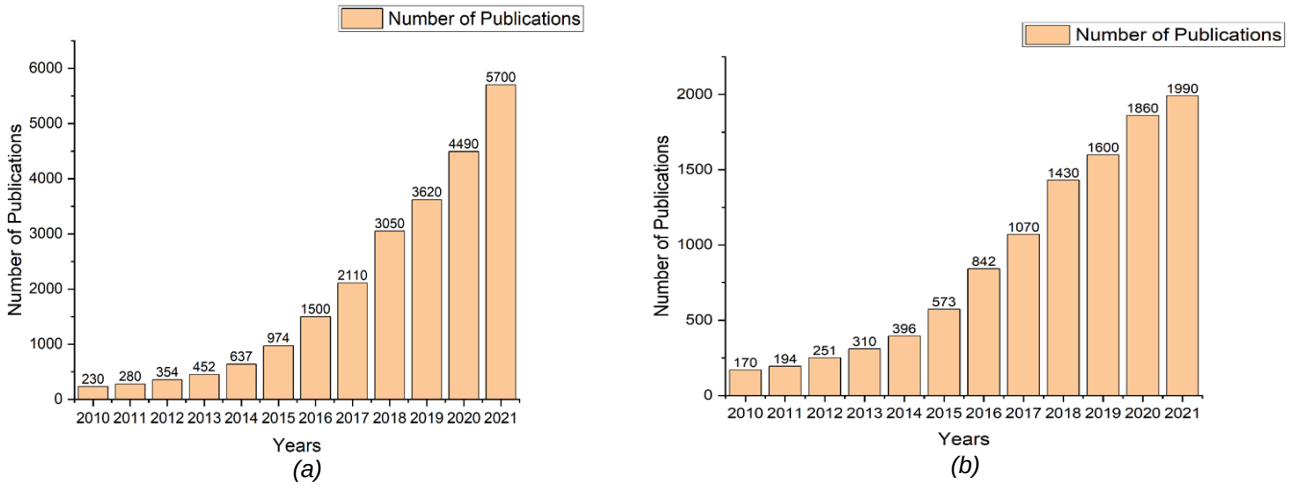


*Figure 1. No. of publications from 2010 to 2021 years @ source: google scholar and caption as (a) EBM of titanium alloys (b) "SLM of titanium alloys"*

### *1.1.2 SLM Process*

In selective laser melting, a complicated metal part can be manufactured by stacking up layers of melted material [57-58]. In the SLM technique, scanning speed, laser power, layer thickness, and hatch spacing are the important parameters to enhance the efficiency of the process. Nevertheless, low scanning speed and high laser may cause the keyhole effect and large material evaporation occurs [59]. The SLM method includes a series of phases from CAD data points to the building parts. Firstly, the CAD data are uploaded as STL (stereolithography) to the SLM to manufacture parts. The manufacturing process begins in a chamber by placing a layer of metal powder (Such as Ti, Fe. etc.) on a substrate plate. Once the powder is placed, a high-energy laser is applied to fuse and melt designated areas corresponding to the processed data. The procedure is then replicated for consecutive layers of powder till the essential parts are fully constructed [60-61]. Fig 1 (b) shows the number of articles published from 2010 to 2021.

*Table 2. Summary of Previous studies performed on Ti alloy by SLM Process.*

| Authors | Remarks |
|---|---|
| Thijs et al. (2010) | This study examined the microstructure of the Ti alloy by light optical microscopy and fabricated by the SLM method. It was found that the path of the extended grains varies with the regional heat transfer condition [62]. |
| Facchini et al. (2010) | The study focused on the variation in the mechanical properties of Ti-6Al-4V alloy manufactured by various variants of the SLM method. However, few microcracks were observed due to the impact of unfinished homologous residual stresses and wetting created by the larger solidification undercooling of the melt pool [63]. |
| Chlebus et al. (2011) | The SLM fabricated Ti alloy showed high mechanical properties in compression and tension tests with thin plates of α′ martensite hardened. Which increases the properties compared to conventional production techniques [64]. |
| Vilaro et al. (2011) | Diverse types of microstructures were investigated after the heat treatments of Ti alloy below the β transit. The results revealed the strong anisotropy of fracture in two loading paths, which is assigned to the fabricated defects. However, the ductility is noticeably increased [65]. |
| Thöne et al. (2012) | The fracture mechanical behaviour of Ti alloy was investigated with the influence of heat treatment following the SLM method. It was found that a decrease in internal stress increases the elongation at breaks in mechanical behaviour [66]. |
| Simonelli et al. (2012) | The microstructure of SLM fabricated Ti alloy revealed that the resultant microstructure is distinct from that examined wrought or cast materials [67]. |

| | |
|---|---|
| Leuders et al. (2013) | Leuders et al. established microstructure connections in cyclic loading for a Ti alloy manufactured by SLM. It was found that the Ti alloy processed by SLM is completed associated with microstructures and tailored by heat treatment. However, Pores in the models indicated a severe impact on the fatigue behaviour of the SLM part [68]. |
| Sun et al. (2013) | The octahedral Ti porous alloy was obtained by determining the load of the simplified model. The results revealed that the microstructure of the porous structure includes many martensites that interlink together and increase the energy needed for crack propagation [69]. |
| Kanazawa et al. (2014) | Kanazawa et al. studied the Ti alloy processed by SLM for maxillary denture and evaluated the microstructure and hardness. It was found that the hardness was higher in SLM samples compared to conventional casting. However, the OM images of SLM samples did not show pores [70]. |
| Yadroitsev et al. (2014) | The evaluation of microstructure was conducted at several heat treatments. The findings revealed that the highest temperature of the molten pool rose with laser power and marginally enhanced with irradiation time [71]. |
| Kasperovich et al. (2015) | This study focused on developing ductility and fatigue resistance of Ti alloy fabricated by the SLM process. It was found that to reduce the pores,' average scanning velocity is desirable. However, at more rapid velocities, the porosity gradually grew again [72]. |
| Agapovichev et al. (2016) | The study was conducted on Ti alloy's microstructure and mechanical properties manufactured by the SLM process. Results indicated that the Ti alloy reveals a high mechanical strength and distinct homogeneous microstructure [73] |
| Dai et al. (2016) | Dai et al. investigated the electrochemical measurements of Ti alloy made by the SLM process. It was found that the SLM samples showed a worse corrosion resistance compared to commercial Grade 5 alloy [74]. |
| Shunmugavel et al. (2017) | Comparative analyses were performed on the mechanical properties of conventional and additively manufactured titanium alloy. It was found that the ultimate tensile strength, yield strength, and hardness properties were greater for additive manufactured parts, but the ductility lacked significantly [75]. |
| Walker et al. (2017) | Walker et al. evaluated the constant loading in Ti alloy samples manufactured by SLM and varied the build direction and layer thickness. However, the computational Modelling was presented with a conventional (LEFM) Linear Elastic Fracture Mechanics approach. It revealed the relationship of the data and showed a way of evaluating the crack initiates defects such as Lack of Fusion (LOF) or porosity [76]. |
| Sing et al. (2018) | In situ alloying was manufactured by the SLM process to produce Ti-tantalum alloy using a tailored powder blend. It was found that the findings show that the dense titanium-tantalum (relative density of $99.85 \pm 0.18\%$.) part can be fabricated from the SLM process [77]. |
| Lu et al. (2018) | Lu et al. investigated the impact of laser shock peening on the hot corrosion behaviour of Ti alloy. The results revealed that the SLM manufactured specimen showed a lower corrosion resistance than the SLM heat-treated specimen [78]. |
| Li et al. (2019) | Li et al. investigated the wear resistance and microhardness of laser polished Ti alloy surface manufactured by SLM. It was found that the yield and tensile strength of polished laser surface were not significantly affected though elongation marginally declined [79]. |
| Zhang et al. (2019) | The probability of the fatigue properties of SLM materials is significant for the safety structures in dynamic load. Zhang et al. studied the low cycle fatigue performance of SLM Ti alloy in high loading states. Results showed that the |

| | |
|---|---|
| | SLM build materials showed improved fatigue performance at low strain amplitudes but low at high strain amplitudes due to increased porosity [80]. |
| Sun et al. (2020) | Similarly, sun et al. examined the fatigue performance of Ti alloy at three distinct build directions such as 0°, 45°, and 90°. It was found that the build path significantly affects the fatigue performance. The fatigue and tensile properties showed better results at 45° [81]. |
| Su et al. (2021) | Su et al. explored that the heat treatment is an efficient technique to change the SEM fabricated tensile properties, while processes like hot isostatic pressing can improve the fatigue properties. It was found that solution treatment at 850 °C observed by water quenching treatment can monitor the tensile, microstructure, and fatigue properties of Ti alloy [82]. |
| Huang et al. (2021) | However, Huang et al. studied the heat treatment impact on SLM fabricated parts and found that it may enhance the ductile property. But yield and tensile strength of samples were lowered [83]. |

## 2. SUMMARY AND RESEARCH TRENDS

This literature survey focused on important findings on EBM and SLM using Ti alloy from 2010 to 2021. Compared to conventional fabrication techniques of metal materials, the SLM and EBM are two advanced direct metal manufacturing methods, which are ideal choices for complicated implants. Fig. 1 show the increasing trend of publication from 2010 to 2021 in both SLM and EDM additive manufacturing. Fig. 2 shows the research contribution on Ti alloy in the areas of fatigue analysis, heat treatments, corrosion performance, FEM analysis, and mechanical properties of Ti alloys. Many researchers have focused on increasing the performance of Ti alloy due to increasing its popularity in medical applications. Studies on EBM and SLM also covered the important parameters, such as the powder size and efficiency, building parameters that affect the material microstructure, and chemical and mechanical properties of the final product [84-89]. The porous metallic shells manufactured by the direct metal method have entirely interlinked and contain the altered pore size and shape and suitable mechanical strength appropriate for the engineering of bone tissue [90-91]. Rafi et al. revealed that the surface of Ti alloy performs a significant role in the connection, differentiation, and proliferation of cells [89]. It was found that the surface roughness of Ti alloy samples fabricated by SLM, and EBM was distinctive from the normal machined samples [92-93]. However, better corrosion resistance was observed in SLM compared to EBM. The explanation for this cause was unspecified, and further studies needed. Zang et al. showed better fatigue performance at low strain amplitudes in the SLM method [80]. However, it was observed that the solution treatment at 850 °C by water quenching treatment influence the tensile, microstructure, and fatigue properties of Ti alloy [82]. In the case of the machining of additive materials, Rotella et al. investigated the surface integrity of machined AM components manufactured from the same powder material.

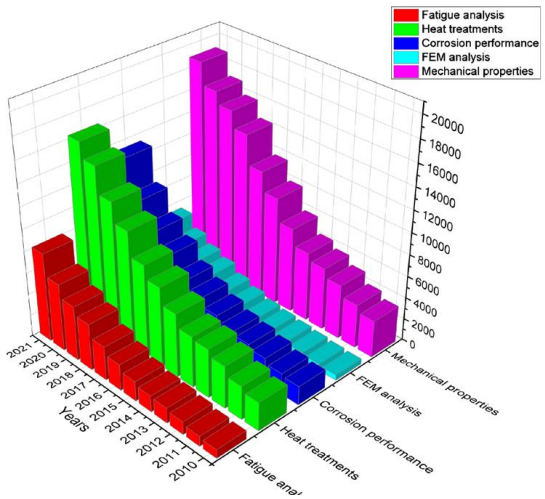


Figure 2. Reported articles from 2010 to 2021 in various areas of Ti alloys. Source: Google scholar

Some studies showed distinct machinability behaviour at different methods (DSLM, EBM) [50]. In addition, Hojati et al. investigated the micro-milling of EBM manufactured Ti alloy concerning the specific cutting energy cutting forces, burr formation, and surface quality. The outcomes show the better surface quality of the EBM manufactured part compared to the extruded part. The produced burr was continuous in extruded parts; however, discontinuity was noted in EBM parts because of the irregular surface [53]. Mechanical properties like hardness are found better in SLM build materials. Kanazawa et al. showed that the hardness was higher in SLM samples compared to conventional casting techniques [70]. Similarly, Shunmugavel et al. studied the comparative analyses on the mechanical properties of conventional and additively manufactured Ti alloy. It was found that the ultimate tensile strength, yield strength, and hardness properties were greater for additive manufactured parts, but the ductility lacked significantly. Furthermore, Ti alloy's microstructure and mechanical properties are manufactured by the SLM process, revealing a high mechanical strength and distinct homogeneous microstructure [73].

## 3. RESEARCH GAP

(i) More studies are needed in the form of biomechanical testing, fatigue testing, and fabrication of patient-specific implants with biodegradable bio ceramics or polymers. These studies would provide better insights to lower the use of metal without losing the needed biomechanical strength.
(ii) Clinical evidence is needed to demonstrate the long-term strength of the prosthesis.
(iii) Future studies are needed to decrease porosity to enhance the mechanical properties of AM-produced material.
(iv) Optimisation of parameters for raw powder production and the EBM process is needed to improve the performance of EBM-manufactured components.
(v) A detailed understanding is required of the impacts of the heat treatments process on the structural properties of EBM fabricated parts for high-integrity applications.
(vi) Further study is needed on the correlation between specific cutting energy and surface roughness.

## 4. CONCLUSION

In this review, the important findings on the EBM and SLM methods of Additive Manufacturing are discussed, especially covering the important parameters that interlinked with machining, heat treatment processes, mechanical properties, and fatigue analysis were discussed. Several differences were observed in the reported studies in Ti alloy about microstructure, chemical, and physical properties. Furthermore, it is emphasized that further studies are needed to evaluate the long-term biocompatibility of Ti implants manufactured using SLM and EBM.

## 5. REFERENCES

Agapovichev, A. V., Kokareva, V. V., Smelov, V. G., & Sotov, A. V. (2016, November). Selective laser melting of titanium alloy: investigation of mechanical properties and microstructure. In IOP conference series: materials science and engineering (Vol. 156, No. 1, p. 012031). IOP Publishing.

Attar H, Bönisch M, Calin M, Zhang LC, Scudino S, Eckert J (2014) Selective laser melting of in situ titanium–titanium boride composites: Processing, microstructure, and mechanical properties. Acta Materialia 76 (9):13–22

Attar H, Calin M, Zhang LC, Scudino S, Eckert J (2014) Manufacture by selective laser melting and mechanical behavior of commercially pure titanium. Materials Science and Engineering: A 593:170-177.

Bannon, B. P., & Mild, E. E. (1983). Titanium alloys in surgical implants. ASTM STP, 796, 7.

Bothe, R. T. (1940). Reaction of bone to multiple metallic implants. Surg Gynecol Obstet, 71, 598-602.

Chan, K. S. (2015). Characterisation and analysis of surface notches on Ti-alloy plates fabricated by additive manufacturing techniques. Surface Topography: Metrology and Properties, 3(4), 044006.

Chan, K. S., Koike, M., Mason, R. L., & Okabe, T. (2013). Fatigue life of titanium alloys fabricated by additive layer manufacturing techniques for dental implants. Metallurgical and Materials Transactions A, 44(2), 1010-1022.

Chlebus, E., Kuźnicka, B., Kurzynowski, T., & Dybała, B. (2011). Microstructure and mechanical behaviour of Ti—6Al—7Nb alloy produced by selective laser melting. Materials Characterisation, 62(5), 488-495.

Chua, C. K., & Leong, K. F. (2014). 3D Printing and additive manufacturing: Principles and applications (with companion media pack)-of rapid prototyping. World Scientific Publishing Company.

Clare, A. T., Chalker, P. R., Davies, S., Sutcliffe, C. J., & Tsopanos, S. (2008). Selective laser melting of high aspect ratio 3D nickel–titanium structures two way trained for MEMS applications. International Journal of Mechanics and Materials in Design, 4(2), 181-187.

Dai N, Zhang LC, Zhang J, Zhang X, Ni Q, Chen Y, Wu M, Yang C (2016) Distinction in Corrosion Resistance of Selective Laser Melted Ti-6Al-4V Alloy on Different Planes. Corrosion Science 111:703-710

Dai, N., Zhang, L. C., Zhang, J., Chen, Q., & Wu, M. (2016). Corrosion behavior of selective laser melted Ti-6Al-4 V alloy in NaCl solution. Corrosion Science, 102, 484-489.

de Formanoir C, Michotte S, Rigo O, Germain L, Godet S (2016) Electron beam melted Ti– 6Al–4V: Microstructure, texture, and mechanical behavior of the as-built and heat-treated material. Materials Science and Engineering: A 652:105-119

de Wild M, Schumacher R, Mayer K, Schkommodau E, Thoma D, Bredell M, et al (2013) Bone regeneration by the osteoconductivity of porous titanium implants manufactured by selective laser melting: a histological and micro computed tomography study in the rabbit. Tissue Engineering: Part A 19(23– 24): 2645–2654.

Facchini, L., Magalini, E., Robotti, P., Molinari, A., Höges, S., & Wissenbach, K. (2010). Ductility of a Ti-6Al-4V alloy produced by selective laser melting of prealloyed powders. Rapid Prototyping Journal.

Froes, F. H., & Dutta, B. (2014). The additive manufacturing (AM) of titanium alloys (Vol. 1019, pp. 19-25). Trans Tech Publications Ltd.

Fukuda, H., Takahashi, H., Kuramoto, K., & Nakano, T. (2012). Effect of energy density of incident beam on mechanical property of titanium alloy products fabricated by electron beam melting (EBM) method. In Materials Science Forum (Vol. 706, pp. 488-491). Trans Tech Publications Ltd.

Galarraga, H., Lados, D. A., Dehoff, R. R., Kirka, M. M., & Nandwana, P. (2016). Effects of the microstructure and porosity on properties of Ti-6Al-4V ELI alloy fabricated by electron beam melting (EBM). Additive Manufacturing, 10, 47-57.

Galarraga, H., Warren, R. J., Lados, D. A., Dehoff, R. R., Kirka, M. M., & Nandwana, P. (2017). Effects of heat treatments on microstructure and properties of Ti-6Al-4V ELI alloy fabricated by electron beam melting (EBM). Materials Science and Engineering: A, 685, 417-428.

Galarraga, H., Warren, R. J., Lados, D. A., Dehoff, R. R., Kirka, M. M., & Nandwana, P. (2017). Effects of heat treatments on microstructure and properties of Ti-6Al-4V ELI alloy fabricated by electron beam melting (EBM). Materials Science and Engineering: A, 685, 417-428.

Gibson, I., Rosen, D. W., Stucker, B., Khorasani, M., Rosen, D., Stucker, B., & Khorasani, M. (2021). Additive manufacturing technologies (Vol. 17). Cham, Switzerland: Springer.

Gu DD, Meiners W, Wissenbach K, Poprawe R (2012) Laser additive manufacturing of metallic components: materials, processes, and mechanisms. International Materials Review 57 (3):133- 164.

Gupta, A., Bennett, C. J., & Sun, W. (2021). The role of defects and characterisation of tensile behaviour of EBM Additive manufactured Ti-6Al-4V: An experimental study at elevated temperature. Engineering Failure Analysis, 120, 105115.

Hao, Y. L., Li, S. J., & Yang, R. (2016). Biomedical titanium alloys and their additive manufacturing. Rare Metals, 35(9), 661-671.

He, G., Liu, P., & Tan, Q. (2012). Porous titanium materials with entangled wire structure for load-bearing biomedical applications. Journal of the mechanical behavior of biomedical materials, 5(1), 16-31.

Hojati, F., Daneshi, A., Soltani, B., Azarhoushang, B., & Biermann, D. (2020). Study on machinability of additively manufactured and conventional titanium alloys in micro-milling process. Precision Engineering, 62, 1-9.

Hrabe, N., & Quinn, T. (2013). Effects of processing on microstructure and mechanical properties of a titanium alloy (Ti–6Al–4V) fabricated using electron beam melting (EBM), part 1: Distance from build plate and part size. Materials Science and Engineering: A, 573, 264-270.

Hrabe, N., Gnäupel-Herold, T., & Quinn, T. (2017). Fatigue properties of a titanium alloy (Ti–6Al–4V) fabricated via electron beam melting (EBM): Effects of internal defects and residual stress. International Journal of Fatigue, 94, 202-210.

Huang, S., Sun, B., & Guo, S. (2021). Microstructure and property evaluation of TA15 titanium alloy fabricated by selective laser melting after heat treatment. Optics & Laser Technology, 144, 107422.

Jin, X., Lan, L., Gao, S., He, B., & Rong, Y. (2020). Effects of laser shock peening on microstructure and fatigue behavior of Ti–6Al–4V alloy fabricated via electron beam melting. Materials Science and Engineering: A, 780, 139199.

Kanazawa, M., Iwaki, M., Minakuchi, S., & Nomura, N. (2014). Fabrication of titanium alloy frameworks for complete dentures by selective laser melting. The Journal of prosthetic dentistry, 112(6), 1441-1447.

Kasperovich, G., & Hausmann, J. (2015). Improvement of fatigue resistance and ductility of TiAl6V4 processed by selective laser melting. Journal of Materials Processing Technology, 220, 202-214.

Koike M, Greer P, Owen K, Guo L, Murr LE, Gaytan SM, et al (2011) Evaluation of titanium alloys fabricated using rapid prototyping technologies-electron beam melting and laser beam melting. Materials 4 (10): 1776–1792.

Koike, M., Martinez, K., Guo, L., Chahine, G., Kovacevic, R., & Okabe, T. (2011). Evaluation of titanium alloy fabricated using electron beam melting system for dental applications. Journal of Materials Processing Technology, 211(8), 1400-1408.

Kok, Y., Tan, X., Tor, S. B., & Chua, C. K. (2015). Fabrication and microstructural characterisation of additive manufactured Ti-6Al-4V parts by electron beam melting: This paper reports that the microstructure and micro-hardness of an EMB

part is thickness dependent. Virtual and Physical Prototyping, 10(1), 13-21.
Krakhmalev, P., & Yadroitsev, I. (2014). Microstructure and properties of intermetallic composite coatings fabricated by selective laser melting of Ti–SiC powder mixtures. Intermetallics, 46, 147-155.
Kruth, J. P., Mercelis, P., Van Vaerenbergh, J., Froyen, L., & Rombouts, M. (2005). Binding mechanisms in selective laser sintering and selective laser melting. Rapid prototyping journal.
Larsson, M., Lindhe, U., & Harrysson, O. L. A. (2003). Rapid manufacturing with Electron Beam Melting (EBM)-A manufacturing revolution? In 2003 International Solid Freeform Fabrication Symposium.
Leuders, S., Thöne, M., Riemer, A., Niendorf, T., Tröster, T., Richard, H. A., & Maier, H. J. (2013). On the mechanical behaviour of titanium alloy TiAl6V4 manufactured by selective laser melting: Fatigue resistance and crack growth performance. International Journal of Fatigue, 48, 300-307.
Leventhal, G. S. (1951). Titanium, a metal for surgery. JBJS, 33(2), 473-474.
Leyens, C., & Peters, M. (Eds.). (2003). Titanium and titanium alloys: fundamentals and applications. John Wiley & Sons.
Li, Y. H., Wang, B., Ma, C. P., Fang, Z. H., Chen, L. F., Guan, Y. C., & Yang, S. F. (2019). Material characterisation, thermal analysis, and mechanical performance of a laser-polished Ti alloy prepared by selective laser melting. Metals, 9(2), 112.
Li, Y. H., Yang, C., Wang, F., Zhao, H. D., Qu, S. G., Li, X. Q., ... & Li, Y. Y. (2015). Biomedical TiNbZrTaSi alloys designed by d-electron alloy design theory. Materials & Design, 85, 7-13.
Liu CK, Jing CX, Tan XY, Xu J, Hu M (2013) Using three-dimensional porous internal titanium scaffold or allogenic bone scaffold for tissue-engineering condyle as a novel reconstruction of mandibular condylar defects. Journal of Medical Hypotheses and Ideas 8(2): 69–73.
Liu YJ, Li SJ, Hou WT, Wang SG, Hao YL, Yang R, Sercombe TB, Zhang LC (2016) Electron beam melted beta-type Ti-24Nb-4Zr-8Sn porous structures with high strength-to-modulus ratio. Journal of Materials Science & Technology 32 (6):505-508
Liu YJ, Li SJ, Wang HL, Hou WT, Hao YL, Yang R, Sercombe TB, Zhang LC (2016) Microstructure, defects and mechanical behavior of beta-type titanium porous structures manufactured by electron beam melting and selective laser melting. Acta Materialia 113:56-67
Liu YJ, Wang HL, Li SJ, Wang SG, Wang WJ, Hou WT, Hao YL, Yang R, Zhang LC (2017) Compressive and fatigue behavior of beta-type titanium porous structures fabricated by electron beam melting. Acta Materialia 126:58-66
Liu, P. C., Yang, Y. J., Liu, R., Shu, H. X., Gong, J. P., Yang, Y., ... & Cai, M. (2014). A study on the mechanical characteristics of the EBM-printed Ti-6Al-4V LCP plates in vitro. Journal of Orthopaedic Surgery and Research, 9(1), 1-6.
Liu, Y. J., Li, S. J., Wang, H. L., Hou, W. T., Hao, Y. L., Yang, R., ... & Zhang, L. C. (2016). Microstructure, defects, and mechanical behavior of beta-type titanium porous structures manufactured by electron beam melting and selective laser melting. Acta materialia, 113, 56-67.
Liu, Y. J., Li, S. J., Wang, H. L., Hou, W. T., Hao, Y. L., Yang, R., ... & Zhang, L. C. (2016). Microstructure, defects, and mechanical behavior of beta-type titanium porous structures manufactured by electron beam melting and selective laser melting. Acta materialia, 113, 56-67.
Liu, Y., Zhang, J., Li, S. J., Hou, W. T., Wang, H., Xu, Q. S., ... & Yang, R. (2017). Effect of HIP treatment on fatigue crack growth behavior of Ti–6Al–4V alloy fabricated by electron beam melting. Acta Metallurgica Sinica (English Letters), 30(12), 1163-1168.
Long, M., & Rack, H. J. (1998). Titanium alloys in total joint replacement—a materials science perspective. Biomaterials, 19(18), 1621-1639.
Lu, H., Wang, Z., Cai, J., Xu, X., Luo, K., Wu, L., & Lu, J. (2021). Effects of laser shock peening on the hot corrosion behaviour of the selective laser melted Ti6Al4V titanium alloy. Corrosion Science, 188, 109558.
Mahamood, R. M., Akinlabi, E. T., Shukla, M., & Pityana, S. L. (2013). Laser metal deposition of Ti6Al4V: a study on the effect of laser power on microstructure and microhardness.
Marin, E., Fusi, S., Pressacco, M., Paussa, L., & Fedrizzi, L. (2010). Characterisation of cellular solids in Ti6Al4V for orthopaedic implant applications: Trabecular titanium. Journal of the Mechanical Behavior of Biomedical Materials, 3(5), 373-381.
Murr L E, Esquivel E V, Quinones S A, Microstructure, and mechanical behavior of porous Ti-6Al-4V parts obtained by selective laser melting et al (2009) Microstructures and mechanical properties of electron beam-rapid manufactured Ti–6Al–4V biomedical prototypes compared to wrought Ti–6Al–4V. Materials Characterization 60(2): 96–105.
Murr LE, Quinones SA, Gaytan SM, Lopez MI, Rodela A, Martinez EY, et al (2009) Microstructure and mechanical behavior of Ti-6Al-4V produced by rapid-layer manufacturing, for biomedical applications. J Mech Behav Biomed Mater 2(1): 20–32. doi: 10.1016/j.jmbbm.2008.05.004 PMID: 19627804
Parthasarathy, J., Starly, B., Raman, S., & Christensen, A. (2010). Mechanical evaluation of porous titanium (Ti6Al4V) structures with electron beam melting (EBM). Journal of the mechanical behavior of biomedical materials, 3(3), 249-259.
Patterson, A. E., Messimer, S. L., & Farrington, P. A. (2017). Overhanging features and the SLM/DMLS residual stresses problem: Review and future research need. Technologies, 5(2), 15.
Ponader S, Vairaktaris E, Heinl P, Wilmowsky CV, Rottmair A, Körner C, et al (2008) Effects of topographical surface

modifications of electron beam melted Ti-6Al-4V titanium on human fetal osteoblasts. J Biomed Mater Res A 2008 15 (4): 1111–9.

Prisco, U., Astarita, A., El Hassanin, A., & Franchitti, S. (2019). Influence of processing parameters on microstructure and roughness of electron beam melted Ti-6Al-4V titanium alloy. Materials and Manufacturing Processes, 34(15), 1753-1760.

Rafi H K, Karthik N V, Gong H J, Starr TL, Stucker BE (2013) Microstructures and mechanical properties of Ti6Al4V parts fabricated by selective laser melting and electron beam melting. Journal of Materials Engineering and Performance, 22(12): 3872–3883.

Rotella, G., Imbrogno, S., Candamano, S., & Umbrello, D. (2018). Surface integrity of machined additively manufactured Ti alloys. Journal of Materials Processing Technology, 259, 180-185.

Safdar, A., He, H. Z., Wei, L. Y., Snis, A., & de Paz, L. E. C. (2012). Effect of process parameters settings and thickness on surface roughness of EBM produced Ti-6Al-4V. Rapid Prototyping Journal.

Sallica-Leva E, Jardini AL, Fogagnolo JB (2013) Microstructure and mechanical behavior of porous Ti- 6Al-4V parts obtained by selective laser melting. J Mech Behav Biomed Mater 26: 98–108. doi: 10. 1016/j.jmbbm.2013.05.011 PMID: 23773976

Sato, M., Takakuwa, O., Nakai, M., Niinomi, M., Takeo, F., & Soyama, H. (2016). Using cavitation peening to improve the fatigue life of titanium alloy Ti-6Al-4V manufactured by electron beam melting. Materials Sciences and Applications, 7(4), 181-191.

Shunmugavel, M., Polishetty, A., Goldberg, M., Singh, R., & Littlefair, G. (2017). A comparative study of mechanical properties and machinability of wrought and additive manufactured (selective laser melting) titanium alloy–Ti-6Al-4V. Rapid Prototyping Journal.

Simonelli, M., Tse, Y. Y., & Tuck, C. (2012, July). Microstructure of Ti-6Al-4V produced by selective laser melting. In Journal of Physics: Conference Series (Vol. 371, No. 1, p. 012084). IOP Publishing.

Sing, S. L., An, J., Yeong, W. Y., & Wiria, F. E. (2016). Laser and electron-beam powder-bed additive manufacturing of metallic implants: A review on processes, materials, and designs. Journal of Orthopaedic Research, 34(3), 369-385.

Sing, S. L., Wiria, F. E., & Yeong, W. Y. (2018). Selective laser melting of titanium alloy with 50 wt% tantalum: Effect of laser process parameters on part quality. International Journal of Refractory Metals and Hard Materials, 77, 120-127.

Springer, J. C., Harrysson, O. L., Marcellin-Little, D. J., & Bernacki, S. H. (2014). In vitro dermal and epidermal cellular response to titanium alloy implants fabricated with electron beam melting. Medical Engineering & Physics, 36(10), 1367-1372.

Su, C., Yu, H., Wang, Z., Yang, J., & Zeng, X. (2021). Controlling the tensile and fatigue properties of selective laser melted Ti–6Al–4V alloy by post treatment. Journal of Alloys and Compounds, 857, 157552.

Sun, J., Yang, Y., & Wang, D. (2013). Mechanical properties of a Ti6Al4V porous structure produced by selective laser melting. Materials & Design, 49, 545-552.

Sun, W., Huang, W., Zhang, W., & Qian, X. (2020). Effects of build direction on tensile and fatigue performance of selective laser melting Ti6Al4V titanium alloy. International Journal of Fatigue, 130, 105260.

Tamayo, J. A., Riascos, M., Vargas, C. A., & Baena, L. M. (2021). Additive manufacturing of Ti6Al4V alloy via electron beam melting for the development of implants for the biomedical industry. Heliyon, 7(5), e06892.

Tan XP, Kok YH, Tan YJ, Descoins M, Mangelinck D, Tor SB, Leong KF, Chua CK (2015) Graded microstructure and mechanical properties of additive manufactured Ti–6Al–4V via electron beam melting. Acta Materialia 97:1-16

Thijs L, kuleuven be, Verhaeghe F, Humbeeck JV, Kruth JP (2010) A study of the microstructural evolution during selective laser melting of Ti–6Al–4V. Acta Materialia 58(9): 3303–3312.

Thijs, L., Verhaeghe, F., Craeghs, T., Van Humbeeck, J., & Kruth, J. P. (2010). A study of the microstructural evolution during selective laser melting of Ti–6Al–4V. Acta materialia, 58(9), 3303-3312.

Thijs, L., Verhaeghe, F., Craeghs, T., Van Humbeeck, J., & Kruth, J. P. (2010). A study of the microstructural evolution during selective laser melting of Ti–6Al–4V. Acta materialia, 58(9), 3303-3312.

Thöne, M., Leuders, S., Riemer, A., Tröster, T., & Richard, H. A. (2012, August). Influence of Heat-Treatment of Selective Laser Melting Products-e.g., Ti6Al4V. In 2012 International Solid Freeform Fabrication Symposium. University of Texas at Austin.

Umer, U., Ameen, W., Abidi, M. H., Moiduddin, K., Alkhalefah, H., Alkahtani, M., & Al-Ahmari, A. (2019). Modeling the effect of different support structures in electron beam melting of titanium alloy using finite element models. Metals, 9(7), 806.

Vaithilingam J, Kilsby S, Goodridge RD, Christie SD, Edmondson S, Hague RJ (2015) Functionalisation of Ti6Al4V components fabricated using selective laser melting with a bioactive compound. Mater Sci Eng C Mater Biol Appl 46: 52–61. doi: 10.1016/j.msec.2014.10.015 PMID: 25491959

Vilaro, T., Colin, C., & Bartout, J. D. (2011). As-fabricated and heat-treated microstructures of the Ti-6Al-4V alloy processed by selective laser melting. Metallurgical and materials transactions A, 42(10), 3190-3199.

Walker, K. F., Liu, Q., & Brandt, M. (2017). Evaluation of fatigue crack propagation behaviour in Ti-6Al-4V manufactured by selective laser melting. International Journal of Fatigue, 104, 302-308.

Wang XJ, Xu SQ, Zhou SW, Xu W, Leary M, Choong P, Qian M, Brandt M, Xie YM (2016) Topological design and additive manufacturing of porous metals for bone scaffolds and orthopaedic implants: a review. Biomaterials 83:127-141

Weiwei, H., Wenpeng, J., Haiyan, L., Huiping, T., Xinting, K., & Yu, H. (2011). Research on preheating of titanium alloy powder in electron beam melting technology. Rare Metal Materials and Engineering, 40(12), 2072-2075.

Yadroitsev, I., Krakhmalev, P., & Yadroitsava, I. (2014). Selective laser melting of Ti6Al4V alloy for biomedical applications: Temperature monitoring and microstructural evolution. Journal of Alloys and Compounds, 583, 404-409.

Yang, C., Liu, L. H., Yao, Y. G., Li, Y. H., & Li, Y. Y. (2014). Intrinsic relationship between crystallisation mechanism of metallic glass powder and microstructure of bulk alloys fabricated by powder consolidation and crystallisation of amorphous phase. Journal of alloys and compounds, 586, 542-548.

Zhang, L. C., Liu, Y., Li, S., & Hao, Y. (2018). Additive manufacturing of titanium alloys by electron beam melting: a review. Advanced Engineering Materials, 20(5), 1700842.

Zhang, L. C., Liu, Y., Li, S., & Hao, Y. (2018). Additive manufacturing of titanium alloys by electron beam melting: a review. Advanced Engineering Materials, 20(5), 1700842.

Zhang, P., He, A. N., Liu, F., Zhang, K., Jiang, J., & Zhang, D. Z. (2019). Evaluation of low cycle fatigue performance of selective laser melted titanium alloy Ti–6Al–4V. Metals, 9(10), 1041.

Zhao XL, Li SJ, Zhang M, Liu YD, Sercombe TB, Wang SG, Hao YL, Yang R, Murr LE (2016) Comparison of the microstructures and mechanical properties of Ti–6Al–4V fabricated by selective laser melting and electron beam melting. Materials & Design 95:21-31

Zhao, X., Li, S., Zhang, M., Liu, Y., Sercombe, T. B., Wang, S., ... & Murr, L. E. (2016). Comparison of the microstructures and mechanical properties of Ti–6Al–4V fabricated by selective laser melting and electron beam melting. Materials & Design, 95, 21-31.

# Additive manufacturing of reinforced polymer composites with stainless steel fibre

Alison Clarke, Andrew Dickson and Denis P. Dowling
University College Dublin.

***Abstract***

This study for the first time investigates the 3D printing of continuous 316L stainless steel fibre (SSF) reinforced polymer composites. The steel fibre bundle used in this printing study consisted of 90 fibres, each with a diameter of 14 µm. This fibre bundle was coated with polylactic acid (PLA), in order to produce PLA-SSF continuous filaments with tailored diameters in the range of 0.9 to 0.5 mm. These were then used to print composite parts using the Fused Filament Fabrication (FFF), 3D printing technique. The steel fibre volume fraction (VF) in the printed composite structures was controlled in the range of 6 to 12VF%. The samples exhibited a homogeneous distribution of steel fibres in the PLA matrix. Increasing the volume fraction and lowering the porosity of the PLA-SSF structure, is achieved by alterations to the 3D printing parameters and printer modifications. Parameters include layer height, path width, temperature and cooling. The evaluation of the PLA-SSF composites includes assessment of its mechanical performance (interlaminar shear strength and tensile property testing), its volume fraction and porosity (CT scans and cross-section studies), as well as morphology (microscopy and SEM examination). The ability of the FFF technique to fabricate PLA polymer-SSF composite structures exhibiting low porosities (approx. 7%), was successfully demonstrated. The SSF reinforcement of the PLA resulted in a significant improvement in mechanical performance i.e., a 5-fold increase in interlaminar shear strength (ILSS), compared with polymer only. The 12 VF% exhibiting significantly increase in both tensile strength and modulus, compared with the 6 VF%. The ILSS of the steel composite at 25.1 MPa, is significantly higher than that reported for carbon fibre composites which is typically reported to be approx. 12 MPa. There is considerable potential for printed steel composites for individualised conductive composite applications. Compared with previous reports from the literature on 3D printed metal fibre reinforced polymer composites, the stainless steel composites were demonstrated to exhibit significantly enhanced mechanical performance.

*Key Words: Stainless steel wire fibre, Fused Filament Fabrication (FFF), composite printing.*

## 1. INTRODUCTION

3D printing (additive manufacturing) enables components to be fabricated by adding material layer-by-layer. A range of 3D printing materials are available to fabricate components including polymers, metals, and composites. Polymer 3D printed components exhibit poor mechanical properties, which can be enhanced by adding reinforcing materials. This study investigated the use of continuous wire filament as a novel reinforcing for polymer composites. Polylactic acid (PLA) and a continuous stainless steel fibre bundle (SSF) are combined to fabricate a composite filament (PLA-SSF) to fabricate 3D printed components. Increasing interest is focusing on the addition of continuous fibres for the reinforcement of polymers.

## 2. LITERATURE REVIEW

One of the most widely used 3D printing techniques is fused filament fabrication (FFF) (Dickson et al., 2018; Dowling et al., 2020; Tekinalp et al., 2014). FFF can be used to produce polymer and composite components. The latter is achieved through the addition of fibres (short or continuous), alternatively powder particles, beads, and pellets as polymer reinforcement. The most commonly used thermoplastic feedstocks include Polylactic acid (PLA), Polycarbonate (PC), Polyamide (PA or nylon), and Acrylonitrile butadiene styrene (ABS) (Dickson et al., 2020; Ibrahim, 2019; Le Duigou et al., 2020; Matsuzaki et al., 2016; Reverte et al., 2020; Saleh et al., 2019). Reinforcing fibres include glass, metal, carbon, basalt and there are a considerable range, as can be seen in the 'Family of Fibres' diagram in Figure 1 (Beckman et al., 2021).

Email : Alison Clarke
alison.clarke1@ucdconnect.ie

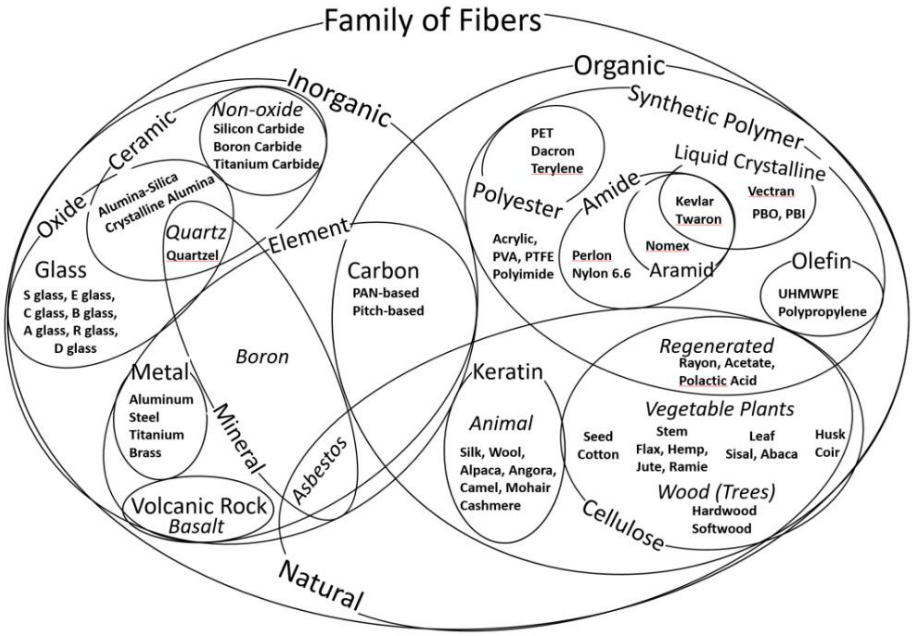


*Figure 1. Family of Fibres (Beckman et al., 2021).*

Stainless steel fibres are used in applications such as automotive body parts, as well as within the marine and aviation industries for sound absorbance, as well as the filtration of oils, in addition to their use in respiration systems for particulate filtration (Baerdemaeker & Vleurinck, 2017; Goux & Van Hooreweder, 2020). Textiles can incoporate them to shield electomagnetic radiation, provide heat or fire retardance (Baerdemaeker & Vleurinck, 2018; Ibrahim et al., 2018; Ozen et al., 2015; Tunakova et al., 2020). Reinforced polymer composites with SSF and carbon fibre (CF) are used for bulletproof vests and car parts, having excellent fatigue resistance leading to an increased life span (Naga Kiran et al., 2019). Stainless steel is, however, susceptible to pitting corrosion (Galvele, 1976; Ryan et al., 2002).

### *2.1 Metal / polymer print technology*

Recently metal-filled polymer filaments have become available commercially and are compatible with FFF 3D printers. The metal filaments come in two types, called metal fill filament and bound metal powder filament. Metal fill filaments are used for aesthetic applications only, the powder metal additive is powder does not provide any significant reinforcement to the polymer's mechanical properties. The bound metal powder filament polymer can be debonded and the remaining metal sintered, to produce metallic parts which are reported to exhibit equivalent mechanical properties to those obtained using laser beam additive manufacturing process. Markforged has developed what they call their 'Metal X' technology, for fused filament fabrication of metals including 17-4 stainless steel, tool steel, Inconel 625, and copper (Markforged, 2018, 2020; Markforged Inc., 2021).

### *2.3 Composite Filament Fabrication*

Composites made by fused FFF generally involve two fabrication approaches, 'ex-situ prepreg' or 'in-situ-fusion'(Botelho et al., 2003; Goh et al., 2018; Hu et al., 2018). The latter is the most widely used approach for the fabrication of continuous fibres and involves direct fibre integration into the print nozzle during 3D printing (Dickson et al., 2020; Pandelidi et al., 2021; Rafiee et al., 2020; Zhuo et al., 2021). As a result of short dwell time, also with the lack of pressure from the nozzle, the polymer matrix can be poorly infused into the fibres. Large temperature gradients between the two materials can cause melt fracture due to the rapid cooling polymer resulting in poor bonding between the two materials (Hu et al., 2018; Mahltig, 2018).

The 'Ex-situ prepreg' production, in contrast, is a two-part process, the composite filament is first fabricated, followed by the 3D printing parts (Dickson et al., 2020). Hu et al. (Hu et al., 2018) described a process for the Ex-situ prepreg with PLA and continuous carbon fibre filament manufacturing. Chen et al. (Chen et al., 2021)

used ex-situ prepreg to 3D print PLA with continuous glass fibre (PLA-CGF) achieving high impregnation into the fibres by optimising the fabrication process.

Ibrahim et al. (Ibrahim, 2019; Ibrahim et al., 2018) and Saleh et al. (Saleh et al., 2019) successfully 3D printed continuous wire polymer composites for sensor applications, combining nickel-chromium wires with a PLA matrix and copper wire in PLA, by in-situ-fusion. Both were single solid wires of diameters of 75 µm. The mechanical properties of the PLA were slightly improved with Nickle-chromium and less impact with copper wire. Intended applications are to be embedded into parts for monitoring, such as aircraft components or biomedical implants. To the authors knowledge no continuous metal reinforced polymer filament are commercially available.

There have been very few publications on the incorporation of steel fibres into 3D printed composites. Quan et al. (Quan et al., 2019) examined laminating a sandwich of SSF with CF in an epoxy matrix, finding a significant increase in fracture toughness. The SSF bundle used by Quan et al. was developed by Bekaert and contained 400 fibres, each with a diameter of 22 µm. In this study, the potential of using a continuous stainless steel fibre bundle for the 3D printing of polymer composites is evaluated for the first time.

## 3. METHODOLOGY

### *3.1. Materials*

The continuous 316L stainless steel fibre (SSF) bundle used in this study has a diameter of 0.15 mm, (Figure 2). The bundle consists of 90 fibres per bundle, each with an individual fibre diameter is 14 µm, has a linear density of 111 decitex (TEX) and torsion per cm of 1. The SSF was obtained from Bekaert.


*Figure 2. Stainless steel fibre bundle, 90 fibres*

SSF is manufactured by a specialist drawing process designed and patented by NV Bekaert SA (Küster et al., 2018; Verlinden et al., 2007). The steel's chemical composition is given in Table 1. Determination of the SSF chemical element composition is evaluated from a surface determination line analysis tool, using energy-dispersive X-ray spectroscopy (EDAX).

*Table 1. EDAX elemental analysis results for the as-received stainless steel fibres*

| Element | Fe | Cr | Ni | Mo | Si | Al |
|---|---|---|---|---|---|---|
| Weight % | 69.6 | 17.9 | 5.6 | 2.1 | 0.5 | 0.4 |

PLA pellets were obtained from Nature Works, commercially called IngeoTM Biopolymer D4043D, from sustainable sources and full recyclable capabilities (NatureWorks, n.d.).

### *3.2 Ex-situ, fused filament fabrication 3D printing technique*

*3.2.1 PLA filament*

Polylactic acid (PLA) filament is produced from pellets which are dried at 55°C for a minimum of 24 hours before extrusion. The fabrication of a PLA - SSF filament was carried out using a laboratory-scale filament maker called the 3devo system. This was modified to facilitate the introduction of the fibre into the molten polymer during filament extrusion. A schematic of the polymer extrusion process is shown in Fig 3(a).

The 3devo filament maker processing parameters used to fabricate the wire reinforced filaments are given in Table 2, for the 0.9 to 0.5 mm diameter PLA-SSF filament. Figure 3 (c) shows a photograph of the 3devo extruding the PLA-SSF filament exiting the die. The modifications successfully achieved a PLA-SSF composite filament of 3D printing quality Fig 3(b).

*Table 2. 3devo filament maker parameters*

| Filament | Fans (%) | Extrusion Speed (rpm) | $T_1$ (°C) | $T_2$ (°C) | $T_3$ (°C) | $T_4$ (°C) |
|---|---|---|---|---|---|---|
| PLA-SSF 0.9mm | 45 | 3.2 | 177 | 187 | 186 | 177 |
| PLA-SSF 0.7mm | 20 | 2.6 | 177 | 187 | 186 | 170 |
| PLA-SSF 0.5mm | 33 | 2.2 | 179 | 186 | 193 | 191 |

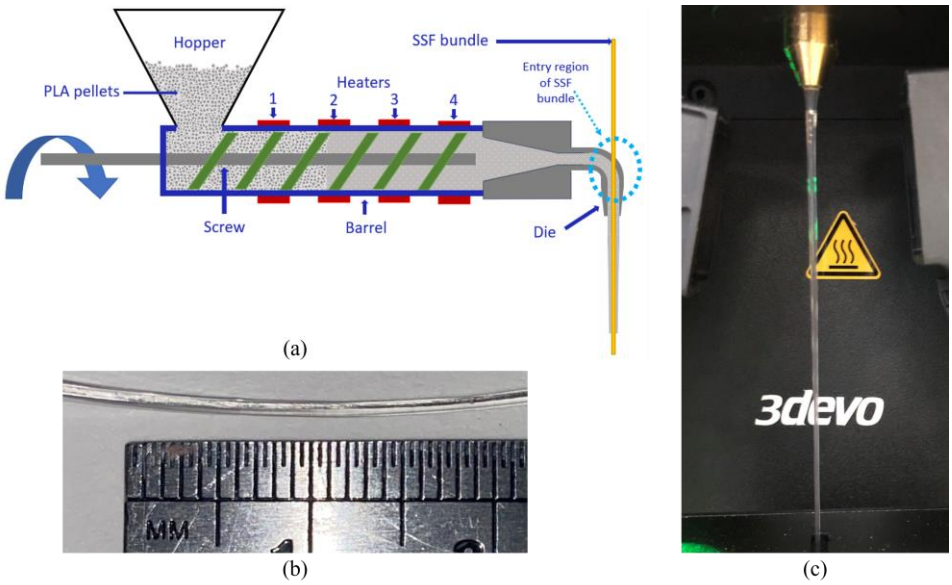


*Figure 3. Schematic of the 3devo filament making (a) with the fibre introduction region indicated by the blue dashed ovals , (b) fabricated PLA-SSF 0.9 mm diameter filament and (c) photograph of the PLA-SSF filament co-extrusion.*

*3.2.2 3D printing*

The components geometries are created in a computer-aided design (CAD) file with Solidworks 2021 software then exported as a stereolithography (STL) file. Open-source slicing software PrusaSlicer is used to slice the STL file generating the g-code for 3D printing.

To successful deposit the PLA-SSF composite parts exhibiting relatively low porosity along with a homogeneous structure, a range of processing parameters were optimised including the software, temperatures, layer height (h), path width (w) Fig 4 (a), speed, and cooling, detailed in Table 3. Testing samples are 3D printed in a unidirectional continuous pattern (0°).

An observation during printing is print ‘stringing’ highlighted by the pink dashed ovals for the SSF-PLA print shown in Fig 4(b). Two reasons account for this, are the layer height which is restricted by filament diameter in addition to the short dwell time.

*3.2.3 PLA-SSF 3D printing: Single samples*

During printing of a range of different part geometries, the PLA-SSF is found to behave differently than other 3D printed continuous fibres (Reverte et al., 2020). The PLA-SSF filament can achieve filament turns of 180° without failing, as show in Figure 4(c). The advantages include reducing printing time and less post processes, such as cutting causing vibrations inducing premature internal failures.

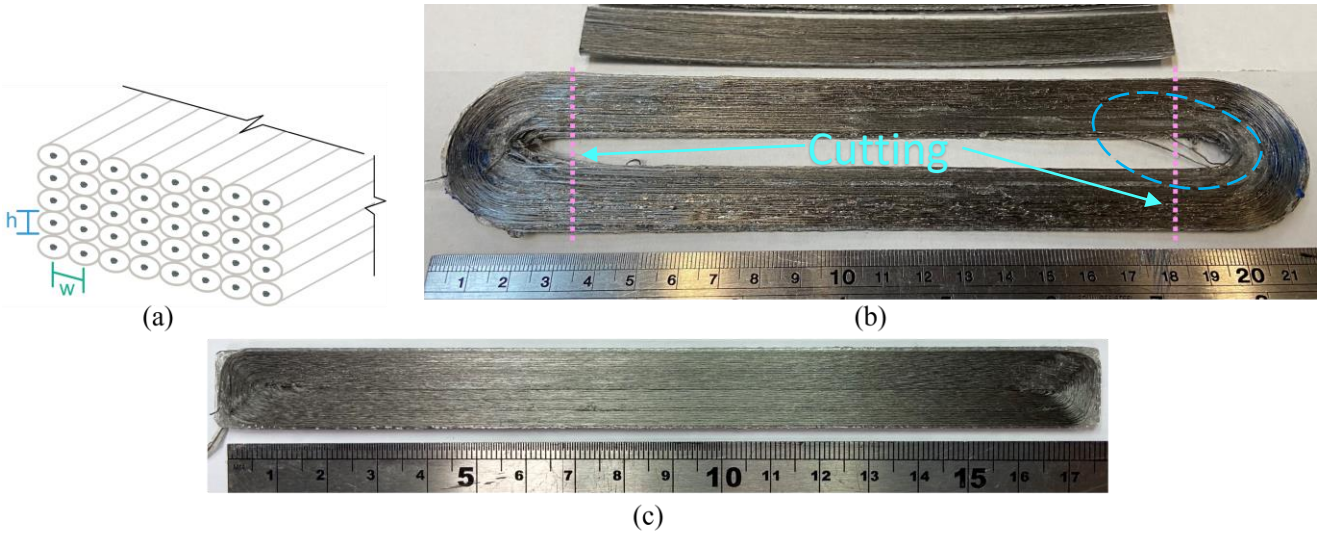


*Figure 4. 3D printing continuous PLA-SSF filament (a) path height and width, (b) Loop geometry, and (c) single tensile sample t35 set*

*Table 3. Examples of composite 3D printing parameters*

| PLA-SSF | Filament Diameter (mm) | Layer Height (mm) | Layer Width (mm) | Speed (mm/s) | $T_{Nozzle}$ (° C) |
|---|---|---|---|---|---|
| L48 (loops) | 0.9-0.7 | 0.48 | 0.8 | 6 | 215 |
| S45 | 0.7 | 0.45 | 0.6 | 4 | 215 |
| S35 | 0.5-0.6 | 0.35 | 0.4 | 5 | 215 |

### *3.3 Characterisation*

The print morphology is examined using a metallurgical microscope and scanning electron microscope (SEM). The porosity and internal structure of the 3D printed components was evaluated using a Computed Tomography (µmCT) scanner, while VG Studios software facility the quantitative measurements. The volume fraction ($\boldsymbol{V_f}$) and the number of fibres in an SSF is also determined using ImageJ and CT scans. The $\boldsymbol{V_f}$ is calculated using equation 1.

$$\boldsymbol{V_f} = \frac{\boldsymbol{A_{SSF}}}{\boldsymbol{A_T}} \tag{1}$$

Where: $A_{SSF}$ is the total cross sectional area of the stainless steel fibres in the bundle and $A_T$ is the overall cross sectional area. The porosity and $V_f$ analysis use different threshold settings to identify the materials. The images include multiple cross-sections of the PLA-SSF filament of at least three separate 3D printed components. The porosity measurements based on CT scan results were cross-referenced with cross sectional microscopy images.

### *3.4 Mechanical performance*

The mechanical performance of the PLA-SSF composites was assessed based on both interlaminar shear strength following the ASTM D2344 and the tensile properties following ASTM D5082 guidance (ASTM, 2002; ASTM D2344, 2003). Tests are conducted using a Zwick Roell Z005 and Lloyd 6000S mechanical testers, with a 10kN and 30kN load cells, respectfully. All tests are performed at room temperature, in atmospheric conditions. Each set consists of at least five specimens.

*3.4.1 Interlaminar shear strength - ILSS*

The interlaminar shear strength (ILSS) or short beam testing is used to investigate cohesion between different material combinations A schematic of the ILSS testing rig shown in Fig. 6. The short beam test is performed at a speed of 1mm/min, (Figure 5).

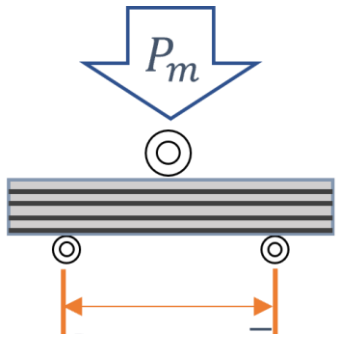


*Figure 6. IILSS testing rig schematic*

Samples are cut to length using a precision saw (Buehler IsometTM High-Speed Pro) and dimensionally shaped using a water grinding wheel. The ILSS sample size is defined by the thickness of the sample (h), the width (b) as 2 x thickness and length (l) as 6 x thickness, final dimensions are 3mm x 6mm x 18mm and beam span S as 12 mm, Fig. 7(b). ILSS strength, $\tau ILSS$, is calculated by using equation 2:

*Figure 5. ILSS PLA-SSF testing*

$$\tau ILSS = \frac{3}{4}\frac{P_m}{b \times h} \qquad (2)$$

Where: $P_m$ is the maximum load or failure load (N), $b$ is the height and $h$ is the width.

*3.4.2 Tensile testing*

The tensile strength and tensile modulus are properties were determined. Samples preparation includes cutting to size from loop prints and grinding to shapes. The final test sample dimensions are 3mm x 15mm x 175mm, with a gauge length of approximately 60 mm as described in Fig 7(a).

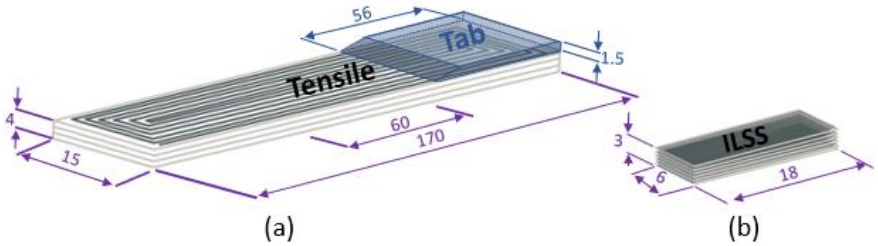


*Figure 7. PLA-SSF 3D printed (a) Tensile sample and tab dimensions and (b) ILSS dimensions*

*Figure 8. S35 PLA-SSF prepared tensile sample set of five samples*

Tabs are bonded to each end and sides of the tensile samples using Loctite 480 Cyanoacrylate. A prepared set of S35 tensile samples are shown in Fig. 8, The PLA-SSF tensile strength ($F_{tu}$) is calculated using equations 4.

$$F_{tu} = \frac{P_{max}}{A} \qquad (4)$$

Where: $P_{max}$ is the maximum force at failure and A is the cross-sectional area. A minimum of five test samples were evaluated under each test condition.

## 4. RESULTS

### *4.1 Geometry analysis*

An example of an optical microscope image of a cross section of an 3D printed tensile sample is given in Figure 9, with each SSF showing as a reflective metallic surface, embedded in the PLA matrix. The perimeter of the SSF bundle exhibits good impregnation and bonding with the PLA matrix. Each SSF bundle retains the circular or oval shape due to the flat sides of each octagonal fibre.


*Figure 9. PLA-SSF 3D printed L41 tensile sample cross-section, Olympus DSX1000 microscope*

A further optimisation of the 3D printing process facilitated higher steel fibre content and lowered porosity in the PLA-SSF structure. This was demonstrated based on SEM examination of printed composite cross sections as shown in Figure 10(a). This demonstrates the impregnation of the PLA matrix into the fibre bundle yielding an improved dispersion of the metal fibres in the composite matrix. Figure 10(b) helps to demonstrate the impregnation of the PLA polymer between the individual fibres. Note that some breakage of polymer is also observed due to the grinding and polishing action, associated with sample preparation.

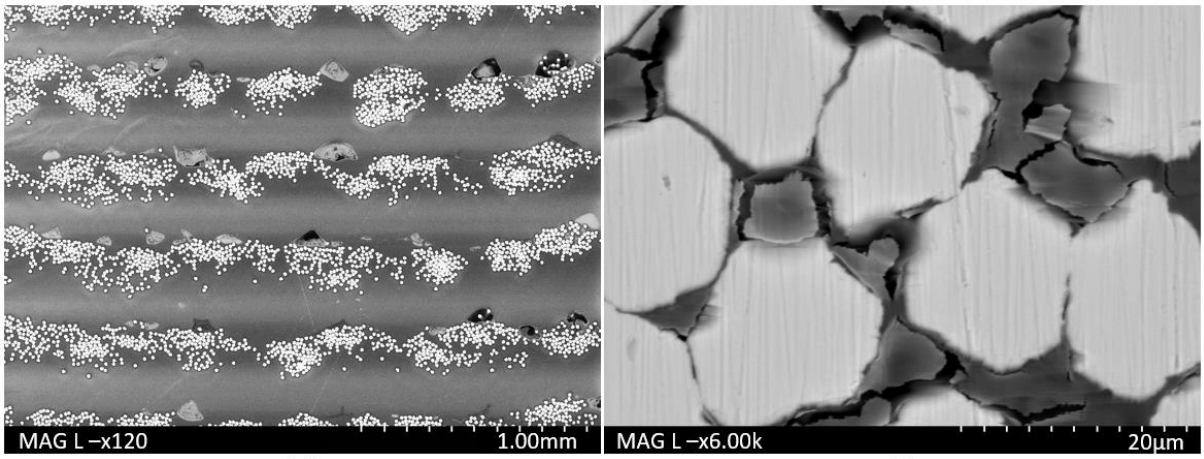


*Figure 10. SEM cross-section images of printed PLA-SSF structure (a) demonstrating the improved dispersion of the fibre filaments in the composite matrix and (b) close-up view demonstrating good diffusion of the PLA into the SSF bundle*

### *4.2 Porosity and volume fraction*

CT scanning along with the examination of composite cross sections using, SEM and optical microscopy were used to evaluate the level of porosity. Table 4 details the porosity results obtained for two of the test samples evaluated (S45 and S35).

*Table 4. Typical volume fraction and porosity results obtained for the printed PLA-SSF composites obtained using CT analysis*

| PLA – SSF Sample | Volume Fraction ($V_f$) | Porosity |
|---|---|---|
| S45 | 7% | 12% |
| S35 | 12% | 6% |

The cross-sectional view in Fig. 11(a) shows the layering of the SSF within the 3D printed structure. Due to the printing pattern used, an increase in porosity is observed around the central region of the composite. Figure 11(b) captures a single layer and longitudinal deposition of each line of PLS-SSF filament. A 3D view of the CT scanned PLA-SSF sample volume shown in Fig. 11(c), demonstrates the uniform steel fibre arrangement. Porosity quantity is influenced by the layer thickness (Le Duigou et al., 2020).

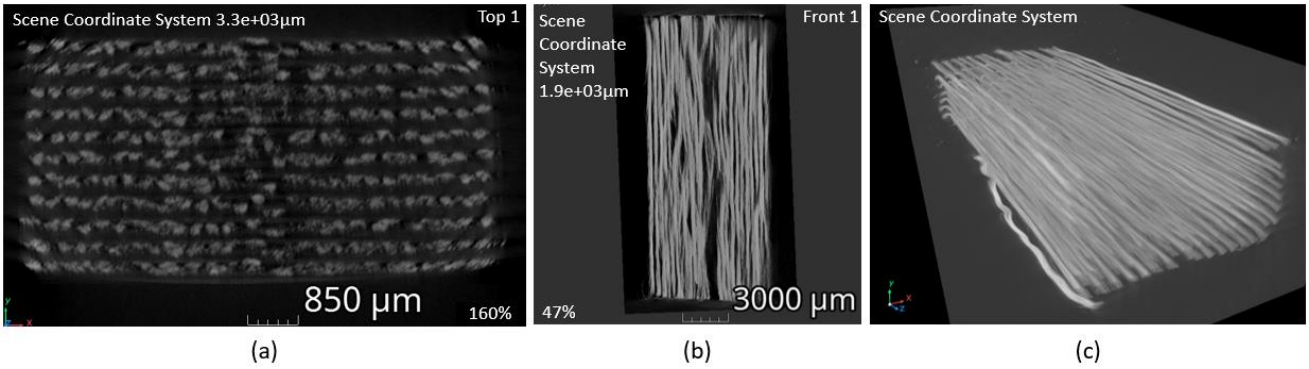


*Figure 11. CT scan of PLA-SSF 3D printed part (a) cross section, (b) longitudinal cross-section and (c) 3D view of SSF in CT scanned volume*

### *4.3 Interlaminar sheer strength*

Interlaminar shear strength (ILSS) testing results are plotted in Figure 12, along with results reported in the literature for 3D printed continuous fibre reinforced PLA composites of glass fibre (PLS-CGF) and carbon fibre (PLA-CF) (Chen et al., 2021; Reverte et al., 2020). The PLA only filament and PLA containing continuous basalt fibres were fabricated and tested at UCD laboratories.

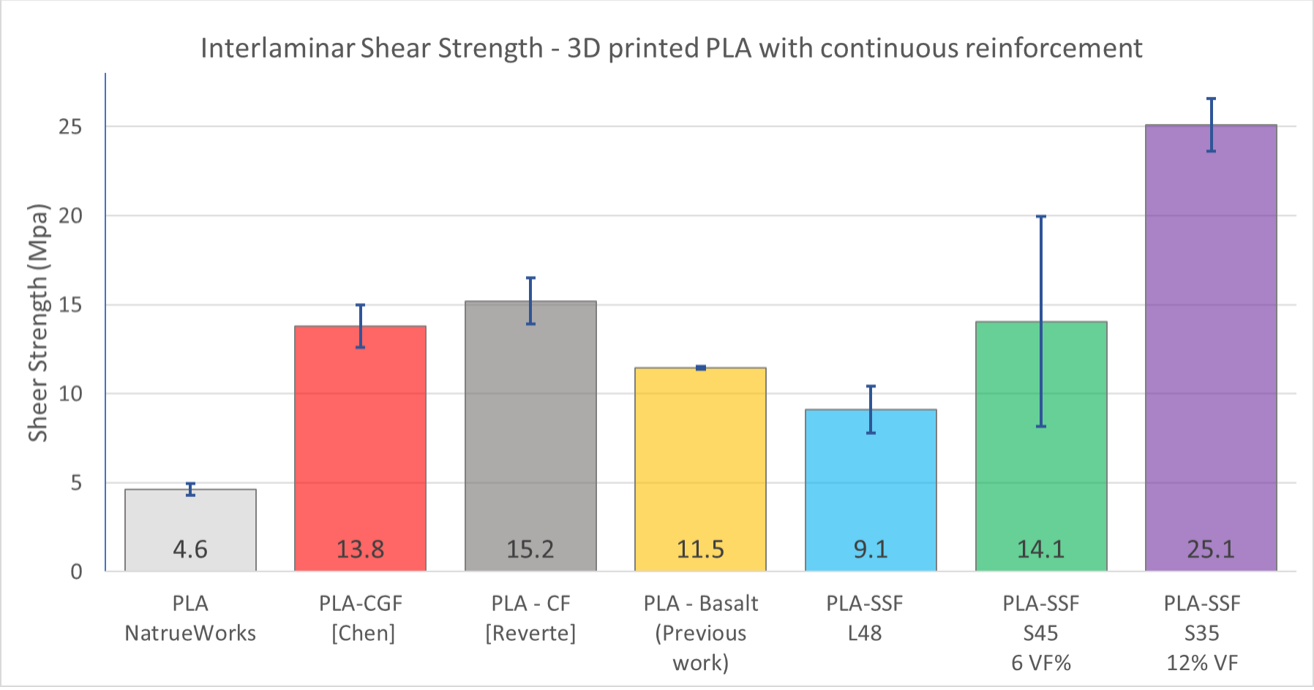


*Figure 12. Interlaminar shear strength results from this study along with those reported in the literature for other fibres*

### 3.4 Tensile testing

The tensile performance properties of PLA and PLA-SSF are plotted in Figure 13, along with the results of a large number of other studies reported in literature for a number of other 3D printed PLA composites (Ferreira et al., 2017; Hamidi & Tadesse, 2019; Nature & Nature, 2007).

The tensile strength of the PLA-SSF is 188 MPa (±20.9) and a tensile modulus of 7.0 GPa (±1.0). Reinforcement materials for PLA include studies on natural fibres, metals, and carbon fibres (continuous and short) (Ibrahim, 2019; Le Duigou et al., 2020; Matsuzaki et al., 2016; Reverte et al., 2020; Saleh et al., 2019).

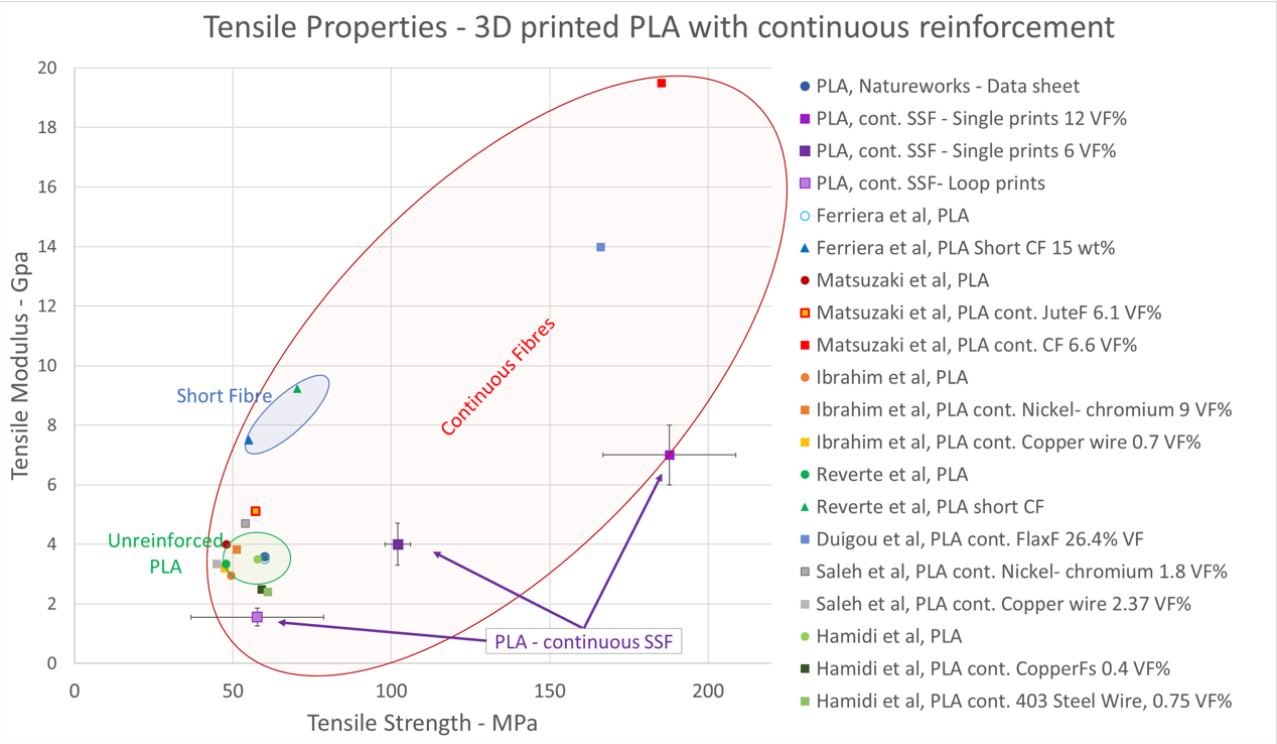


*Figure 13. PLA and reinforced PLA results and literature comparison of tensile properties.*

The PLA-SSF samples tensile strength is three times that of PLA, while the tensile modulus is twice that of the unreinforced polymer. A summary of the volume fraction and tensile strength of some 3D printed reinforced PLA materials are tabulated in table 5.

*Table 5. PLA reinforced materials tensile properties of % strength of PLA-SSF*

| PLA reinforcement | $V_f$ % | Tensile Strength (Mpa) | Reference |
|---|---|---|---|
| Continuous Stainless steel fibre bundle | 12 | 187.8 | This work |
| Continuous Stainless steel fibre bundle | 6 | 102.0 | This work |
| Continuous Flax fibre | 26.4 | 166.0 | (Le Duigou et al., 2020) |
| Continuous Sprint-Back 304 stainless steel wire Wire diameter = 0.1778 mm | 0.8 | 61.0 | (Hamidi & Tadesse, 2019) |
| Continuous Nickel-Chromium Wire diameter = 75 µm | 1.8 | 53.8 | (Saleh et al., 2019) |
| Continuous Nickel-Chromium Wire diameter = 75 µm | 9.0 | 51.2 | (Ibrahim et al., 2018) |
| Continuous Copper wire Wire diameter = 0.127mm | 0.4 | 59.0 | (Hamidi & Tadesse, 2019) |
| Continuous Copper wire Wire diameter = 75 µm | 2.4 | 44.9 | (Saleh et al., 2019) |
| Continuous Copper wire Wire diameter = 75 µm | 0.7 | 47.5 | (Ibrahim et al., 2018) |
| Continuous Carbon Fibre | 6.6 | 185.2 | (Matsuzaki et al., 2016) |
| Short Carbon Fibre | 15 | 53.4 | (Ferreira et al., 2017) |

## 5. DISCUSSION

### *5.1 Interlaminar sheer strength*

PLA's ILSS mode of failure was observed to be by tensile fracture with minimum shearing observed between the layers. The interlaminar shear strength of the PLA-SSF is found to be 25.1 MPa (±1.5). The SSF reinforcement with a volume fraction of 12 % shows a fivefold improvement over that obtained for PLA only. A factor influencing this improvement is good adhesion and impregnation of the PLA with the SSF bundle, the quantity of SSF in the sample and low porosity helping to reduce reducing crack propagation sites.

An image of a sample side profile before ILSS testing is shown in the SEM image in Fig 14(a). The same sample is captured after ILSS testing in Fig 14(b), the fractured samples demonstrated the tensile fracture failure mode. The Fig 14(c) and 14(d) SEM images demonstrate good impregnation and adhesion of the PLA matrix into the SSF. Also illustrated are individual SS fibre pull-out, SS fibre necking and bounce back. Bounce back is where a fibre pulls out of the matrix at the point of failure. Necking of the individual fibres which have fractured is shown in Fig 14(d), where a portion of the fibres in the SSF fractured close to the PLA fractured surface and others have pulled out of the matrix before failure.

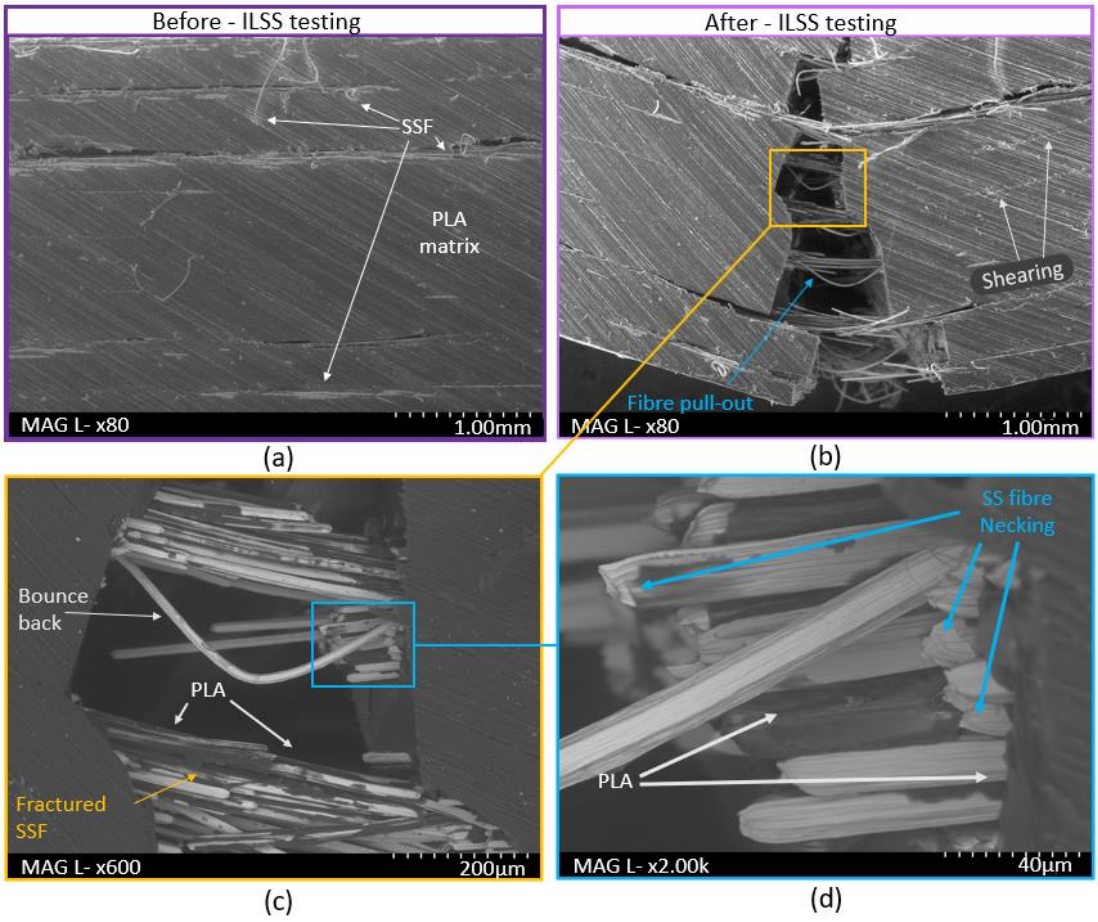


*Figure 14. ILSS sample (a) prior to testing, (b) Interlaminar sheering and tensile fracture, (c) Fibre pull out and necking and (d) SSF necking and extension.*

### *5.2 Tensile testing*

The highest volume fraction of 26.4% as shown in Figure 13 is for a 3D printed composited formed using PLA-flax, which has significantly improved the tensile properties of PLA only polymer. This infers that increasing the SS fibre content in the PLA could potentially improve tensile properties. PLA-SSF tensile strength and modulus values show the highest values for all the metal reinforcements. It is concluded from the results shown in Figure 13, that the higher the volume of fibre within the composites, the higher the strength.

After tensile testing, the fractured surface is investigated using SEM, as demonstrated in Figure 15 for a cross-section of an SSF bundle within the PLA matrix after tensile testing. There is good adhesion between the PLA and SS fibres is good around most, however, some fibre pull-out is seen in Fig 15(a), where impregnation into the middle of the bundle is low leading to voids or porosity in the structure. Every SS fibre displays necking even if the SS fibre is pulled out of the PLA matrix. The fibres in Figure 15(b) all failed at the surface, inferring a good bond between the materials.

Gaps in the PLA around a number of the SS fibres can be due to elongations and cross sectional shrinkage of the fibre experienced during necking before ultimate failure. PLA is stiffer than the SSF and failure is brittle, this leaves what appears like a 'popped bubble' surface on the PLA's fractured surface.

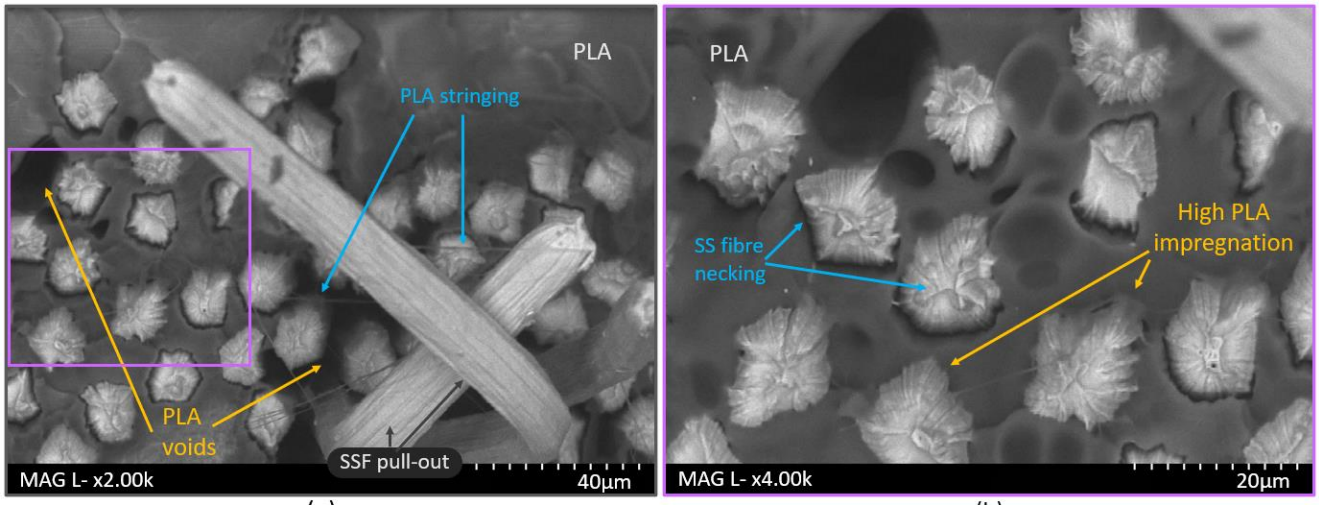


*Figure 15. SEM of SSF bundle after tensile testing, (a) note the 'pull-out' of the 14 µm diameter filaments and (b) SS fibre necking and high impregnation around the SS fibres*

## 6. CONCLUSION

Filaments of continuous stainless steel fibre bundles within a polylactic acid (PLA) polymer were fabricated. These filaments were then used to 3D print composites by fused filament fabrication. The printed composites exhibited a fibre volume fraction between 7% and 12%. Good impregnation and adhesion of the PLA matrix into the stainless steel fibre were found based on a CT analysis, with porosity as low as 6%. Interlaminar shear strength of the PLA-SSF with a volume fraction of 12% is found to be 25.1 MPa (±1.5). The interlaminar shear strength of the fibre reinforced composite was over four time that of PLA only prints. Tensile properties of the PLA-SSF have the highest mechanical strength with respect to metal fibre reinforced composites, reported in literature. Tensile strength and a tensile modulus of 188 MPa (±20.9) and 7.0 GPa (±1.0) respectfully. A significant improvement to the PLA tensile properties. The potential applications for a 3D printed reinforced polymer with SSF are very considerable based on the composites unique material properties, in addition to having the sustainability advantage of being potentially recyclable.

## 5. REFERENCES

ASTM, D. (2002). Standard Test Method for Tensile Properties of Reinforced Thermosetting Plastics. *ASTM Standards*, *June*, 1–9. https://doi.org/10.1520/D5083-17.1

ASTM D2344. (2003). ASTM D2344/D2344M: Standard Test Method for Short-Beam Strength of Polymer Matrix Composite Materials and Their Laminates. *Annual Book of ASTM Standards*, *3*(2), 136–140.

Baerdemaeker, J. De, & Vleurinck, J. (2017). An Introduction to Metal Fibre Technology. *Whitepaper*, 1–9.

Baerdemaeker, J. De, & Vleurinck, J. (2018). *Whitepaper 2 Overview Metal Fibers Applications EN.PDF*.

Beckman, I., Lozano, C., Freeman, E., & Riveros, G. (2021). Fiber Selection for Reinforced Additive

Manufacturing. *Polymers*, 1–53.
Botelho, E. C., Figiel, Rezende, M. C., & Lauke, B. (2003). Mechanical behavior of carbon fiber reinforced polyamide composites. *Composites Science and Technology*, *63*(13), 1843–1855. https://doi.org/10.1016/S0266-3538(03)00119-2
Chen, K., Yu, L., Cui, Y., Jia, M., & Pan, K. (2021). Optimization of printing parameters of 3D-printed continuous glass fiber reinforced polylactic acid composites. *Thin-Walled Structures*, *164*(November 2020), 107717. https://doi.org/10.1016/j.tws.2021.107717
Dickson, A. N., Abourayana, H. M., & Dowling, D. P. (2020). 3D printing of fibre-reinforced thermoplastic composites using fused filament fabrication-A review. *Polymers*, *12*(10), 1–20. https://doi.org/10.3390/POLYM12102188
Dickson, A. N., Ross, K. A., & Dowling, D. P. (2018). Additive manufacturing of woven carbon fibre polymer composites. *Composite Structures*, *206*(July), 637–643. https://doi.org/10.1016/j.compstruct.2018.08.091
Dowling, D. P., Abourayana, H. M., Brantseva, T., Antonov, A., & Dobbyn, P. J. (2020). Enhancing the mechanical performance of 3D-printed basalt fiber-reinforced composites using in-line atmospheric plasma pretreatments. *Plasma Processes and Polymers*, *17*(1), 1–8. https://doi.org/10.1002/ppap.201900143
Ferreira, R. T. L., Amatte, I. C., Dutra, T. A., & Bürger, D. (2017). Experimental characterization and micrography of 3D printed PLA and PLA reinforced with short carbon fibers. *Composites Part B: Engineering*, *124*, 88–100. https://doi.org/10.1016/j.compositesb.2017.05.013
Galvele, J. R. (1976). Transport Processes and the Mechanism of Pitting of Metals. *Journal of The Electrochemical Society*, *123*(4), 464–474. https://doi.org/10.1149/1.2132857
Goh, G. D., Dikshit, V., Nagalingam, A. P., Goh, G. L., Agarwala, S., Sing, S. L., Wei, J., & Yeong, W. Y. (2018). Characterization of mechanical properties and fracture mode of additively manufactured carbon fiber and glass fiber reinforced thermoplastics. *Materials and Design*, *137*, 79–89. https://doi.org/10.1016/j.matdes.2017.10.021
Goux, A., & Van Hooreweder, M. (2020). *Metal fibers for HEPA and ULPA filtration*.
Hamidi, A., & Tadesse, Y. (2019). Single step 3D printing of bioinspired structures via metal reinforced thermoplastic and highly stretchable elastomer. *Composite Structures*, *210*(November 2018), 250–261. https://doi.org/10.1016/j.compstruct.2018.11.019
Hu, Q., Duan, Y., Zhang, H., Liu, D., Yan, B., & Peng, F. (2018). Manufacturing and 3D printing of continuous carbon fiber prepreg filament. *Journal of Materials Science*, *53*(3), 1887–1898. https://doi.org/10.1007/s10853-017-1624-2
Ibrahim, Y. (2019). *3D Printing of Continuous Wire Polymer Composite for Mechanical and Thermal Applications*. *February*.
Ibrahim, Y., Melenka, G. W., & Kempers, R. (2018). Fabrication and tensile testing of 3D printed continuous wire polymer composites. *Rapid Prototyping Journal*, *24*(7), 1131–1141. https://doi.org/10.1108/RPJ-11-2017-0222
Küster, K., Barburski, M., Lomov, S. V., & Vanclooster, K. (2018). Metal Fibers-Steel. In *Inorganic and Composite Fibers: Production, Properties, and Applications* (pp. 219–241). https://doi.org/10.1016/B978-0-08-102228-3.00010-4
Le Duigou, A., Chabaud, G., Matsuzaki, R., & Castro, M. (2020). Tailoring the mechanical properties of 3D-printed continuous flax/PLA biocomposites by controlling the slicing parameters. *Composites Part B: Engineering*, *203*(July), 108474. https://doi.org/10.1016/j.compositesb.2020.108474
Mahltig, B. (2018). Introduction to Inorganic Fibers. In *Inorganic and Composite Fibers: Production, Properties, and Applications* (Issue 105, pp. 1–29). Elsevier Ltd. https://doi.org/10.1016/B978-0-08-102228-3.00004-9
Markforged. (2018). H13 Tool Steel. *Material Datasheet*, 1. http://www.astmsteel.com/product/h13-tool-steel-x40crmov5-1-skd61-hot-work-steel/
Markforged, I. (2020). *Material Datasheet 17-4 PH Stainles Steel*. 1–2.
Markforged Inc. (2021). *Metal X*. *Gen 2*, 1–2. https://www.mark3d.com/en/wp-content/uploads/sites/6/2021/01/MetalX_Spec_Flyer_Januar2021_web.pdf
Matsuzaki, R., Ueda, M., Namiki, M., Jeong, T. K., Asahara, H., Horiguchi, K., Nakamura, T., Todoroki, A., & Hirano, Y. (2016). Three-dimensional printing of continuous-fiber composites by in-nozzle impregnation. *Scientific Reports*, *6*(December 2015), 1–8. https://doi.org/10.1038/srep23058
Naga Kiran, S. D., Jayakumar, V., & Madhu, S. (2019). Evaluation of Mechanical Characterization of CFRP

Reinforced Stainless Steel (SS304) Wire Mesh Polymer Composite. *IOP Conference Series: Materials Science and Engineering*, *574*(1). https://doi.org/10.1088/1757-899X/574/1/012024

Nature, G. B., & Nature, G. B. (2007). Chapter 17 New technologies. *Pergamon Materials Series*, *11*, 475–517. https://doi.org/10.1016/S1470-1804(07)80021-6

NatureWorks. (n.d.). *Ingeo ™ Biopolymer 3D850 Technical Data Sheet 3D Printing Monofilament – General Purpose Grade*. *4*, 1–4.

Ozen, M. S., Sancak, E., & Akalin, M. (2015). The effect of needle-punched nonwoven fabric thickness on electromagnetic shielding effectiveness. *Textile Research Journal*, *85*(8), 804–815. https://doi.org/10.1177/0040517514555794

Pandelidi, C., Bateman, S., Piegert, S., Hoehner, R., Kelbassa, I., & Brandt, M. (2021). The technology of continuous fibre-reinforced polymers: a review on extrusion additive manufacturing methods. *International Journal of Advanced Manufacturing Technology*, *113*(11–12), 3057–3077. https://doi.org/10.1007/s00170-021-06837-6

Quan, D., Flynn, S., Artuso, M., Murphy, N., Rouge, C., & Ivanković, A. (2019). Interlaminar fracture toughness of CFRPs interleaved with stainless steel fibres. *Composite Structures*, *210*(1), 49–56. https://doi.org/10.1016/j.compstruct.2018.11.016

Rafiee, M., Farahani, R. D., & Therriault, D. (2020). Multi-Material 3D and 4D Printing: A Survey. *Advanced Science*, *7*(12), 1–26. https://doi.org/10.1002/advs.201902307

Reverte, J. M., Caminero, M. ángel, Chacón, J. M., García-Plaza, E., Núñez, P. J., & Becar, J. P. (2020). Mechanical and geometric performance of PLA-based polymer composites processed by the fused filament fabrication additive manufacturing technique. *Materials*, *13*(8). https://doi.org/10.3390/MA13081924

Ryan, M. P., Williams, D. E., Chater, R. J., Hutton, B. M., & McPhail, D. S. (2002). Why stainless steel corrodes. *Nature*, *415*(6873), 770–774. https://doi.org/10.1038/415770a

Saleh, M. A., Kempers, R., & Melenka, G. W. (2019). 3D printed continuous wire polymer composites strain sensors for structural health monitoring. *Smart Materials and Structures*, *28*(10). https://doi.org/10.1088/1361-665X/aafdef

Tekinalp, H. L., Kunc, V., Velez-Garcia, G. M., Duty, C. E., Love, L. J., Naskar, A. K., Blue, C. A., & Ozcan, S. (2014). Highly oriented carbon fiber-polymer composites via additive manufacturing. *Composites Science and Technology*, *105*, 144–150. https://doi.org/10.1016/j.compscitech.2014.10.009

Tunakova, V., Tunak, M., Bajzik, V., Ocheretna, L., Arabuli, S., Kyzymchuk, O., & Vlasenko, V. (2020). Hybrid knitted fabric for electromagnetic radiation shielding. *Journal of Engineered Fibers and Fabrics*, *15*. https://doi.org/10.1177/1558925020925397

Verlinden, B., Driver, J., Samajdar, I., & Doherty, R. D. (2007). Microstructure and Properties. In B. Verlinden, J. Diver, I. Samajdar, & R. D. Doherty (Eds.), *Pergamon Materials Series* (Vol. 2, Issue 2, pp. 9–30). Pergamon. https://doi.org/10.1016/S1470-1804(07)80015-0

Zhuo, P., Li, S., Ashcroft, I. A., & Jones, A. I. (2021). Material extrusion additive manufacturing of continuous fibre reinforced polymer matrix composites: A review and outlook. *Composites Part B: Engineering*, *224*(July), 109143. https://doi.org/10.1016/j.compositesb.2021.109143

# Examining the Quality of New and Reused Powder in the Powder Bed Fusion Process via Optical Microscopy

Courtney Gallagher, Ulster University
Ryan Harkin, Ulster University
Emmett Kerr, Ulster University
Shaun McFadden, Ulster University

***Abstract***

The quality of the powder used in Laser-based Powder Bed Fusion (L-PBF) additive manufacturing processes plays a key role in the properties of the fabricated part. The particle size distribution (PSD) and morphology of the powder particles affects the flowability of the powder and can adversely affect the quality of the final part. Ti6Al4V powder for additive manufacturing processes is relatively expensive, making L-PBF a costly process. One method of reducing the associated costs by making the process more sustainable is to reuse unconsolidated powder from the breakout step of a prior build for subsequent part builds. However, reused powder will have been exposed to the environment of the L-PBF build chamber and spatter particles from the L-PBF melt pool leads to the formation of partially-melted and agglomerated particles. Composition assessment of the powder quality is required between powder re-use cycles to ensure it remains within specification for subsequent part builds, however, the Inert Gas Fusion method used for detecting interstitial elements at these very low composition thresholds is not typically available at the manufacturing premises. Industry, therefore, requires an effective and low-cost proxy method of assessing powder quality. Two different sample preparation techniques are used in this investigation to obtain digital images of Ti6Al4V powder in the virgin state and of the sieve-captured powders after seven reuse cycles. This paper provides an overview of changes in powder properties between virgin powder and the sieve-captured powders after seven reuses. A discussion of the advantages and limitations of both powder preparation and imaging techniques is provided. It is proposed that the development of optical-based image analysis techniques can be used to get a reasonable classification of powder quality for the L-PBF process.

*Key Words: Powder Characterisation, Ti6Al4V, Additive Manufacturing, Laser Powder Bed Fusion.*

## 1. INTRODUCTION

Additive manufacturing powders have many stringent technical requirements for good manufacturability and are therefore expensive. To facilitate economical use of the powders they must be reused, however, this creates several issues. The technical requirements include the need for the powder to have the correct composition, a well-graded Particle Size Distribution (PSD), spherical morphology, and low porosity, to name a few. A well-graded PSD and spherical morphology are desired to ensure good flowability in order to allow for a thin layer of powder to be uniformly spread over the powder bed during the recoating stage of the PBF process (Brika et al., 2020). Powder feedstock additive manufacturing processes enable highly intricate parts to be manufactured and are particularly attractive in the aerospace, medical and automotive industries (Harkin et al., 2021; Zhang et al., 2021). Currently, Laser-based Powder Bed Fusion (L-PBF) offers the best dimensional accuracy and reproducibility for part production and is well researched within academia and industry (Gordon et al., 2020). Typically, only 10-50% of the powder within the build chamber is used in the L-PBF process, highlighting the importance of reusing powder across build cycles (Santecchia et al., 2020). The general procedure for part fabrication via L-PBF is as follows:

(i) A layer of metal powder is spread onto the machine build plate by a recoater blade that ensures even distribution and a specified layer thickness (typically 20 to 60 μm (Sun et al., 2018));
(ii) A travelling laser beam selectively melts particles in the desired area of the powder layer, as determined by a CAD model that is post processed by a slicing software;
(iii) The build plate moves down incrementally to allow the next layer of powder to be spread on the build plate; and the process is repeated until part fabrication is completed.

Email: Courtney Gallagher
Gallagher-c64@ulster.ac.uk

One of the most widely investigated alloys in metal powder feedstock additive manufacturing is Ti-6wt%Al-4wt%V (Ti6Al4V), which is an α + β titanium alloy that possesses relatively high strength and fracture toughness with relatively low density. The strength-to-weight ratios of Ti6Al4V make it attractive for many applications including structural airframe components (Cui et al., 2011). Ti6Al4V has good biocompatibility and corrosion resistance making it a suitable alloy for medical implants (Hao et al., 2016). Ti6Al4V is available in the market at two grades: Grade 5 and Grade 23. Grade 5 is the standard grade for many structural applications. Grade 23 is also known as the Extra Low Interstitial (ELI) or biomedical grade and has stricter compositional requirements on interstitial elements that go into solid solution, namely hydrogen, carbon, nitrogen and oxygen as these impact the mechanical properties of the alloy by lowering the ductility (Sun et al., 2018).

In L-PBF, the laser impacts the powder aggressively at the micro-scale. Most of the powder particles will be melted by the laser and consolidate the layer, however, some will become spatter particles which are partially melted and ejected from the melt pool. Spatter particles are problematic because they may land in the part, causing defects in the part, or they may land in the adjacent powder, thereby polluting the surrounding unconsolidated powder. This compromises the powder quality as changes in the morphology of the particles can change the flowability of the powder, whilst the presence of internal cavities within the powder particles may lead to defects in the fabricated part (Gordon et al., 2020). Spatter particles need to be removed via a sieving process which typically involves two stages using different mesh sizes, however, it is not guaranteed to remove all spatter particles as some can pass through the mesh.

A question that arises in the classification of powder particles is how to distinguish between the different forms of particle. Powder is expected to come in spherical form but deviations from this ideal morphology are apparent. Nichols et al. (2002) proposed that the term “agglomerate” be used exclusively to describe particle assemblages. Particle morphologies can therefore be divided into primary particles (individual, highly spherical particles) and agglomerated particles. Three subcategories of agglomerated particles are used in this paper: “Satellites” (small particles joined to a larger particle, Figure 1(a)), “Chain-Like Agglomerations” (two or more particles joined to form a chain, Figure 1(b)), and “Cluster Agglomerations” (particles joined together as a cluster, Figure 1(c)).

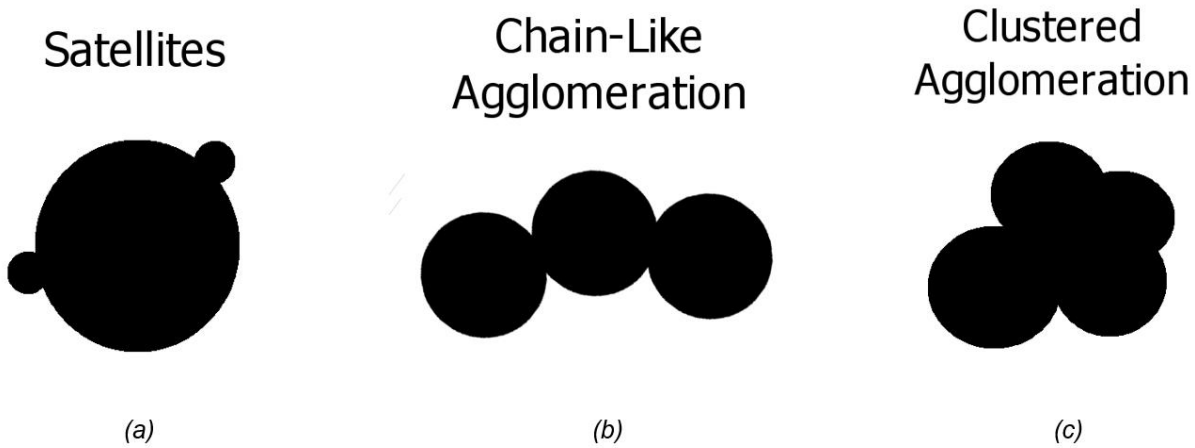


*Figure 1. Morphological representations of (a) satellites, (b) chain-like agglomerations and (c) clustered agglomerations.*

Furthermore, studies have shown that powder composition is affected during the laser fabrication process, primarily an increase in oxygen content is observed (Carrion et al., 2019; Harkin et al., 2022). Hence, oxygen levels can exceed the compositional limit even after a few reuse cycles, especially when the alloy is specified with the grade 23 designation. It is therefore useful to develop powder characterisation methods to quickly and accurately characterise powder properties during reuse cycles to ensure the powder remains within specification. Inert Gas Fusion is required for detecting the presence of interstitial elements and a Scanning Electron Microscope (SEM) is typically used to obtain detailed images of the powder particles. An example of an SEM image of virgin Ti6Al4V powder is provided in Figure 2. Simpler characterisation methods will be beneficial within industry, reducing the time and cost associated with powder analysis. With improved computer image analysis techniques, more information may be extracted by simple metallurgical preparation and digital imaging.

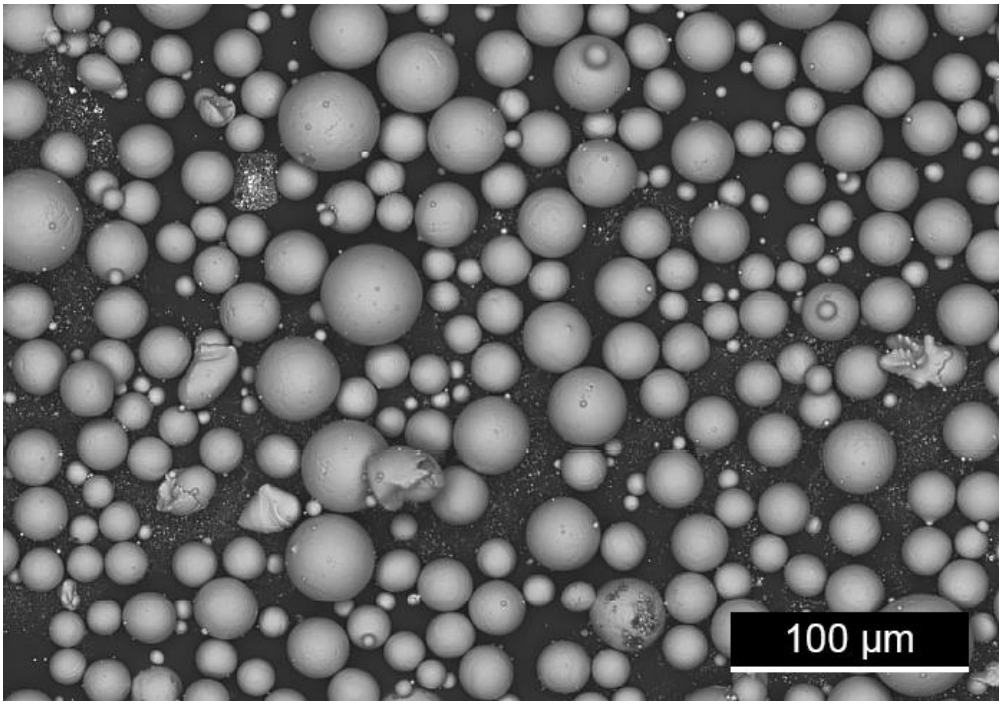


*Figure 2. SEM micrograph depicting the particles of virgin Ti6Al4V powder.*

The aim of this paper is to demonstrate Ti6Al4V powders used in the L-PBF additive manufacturing process and some of the issues that arise through digital imaging using an automatic focus of the powder, as well as cross-sectioning and imaging. A discussion of the advantages and limitations of each method presented is provided.

## 2. MATERIALS AND METHODS

Plasma-atomised ELI (Grade 23) Ti6Al4V powder (Carpenter Additive, Widnes, UK) is investigated in this study. L-PBF fabrication was performed using an MLab Cusing R machine. Part fabrication was performed within an argon enriched atmosphere in which the oxygen levels were kept within the range of 0.1 – 0.2%. A top-up powder reuse strategy was implemented. After each fabrication stage, unconsolidated powder within the build chamber was collected and sieved via a two-stage process using a mechanically vibrating Retsch AS 200 sieve at an amplitude of 60 Hz for 10 mins. The first sieving stage utilised a 63-µm mesh, followed by sieving using a 50-µm mesh. The powder was then topped-up and blended with virgin powder using the 63-µm mesh sieve. Further details about the fabrication process and powder reuse strategy may be found in Harkin et al. (2020, 2021). Three powder samples were taken. The first was a sample of as-supplied virgin powder. The second and third samples were taken from powder captured during the sieving process, after seven reuse cycles: one sample captured from the 63-µm sieve and the other from the 50-µm sieve.

### *2.1 Sample Preparation*

Two different sample preparation methods were used in this investigation: tape-mounted samples and cross-sectioned samples.

#### *2.1.1 Preparation of tape-mounted samples*

Cylinders of Bakelite powder were formed via a hot-mounting press to a depth of approximately 20 mm. A section of double-sided mounting tape was applied to the flat surface of the Bakelite cylinder. A small sample of the loose powder was then deposited onto the double-sided tape. The cylinder was lifted and moved around gently to encourage even spreading of the powder particles over the surface of the double-sided tape. The Bakelite cylinder was then tapped on its curved side to allow any powder which had not adhered to the double-sided tape to drop-off, thereby leaving a thin coating of powder particles on the surface of the tape. This is a similar process to that used for mounting powders for analysis in SEM using conductive tape.

*2.1.2 Cross-sectioned sample preparation*

Samples of collected powder were spread on the sample stage of a hot-mounting press before being back filled with Bakelite powder. The hot mounting press then formed cylindrical samples with the powder sample becoming infiltrated into the Bakelite on the bottom face to a depth of about 100 μm. Each mounted sample was then cut along its axial direction, and repositioned on the hot mount stage with the infiltrated layer of powder at 90 degrees orientation to that of the first mounting cycle. The repositioned sample was then back filled with Bakelite and remounted so that the initial layer of powder became aligned along the axial direction of the cylindrical sample. A schematic diagram depicting this remounting procedure is provided in Figure 3. The reason for cutting and remounting the sample was to minimise the potential of grinding through the entirety of the mounted powder sample, as it is a very thin layer, and in particular to minimise issues associated with grinding out the very small-scale particles that may have settled on the base plate, which is possible even with very low grinding depths. An ATM Saphir 520 semi-automatic grinding and polishing machine was used to perform the grinding and polishing stages. Complementary rotation was used throughout with grinding performed using P2500 SiC paper and fine polishing performed using 1-μm diamond suspension.

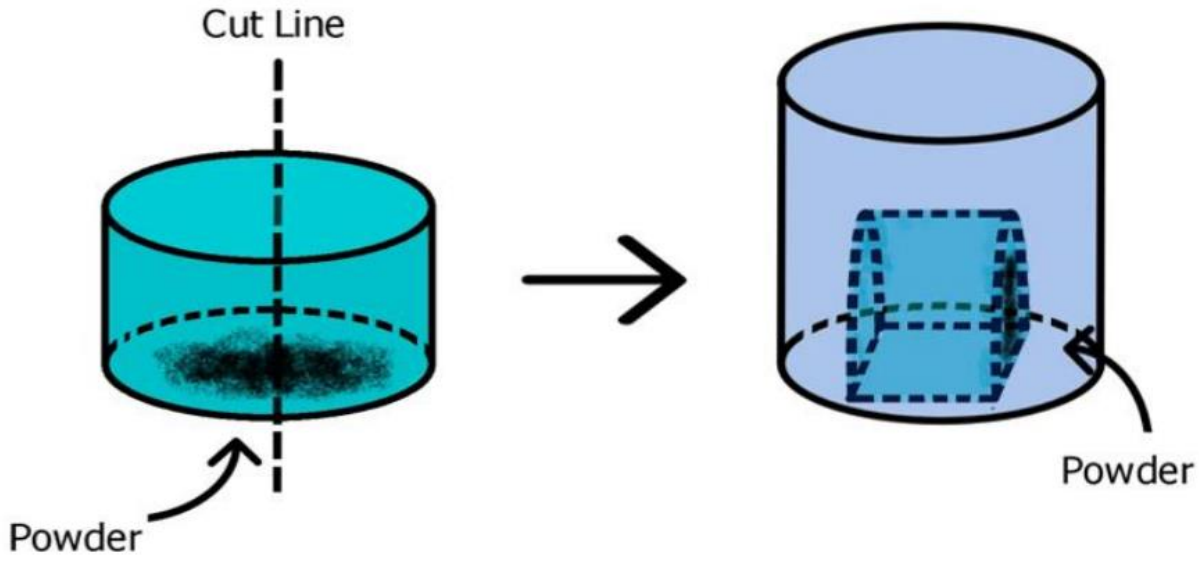


*Figure 3. Schematic diagram depicting the remounting process.*

***2.2 Digital Imaging***

Two methods were used to image the prepared powder samples. For the tape-mounted powder samples, a ZEISS Smartzoom 5 Digital Microscope was used to obtain digital images of the 3D powder particles using mixed coaxial brightfield and ring-light illumination and automatic focusing via telecentric lens. For those samples which had been hot mounted and sectioned, a Leica DMi8 C Inverted Microscope with a fixed lens was used with brightfield illumination to obtain images.

## 3. RESULTS

Figure 4 shows representative images of the virgin powder sample. Figure 4(a) is an image captured using the digital microscope of virgin powder that is tape mounted. Figure 4(b) is an image captured using the inverted microscope of the same powder mounted in Bakelite and cross sectioned as described earlier. Red squares in these images highlight examples of satellite particles. An example of a chain-like agglomerated particle is indicated by the red circle in Figure 4(b). Overall, the primary particles seen in these images are highly spherical/circular.

Figure 5 shows images captured via the inverted microscope of the sieve captured powder samples. Figure 5(a) and Figure 5(b) show powder particles that had been captured by the 63-μm mesh sieve after the seventh reuse cycle. In both these images, a lower proportion of circular primary particles is evident with a significant proportion of agglomerated particles now present. In Figure 5(a), it is observed that a few particles contain

internal gas pores (an example is highlighted by the red circle). In Figure 5(b), a larger PSD range for this sieve-captured powder is seen in the presence of large agglomerated particles and many very small particles.

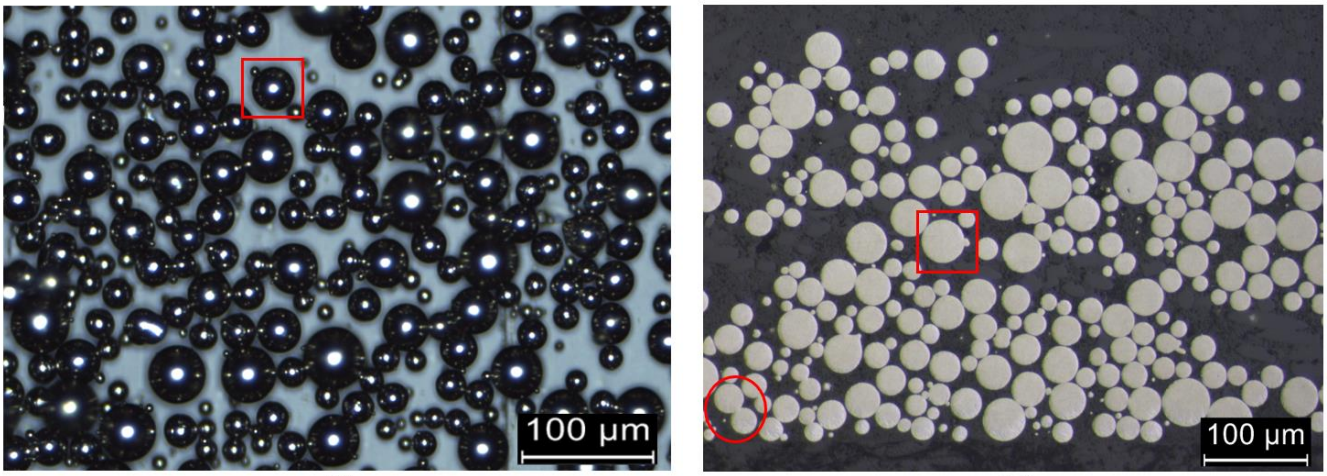


*Figure 4. Digital images of the (a) tape-mounted and (b) cross-sectioned virgin powder sample. Red squares highlight particle satellites and the red circle highlights an example of a chain-like agglomerated particle.*

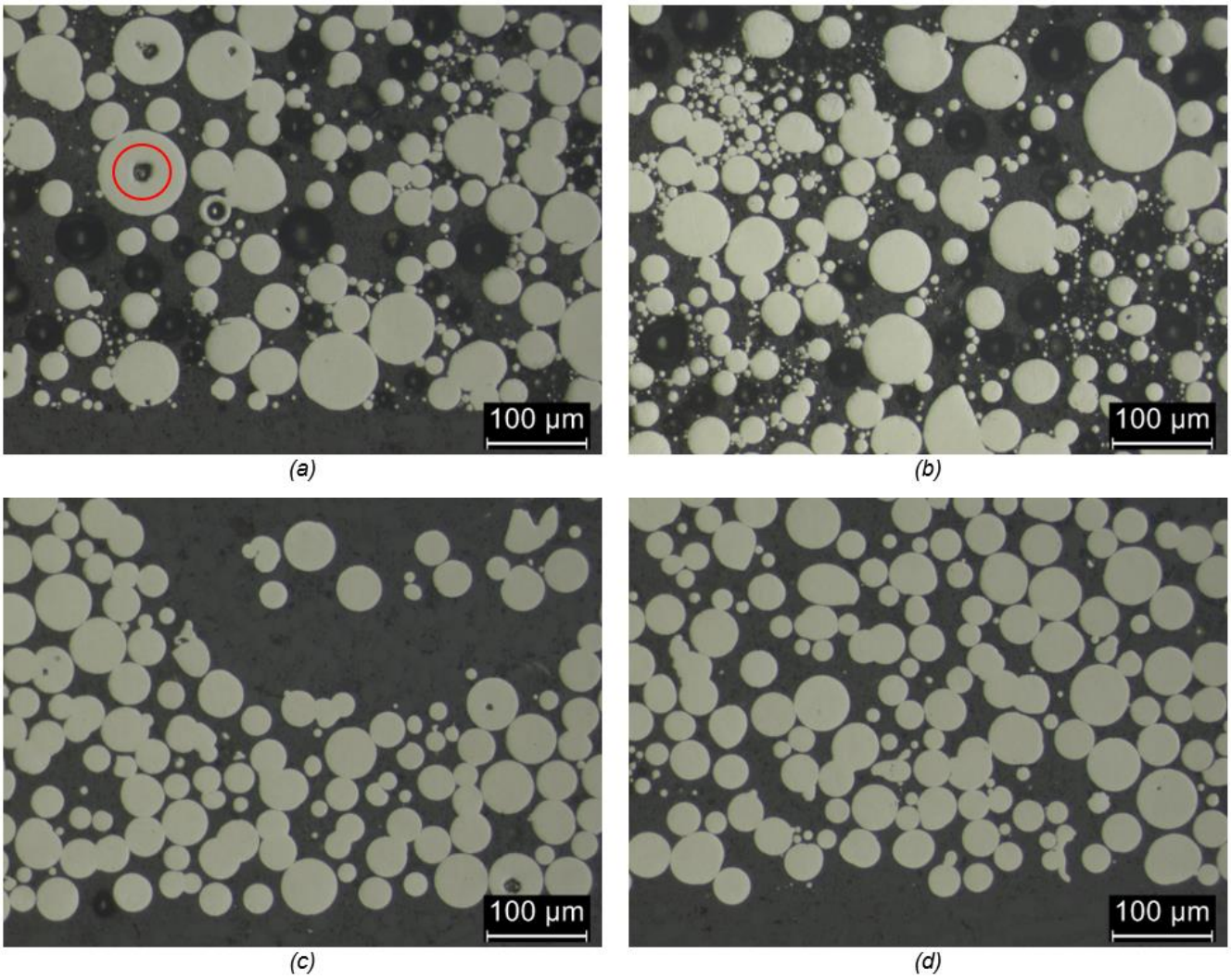


*Figure 5. Cross-sectioned sieve-captured powders from the 63-µm mesh ((a) and (b)) and the 50-µm mesh ((c) and (d)). The red circle in (a) highlights an example of an internal gas pore. All images taken at 200x magnification.*

Images of the cross-sectioned, sieve-captured powder collected from the sieve with a 50-μm mesh are shown in Figure 5(c) and Figure 5(d). It is evident from these images that the powder is returning to a state closer to that of the virgin powder with the presence of some circular primary particles but there are still several agglomerated particles present. There is evidence of internal defects, including porosity, within particles shown in Figure 5(c).

In the images depicting cross-sectioned powder particles (Figure 4(b) and Figure 5(a) – (d)), there are black circles evident (most clearly depicted in Figure 5(a) and Figure 5(b)). These black circles are due to "pull-outs" which are areas in which a powder particle had been embedded within the Bakelite but were extracted during grinding and polishing stages, thereby leaving behind a crater in the Bakelite. These pull outs can be ignored.

## 4. DISCUSSION

In Figure 4(b), showcasing the cross-sectioned virgin powder, the primary particles are highly circular as expected with some evidence of low-order, chain-like agglomerations as depicted by the red circle. In comparison, the images of the cross-sectioned, sieve-captured powders (see Figure 5) clearly show more evidence of agglomeration, in particular, cluster and chain-like agglomerations are evidenced. It is important to ensure removal of as many of these agglomerated particles as possible during powder replenishing procedures as they typically have a detrimental effect on the powder flowability for subsequent build cycles. Due to the presence of the large number of agglomerated particles in the images of the sieve-captured powders (see Figure 5), it can be inferred that the sieving process effectively removes a large proportion of the agglomerated particles that are most likely caused by spatter from the melt pool contaminating the powder bed.

The presence of internal gas porosity is also evident in the cross-sectioned powder images. Gordon et al. (2020) suggested that around 10% of gas pores in the initial powder feedstock can survive the PBF process and present themselves as similar defects in the finished part. Therefore, it is desirable to remove any powder particles with internal porosity. As the gas pores are observed in the larger particles (> 40 μm) removed by sieving, the sieving process should also be beneficial in reducing defects in the final parts.

In previous studies (Harkin et al., 2020, 2021), the oxygen content of these sieve-captured powders was found to be 0.43 wt.% for the 63-μm sieve-captured powder and 0.40 wt.% for the 50-μm sieve-captured powder which are higher than that of the virgin powder (0.095 wt.%) and in fact exceed the maximum thresholds specified for both the Grade 23 and Grade 5 specifications of 0.13 wt.% and 0.2 wt.% respectively. However, the oxygen content returns to below the Grade 23 requirement after sieving and powder replenishment. Detecting the interstitial elements present in the powder at these low composition thresholds is done via Inert Gas Fusion, however many manufacturing premises do not have access to the equipment to conduct this analysis. As the sieve-captured powder samples consist of a large number of agglomerated particles, it may therefore be possible to use the presence of agglomerated particles as a proxy method of determining the powder composition using digital imaging and image analysis techniques.

In relation to digital imaging of the powder samples, it was found that optical imaging of the 3D powder particles mounted on double-sided tape presented issues relating to the presence of glare coming from the light reflecting off the individual powder particles, something that is not an issue when using SEM. This artefact impacts the development of image analysis algorithms to effectively characterise the powder particles, particularly in the segmentation of powder particles in a binarized image. Cross-sectioning of the powder particles via hot-mounting of the powder sample enables identification of internal defects and porosity within individual particles that is not possible with auto-focussed digital imaging. However, this method has limitations as smaller particles may be removed, depending on the depth of the grind, and issues due to 3D particles being viewed in a 2D plane. Particle measurements, such as diameter, are therefore not true to the actual particle size and are instead most likely to be an underestimation of the true particle size. In order to determine the 3D PSD, stereological techniques must be applied to the 2D section size distribution data, such as in the work by Susan (2005). Furthermore, proper classification of primary, agglomerated and satellited particles is required to determine how best to segment the images during image processing to ensure accurate characterisation of powder samples. Table 1 provides an overview of the advantages and drawbacks of each of these digital imaging methods, compared against SEM imaging.

*Table 1. Table outlining the main advantages and disadvantages of each powder imaging method specified.*

| Imaging Method | Advantages | Drawbacks |
|---|---|---|
| SEM | Provides detailed three-dimensional and topographical images, can readily see agglomerated and satellites particles | Expensive, requires highly trained personnel, specialised access |
| Optical imaging of tape-mounted particles | Provides images of the three-dimensional particles, can readily see satellited particles | Issues with glare from reflection of light on particles |
| Optical imaging of cross-sectioned powder samples | Visualise internal defects | Need to apply stereological corrections, potential loss of information due to removal of small particles |

## 5. CONCLUSION

In this paper, Ti6Al4V powders used in L-PBF have been demonstrated and a discussion of some of the issues arising during digital imaging of powder particles using automatic focus, as well as cross-sectioning of powders and imaging using a fixed lens, has been provided with the associated advantages and limitations of each method.

Two different digital imaging techniques were utilised in this paper: imaging of tape-mounted particles and of cross-sectioned particles. The advantages of acquiring images from tape-mounted powder samples are that agglomerated and satellited particles are readily seen and very small particles remain bound to the tape so small-scale information is not lost, but issues arise due to the presence of glare from light reflected off individual powder particles. In comparison, the cross-sectioning method enables analysis of internal features and defects, such as gas porosity, which is unobservable using the tape-mounting method. However, the cross-sectioning method has drawbacks in that smaller particles may be removed depending on the depth of the grind. Issues arise due to the fact 3D particles are observed in a 2D plane. Hence, particle size measurements from the images of the cross-sectioned particles are likely to be an underestimation of the true particle size. It is therefore important to ensure that stereology corrections are accounted for in determining the true size distribution of the powder.

By examining the images, it was found that the morphologies of virgin powder particles were highly spherical in comparison to the sieve-captured powder samples which were compromised by the presence of agglomerated particles. The presence of a high proportion of agglomerated particles in the sieve-captured powders indicates the effectiveness of the sieving process in removing agglomerated and spatter particles which would otherwise have a detrimental effect on powder flowability in subsequent build cycles. Furthermore, the oxygen content in the sieve-captured powders (0.43 wt.% and 0.40 wt.% for the 63-μm and the 50-μm sieve-captured powders respectively) was shown elsewhere to be higher than that of the virgin powder (0.095 wt.%), in fact exceeding the maximum thresholds specified by both Grade 23 (0.13 wt.%) and Grade 5 (0.20 wt.%) designations. It is therefore interesting to investigate if a relationship between the powder composition and the presence of agglomerated particles exists.

Most industrial labs do not have access to highly-specialised equipment such as SEM to image powders, but they typically do have access to simple metallurgical preparation techniques. By developing automatic image analysis algorithms to characterise powders from digital images obtained via digital optical microscopy, industry will benefit from lower-cost, quicker, proxy methods of determining powder properties at various stages in the powder reuse cycles.

## 6. REFERENCES

Brika, S. E., Letenneur, M., Dion, C. A., & Brailovski, V. (2020). Influence of particle morphology and size distribution on the powder flowability and laser powder bed fusion manufacturability of Ti-6Al-4V alloy. *Additive Manufacturing*, *31*(November 2019), 100929. https://doi.org/10.1016/j.addma.2019.100929

Carrion, P. E., Soltani-Tehrani, A., Phan, N., & Shamsaei, N. (2019). Powder Recycling Effects on the Tensile and Fatigue

Behavior of Additively Manufactured Ti-6Al-4V Parts. *Jom*, *71*(3), 963–973. https://doi.org/10.1007/s11837-018-3248-7

Cui, C., Hu, B. M., Zhao, L., & Liu, S. (2011). Titanium alloy production technology, market prospects and industry development. *Materials and Design*, *32*(3), 1684–1691. https://doi.org/10.1016/j.matdes.2010.09.011

Gordon, J. V., Narra, S. P., Cunningham, R. W., Liu, H., Chen, H., Suter, R. M., Beuth, J. L., & Rollett, A. D. (2020). Defect structure process maps for laser powder bed fusion additive manufacturing. *Additive Manufacturing*, *36*, 101552. https://doi.org/10.1016/j.addma.2020.101552

Hao, Y. L., Li, S. J., & Yang, R. (2016). Biomedical titanium alloys and their additive manufacturing. *Rare Metals*, *35*(9), 661–671. https://doi.org/10.1007/s12598-016-0793-5

Harkin, R., Wu, H., Nikam, S., Quinn, J., & McFadden, S. (2020). Reuse of grade 23 ti6al4v powder during the laser-based powder bed fusion process. *Metals*, *10*(12), 1–14. https://doi.org/10.3390/met10121700

Harkin, R., Wu, H., Nikam, S., Quinn, J., & McFadden, S. (2021). Analysis of spatter removal by sieving during a powder-bed fusion manufacturing campaign in grade 23 titanium alloy. *Metals*, *11*(3), 1–13. https://doi.org/10.3390/met11030399

Harkin, R., Wu, H., Nikam, S., Yin, S., Lupoi, R., McKay, W., Walls, P., Quinn, J., & McFadden, S. (2022). Powder Reuse in Laser-Based Powder Bed Fusion of Ti6Al4V—Changes in Mechanical Properties during a Powder Top-Up Regime. *Materials*, *15*(6). https://doi.org/10.3390/ma15062238

Nichols, G., Byard, S., Bloxham, M. J., Botterill, J., Dawson, N. J., Dennis, A., Diart, V., North, N. C., & Sherwood, J. D. (2002). A review of the terms agglomerate and aggregate with a recommendation for nomenclature used in powder and particle characterization. *Journal of Pharmaceutical Sciences*, *91*(10), 2103–2109. https://doi.org/10.1002/jps.10191

Santecchia, E., Spigarelli, S., & Cabibbo, M. (2020). Material reuse in laser powder bed fusion: Side effects of the laser—metal powder interaction. *Metals*, *10*(3), 1–21. https://doi.org/10.3390/met10030341

Sun, Y., Aindow, M., & Hebert, R. J. (2018). Comparison of virgin Ti-6Al-4V powders for additive manufacturing. *Additive Manufacturing*, *21*(April 2017), 544–555. https://doi.org/10.1016/j.addma.2018.02.011

Susan, D. (2005). Stereological analysis of spherical particles: Experimental assessment and comparison to laser diffraction. *Metallurgical and Materials Transactions A: Physical Metallurgy and Materials Science*, *36*(9), 2481–2492. https://doi.org/10.1007/s11661-005-0122-3

Zhang, J., Habibnejad-korayem, M., Liu, Z., Lyu, T., Sun, Q., & Zou, Y. (2021). A Computer Vision Approach to Evaluate Powder Flowability for Metal Additive Manufacturing. *Integrating Materials and Manufacturing Innovation*. https://doi.org/10.1007/s40192-021-00226-3

# A novel approach for the measurement of the roughness of overhang structures printed using additive manufacturing

John Power, I-Form Centre, School of Mechanical and Materials Engineering, UCD, Belfield, Dublin 4
Mark Hartnett, Irish Manufacturing Research, Block A, Collegeland, Rathcoole, Co. Dublin, D24 WC04
Owen Humphreys, I-Form Centre, School of Mechanical and Materials Engineering, UCD, Belfield, Dublin 4
Darragh Egan, I-Form Centre, School of Mechanical and Materials Engineering, UCD, Belfield, Dublin 4
Denis P. Dowling, I-Form Centre, School of Mechanical and Materials Engineering, UCD, Belfield, Dublin 4

***Abstract***

Additive manufacturing (AM) is widely used in the fabrication of metallic parts in sectors such as medical devices and aerospace. One key characteristic used to measure the quality of an AM produced part is the roughness of the printed alloy surface. Conventional methods for measuring roughness, such as the stylus and optical profilometer, have considerable difficulty obtaining measurements on difficult to access geometric features, such as overhang structures. In this work, a Line Edge Roughness (LER) approach is evaluated to provide a quantitative assessment of the roughness of printed alloy parts. The LER technique quantitatively defines the roughness of a printed part edge based on an analysis of ImageJ software data obtained from cross-section microscopy images of that edge. The measurements were obtained from cross-section optical microscopy images of Ti-6Al-4V overhang features, printed using the laser powder bed fusion technique. The printing was carried out using laser powers in the range of 7 to 200 W, in order to investigate the effect of laser energy on the roughness of the resulting overhang features. The roughness measurements were assessed based on the deviation from an ideal shape. At higher laser powers during printing, an increase in the roughness of the part was observed, probably due to overheating of the meltpool. This is likely to be associated with the reduced ability of the powder particles directly underneath the overhang structure to remove heat due to the lower thermal conductivity of powder particles compared with the solid alloy structure. The LER method was evaluated by comparing its measurements to those obtained optical profilometry measurements of the same sample surfaces. Both measurement methods identified a similar trend, with an increase in the roughness of the overhang structure as the laser energy used to print the overhang layers increased. Furthermore, the LER method can facilitate the identification of defects that would remain hidden due to the line of sight limitation of optical profilometry measurements.

*Key Words: Additive Manufacturing, Roughness, Overhang structures, Ti-6Al-4V.*

## 1. INTRODUCTION

Additive manufacturing (AM) can create complex geometries and internal features that conventional formative and subtractive manufacturing cannot readily produce. For this reason, AM has seen increased use in the biomedical (Murr et al., 2009) and aerospace sectors (Liu, Wang, Sparks, Liou, & Newkirk, 2017). One of the critical limitations of AM, however, is the ability to control the as-built surface quality of printed parts (Fox, Moylan, & Lane, 2016). Rough surfaces are detrimental, for example, to the fatigue performance of metallic materials, which is an essential consideration in the design of components which will experience repeated loading and unloading during their use. In a study which investigated a significant reduction in printed part porosity, there was no corresponding improvement in the fatigue life of AM Ti-6Al-4V parts (Greitemeier, Dalle Donne, Syassen, Eufinger, & Melz, 2016). This study suggests that the roughness of an alloy may play a dominant role in the fatigue performance of AM Ti-6Al-4V parts, arising from stress concentrations at the alloy's surface, which can serve as the starting point for crack propagation.

A high degree of roughness is desirable in specific applications, *e.g.*, osteointegration. Previous research has observed that as the roughness of an implant increases, the interface between the bone and implant linearly increases (Wong, Eulenberger, Schenk, & Hunziker, 1995). Manufacturers need to control the roughness of AM produced parts to meet specific applications and create homogenous surfaces to improve the fatigue life of these parts. While the roughness of external surfaces can be readily determined using techniques such as optical

Email: John Power
john.power1@ucdconnect.ie

profilometry, there are considerable difficulties in non-destructively determining the roughness of internal surfaces.

## 2. STATE OF THE ART

### *2.1. AM process parameters which affect surface quality*

The rough surface of AM parts comes from the layered nature of the process, the process parameters used, and the partially melted surface particles. The roughness caused by the layering process is referred to as the staircase effect, and this effect is due to the stepped approximation by layers of curved and inclined surfaces. The average Ra roughness depends on the layer thickness and the build angle (Rahmati & Vahabli, 2015). Increased roughness has also been observed at higher powder layer thicknesses (Qiu et al., 2015). This increased roughness was caused by the increasingly misaligned and irregular-shaped scan tracks suggesting that at larger powder layer thicknesses, the meltpool became unstable, and discontinuities of melted material can occur, causing surface pores.

Laser-Powder Bed Fusion (L-PBF) processing parameters can affect the formation of rough surfaces due to the poor melting of powder particles along with the balling phenomenon. Increased laser scanning speed has been shown to correlate with an increase in the measured roughness of L-PBF made parts (Gockel, Sheridan, Koerper, & Whip, 2019). At high scanning speeds, the balling of molten powder can occur, disrupting the edge of the meltpool, and affecting the layer's shape (Wang, Yang, Yi, & Su, 2013). Due to Raleigh instability, the molten pool elongates at high scanning speeds, breaking into small islands (Lee & Zhang, 2015). This is due to the surface tension gradient-driven flow inside the molten pool. These small islands or balls are dragged to the outer edge of the molten pool. A reduction in the measured surface roughness has been found to correlate with an increase in the laser power (Gockel et al., 2019). Some powder particles will also not be wholly melted when insufficient energy is added to the powder bed, and this partially melted powder material adheres to the surface of the build. The average roughness caused by these un-melted particles is on the same order of magnitude as the powder diameter (DebRoy et al., 2018). Therefore, roughness is expected to be reduced with higher energy input.

Gravity can also affect the surface finish of downward-facing overhangs in an L-PBF part. These overhangs can sag into the un-melted powder material beneath them, resulting in a rougher surface finish. A further factor influencing the surface finish of downward-facing overhangs, is the unequal heat distribution rates in the powder compared to the solid material, creating large thermal gradients which can destabilise the meltpool and disrupt the shape of the layer edge (Gusarov & Kovalev, 2009). These large thermal gradients lead to the overheating of the laser meltpools and have been shown to correlate with an increase in the roughness of overhangs in L-PBF produced parts (Craeghs, Clijsters, Kruth, Bechmann, & Ebert, 2012).

### *2.2. Measuring surface roughness of additive manufacturing features*

The complex surface finish of a L-PBF-produced part, makes it difficult to determine what drives the formation of rough surfaces. Typically, average roughness values are used to implement process optimisation to improve the surface finish of parts. Ra, defined as the arithmetic mean of the absolute values of the ordinate values (*ISO 21920-2:2021 Geometrical product specifications (GPS) - Surface texture: Profile - Part 2: Terms, definitions and surface texture parameters*, 2021), is the most commonly used. However, using Ra as the only metric of roughness is unreliable, and many studies have concluded that it is insufficient as a single measurement to describe the roughness of AM components (Arola & Ramulu, 1999).

Rt is the sum of the largest height and depth of the surface profile (*ISO 21920-2:2021 Geometrical product specifications (GPS) - Surface texture: Profile - Part 2: Terms, definitions and surface texture parameters*, 2021). Studies have shown a relationship between the Rt roughness value and the high cycle fatigue life of L-PBF parts. In studies which compare the Ra and Rt roughness parameters of L-PBF parts, the Rt values were found to have a more significant influence on the high cycle fatigue life (Greitemeier et al., 2016).

The line of sight limitation of profilometry techniques leads to the necessity of a novel and robust approach for measuring the roughness of L-PBF-produced parts. Line edge roughness (LER), which is defined as a deviation of a feature edge from an ideal shape, is one such approach. LER is widely used in the semiconductor industry

to describe the variation on the edges of features (Bunday et al., 2004; Croon et al., 2002). In work by Croon et al., images of semiconductor transitions were taken using scanning electron microscopy, at the nm scale. The study demonstrated that the transistor edge roughness measured using LER does not significantly contribute to parameter fluctuations.

In the current work, the application of the LER approach to microscopy images of L-PBF printed alloy parts is investigated. While LER has to date not been applied to microscopy images, a similar image-based approach for measuring the profile roughness has been investigated by Triantaphyllou et al. (Triantaphyllou et al., 2015). They used a MATLAB-based program to detect abnormal surface features along the edge of the profile obtained from an image of a sample's cross-section. The authors however, did not report on roughness measurements gathered using this approach.

The objective of this study is to evaluate if the LER method can be used to measure the roughness of overhang features printed on Ti-6Al-4V parts. The performance of the LER method will be evaluated against optical profilometry roughness measurements obtained from the same parts.

## 3. METHODOLOGY

### *3.1. Part design*

Figure 1 shows the design of the test piece used in this study; it is used to simulate a flat overhang structure with no print supports. The overhang area of the test piece was 2 mm x 10 mm. A similarly sized 'fin' shape was included at the top of the test piece, which facilitated part mounting on a precision saw, in order to remove the legs on either side of the overhang surface. This facilitates the line of sight required for the optical profilometry measurements. The test pieces were printed using Ti-6Al-4V powder using a Renishaw 500AM L-PBF machine.

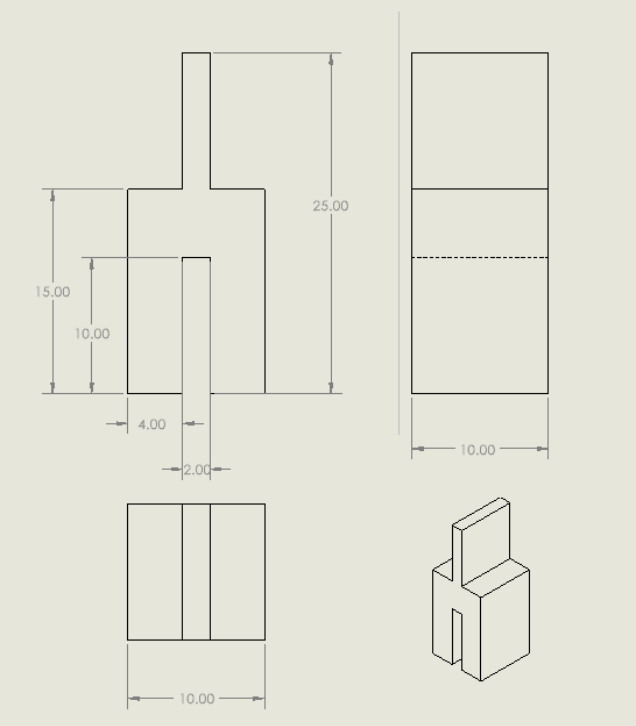


*Figure 1: Schematic of the overhang test piece and dimensions used in this study. All units are in millimetres.*

*3.1.1 Print laser parameters*

Printing overhang structures without supports can lead to an increase in part's defects, such as increased porosity and roughness (Gusarov & Kovalev, 2009, Craeghs et al., 2012)). Figures 2 and 3 show the increase in meltpool temperature detected based on optical emission and infrared (IR) sensor data obtained during the printing of the layers immediately above the overhang structure. Two factors are associated with this overheating. Firstly, the standard operating procedure for printing flat overhangs on a Renishaw 500AM system is to reduce the laser

power from 100% to 20% for the first three layers immediately above an overhang region. Without this reduction, the laser power level used in the processing of the alloy bulk, can result in add a significant overheating when applied to the overhang region. This is partially associated with the reduced thermal conductivity of the powder immediately below the overhang structure, compared with that of the solid alloy material, as discussed in the literature review. The parameters used in this study were selected in order to reduce the excess heating of the meltpool at the overhang region.

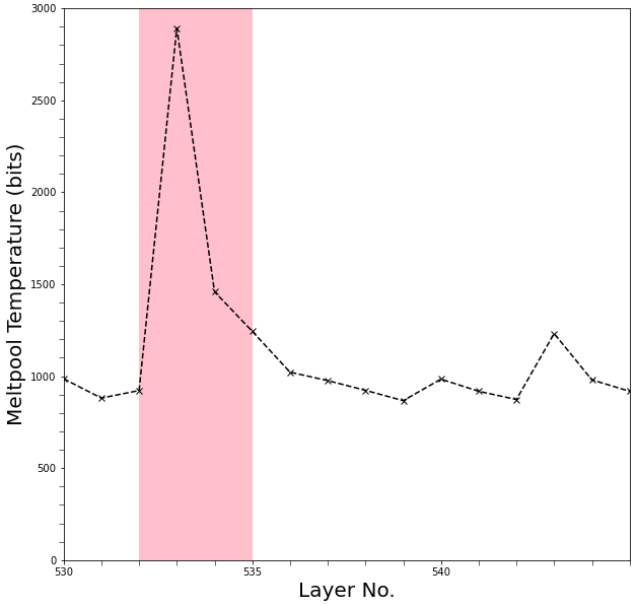


*Figure 2: Meltpool temperature (bits) measured using an IR sensor. A significant increase in meltpool temperature is detected after the first overhang layer (layer 533) is printed, as highlighted in pink. This illustrates the necessity to reduce the laser energy in the print region immediately above an overhang region.*

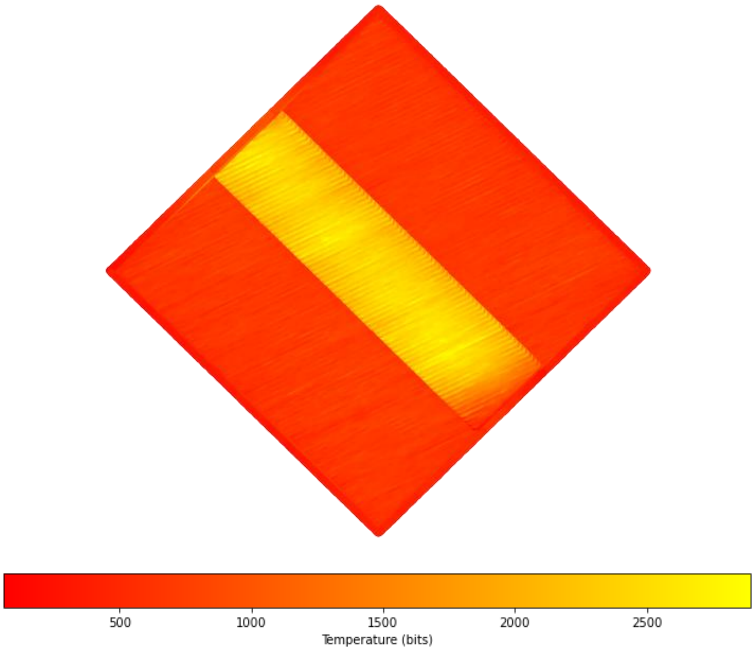


*Figure 3: Image of overhang layer (layer 533) constructed from the IR data collected during the build process. The overhang region in the square's centre emits more IR energy, indicating that the meltpool in this region was at a higher temperature.*

In this study, two print parameters were varied: laser power and the number of print layers over which a reduction in laser input power was applied. The objective was to investigate how altering the input laser energy, along with the number of print layers from the overhang, resulted in changes to the measured overhang roughness. It was hypothesised that the overheating due to the significant step change in laser power could be prevented by gradually increasing the laser power back to nominal over a number of layers. Table 1 lists the percentage reduction applied to the laser power, along with the number of print layers over which this was applied. Figure 4

graphs the resultant parameter values at each overhang layer. As an example, consider experimental run 4 in figure 4, for which the laser power is 68.7 W for the first print layer above the overhang. Over the following seven layers, the laser power is gradually increased in steps of 12.5% until it returns to 200 W for the ninth overhang layer. The optimised laser parameters shown in Table 1 and figure 4 were taken from a design of experiment (DOE) study, whose aim was to reduce the overheating and part porosity in the overhang region by systematically altering the laser energy below the nominal (10000 J) conditions used for the overall alloy structure. A total of seven parameters with three replicates per parameter set were investigated.

*Table 1. Percentage change in laser power for the seven parameter sets used in this study.*

| Experimental Run | Laser power reduction per layer (%) | No. of layers where laser power was reduced | Overall laser power reduction up to layer 15 from the overhang (%) |
|---|---|---|---|
| 1 | 12.5 | 1 | 12.5 |
| 2 | 5.0 | 1 | 5.0 |
| 3 | 5.0 | 8 | 33.7 |
| 4 | 12.5 | 8 | 65.6 |
| 5 | 20.0 | 15 | 96.5 |
| 6 | 5.0 | 15 | 53.7 |
| Optimal | 20.0 | 7 | 79.0 |

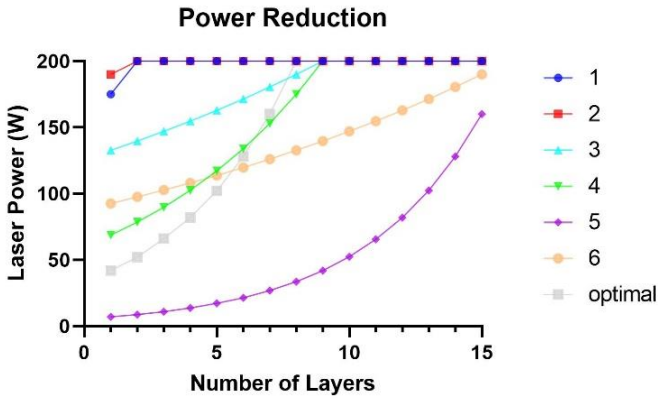


*Figure 4: Laser power settings used for the first fifteen print layers above the overhang for each parameter set.*

### *3.2. Optical profilometry*

The roughness of the overhang surfaces was also measured using a Bruker NPFLEX white-light interferometer. Measurements were taken using single field of view (FOV) acquisitions and a lens with 2.5X magnification. Due to the very high roughness values observed for the samples in this study (≈ 20 µm), an 8 mm cut-off length would be necessary to take a profile measurement of the roughness according to ISO guidelines (*ISO 21920-3:2021 Geometrical product specifications (GPS) - Surface texture: Profile - Part 3: Specification operators*, 2021). Therefore, only S-parameter roughness values could be acquired from optical profilometry measurements in this study. The measurement area was 1.7 mm by 1.7 mm, and the L-filter nesting index was established using an area scale analysis method, which calculates the surface area of the measured topography as a function of scale.

### *3.3. Line edge roughness image analysis method*

The evaluation of the roughness of the overhang samples using the Line Edge Roughness (LER) method, involved sectioning, resin mounting, grinding and polishing down to a cross-section of the overhang, as would be required for typical microstructure analysis. A preparation method developed by Struers Ltd for titanium alloys was followed (Taylor & Weidmann, 2016). The sectioned overhang surfaces were imaged using an Olympus GX51 microscope, at 5x magnification.

The LER method was implemented using an ImageJ script developed specifically for this application. Firstly the script removed satellite particles not directly attached to the layer edge and applied a greyscale to the image to

locate and isolate its layer edge. Next, the ImageJ script analyses the edge pixels within a user-selected ROI and measures the edge roughness. The script isolates and discretises the edge in the ROI and then determines the location of each discrete point of the edge and calculates its angle of orientation to a reference line. The script then refines the selection of contiguous edge segments and collects the gradient data, which is used to calculate the roughness parameters, Ra and Rt. The cross-sectional profile of each sample was split into several regions of interest, and the surface measurements from each region were averaged and taken as the surface value for the entire cross-section.

## 4. RESULTS AND DISCUSSIONS

### *4.1. Optical profilometry results*

The optical profilometry roughness parameters Sv (maximum pit height) and Ssk (surface skewness), were selected for the evaluation of the roughness of the printed overhang structures (*ISO 21920-2:2021 Geometrical product specifications (GPS) - Surface texture: Profile - Part 2: Terms, definitions and surface texture parameters*, 2021). Sv measures the maximum valley below the mean line. Figure 5 plots the Sv parameter against the overall percentage reduction in laser power across the first fifteen overhang layers. As the graph shows, the samples where the overhang layers were printed with less laser power displayed a smaller Sv measurement.

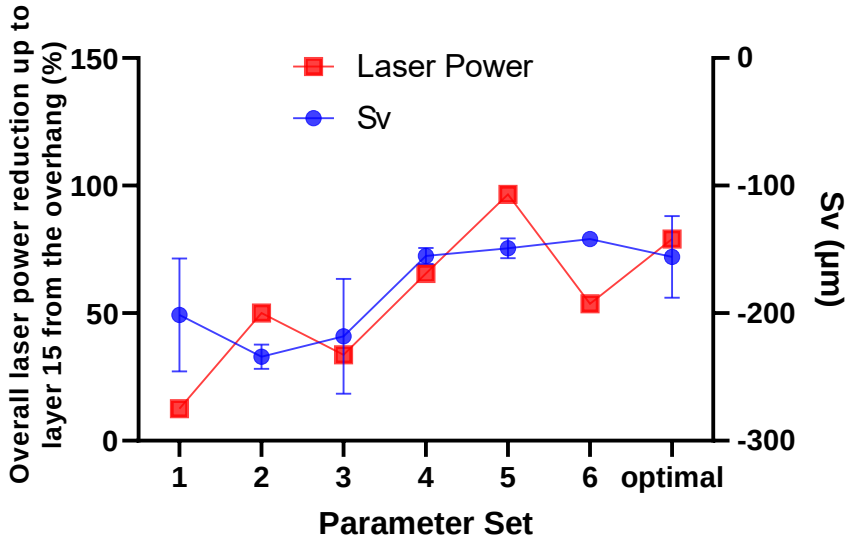


*Figure 5: Comparison between the Sv parameter and the overall laser power reduction up to layer 15 from the overhang layer.*

The Ssk parameter provides a measure of a surface's skewness or the shape of the distribution of the height of the surface. An increase in skewness indicates that the number and severity of valleys are decreasing and that more of the surface features are found to be higher than the average surface. Figure 6 shows the Ssk parameter for each sample measured using the optical profilometer. The skewness increased, indicating a surface with smaller surface deviations on it, as the laser power used to print the surface decreased. A reduction in the laser energy added to meltpool of an overhang section has been previously linked to reduced measured roughness values (Craeghs et al., 2012), so this trend is to be expected. The Sv and Ssk parameters will be used to evaluate if the LER method can evaluate a trend of increased roughness with increased laser energy.

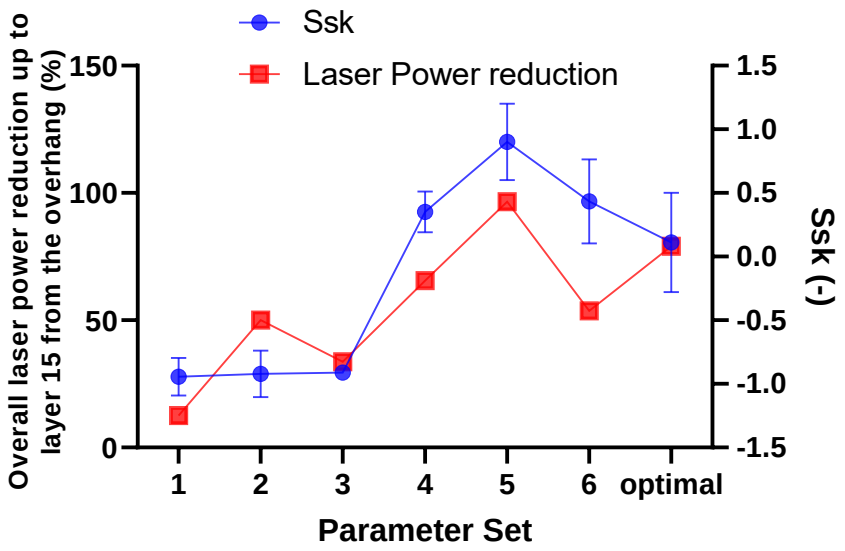


*Figure 6: Comparison between the Sv parameter and the overall laser power reduction up to layer 15 from the overhang layer.*

### *4.2. Evaluation of LER results*

To evaluate the LER method, a comparison between the Ra results from the LER results and the Ssk and Sv measurements for the optical profilometry measurements was undertaken. Figure 7 plots the Ra results against the Ssk parameter. As discussed earlier, an increase in Ssk values indicates a smoother, less skewed surface, which was found to occur as the laser power used decreased. The Ra measurements obtained using LER, also saw a decrease, indicating a smoother surface. These results are in line with previous studies, which linked a decrease in the laser energy to print a surface to a decrease in the measured roughness of a surface of an overhang surface (Craeghs et al., 2012; Gusarov & Kovalev, 2009),.

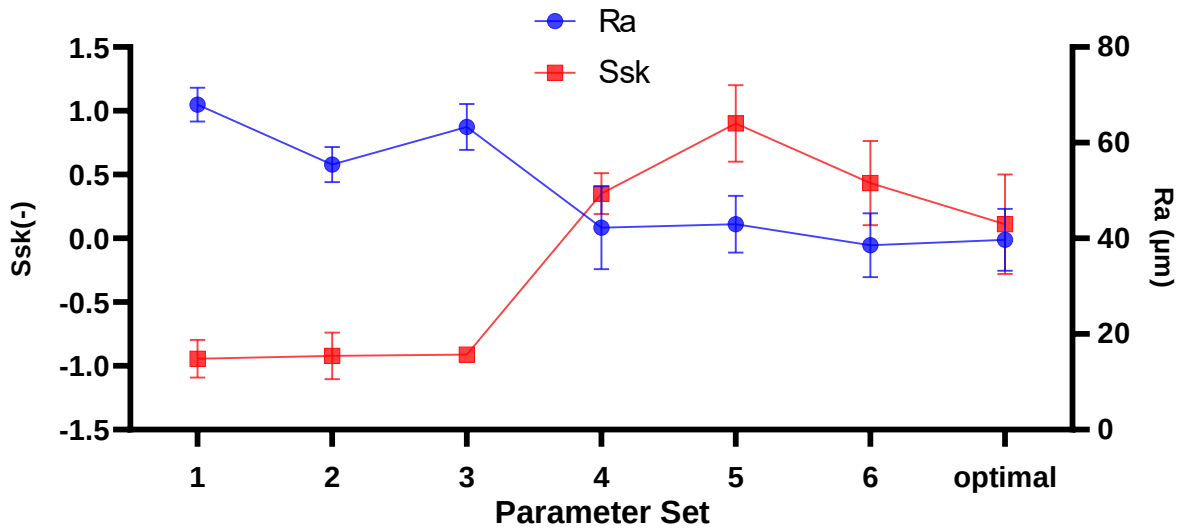


*Figure 7: Comparison between the Ssk parameter and Ra roughness, measured using the LER technique.*

Figure 8 compares the Ra obtained using LER measurements, with Sv which was obtained using optical profilometry. A decrease in the Sv parameters means that a decrease in the maximum valley depth on a surface. Ra is the arithmetic average of the profile's roughness, i.e. the average of the peak and valley heights measured along that profile. Therefore, it is anticipated that if the Sv value for a surface decreased, then the Ra value would also decrease for the same surface. This is indeed the trend that is observed in Figure 8 with the Sv becoming less negative in correlation with the decrease in Ra roughness.

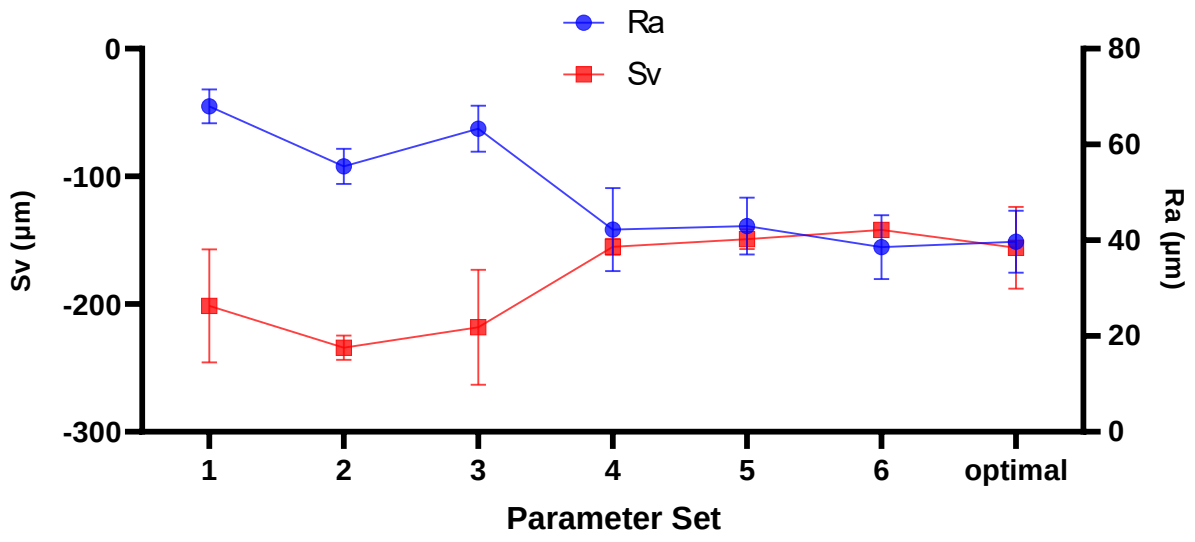


*Figure 8: Comparison between the Sv parameter and the Ra parameter.*

The LER measurements therefore provided a similar correlation between the overhang roughness with laser energy, as obtained using optical profilometry. Once the cross-sectional images are available, the measurements of the cross-sectional images can be automated with little user input. The LER method does require a considerably higher level of sample preparation however prior to part examination. The examination of additional cross-sections of individual samples is also required in order to provide a more statistically significant sample size, compared with the single cross sectional measurements obtained in this study. The LER measurements however for this study, were carried out on a difficult to access overhang feature, for which the use of an optical profilometer would not have been suitable due to the difficulty in accessing the internal surface of the part.

### *4.3. Outlying surface features and their effect on LER results*

Single profile features such as protrusions and deep valleys can have a significant impact on the obtained roughness parameters. Figure 9 shows an example of part of an alloy sample cross-section, with some surface protrusions highlighted, which appeared to be associated with powder particles which appear to be 'weakly' bonded to the surface. These powder particles are unlikely to contribute to stress but have a significant effect on the profile's roughness measurements obtained using the LER method. The deep notches observed on the profile, figure 9 (b), are potentially caused by meltpool instabilities caused by the powder bed underneath the overhang (Gusarov & Kovalev, 2009). These notches are important to consider when predicting the mechanical and fatigue performance of the part.

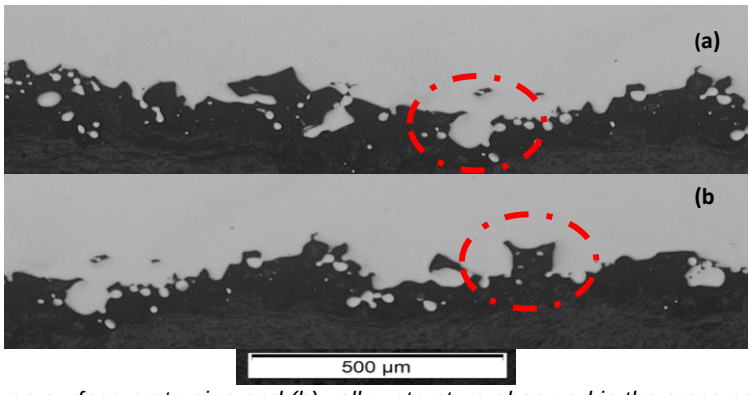


*Figure 9: (a) Abnormally large surface protrusion and (b) valley structure observed in the cross-sections of the titanium alloy*

The effect of surface protrusions on the LER roughness results were investigated based on the use of ImageJ software, to remove these protrusions. ImageJ can identify circular features, and these functions were used to exclude surface protrusions from the LER analysis of the profile. Figure 10 shows the Ra roughness, measured by the LER method with and without the use of the surface protrusions filter. As anticipated, the Rq, Rz, and Rt

roughness measurements were all found to decrease when the surface protrusions were excluded from the analysis. While this approach is subjective, it has the potential to enhance the accuracy of the roughness measurements by removing individual 'abnormal' features, which can distort the measured roughness values obtained from the cross sections.

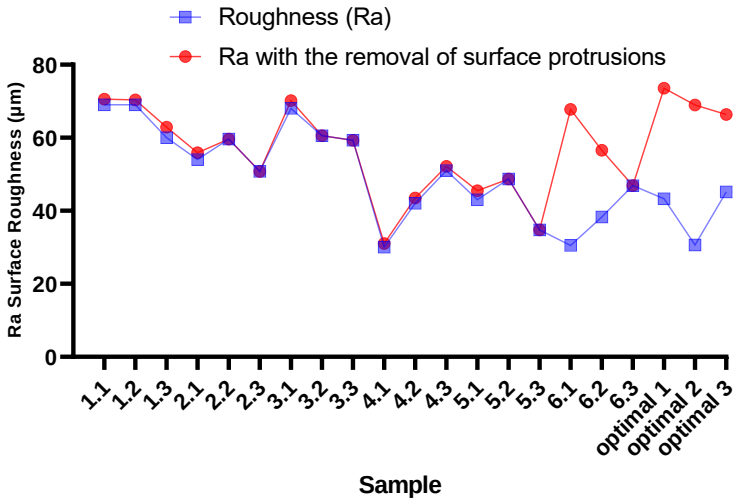


*Figure 10: Ra roughness as determined using the LER technique with and without the use of a surface protrusions filter.*

As demonstrated in Figure 11, on applying the surface protrusion filter, the Ra measurements for samples 6.1, 6.2, and the three samples printed with the optimal parameters decreased significantly when compared to the other samples. The more considerable decrease was due to the presence of substantial surface protrusions on the edges of the cross-sections for these samples. Figure 12 helps to illustrate this, demonstrating the presence of surface defects, with a diameter of approx. 250 µm long, on the cross-section obtained for sample 6.2. This type of defect is likely caused by powder at the edge of the printed part adhering to the overhang surface as it cools.

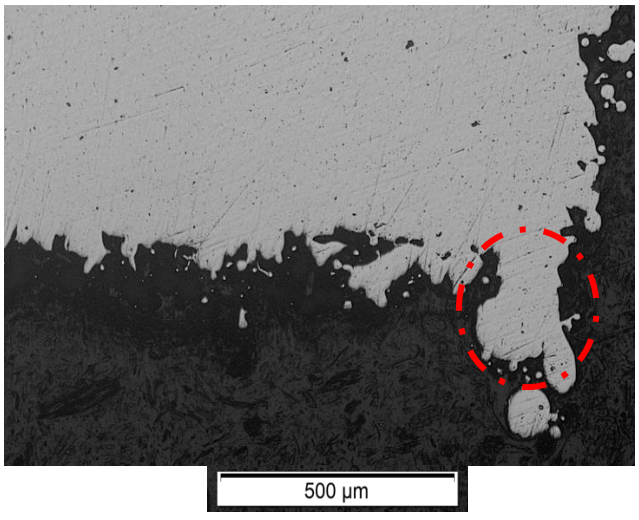


*Figure 11: A large surface protrusion, ≈250 µm, on sample 6.2's cross-section.*

All of the cross-section profiles were analysed qualitatively, and it was found that the distribution of surface defects, e.g. valleys, powder sticking to the surface, were distributed in a random manner. Going forward, it may be necessary to select a size of a peak or valley, above which a decision should be made if the feature should be included or not in the roughness measurement used to determine the sample LER.

## 5. CONCLUSIONS AND FURTHER WORK

The objective of this study was to evaluate for the first time, if the LER method could be used to measure the roughness of internal L-PBF-produced Ti-6Al-4V structures, based on microscopy images. The LER

measurements were compared to the Roughness measurements using optical profilometry were used for comparison with the LER measurements, just to stress that the LER provides results for a single edge profile, while the optical profilometry measurements were carried out over an area of 1.7 x 1.7 µm. It was demonstrated that the LER measurements could identify the same trends between the laser energy used to print the overhang features and the roughness of the overhang features.

The LER method can provide an indication of the alloy's surface profile in terms of its maximum valleys and peaks. However, it is essential to consider that a profile measurement only examines a small sample of the alloy surface and can be significantly influenced by features such as adherent powder particles. These abnormal features can significantly affect the roughness values obtained, and removing them may allow for a more accurate measurement of the part roughness. An approach to systematically remove these abnormal features using ImageJ software was demonstrated.

The LER method facilitates the evaluation of the roughness of hard-to-access features, which gives it an advantage over optical profilometry. However, this method requires significantly more experimental time and material to complete. Further work is required to examine multiple cross-sections of the overhang to determine if the results vary significantly and to investigate the feasibly of using this method on other L-PBF printed surfaces.

## 6. REFERENCES


Arola, D., & Ramulu, M. (1999). An examination of the effects from surface texture on the strength of fiber reinforced plastics. *Journal of Composite materials, 33*(2), 102-123.

Bunday, B. D., Bishop, M., McCormack Jr, D. W., Villarrubia, J. S., Vladar, A. E., Dixson, R., . . . Allgair, J. A. (2004). *Determination of optimal parameters for CD-SEM measurement of line-edge roughness.* Paper presented at the Metrology, Inspection, and Process Control for Microlithography XVIII.

Craeghs, T., Clijsters, S., Kruth, J. P., Bechmann, F., & Ebert, M. C. (2012). Detection of Process Failures in Layerwise Laser Melting with Optical Process Monitoring. *Physics Procedia, 39*, 753-759. doi:https://doi.org/10.1016/j.phpro.2012.10.097

Croon, J. A., Storms, G., Winkelmeier, S., Pollentier, I., Ercken, M., Decoutere, S., . . . Maes, H. E. (2002, 8-11 Dec. 2002). *Line edge roughness: characterization, modeling and impact on device behavior.* Paper presented at the Digest. International Electron Devices Meeting.

DebRoy, T., Wei, H. L., Zuback, J. S., Mukherjee, T., Elmer, J. W., Milewski, J. O., . . . Zhang, W. (2018). Additive manufacturing of metallic components – Process, structure and properties. *Progress in Materials Science, 92*, 112-224. doi:https://doi.org/10.1016/j.pmatsci.2017.10.001

Fox, J. C., Moylan, S. P., & Lane, B. M. (2016). Effect of Process Parameters on the Surface Roughness of Overhanging Structures in Laser Powder Bed Fusion Additive Manufacturing. *Procedia CIRP, 45*, 131-134. doi:https://doi.org/10.1016/j.procir.2016.02.347

Gockel, J., Sheridan, L., Koerper, B., & Whip, B. (2019). The influence of additive manufacturing processing parameters on surface roughness and fatigue life. *International Journal of Fatigue, 124*, 380-388. doi:https://doi.org/10.1016/j.ijfatigue.2019.03.025

Greitemeier, D., Dalle Donne, C., Syassen, F., Eufinger, J., & Melz, T. (2016). Effect of surface roughness on fatigue performance of additive manufactured Ti–6Al–4V. *Materials Science and Technology, 32*(7), 629-634.

Gusarov, A., & Kovalev, E. (2009). Model of thermal conductivity in powder beds. *Physical Review B, 80*(2), 024202.

*ISO 21920-2:2021 Geometrical product specifications (GPS) - Surface texture: Profile - Part 2: Terms, definitions and surface texture parameters*. (2021). Geneva: International Organization for Standardization.

*ISO 21920-3:2021 Geometrical product specifications (GPS) - Surface texture: Profile - Part 3: Specification operators*. (2021). Geneva: International Organization for Standardization.

Lee, Y., & Zhang, W. (2015). *Mesoscopic simulation of heat transfer and fluid flow in laser powder bed additive manufacturing.* Paper presented at the 2015 International Solid Freeform Fabrication Symposium.

Liu, R., Wang, Z., Sparks, T., Liou, F., & Newkirk, J. (2017). 13 - Aerospace applications of laser additive manufacturing. In M. Brandt (Ed.), *Laser Additive Manufacturing* (pp. 351-371): Woodhead Publishing.

Murr, L. E., Quinones, S. A., Gaytan, S. M., Lopez, M. I., Rodela, A., Martinez, E. Y., . . . Wicker, R. B. (2009). Microstructure and mechanical behavior of Ti–6Al–4V produced by rapid-layer manufacturing, for biomedical applications. *Journal of the Mechanical Behavior of Biomedical Materials, 2*(1), 20-32. doi:https://doi.org/10.1016/j.jmbbm.2008.05.004

Qiu, C., Panwisawas, C., Ward, M., Basoalto, H. C., Brooks, J. W., & Attallah, M. M. (2015). On the role of melt flow into the surface structure and porosity development during selective laser melting. *Acta Materialia, 96*, 72-79.

Rahmati, S., & Vahabli, E. (2015). Evaluation of analytical modeling for improvement of surface roughness of FDM test part using measurement results. *The International Journal of Advanced Manufacturing Technology, 79*(5), 823-829.

Taylor, B., & Weidmann, E. (2016). Metallographic preparation of titanium. Retrieved from https://www.struers.com/-/media/Struers-media-library/Materials/Application-reports/Application_Note_Titanium_2015_ENG.pdf

Triantaphyllou, A., Giusca, C. L., Macaulay, G. D., Roerig, F., Hoebel, M., Leach, R. K., . . . Milne, K. A. (2015). Surface texture measurement for additive manufacturing. *Surface topography: metrology and properties, 3*(2), 024002.

Wang, D., Yang, Y., Yi, Z., & Su, X. (2013). Research on the fabricating quality optimization of the overhanging surface in SLM process. *The International Journal of Advanced Manufacturing Technology, 65*(9), 1471-1484.

Wong, M., Eulenberger, J., Schenk, R., & Hunziker, E. (1995). Effect of surface topology on the osseointegration of implant materials in trabecular bone. *Journal of biomedical materials research, 29*(12), 1567-1575.

# Accessing Injection Mould Cooling Enhancement Delivered by Additive Manufactured Lattices Based on Triply Periodic Minimal Surfaces

Seyed Mahdi Akbarimoosavi, Centre for Precision Engineering, Materials and Manufacturing Research and Department of Mechanical and Manufacturing Engineering, Atlantic Technological University-Sligo, Ash Lane, Sligo, Ireland

John Lohan, Integrated Sustainable Energy Technologies (iSET) Research Group and Department of Mechanical and Industrial Engineering, Atlantic Technological University- Galway, Dublin Road, Galway, Ireland

Denis O'Mahoney, Department of Mechanical and Industrial Engineering, Atlantic Technological University- Galway, Dublin Road, Galway, Ireland

Gerard McGranaghan, Centre for Precision Engineering, Materials and Manufacturing Research and Department of Mechanical and Manufacturing Engineering, Atlantic Technological University-Sligo, Ash Lane, Sligo, Ireland, I-Form, The SFI Advanced Manufacturing Research Centre, Ireland

***Abstract***

Heat transfer enhancement during the cooling stage of injection moulding reduces cycle time and boosts production. In addition, controlled and more uniform cooling alleviates residual stresses which cause deformation and weak points. This study focuses on a novel method for improving the cooling rate within an injection mould using Triply Periodic Minimal Surface (TPMS) lattices in a channel creating conformal cooling of the core and cavity. These complex geometries cannot be made using traditional methods of machining, forging, or drilling and are only possible with recent advancements in additive manufacturing. In this simulation study, the performance of a normal cubic lattice is compared against a three-dimensional mathematically defined TPMS structure called Solid/Skeletal Diamond periodic lattice. The cells are of size 20 mm by 10 mm by 10 mm and are contained in a 40 mm long parallel plate channel. A periodic boundary condition is used on the sides for modelling the parallel channel and the lattice inside. The material of lattices and channels is maraging steel, the working fluid is water which is fully developed at the inlet. One side under the lattice is held at a constant temperature for heat input. The lattices have porosities ranging from 50% to 90% and their heat and mass transfer performance is investigated in steady-state using the Computational Fluid Dynamics (CFD) method in ANSYS Fluent. In the model, the flow and heat transfer are coupled in fluid and solid domains. The cooling rate, convection coefficient and pressure drop characteristics are presented for Reynolds numbers in the range of 1,250 to 10,000. A trade-off analysis between pressure drop and cooling rate improvement is conducted using the Performance Evaluation Criteria (PEC) to determine optimal porosity and structure.

Results indicate that the cubic and Solid Diamond structures deliver up to 580% and 520% in heat transfer enhancement in terms of Nusselt number due to their high surface area to volume ratio and the flow characteristics within them when compared with the open channel. It was revealed that decreasing the porosity of the TPMS structures can considerably enhance the convective heat transfer coefficient at the expense of pressure drop increment. The lattices suffer more from pressure drop at higher Reynolds numbers since the rate of growth in the pressure drop rises with increasing inlet velocity. After considering all the factors and compared to an Open Channel, the Solid/Skeletal Diamond structure with 50% porosity and inlet Re of 2,500, performs the best among the studied cases by increasing the Nusselt number by 520% with a PEC of 1.1. It was also revealed that a more uniform cooling is achieved using the lattices. The velocity magnitude distribution and temperature contours show that the heat transfer enhancement is achieved due to several reasons, including more available wetted surface area, increased fluid velocity and turbulence intensity within the TPMS structure, thinner boundary layers, and consequently lower thermal resistance. These results show the potential of TPMS-based structure to not only deliver enhanced thermal control of injection moulds but simultaneously facilitate space, weight, and material savings.

*Key Words: Triply Periodic Minimal Surfaces, Additive Manufactured Injection Moulds, Conformal Cooling, Computational Fluid Dynamics, Enhanced Thermal Control*

Email: Seyed Mahdi Akbarimoosavi
Seyedmahdi.akbarimoosavi@mail.itsligo.ie

## 1. INTRODUCTION

Periodic cellular structures have not been studied as much as foams in terms of mass and heat transfer in the literature, due to their complex topology and fabrication difficulties. However, such heat transfer studies are now required as recent advancements in additive manufacturing have not only made their fabrication possible but also enable desirable characteristics such as permeability, surface-to-volume ratio, and stiffness-to-weight ratios to be controlled. They have received high interest in making lighter mechanical parts without compromising on mechanical properties (Abueidda et al., 2017; Maskery et al., 2018; Khogalia, Choo, & Yap, 2020). Lattices have also shown a high potential for heat dissipation in heat exchangers and heat sinks (Al-Ketan et al., 2021). Combining the aforementioned applications is the starting point for using periodic cellular structures and specifically, those based on Triply Periodic Minimal Surfaces (TPMSs) in the fabrication of injection moulds that offer reduced weight, predictable and higher heat transfer rates with greater uniformity in heat transfer and a reduced cooling time during the injection moulding cycle (Tang, Gao, & Zhao, 2019; Oh, Ha, & Park, 2022).

## 2. LITERATURE REVIEW

The term cellular structure refers to materials that have intentionally incorporated voids (Al-Ketan, Rowshan, & Al-Rub, 2018). If the voids are arranged periodically, they form lattices. There are a variety of periodic cellular structures including two-dimensional symmetric lattices such as honeycomb and prismatic, and three-dimensional symmetric structures like strut-based lattices. Another group of lattices are based on TPMSs which are defined with mathematical equations that create surfaces which divide the space into two or more volumes. The volume trapped inside these surfaces can shape and produce structures called solid/skeletal lattices. Thickening these surfaces can also create structures called Sheet lattices (Ali et al., 2020; Al-Ketan et al., 2018). There are a variety of TPMS-based lattices such as Sheet-based and Skeletal/Solid-based Gyroid, Diamond, IWP, and Primitive. Due to the TPMS-based structures' high mechanical energy absorption, and their relatively high permeability in comparison with conventional lattices (Ali et al., 2020; Al-Ketan et al., 2018; Chen et al., 2019) their utilisation has been recommended in the literature for applications that work at high temperatures, components that undergo severe fatigue loads, and for heat-exchangers (Ali et al., 2020).

TPMS-based lattices have not received much attention in the literature due to their fabrication challenges which have only recently been alleviated by additive manufacturing. 3D printing is based on adding materials layer by layer enabling fabrication of complex geometries in a short time with less wasted material. For metals which are the subject of this study due to their higher thermal conductivity and mechanical properties, powder bed fusion techniques are used including selective laser melting, selective electron beam melting, and selective laser sintering where a laser or electron beam melts or sinters the layers of metal powder and fabricates such complex lattice structures (Al-Ketan et al., 2018).

Some TPMS-based structures were studied numerically and experimentally (Abueidda et al., 2016; Catchpole-Smith et al., 2019) for their effective electrical/thermal conductivities and elastic moduli with no convective medium showing that conductivities change linearly with porosity (volume of void divided by the volume of structure). In a CFD analysis (Al-Ketan et al., 2021), square channels with TPMS lattices were used as air-cooled heatsinks in the turbulent region. It was reported that Sheet Gyroid has a high convective heat transfer coefficient because of its high surface-to-volume ratio and topological tortuosity with a higher pressure drop penalty.

There are only a few studies conducted on the application of lattices in injection moulds. Au and Yu (2007) simulated injection moulds with a uniform-sized cubic lattice architecture for conformal cooling. They could provide more uniform cooling with less residual stresses than the conventional methods within the moulded part. They could avoid the common defects such as thermal stress residuals and warpage without losing the required mechanical properties of the mould for withstanding any force or load produced during mould opening and closing with the common materials. Another conformal porous structure within an injection mould was modelled (Tang et al., 2019) resulting in achieving a more uniform mould surface temperature distribution and a lower pressure drop in the cooling system in comparison with the existing cooling methods. In the most recent paper (Oh et al., 2022) Sheet Gyroid and Sheet Diamond lattices were used in the core of an injection mould and the effectiveness of these structures was examined numerically and experimentally resulting in a 40% decrement in the cooling time.

In this work, the thermal and hydraulic performance of Solid Diamond lattice and normal Cubic scaffold as heat sinks in a water-cooled parallel plate channel is explored using CFD. Forced convection in laminar, transition, and turbulent regions is accessed to establish the potential of TPMS-based structures in injection mould cooling and their advantages over more simple Cubic lattices.

## 3. METHODOLOGY

In this study, MSLattice software was used to design the Solid/Skeletal Diamond lattices and ANSYS was used to design the Cubic lattices and generate the required mesh. To solve the coupled heat and mass transfer in a parallel plate channel with different lattices and to predict the thermal and hydraulic performance of the cooling system, ANSYS Fluent's laminar, K-ω-γ transition, and the K-Ɛ, Realizable with the Enhanced Wall Treatment models were applied. Very small-sized cells were generated close to the walls in the fluid region to include the boundary sublayers. The working fluid is water; therefore, the flow is considered incompressible in the fluid domain. The energy equation was selected for both the fluid and solid domains. Gravity was neglected since the temperature differences in the fluid were small and the consequent buoyancy force is low. Due to the low temperatures in all regions, radiation was not considered either.

### *3.1. Governing equations*

Coupled conservation of mass (Eq. 1), Navier-Stokes momentum equations (Eq. 2,3 and 4) and conservation of energy (Eq. 5, 6) in the fluid region and the simplified equation of energy (Eq. 7) in the solid region were solved using the Finite Volume Method. For incompressible flow, Newtonian fluid, and assuming constant density, viscosity, thermal conductivity, and specific heat, and neglecting gravity in steady-state and in the absence of volumetric energy generation, the governing equations are presented in Equations 1 through 8.

$$\frac{\partial u}{\partial x}+\frac{\partial v}{\partial y}+\frac{\partial w}{\partial z}=0 \quad \text{(Eq. 1)}$$

$$u\frac{\partial u}{\partial x}+v\frac{\partial u}{\partial y}+w\frac{\partial u}{\partial z}=-\frac{1}{\rho}\frac{\partial p}{\partial x}+\frac{\mu}{\rho}\left(\frac{\partial^2 u}{\partial x^2}+\frac{\partial^2 u}{\partial y^2}+\frac{\partial^2 u}{\partial z^2}\right) \quad \text{(Eq. 2)}$$

$$u\frac{\partial v}{\partial x}+v\frac{\partial v}{\partial y}+w\frac{\partial v}{\partial z}=-\frac{1}{\rho}\frac{\partial p}{\partial y}+\frac{\mu}{\rho}\left(\frac{\partial^2 v}{\partial x^2}+\frac{\partial^2 v}{\partial y^2}+\frac{\partial^2 v}{\partial z^2}\right) \quad \text{(Eq. 3)}$$

$$u\frac{\partial w}{\partial x}+v\frac{\partial w}{\partial y}+w\frac{\partial w}{\partial z}=-\frac{1}{\rho}\frac{\partial p}{\partial z}+\frac{\mu}{\rho}\left(\frac{\partial^2 w}{\partial x^2}+\frac{\partial^2 w}{\partial y^2}+\frac{\partial^2 w}{\partial z^2}\right) \quad \text{(Eq. 4)}$$

$$\rho C_p\left(u\frac{\partial T}{\partial x}+v\frac{\partial T}{\partial y}+w\frac{\partial T}{\partial z}\right)=k_f\left(\frac{\partial^2 T}{\partial x^2}+\frac{\partial^2 T}{\partial y^2}+\frac{\partial^2 T}{\partial z^2}\right)+\mu\phi \quad \text{(Eq. 5)}$$

where ϕ is equal to:

$$\mu\phi=\mu\left\{2\left[\left(\frac{\partial u}{\partial x}\right)^2+\left(\frac{\partial v}{\partial y}\right)^2+\left(\frac{\partial w}{\partial z}\right)^2\right]+\left(\frac{\partial u}{\partial y}+\frac{\partial v}{\partial x}\right)^2+\left(\frac{\partial u}{\partial z}+\frac{\partial w}{\partial x}\right)^2+\left(\frac{\partial v}{\partial z}+\frac{\partial w}{\partial y}\right)^2\right\}-\frac{2}{3}\mu\left(\frac{\partial u}{\partial x}+\frac{\partial v}{\partial y}+\frac{\partial w}{\partial z}\right)^2 \quad \text{(Eq. 6)}$$

where u, v, and w are velocity components in x, y, and z directions, ρ is fluid density, μ is fluid dynamic viscosity, ϕ is the viscous dissipation term, and T is temperature.

$$\frac{\partial^2 T}{\partial x^2}+\frac{\partial^2 T}{\partial y^2}+\frac{\partial^2 T}{\partial z^2}=0 \quad \text{(Eq. 7)}$$

At the interface of the solid and fluid regions where coupling happens, the following conditions exist:

$$T_f = T_s \text{ and } -k_f \frac{T_{interface} - T_f}{\Delta m_f} = -k_s \frac{T_{interface} - T_s}{\Delta m_s} \quad \text{(Eq. 8)}$$

where $k_f$ is fluid thermal conductivity, $T_{interface}$ is the interface temperature, $T_f$ is the temperature of fluid at the cell attached to the wall, $k_s$ is the solid thermal conductivity, $T_s$ is the solid adjacent to interface cell temperature, $\Delta m_f$ and $\Delta m_s$ are the height of the interface neighbour cell centres in the fluid and solid domains.

### *3.2. Design and boundary condition*

The three-dimensional model of the parallel plate channel is illustrated in Figure 1. The 2×1×1 cells of Solid/Skeletal Diamond lattice and 8×4×4 cubic cells are shown in Figure 1(a) and (b) respectively. The length of the channel is 40 mm with inner height of 10 mm and wall thickness is 3 mm. Hydraulically fully developed water enters the channel from the inlet at x=0 with an average velocity of $u_{inlet}$ with Reynolds numbers (Re) in the range of 1,250 to 10,000 and a uniform temperature of $T_{inlet}$=25 °C. One external side of the 20×10×10 mm area of the channel wall under the lattice at z=0 (highlighted by orange colour in Figure 1) is kept at a constant temperature of $T_h$=40 °C. Water passes through the lattices with porosities varying between 50% to 90% and removes heat. Zero-gauge pressure is considered at the outlet at x=40 mm, and periodic boundary condition is considered at y=5 mm and y=-5 mm on both open sides of the channel. The material properties applied are listed in Table 1.

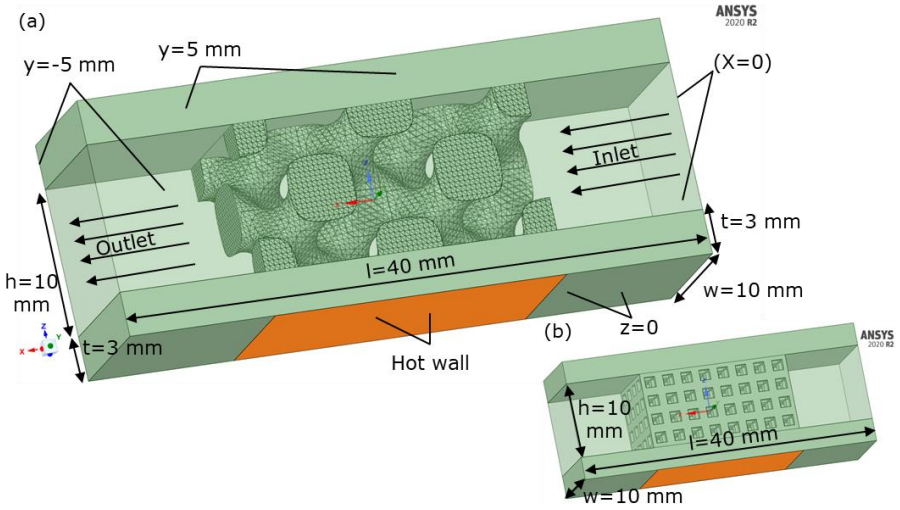


*Figure 1. Parallel channel with 60% Porosity Solid/Skeletal Diamond TPMS (a) and Cubic lattice (b)*

*Table 1. Material properties applied for both TPMS and Cubic lattice structures*

| Materials | ρ (kg/m³) | $C_p$ (J/kg.K) | k (W/m.K) | μ (kg/m.s) |
|---|---|---|---|---|
| Water (Fluid Domain) | 998.2 | 4182 | 0.6 | 0.001003 |
| Maraging Steel (Solid Domain) | 8030 | 502 | 25.3 | - |

### *3.3. Definitions*

Re is calculated using the Equation 9.

$$Re = \frac{\rho u_{inlet} D_h}{\mu} \quad \text{(Eq. 9)}$$

where all the variables including ρ (density of water), $u_{inlet}$ (average inlet velocity), $D_h$ (hydraulic diameter), and μ (dynamic viscosity) are known.

Equivalent average convection coefficient is calculated by Equation 10:

$$h_m = \frac{Q}{A(T_{i,h} - T_{f,ave})} \quad \text{(Eq. 10)}$$

where Q is the cooling rate from the internal side of the hot wall, A is the surface area of the internal side of the hot wall, $T_{i,h}$ is the average temperature of the internal side of the hot wall, and $T_{f,ave}$ is the average fluid temperature of the inlet and outlet. Once the average convection coefficient is established, the average Nusselt number is calculated using Equation 11:

$$Nu_m = \frac{h_m D_h}{k_f} \quad \text{(Eq. 11)}$$

where $k_f$ is the fluid conductivity. Finally, the friction factor is calculated using the Equation 12.

$$f = \frac{2\Delta p}{\rho {u_{inlet}}^2} \frac{D_h}{L} \quad \text{(Eq. 12)}$$

where Δp is the pressure drop in the channel and L is the length of the lattice (20 mm) in the flow direction.

### *3.4. Validation and mesh converging study of the CFD model*

For benchmarking the model, flow and heat transfer in a circular tube of diameter of 20 mm and constant wall temperature of 40 °C was modelled with 800,000 cells. The flow was fully developed and the Re of 1,250, 2,500, 5,000, and 10,000 were modelled. The resulting average Nusselt numbers and friction factors had root mean square errors of 13.4% and 7.7% respectively showing a good agreement with internal laminar fully developed flow in the literature (Bergman, Lavine, Incropera, & DeWitt, 2011) and internal fully developed turbulent flow correlations (Hartnett, Irvine, Greene, & Cho, 1998; Dittus, & Boelter, 1930).

The results of the studied mesh convergence conducted for the case of Solid Diamond lattice with 40% porosity with Re of 10,000 are presented in Table 2. The percentage difference in friction factor and Nusselt number is less than 1 percent between Mesh No. 2 and 1, showing that there is a convergence in the results in the mesh with 6.7 million cells which was then chosen for this case.

*Table 2. Mesh convergence study*

| Mesh Number | Number of cells (millions) | Friction Factor (f) | Error in f compared to Mesh 1 | Nusselt Number (Nu) | Error in Nu compared to Mesh 1 |
|---|---|---|---|---|---|
| Mesh No. 1 | 6.7 | 14.63 | 0% | 460.98 | 0% |
| Mesh No. 2 | 4.9 | 14.76 | 0.91% | 461.52 | 0.12% |
| Mesh No. 3 | 2.5 | 15.65 | 6.99% | 495.13 | 7.41% |

6 to 8 million cells were generated in ANSYS Fluent (Figure 2) for the Solid Diamond and Cubic lattices cases and since K-ω-γ and K-Ɛ Realizable with Enhanced Wall Treatment was used for modelling transition and turbulent flow, the height of the cells in fluid region were chosen small enough on the fluid-wall interface to keep $y^+$ close to 1. A Core i9 computer with 32 GB RAM was used for the modelling and the average convergence time of the simulations was around 2.5 hours.

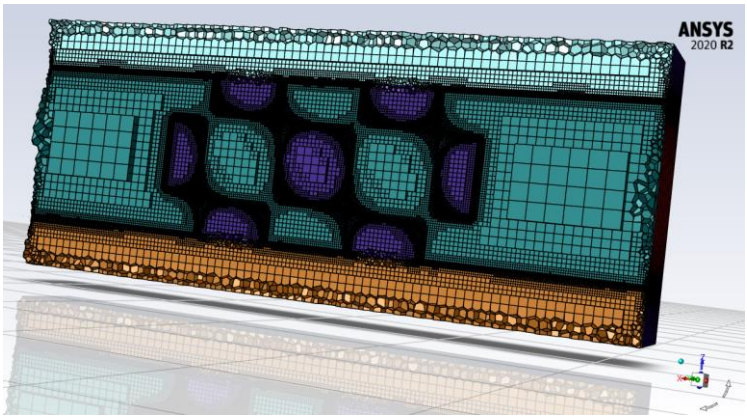


*Figure 2. Generated Poly-Hexacore Mesh (6.7 million cells for the Solid Diamond case with 60% porosity, calculation time is about 4 hours after 400 iterations on average)*

## 4. RESULTS

### *4.1. Results of CFD analysis*

The result of the CFD models with Re varying from 1,250 to 10,000 and porosities between 50% to 90% for Cubic and Solid/Skeletal Diamond lattices are presented in Figures 3, 4, and 5. It is observed in Figure 3 that by increasing the Re and decreasing the porosity, higher values of cooling rate and Nusselt number can be achieved. In laminar and transition regions, the Solid Diamond network has a better cooling performance where with the 50% porosity a 474% (at Re=1,250) and 520% (at Re=2,500) rise in the Nusselt number can be seen. Conversely, the Cubic lattice has the upper hand in turbulent regions, enhancing the Nusselt number by 580% at Re=5,000 and 468% at Re=10,000 with the 50% porosity.

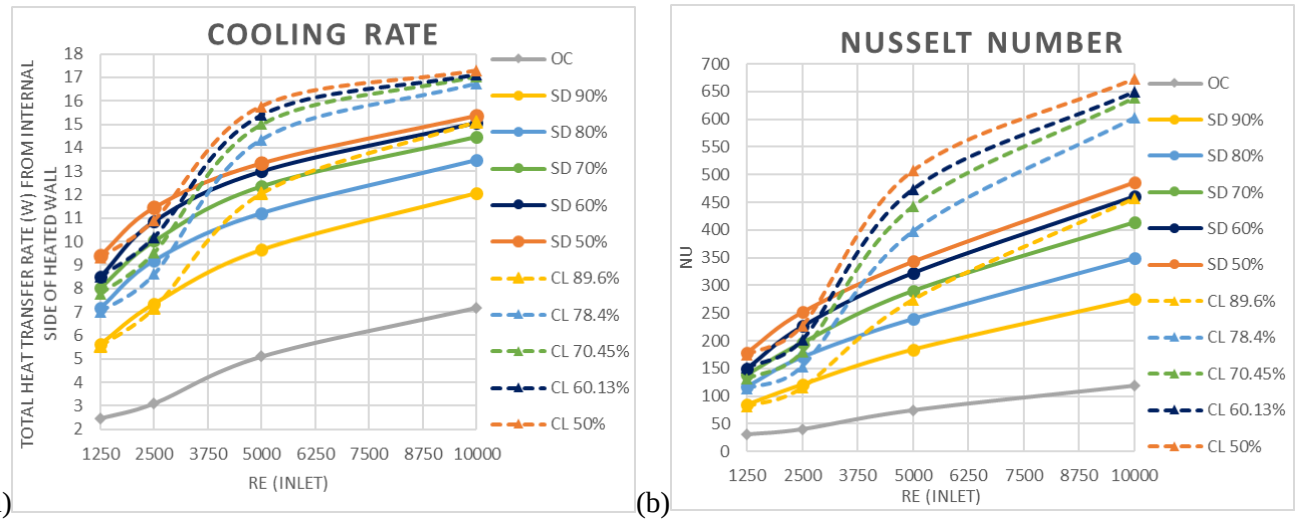


*Figure 3. (a) The total heat transfer rate from the internal side of the heated wall (to fluid and to lattice) versus Re in an Open Channel (OC) and channels with Solid Diamond (SD) and Cubic lattices (CL) with porosities of 50% to 90% (b) Average Nusselt number versus Re in an Open Channel (OC) and in channels with Solid Diamond (SD) and Cubic lattices (CL) with porosities of 50% to 90%*

The results for pressure drop and friction factor shown in Figure 4 both reveal an expected considerable increase when compared with the Open Channel. For instance, adding the 80% porosity Solid Diamond lattice in the channel results in a 6233% increase in average pressure drop compared to the Open Channel. Reducing the porosity further increases both pressure drop and friction factor. Increasing the Re increases the pressure drop with a higher rate of increment at higher Re. However, by increasing the inlet velocity, friction factor declines in the laminar region till it reaches a minimum around Re=2,500 and then it grows till it hits a peak when the flow becomes turbulent (around Re=5,000) beyond which it decreases slightly with Re. The minimum and maximum of friction factor can be observed in Cubic lattices, but they are not observed in the Solid Diamond case at the studied Re; therefore, more intermediate Reynolds numbers need to be investigated in the transition region in the future to be a able to observe the complete trend of friction factor in this region because the transition to turbulence probably shifts to lower Re due to the topological characteristics of Solid/Skeletal Diamond network. Generally, the results show that Cubic lattice have much higher pressure drop and friction factor in all regions.

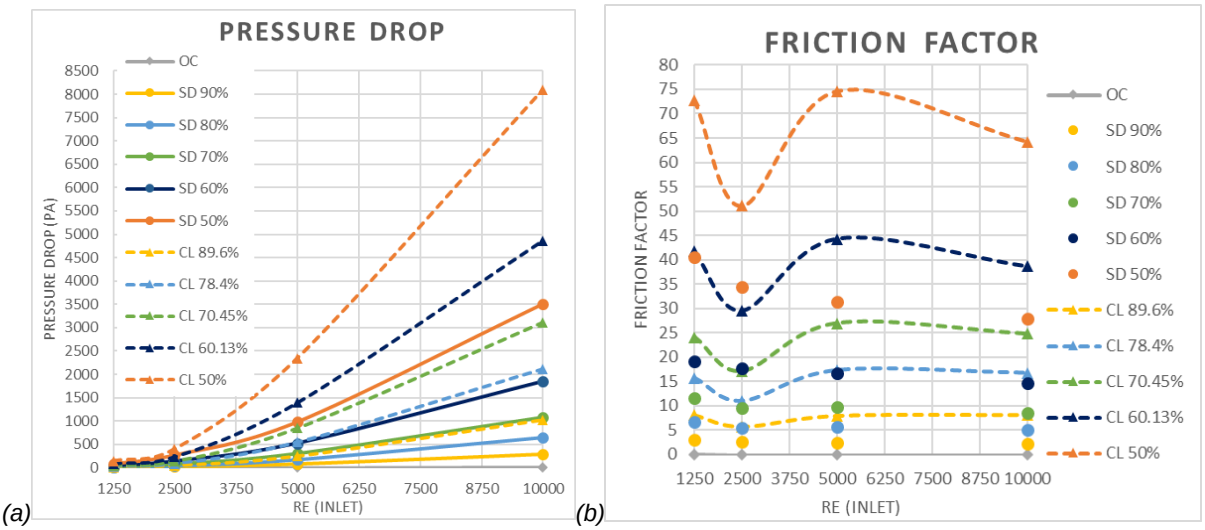


(a) (b)

*Figure 4. (a) Pressure drop versus Re in Open Channel (OC) and in channels with Solid Diamond (SD) and Cubic Lattices (CL) with porosities of 50% to 90% (b) Friction Factor versus Re in Open Channel (OC) and in channels with Solid Diamond (SD) and Cubic Lattices (CL) with porosities of 50% to 90%*

Higher uniformity of heat flux from the hot wall is important as it produces a more uniform temperature distribution for injection mould and it reduces the residual stresses during product cooling; therefore, the effect of the using the lattices on uniformity of heat flux from the hot wall was investigated (Figure 5). For this purpose, the area-weighted uniformity-index of h (heat flux) is calculated using the following equation:

$$\gamma_a = 1 - \frac{\sum_{i=1}^{n}[(|h_i - \bar{h}_a|)A_i]}{2|\bar{h}_a|\sum_{i=1}^{n} A_i} \quad \text{(Eq. 15)}$$

where i is the facet index of a surface with n facets $A_i$ is the facets area, and $\bar{h}_a$ is the average value of heat flux over the surface.

$$\bar{h}_a = \frac{\sum_{i=1}^{n}[h_i A_i]}{\sum_{i=1}^{n} A_i} \quad \text{(Eq. 16)}$$

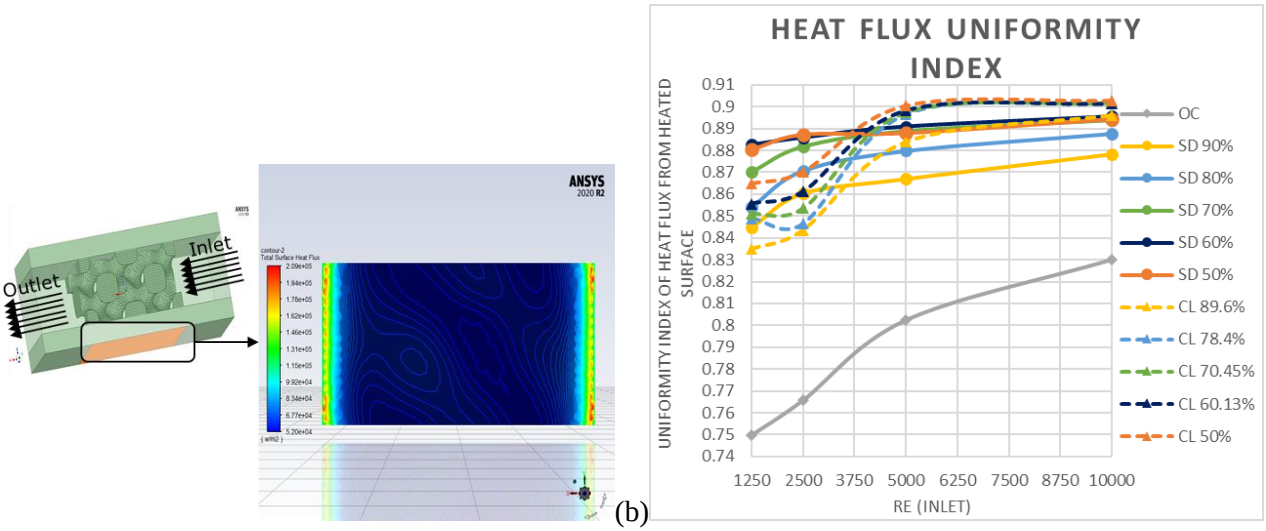


(a) (b)

*Figure 5. (a) The contours of surface heat flux on the hot wall in the channel with 60% porosity Solid Diamond lattice, Re=2,500, and $T_h$=40 °C (b) Area-weighted uniformity-index of hot wall's surface heat flux versus Re in Open Channel (OC) and in channels with Solid Diamond (SD) and Cubic Lattices (CL) with porosities of 50% to 90%*

The results reveal that using lower porosities and higher Re, a more uniform cooling can be attained. For Re of 1,250 and 2,500 the uniformity-index is higher for Solid Diamond lattice, but Cubic lattice performs better in turbulent regions. By using the 50% Solid Diamond in the channel, the uniformity-index increases by 13 % on average.

The share of cooling rate between lattice and wall at Re of 2,500, in the Open Channel, Solid Diamond, and Cubic lattices is presented in Figure 6 (a). By adding lattices, the cooling rate is enhanced by 87% to 285%. In Solid Diamond network cases, the wall has a significant share in cooling reaching a maximum at in 80% porosity. On the other hand, Cubic Lattices have a major share in cooling. Lowering the porosity increases the contribution of the lattice in heat transfer in all cases.

Velocity streamlines, velocity contours, and velocity vectors at the cross-sections of the channel, for the case with 60% porosity Solid Diamond and Re of 2,500 are shown in Figures 6 (b), and 7. It can be observed that high velocity magnitudes and disturbance in the fluid close to the heated wall can be provided by the lattice which elevates the heat transfer. Figure 8 presents the temperature distribution at the cross-sections of the channel and on the lattice surface. The temperature rise in almost half of the height of the lattice can be observed.

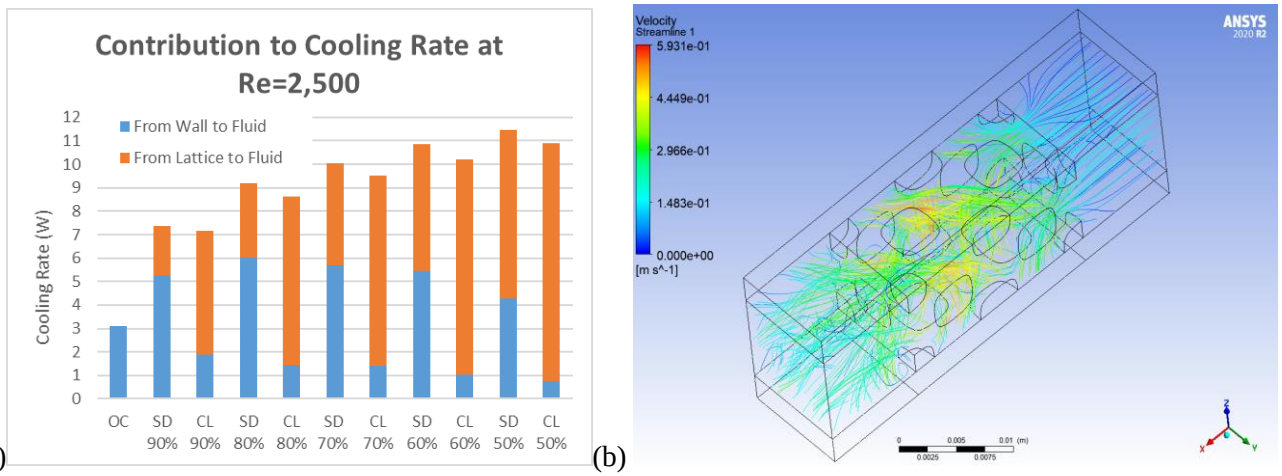


*Figure 6. (a) share of heat transfer from internal side of heated wall to fluid, and lattice to fluid for inlet Re=2,500 in Open Channel (OC) and in channels with Solid Diamond (SD) and Cubic Lattices (CL) with porosities of 50% to 90% (b) Streamlines for Solid Diamond lattice of 60% porosity, Re=2,500, and $T_h$=40 °C*

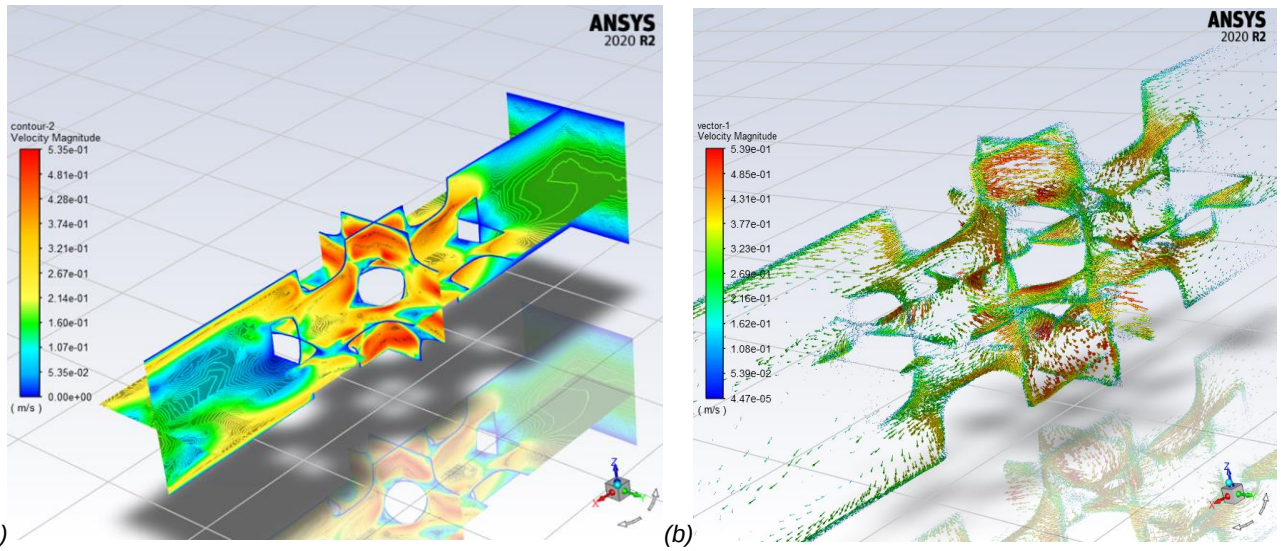


*Figure 7. (a) Velocity contours at the inlet and cross-sections of the channel with 60% porosity Solid Diamond lattice, Re=2,500, and $T_h$=40 °C (b) Velocity vectors at the cross-sections of the channel in the same case*

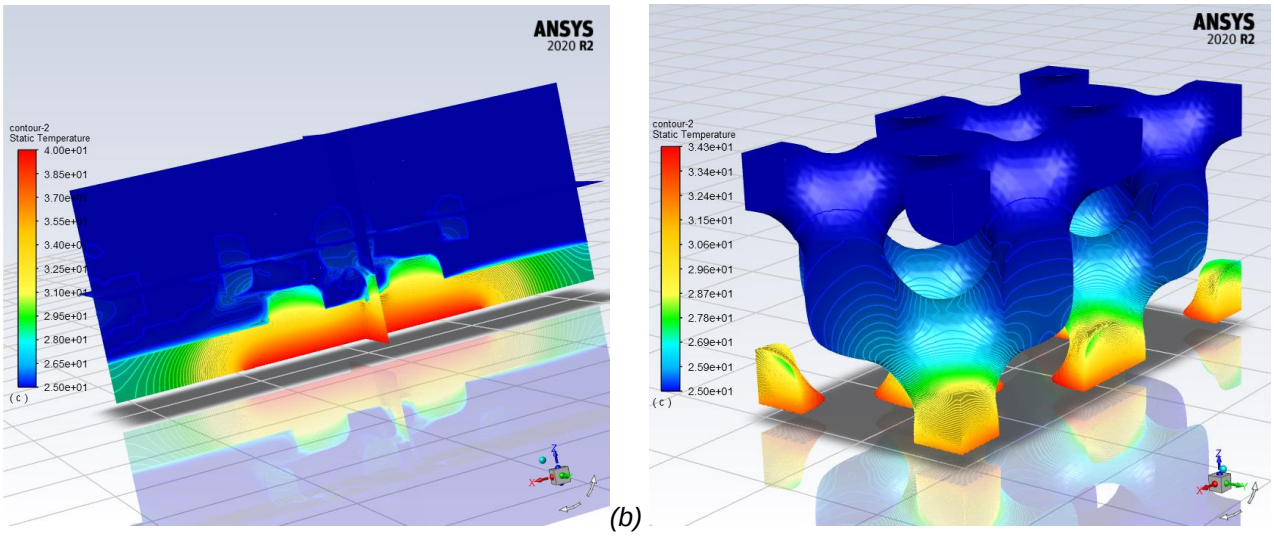


*Figure 8. (a) Temperature field at cross-sections of the channel with 60% porosity Solid Diamond lattice, Re=2,500, and $T_h$=40 °C (b) Temperature field in lattice in the same case*

### *4.2. Performance Evaluation Criteria analysis*

In order to calculate the performance of lattice heat sinks considering pumping power and also heat transfer enhancement, a trade-off analysis between friction factor and Nusselt number is conducted using the Performance Evaluation Criteria (PEC) or Thermal Performance Factor (TPF) in both turbulent (Webb, 1981) and laminar regions (Suresh, Venkitaraj, & Selvakumar, 2011), as defined by Equations 13 and 14.:

$$PEC\ (TPF)_{Turbulent} = \frac{\overline{Nu}/\overline{Nu}_{Base}}{\left(f/f_{Base}\right)^{1/3}} \quad \text{(Eq. 13)}$$

$$PEC\ (TPF)_{Laminar} = \frac{\overline{Nu}/\overline{Nu}_{Base}}{\left(f/f_{Base}\right)^{1/6}} \quad \text{(Eq. 14)}$$

The PEC analysis results are presented in Figure 9. Having a thermal performance of 1 or higher indicates that the cooling system works efficiently considering the pressure drop penalty versus improved cooling rate. The results reveal that the 50% porosity Solid Diamond lattice has the highest performance at Re=1,250 and 2,500 while at higher Re, the 78.4% porosity Cubic lattice performs better.

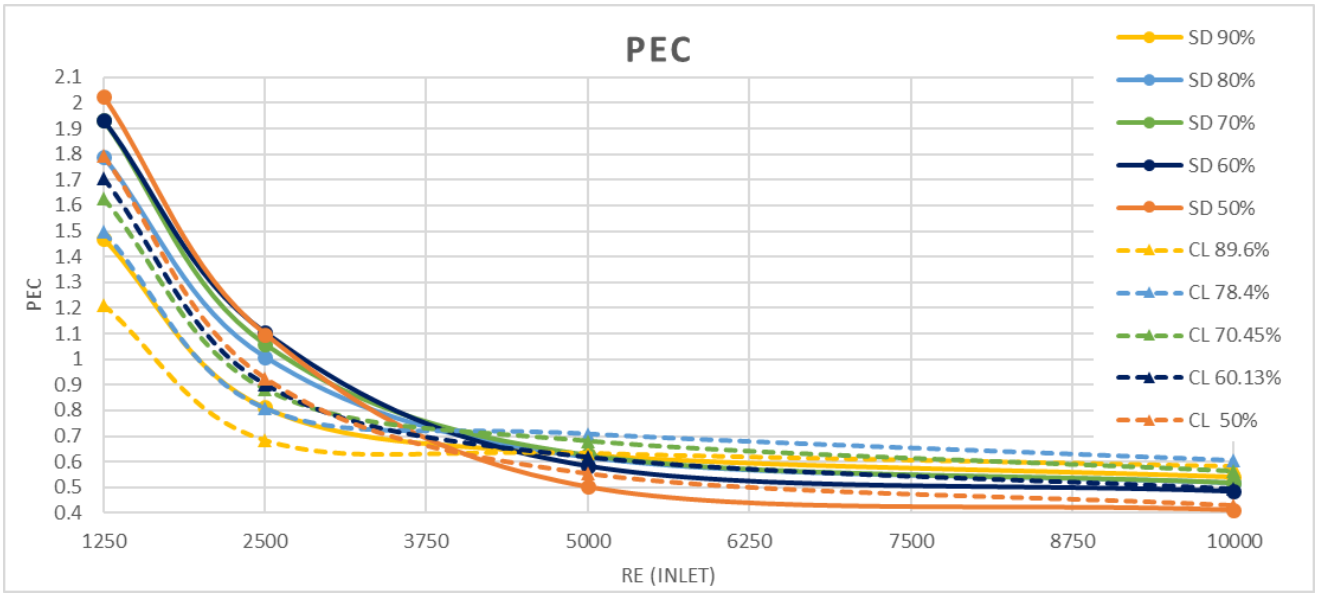


*Figure 9. Performance Evaluation Criteria versus Re in channels with Solid Diamond (SD) and Cubic Lattices (CL) with porosities of 50% to 90%*

## 5. DISCUSSION

Usage of lower porosities and applying higher Re elevates the Nusselt number and uniformity of heat flux significantly. The reasons are more wetted surface area especially provided by cubic lattices and higher disturbance and consequently higher turbulence intensity particularly provided by adding Solid/Skeletal Diamond lattices. Theses advantages result in thinner boundary layers which lower the thermal resistance. On the other hand, the proposed cooling system with lattice structures suffer from high pressure drop specifically in the turbulent region which leads to PEC values lower than 1. TPMS-based Solid/Skeletal Diamond cases with porosities less than 80% have shown PECs above 1 at lower Re in the studied transition and laminar regions which are promising in terms of energy and heat transfer enhancement and lower friction factor. Besides, the increase in the heat flux uniformity-index of the hot wall provides more uniform temperature distribution on the product surfaces which leads to lower residual stresses and warpage during the cooling process. Considering all the aspects, Solid/Skeletal Diamond Lattice with 50% porosity with Re of 2,500 has shown the best performance among the 2 types of lattices studied by providing a heat flux removal of 57,000 $W/m^2$ and increasing the cooling rate by 270%, Nusselt number by 520%, and heat flux uniformity-index by 15.85% with a PEC of 1.1 compared to the Open Channel. These results show that the use of TPMS-based Solid Diamond can enhance the efficiency of conformal cooling with PECs higher than Cubic lattice leading to less required pumping power. In addition, it reduces the residual stresses by increasing the uniformity of heat flux.

## 6. CONCLUSION

In this work, novel cooling channels based on Cubic and Solid/Skeletal Diamond TPMS-based lattices were designed and analysed numerically for the purpose of heat transfer enhancement in channels for conformal cooling of injection moulds. The effect of porosity and Re were investigated for average Nusselt number, friction factor, uniformity-index of heat flux on the heated wall, and PEC/thermal performance factor. The predicted results were promising for cooling and heat flux uniformity in all cases but at the cost of pressure drop. PEC analysis revealed that the designed Solid Diamond lattices with porosities less than 80% at Reynolds numbers of 1,250 and 2,500 are more efficient among the studied cases considering both Nusselt number and friction factor. In conclusion, applying TPMS-based Solid Diamond have a superiority over Cubic lattice in terms of PEC. Using them in Re in the range of 1,250 to 2,500 leads to a cooling enhancement with reasonable PECs, higher heat flux uniformity-index and less pumping power needed providing the required heat flux for conformal cooling of injection moulds. Besides, the increased heat flux uniformity will lead to higher quality of the products.

## 7. REFERENCES

Abueidda, D. W., Al-Rub, R. K. A., Dalaq, A. S., Lee, D. W., Khan, K. A., & Jasiuk, I. (2016). Effective Conductivities and Elastic Moduli of Novel Foams with Triply Periodic Minimal Surfaces. *Mechanics of Materials, 95*, 102-115.

Abueidda, D. W., Bakir, M., Al-Rub, R. K. A., Bergström, J. S., Sobh, N. A., & Jasiuk, I. (2017). Mechanical Properties of 3D Printed Polymeric Cellular Materials with Triply Periodic Minimal Surface Architectures. *Materials & Design*, *122*, 255-267.

Ali, M. I. H., Al-Ketan, O., Khalil, M., Baobaid, N., Khan, K., & Abu Al-Rub, R. K. (2020, July). 3D Printed Architected Heat Sinks Cooling Performance in Free and Forced Convection Environments. In *Heat Transfer Summer Conference* (Vol. 83709, p. V001T09A012). American Society of Mechanical Engineers.

Al-Ketan, O., Ali, M., Khalil, M., Rowshan, R., Khan, K. A., & Abu Al-Rub, R. K. (2021). Forced Convection Computational Fluid Dynamics Analysis of Architected and Three-Dimensional Printable Heat Sinks Based on Triply Periodic Minimal Surfaces. *Journal of Thermal Science and Engineering Applications*, *13*(2).

Al-Ketan, O., Rowshan, R., & Al-Rub, R. K. A. (2018). Topology-Mechanical Property Relationship of 3D Printed Strut, Skeletal, and Sheet Based Periodic Metallic Cellular Materials. *Additive Manufacturing*, *19*, 167-183.

Au, K. M., & Yu, K. M. (2007). A Scaffolding Architecture for Conformal Cooling Design in Rapid Plastic Injection Moulding. *The International Journal of Advanced Manufacturing Technology*, 34(5), 496-515.

Bergman, T. L., Lavine, A. S., Incropera, F. P., & DeWitt, D. P. (2011). *Introduction to heat transfer*. John Wiley & Sons.

Catchpole-Smith, S., Sélo, R. R. J., Davis, A. W., Ashcroft, I. A., Tuck, C. J., & Clare, A. (2019). Thermal Conductivity of TPMS Lattice Structures Manufactured via Laser Powder Bed Fusion. *Additive Manufacturing*, *30*, 100846.

Chen, Z., Xie, Y. M., Wu, X., Wang, Z., Li, Q., & Zhou, S. (2019). On Hybrid Cellular Materials Based on Triply Periodic Minimal Surfaces with Extreme Mechanical Properties. *Materials & Design*, *183*, 108109.

Dittus, F. W., & Boelter, L. M. K. (1930). *Heat Transfer in Automobile Radiators of the Tubular Type*. Berkeley, Calif: University of California Press

Hartnett, J. P., Irvine, T. F., Greene, G. A., & Cho, Y. I. (1998). *Advances in Heat Transfer*. Academic Press.

Khogalia, E. H., Choo, H. L., & Yap, W. H. (2020, May). Performance of Triply Periodic Minimal Surface Lattice Structures under Compressive Loading for Tissue Engineering Applications. In *AIP Conference Proceedings* (Vol. 2233, No. 1, p. 020012). AIP Publishing LLC.

Maskery, I., Sturm, L., Aremu, A. O., Panesar, A., Williams, C. B., Tuck, C. J., ... & Hague, R. J. (2018). Insights into the Mechanical Properties of Several Triply Periodic Minimal Surface Lattice Structures Made by Polymer Additive Manufacturing. *Polymer*, *152*, 62-71.

Oh, S. H., Ha, J. W., & Park, K. (2022). Adaptive Conformal Cooling of Injection Molds Using Additively Manufactured TPMS Structures. *Polymers*, *14*(1), 181.

Suresh, S., Venkitaraj, K. P., & Selvakumar, P. (2011). Comparative Study on Thermal Performance of Helical Screw Tape Inserts in Laminar Flow Using Al2O3/Water and CuO/Water Nanofluids. *Superlattices and Microstructures*, *49*(6), 608-622.

Tang, Y., Gao, Z., & Zhao, Y. F. (2019). Design of Conformal Porous Structures for the Cooling System of an Injection Mold Dabricated by Additive Manufacturing Process. *Journal of Mechanical Design*, *141*(10).

Webb, R. L. (1981). Performance Evaluation Criteria for Use of Enhanced Heat Transfer Surfaces in Heat Exchanger Design. *international journal of heat and mass transfer*, *24*(4), 715-726.

# Experimental plan for the investigation of condition monitoring of additively manufactured die plates under cyclic loading.

Albert Weinert, Centre for Precision Engineering, Materials and Manufacturing (PEM Centre), ATU Sligo, Ireland.
David Tormey, Centre for Precision Engineering, Materials and Manufacturing (PEM Centre), ATU Sligo, Ireland.
Christopher O'Hara, Centre for Precision Engineering, Materials and Manufacturing (PEM Centre), ATU Sligo, Ireland.
Marion McAfee, Centre for Precision Engineering, Materials and Manufacturing (PEM Centre), ATU Sligo, Ireland.

***Abstract***

Additive manufacturing (AM) is seeing an increased uptake in the production of tools and dies due to its ability to print more complex geometries, which are typically exceedingly difficult to achieve with conventional machining (Thompson et al. 2016). Many industries are adapting AM due to its capabilities and one of the industries which have witnessed an increased interest in the technology is Injection Moulding (IM). AM tooling allows for the dies to incorporate a modern form of cooling channels, known as conformal cooling, which reduces process cycle time and enhances control over product quality (Park et al. 2020). However, concerns remain about the viability of AM-produced mould tools and their ability to withstand the mechanical and thermal stresses associated with the injection moulding process over a high number of production cycles. Failure events within IM tooling are typically sudden and catastrophic, causing damage to the machine and resulting in extended downtime (Saputro et al. 2021).

In this experimental plan, the four bodies of work, as identified for the development of a tool condition monitoring system for additively manufactured die plates will be outlined. Starting with an overview into the sample design for accelerated defect formation in 3D printed samples. The failure initiation will be monitored during cyclic loading performed on a constructed bench rig. A sensor-based tool condition monitoring (TCM) system is proposed to monitor the structural health of samples. In recent years, TCM systems have proven to be effective in machining processes, resulting in manufacturing/maintenance cost reduction and quality improvement (Kuntoğlu et al. 2021; Mohanraj et al. 2020). However, to date, there are no reports in the literature on the development of such a system for injection mould tools, especially regarding AM tooling within this industry. Sensors including acoustic emission, accelerometer and ultrasound are used to monitor the initiation and propagation of material defects during cyclic loading. The defects under investigation, simulated in the samples used in this study, are common within the IM and AM industries and include cracking, delamination, and deformation.

*Key Words: Injection Moulding, Additive Manufacturing, Tool Condition Monitoring*

## 1. INTRODUCTION

Injection Moulding (IM) is a method of obtaining moulded products by injecting molten plastic materials into a mould, followed by cooling and solidification (Kazmer 2016). This process is used for manufacturing over 30% of plastic parts in industries including food and beverages, medical and pharmaceutical, electronics, toys, car parts and many more (Singh and Verma 2017). To be able to produce such a mass number of products for each of the industries, the tooling plays a significant role. Any malfunction of the mould tools may lower the productivity of the tool, bringing significant financial losses to the process (Nwanya, Udofia, and Ajayi 2017; Umar Nisbantoro, Jinan, and Hardi Purba 2018). Tool failures cannot be predicted within conventional tooling and often result in catastrophic damage and unscheduled machine downtime. In injection moulding, the tool's complexity is usually dependent on the complexity of the part to be manufactured, with a more complex part resulting in higher design and production costs. The manufacturing of the injection mould tool requires highly experienced mould toolmakers to design the two halves of the tool containing all the geometry and features that make up the part specification. The design of the tool is complicated by the need to achieve rapid and even cooling of the part to achieve fast cycle times whilst maintaining high dimensional stability of the part.

The IM process exerts high cyclic pressures and stresses, which must be withstood by the mould tooling. Tooling defects such as cracking, deflection, wear and blockages of cooling channels are common and must be addressed by the machine operators. Mechanical defects of tooling can influence the final parts, which could cause issues such as flash or line marks. Mould tooling is often complicated, as it needs to provide high precision whilst also

Email: Albert Weinert
albert.weinert@mail.itsligo.ie

providing rapid and even cooling of the parts. Due to the use of conventional cooling, formed by drilling straight bores, the simulated times for the optimum cooling stage are not met, and parts cannot be rapidly and evenly cooled. This results in the formation of hot regions known as 'hot spots' within the moulded components causing uneven cooling and warping of parts. Uneven cooling can cause further issues with part quality, and part defects such as shrinkage, delamination, sink marks, flow line and weld lines. One of the advantages which Additive Manufacturing offers for injection mould tooling is the integration of conformal cooling channels into the tool design. Conformal cooling channels can be located closer to the cavity walls and in effect follow its geometry, providing more effective and consistent heat transfer (Feng, Kamat, and Pei 2021). This result is much shorter cooling times, even cooling of parts and obtaining the required dimensional stability of complex geometry parts.

First attempts at predicting the tool wear in injection moulding process were based on collected process data (Frumosu, Rønsch, and Kulahci 2020). The monitored data included tool information such as mould status, mould characteristics, mould running settings, maintenance data and production data. It presented the possibility of using the process data to create tool wear-out projection curves. Uses of external sensors has been explored by Kek et al. (2015) where acoustic emission sensors have been evaluated for detection of micro-cracks in conventional tool inserts. The collected data showed a successful identification of cracks by comparison of signal amplitudes during injection moulding process. However, there have been no attempts at creating a condition monitoring system of AM mould tools reported in the literature to date.

Many manufacturing industries, including injection moulding, are in the process of adapting the principles of Industry 4.0 and the new operational and business models that come with it. The fourth wave of Industrial advancement introduces new digital technology, where sensors, machines, workpieces, tooling and IT (Information Technology) system connect along the value chain beyond a single enterprise (Milutinović et al. 2021). Introducing additive manufacturing into the injection moulding process opens the possibility to integrate higher sensorisation of tooling and delivering a real-time tool monitoring capability (Moreira et al. 2020). Richer information collected from the tooling can significantly benefit injection mould tooling. This could facilitate tool manufacturers and/or end-user injection moulding companies to monitor the wear of their tools and schedule predictive maintenance, accordingly, enabling them to avoid unnecessary downtime of their processes.

This work looks at simulating the cyclic loading forces experienced by injection mould tooling in 3D printed 316L samples to examine the potential for acoustic emission and accelerometers to detect the early onset. This experiment is conducted on samples which have designed in flaws which act as crack initiation points. Additionally, a high-speed camera will be mounted on the test rig to verify the exact point of failure.

## 2. CONDITION MONITORING SYSTEM

Condition Monitoring of machinery, through the deployment of sensors into critical components of the machinery, shows significant potential in industries such as civil and mechanical engineering, infrastructure, aerospace, and machining. Primarily in machining, TCM systems have been used as indicators for how worn the tools are and when replacement is required to avoid unnecessary downtime or equipment failure. In structural health monitoring, the structure of interest is equipped with sensors to monitor its material and geometric properties (Farrar and Worden 2007). Types of sensors which are used for monitoring the condition of tools, wings, blades, and other structures include ultrasound, acoustic emission, accelerometers, strain gauges, force sensors, optical sensors, and thermography. Depending on the application and fault type, different sensors are used to monitor the relevant type of wear and its development. However, the overall framework of the condition monitoring systems is similar as shown in Figure 1.

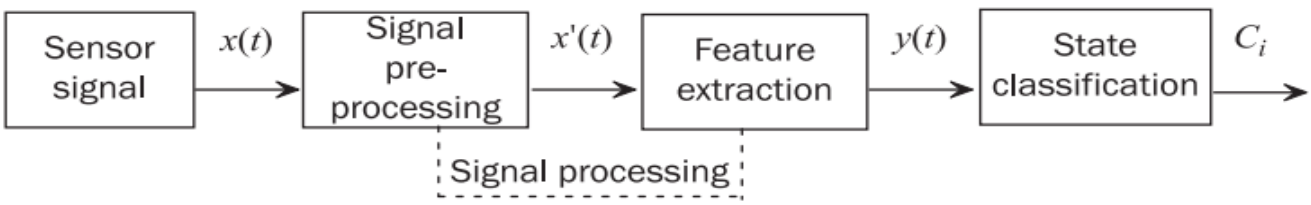


*Figure 1. A condition monitoring system as a pattern recognition system. (Kunpeng et al., 2012).*

At present, the design of injection mould tooling is often complex and integration of internal probes into conventionally machined tools can be challenging. Machining of suitable slots or pockets in existing tooling to embed a probe in a required location can, in some cases, be expensive. AM can more easily create the required space for probes in the mould tools, as well as facilitate the fabrication of complex conformal cooling channels.

### *2.1 Identification of defect development*

Despite offering considerable design flexibility, the Additive Manufacturing process can result in significantly more tool defects than conventional machining processes. Figure 2 presents examples of common AM defects as outlined by Molitch-Hou (2017). AM results in a poor surface finish, and post-machining is required for tooling to be used in the IM process. Warpage occurs when poor heat transfer causes the parts to deform. Residual stresses develop in the part, due to poor heat transfer during the print process, causing deformation of printed components. Porosity in the build is an AM specific issue that must be monitored. It is considered as the most significant issue, as when small voids between layers occur and external forces are exerted on the printed components, the presence of voids can lead to the onset of defects such as cracking or delamination.

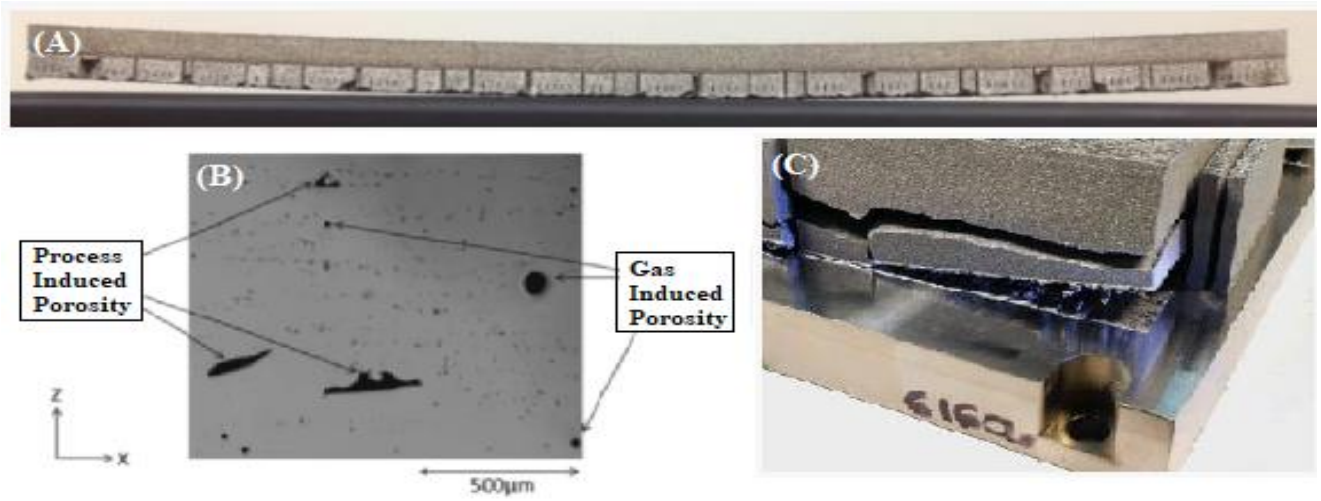


*Figure 2. Examples of Additive Manufacturing defects: (A) Warpage, (B) Porosity and (C) Residual Stresses (Molitch-Hou 2017).*

### *2.2 Identification of defect development*

The presented work examines the effectiveness of accelerometer and acoustic emission sensors for early identification of the development of faults in 3D printed samples under cyclic loading. A high-speed camera is used as an additional source of information for post verification of results. The 3D printed samples were manufactured with features located in strategic locations, most liable to failure during the cyclic loading, to accelerate the onset of failures such as cracking and deformation. The selected probes have proven to be highly effective for early identification of such defects in other industries (Nath 2020; Serin et al. 2020).

## 3. EXPERIMENTAL WORK

### *3.1 Manufacturing of samples*

The tested samples were designed and manufactured in collaboration with a research partner, SEAM (South Eastern Applied Materials). An EOS M280 metal 3D printed was used to print three samples using Stainless Steel 316L powder. The process parameters for manufacturing the samples are listed in Table 1.

*Table 1. Additive Manufacturing process settings*

| Layer Thickness | Laser Scanning | Laser Power | Laser Speed |
|---|---|---|---|
| 20µm | 67° | 200W | 1200mm/s |

The three samples are of identical shape but contain unique features as shown in Figure 3, each of the plates contain a different feature intended to accelerate the testing of failures. These features aim to accelerate the occurrence and presence of failures at the designed locations for better monitoring. Each of the probes are intended to monitor the development of material deformation and crack formation during the cyclic testing. A high-speed camera will monitor the exact time of deformation and mechanical failure of the tested samples.


*Figure 3. Three samples manufactured using 3D printing.*

### *3.2 Experimental Setup*

The samples were tested on a custom-built bench rig with acoustic emission and accelerometer probes attached to the samples. The cyclic testing will have a pre-set cut off time of 20 minutes for conventional and 30 minutes for AM samples.

The signal from the Vallen Systeme, passive piezoelectric AE (Acoustic Emission) probe (VS160-NS), which has a resonant frequency of 160 kHz, is connected to a preamplifier and a decoupler from Vallen Systeme to a Data Acquisition Device (DAQ) for sampling. The accelerometer used is a CTC (MEB221) rated at 10mV/g with a dedicated signal conditioner and connected to a DAQ unit. Additionally, a Ximea high-speed camera with a 9mm lens has been mounted on the rig for monitoring the deformation of the samples. The sampling rate was set at 200 samples/sec for the acoustic sensors. 200 samples/sec for the accelerometer and 500 frames for the high-speed camera. All devices are directly connected to a PC for data collection and storage during the testing of the samples. The captured data is analysed using Matlab software.

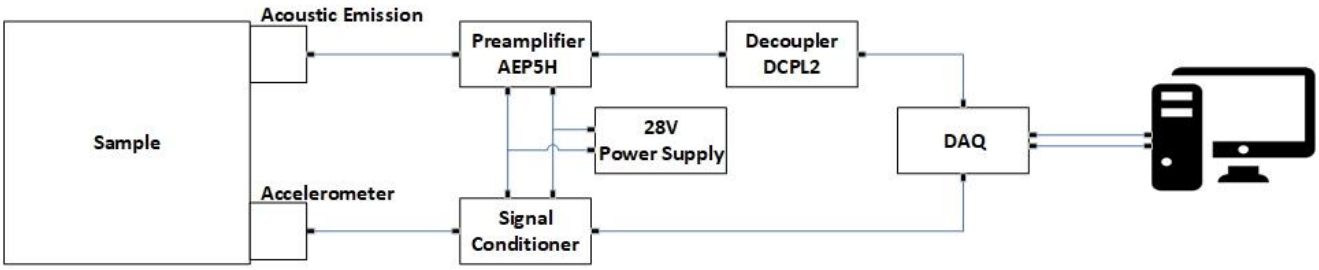


*Figure 4. Schematic Diagram of the setup.*

## 4. RESULTS

**Error! Reference source not found.** presents the preliminary results from cyclic loading of the samples using a pneumatic cylinder exerting a force of 480N on localised region of $2mm^2$ on the samples. The testing has been

conducted over a duration of 20 minutes for conventional and 30 minutes for each of the AM samples. The preliminary results are discussed in the next section.

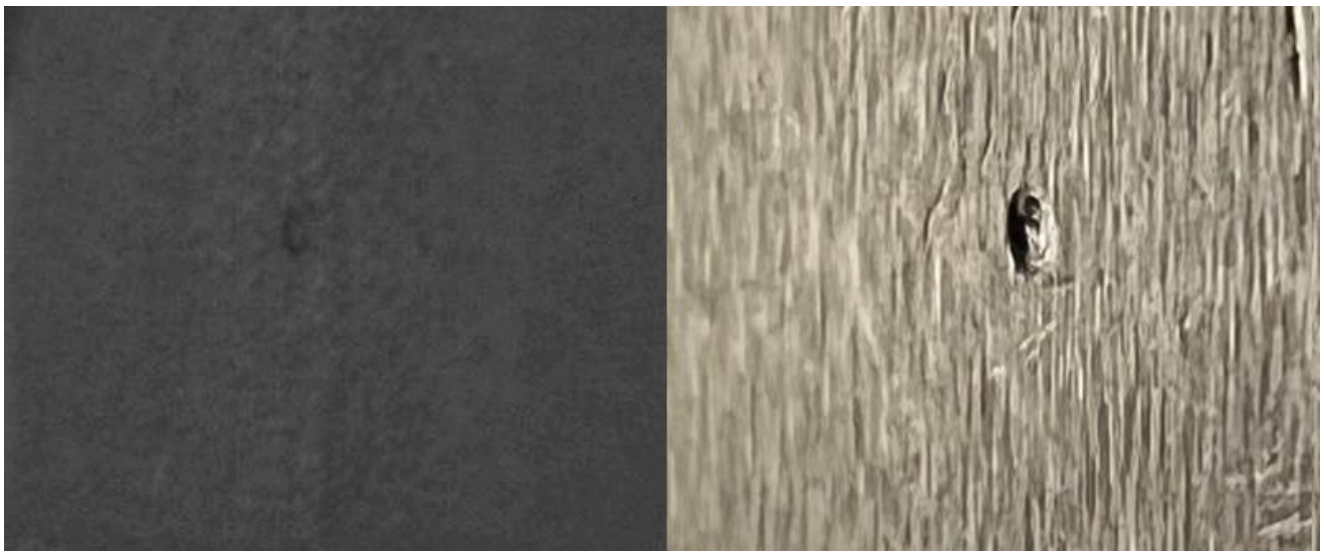

*Figure 5. AM sample (Right) vs Conventional (Left) Sample after cyclic loading.*

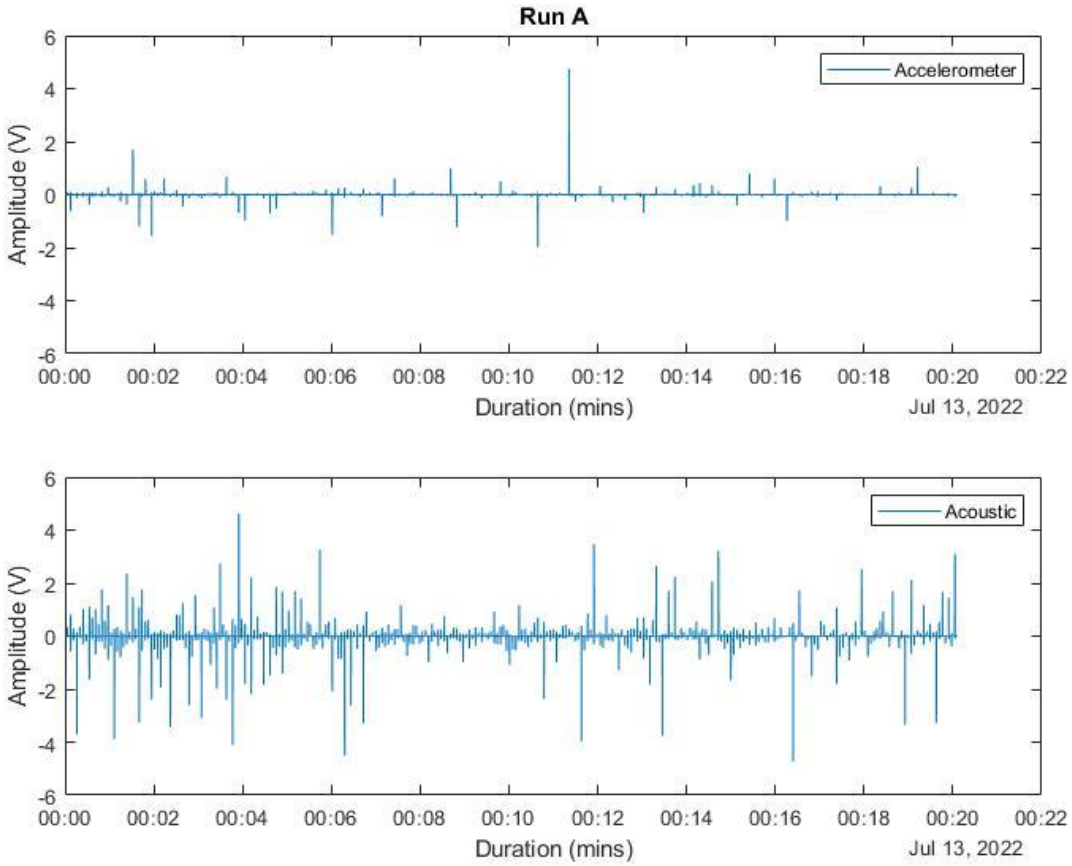


*Figure 6. Sensor data from a 20-minute test on conventional sample.*

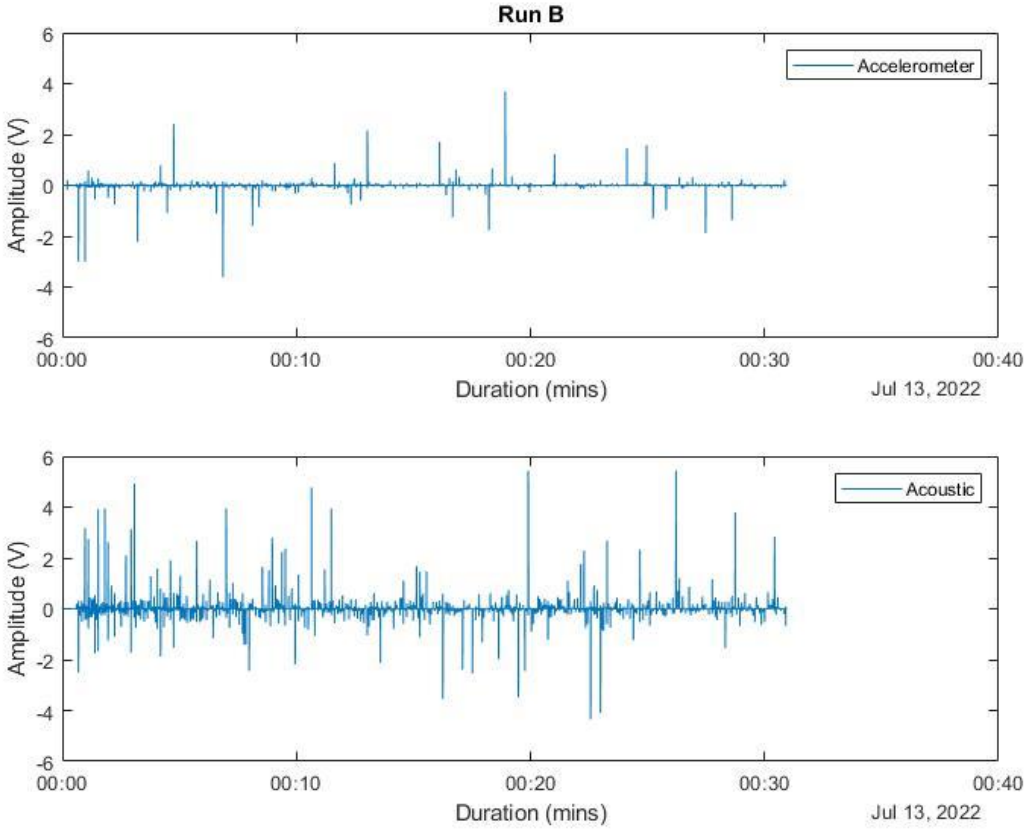


*Figure 7. Sensor data from a 30-minute test on AM sample (A).*

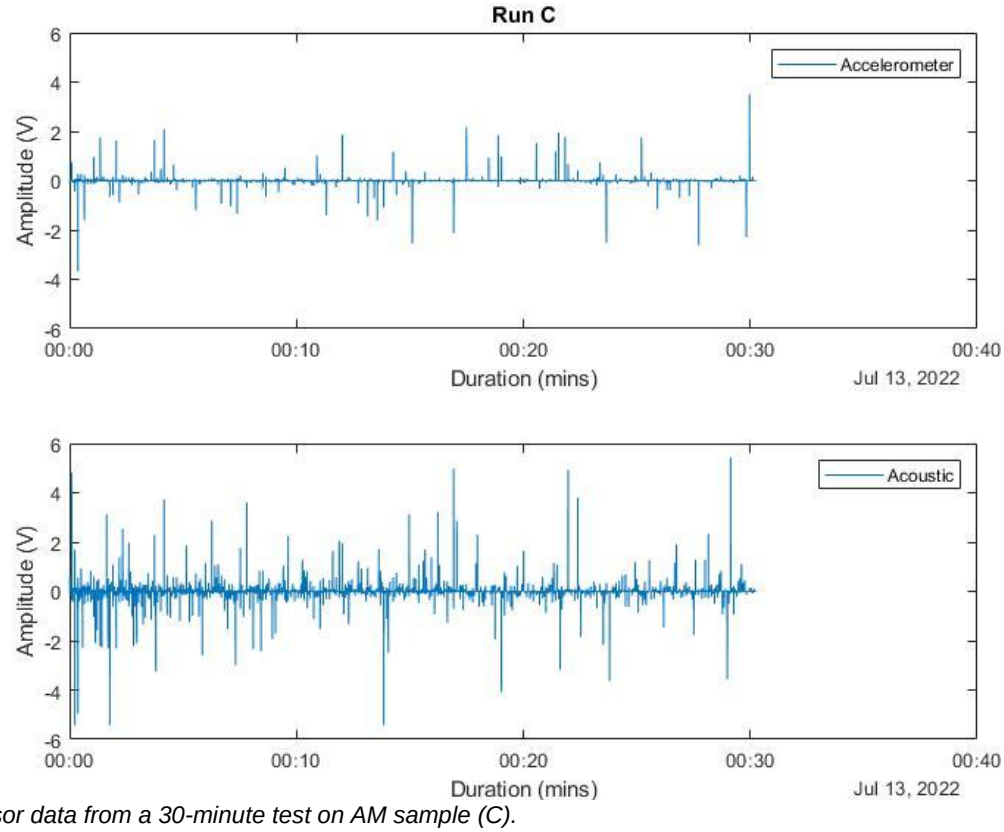


*Figure 8. Sensor data from a 30-minute test on AM sample (C).*

## 5. DISCUSSION

The preliminary results collected during initial trails showed an increased hardness in the AM samples compared to the conventionally machined 316L steel sample. The 3D printed samples have not undergone any additional post processing, such as hardening, and they showed a much higher strength in comparison to the conventional samples under the same test conditions. Figure 5 shows a comparison between the two types of samples and a significant difference can be observed where the conventional steel is clearly dented, where the agitator caused a surface defect on the sample. The collected data from both sensors has not shown any clear results, further analysis of the data using unsupervised learning will be conducted to analyse the data in greater detail. The high-speed camera has shown no wear on the AM sample apart from a small mark (where the roughness was smoothed) which has been caused by the point of contact between the sample and the agitator as shown in Figure 5. This is in comparison to the noticeable dent on the conventionally machined sample. The collected data presented in Figure 6-8 is recorded on one conventional sample and two AM samples. The collected data requires further analysis and filtering due to a large amount of background noise. The final sample requires testing for full understanding of the sensor behaviour during cyclic loading. Thus far, the collected data has not shown any similar patterns between samples, and further analysis is required to understand the data.

## 6. CONCLUSION

The conducted preliminary experiment has shown that AM samples without post-processing appears to be a lot harder when compared to conventional steel. The work has provided an understanding relevant to the performance of the samples and design options which can be later implemented into the final mould tool design where greater forces are present and accelerated tooling defects will be easier to accomplish. The designed samples will be retested using an increased force and compared once again with the conventional sample of identical size to finalise the results. The testing will be conducted with a higher load by upgrading to a larger bore pneumatic cylinder and applying a higher load to the direct point of contact, for acceleration of the test to accommodate the increased sample hardness. Additionally, the third sample, which was on a long lead time at the time of this preliminary test, will be included with the new testing conditions and it will undergo the same steps for data analysis and filtering to understand the behaviour of the sensors under loading and how they respond to tooling failure.

## 7. REFERENCES

Farrar, Charles R., and Keith Worden. 2007. "An Introduction to Structural Health Monitoring." *Mathematical Physical & Engineering Sciences* (365):303–315. doi: 10.1098/rsta.2006.1928.

Feng, Shaochuan, Amar M. Kamat, and Yutao Pei. 2021. "Design and Fabrication of Conformal Cooling Channels in Molds: Review and Progress Updates." *International Journal of Heat and Mass Transfer* 171:121082. doi: 10.1016/j.ijheatmasstransfer.2021.121082.

Frumosu, Flavia Dalia, Georg Ørnskov Rønsch, and Murat Kulahci. 2020. "Mould Wear-out Prediction in the Plastic Injection Moulding Industry: A Case Study." *International Journal of Computer Integrated Manufacturing* 33(12):1245–58. doi: 10.1080/0951192X.2020.1829062.

Kazmer, David O. 2016. *Injection Mold Design Engineering*. 2nd ed. edited by C. Hamiltion. Munich: Hanser Publishers.

Kek, Tomaz, Dragan Kusic, Ales Hancic, and Janez Grum. 2015. "Acoustic Emission Crack Detection in Injection Molding." *NDT in Progress 2015 - 8th International Workshop of NDT Experts, Proceedings* 81–88.

Kuntoğlu, Mustafa, Abdullah Aslan, Danil Yurievich Pimenov, Üsame Ali Usca, Emin Salur, Munish Kumar Gupta, Tadeusz Mikolajczyk, Khaled Giasin, Wojciech Kapłonek, and Shubham Sharma. 2021. "A Review of Indirect Tool Condition Monitoring Systems and Decision-making Methods in Turning: Critical Analysis and Trends." *Sensors (Switzerland)* 21(1):1–33. doi: 10.3390/s21010108.

Milutinović, Mladomir, Mijodrag Milošević, Jovica Ilić, Dejan Movrin, Milija Kraišnik, Saša Ranđelović, and Dejan Lukić. 2021. "Industry 4.0 and New Paradigms in the Field of Metal Forming." *Tehnički Glasnik* 15(2):250–57. doi: 10.31803/tg-20210524192249.

Mohanraj, T., S. Shankar, R. Rajasekar, N. R. Sakthivel, and A. Pramanik. 2020. "Tool Condition Monitoring Techniques in Milling Process-a Review." *Journal of Materials Research and Technology* 9(1):1032–42. doi: 10.1016/j.jmrt.2019.10.031.

Molitch-Hou, Michael. 2017. "Issues to Look Out for in Metal 3D Printing." *3D Printing*. Retrieved March 16, 2020 (https://www.engineering.com/3DPrinting/3DPrintingArticles/ArticleID/15202/7-Issues-to-Look-Out-for-in-Metal-3D-Printing.aspx#:~:text=In the metal 3D printing,warping%2C cracking and surface finish.).

Moreira, Eurico Esteves, Filipe Serra Alves, Marco Martins, Gabriel Ribeiro, António Pina, Diogo E. Aguiam, Edoardo Sotgiu, Elisabete P. Fernandes, and João Gaspar. 2020. "Industry 4.0: Real-Time Monitoring of an Injection Molding Tool for Smart Predictive Maintenance." *IEEE International Conference on Emerging Technologies and Factory Automation, ETFA* 2020-Septe:1209–12. doi: 10.1109/ETFA46521.2020.9212167.

Nath, Chandra. 2020. "Integrated Tool Condition Monitoring Systems and Their Applications: A Comprehensive Review." *Procedia Manufacturing* 48:852–63. doi: 10.1016/j.promfg.2020.05.123.

Nwanya, S. C., J. I. Udofia, and O. O. Ajayi. 2017. "Optimization of Machine Downtime in the Plastic Manufacturing." *Cogent Engineering* 4(1). doi: 10.1080/23311916.2017.1335444.

Park, Hong-Seok, Xuan-Phuong Dang, Dinh-Son Nguyen, and Saurabh Kumar. 2020. "Design of Advanced Injection Mold to Increase Cooling Efficiency." *International Journal of Precision Engineering and Manufacturing-Green Technology* 7(2):319–28. doi: 10.1007/s40684-019-00041-4.

Saputro, Iwan, Erry Rimawan, Alib Sabaruddin, and Wahyu Abadi. 2021. "Performance Measurement Analysis of Injection Molding Machine JSW J450AD Using Methods Overall Effectiveness ( OEE ) And Failure Mode Effect Analysis ( FMEA ) In The Plastics Industry." 6(8):1193–99.

Serin, G., B. Sener, A. M. Ozbayoglu, and H. O. Unver. 2020. "Review of Tool Condition Monitoring in Machining and Opportunities for Deep Learning." *International Journal of Advanced Manufacturing Technology* 109(3–4):953–74. doi: 10.1007/s00170-020-05449-w.

Singh, Gurjeet, and Ajay Verma. 2017. "A Brief Review on Injection Moulding Manufacturing Process." *Materials Today: Proceedings* 4(2):1423–33. doi: 10.1016/j.matpr.2017.01.164.

Thompson, Mary Kathryn, Giovanni Moroni, Tom Vaneker, Georges Fadel, R. Ian Campbell, Ian Gibson, Alain Bernard, Joachim Schulz, Patricia Graf, Bhrigu Ahuja, and Filomeno Martina. 2016. "Design for Additive Manufacturing: Trends, Opportunities, Considerations, and Constraints." *CIRP Annals - Manufacturing Technology* 65(2):737–60. doi: 10.1016/j.cirp.2016.05.004.

Umar Nisbantoro, Faisal, Riyadil Jinan, and Humiras Hardi Purba. 2018. "Measurement Overall Equipment Effectiveness on Injection Moulding Machine: A Case Study in Injection Moulding Manufacturing Industry." *International Journal of Engineering Research and Advanced Technology* 4(8):62–69. doi: 10.31695/ijerat.2018.3302.

# Chapter 4: Forming Processes (Plastic Injection Moulding)Additive Manufacturing

# Model-based pressure tracking using a feedback linearisation technique in thermoplastic injection moulding

Mandana Kariminejad, Centre for Precision Engineering, Material and Manufacturing (PEM), Atlantic Technological University Sligo, I-Form Advanced Manufacturing Research Centre
David Tormey, Centre for Precision Engineering, Material and Manufacturing (PEM), Atlantic Technological University Sligo, I-Form Advanced Manufacturing Research Centre
Marion McAfee, Centre for Precision Engineering, Material and Manufacturing (PEM), Atlantic Technological University Sligo, I-Form Advanced Manufacturing Research Centre

***Abstract***

Injection moulding is a well-established automated process for manufacturing a wide variety of plastic components in large volumes and with high precision. There are, however, process control challenges associated with each stage of injection moulding, which should be monitored and controlled precisely to prevent defects in the injection moulded component. One of the process variables is the pressure profile during the injection and packing phases, which has a direct impact on the quality of the manufactured part. This research proposes a model-based controller design for the injection and cavity pressure during the moulding cycle, with a feedback linearisation controller. First, the injection and packing phases were mathematically modelled and converted to a state-space model. The procedure of designing the controller for the process was outlined. A pressure profile was defined as the target trajectory in the proposed controller and the ability of the designed controller in following the set profile was explored.

*Key Words: Injection Moulding, Cavity pressure, Feedback Linearisation.*

## 1. INTRODUCTION

One of the most developed processes to produce plastic components is injection moulding. In general, this process contains three main steps: the filling stage in which melted polymer pellets are injected into the cavity, the packing stage which prevents excessive shrinkage by injecting extra polymer when the cavity is full, and the cooling stage where the polymer solidifies and becomes ready for ejection (Kazmer, 2007). There are process control challenges associated with each stage of injection moulding, critical process variables should be monitored and controlled precisely to prevent defects in the injection moulded component. One of the process variables of interest, is the pressure profile during the packing and injection phases, which has a direct impact on the quality of the manufactured part. Non-optimised pressure will lead to part defects such as weldlines, shrinkage, and warpage (Chen et al., 2019; Kurt et al., 2009).

Real-time and online control of the injection moulding process is a challenge. One of the main challenges is to control and model the batch nature of the process, which is different from classical continuous process models due to the levels of inherent process variation. This process is also nonlinear with a high number of complex and dynamic variables, making the design of a controller more difficult. Several studies have been done to control the process by using a classical controller such as PID (C. J. Chen et al., 2021; Jeong et al., 2015; Pannawan & Sudsawat, 2021). However, these controllers are not able to control the complexity, uncertainties, and nonlinearity of batch processes like injection moulding.

A feedback linearisation controller is a powerful controller which has an acceptable control performance for many nonlinear systems, and it addresses two of the main challenges in control theory: robustness and stability. In this method, a nonlinear system is transformed into a fully or partially decoupled linear system by using nonlinear transformation and cancelling the nonlinearities of the system through feedback. After linearisation, linear control techniques can be applied to control the desired output (Wu & Blaabjerg, 2021). The linear design tool used in this research is input-output linearisation, which can be achieved by differentiating the output several times and has been applied to obtain a linear input-output description.

Email: Mandana Kariminejad
Mandana.kariminejad@mail.itsligo.ie

In this project, design of a feedback linearisation controller is explored for the nonlinear model of a servo-electric injection moulding machine to control and track the desired pressure profile and find the optimum input, which is the voltage of the servo-electric motor, for the desired pressure profile. In the following sections the nonlinear model of servo-electric injection moulding is outlined and the feedback linearisation method and resulting simulation are discussed. To conclude, a discussion regarding the controller result and further research opportunities for the improvement of the controller are explained.

## 2. METHODOLOGY

### *2.1. Nonlinear model of a servo-electric injection moulding*

This study utilises the nonlinear model developed by Stemmler et al. (Stemmler et al., 2019) for a servo-electric injection moulding machine. They modelled the servo-electric drive, plastification unit, nozzle, and cavity. In their model, the servo-electric drive was estimated by a second-order system to relate the input voltage *U* to the desired drive velocity *v*. The transfer function for this second-order system by the Laplace transformation is presented in equation (1). In the function, the values gain *K*= 23.4, damping *D*=0.79 and cut-off frequency $w_0$=133s$^{-1}$ are estimated.

$$G(s) = \frac{V(s)}{U(s)} = \frac{K{w_0}^2}{s^2 + 2Dw_0 s + w_0^2} e^{-sT_d} \tag{1}$$

The plastification unit was approximated as a hydraulic cylinder and the pressure was derived by the mass continuity equation as equation (2). $\beta_s$ is the bulk modulus, $v_s$ is the specific volume and $\dot{m}_n$ is the mass flow through the nozzle and can be also estimated by equation (3).

$$\frac{dp_s}{dt} = \frac{\beta_s}{x}(-v - \dot{m}_n v_s + m_s \dot{v}_s) \tag{2}$$

The mass flow through the nozzle ($\dot{m}_n$) was found by assuming a steady-state flow of a Newtonian fluid. In this equation, the radius and length of the nozzle are *R*=0.2 cm and *L*=8cm respectively. The viscosity $\mu$ is considered constant and equal to 60 kg m$^{-1}$ s$^{-1}$.

$$\dot{m}_n = \frac{\pi R^4}{8 v_s L \mu}(p_s - p_c) \tag{3}$$

The cavity was modelled, similarly to equation (2), by modelling the mass flow through the nozzle and shrinkage of the melt flow in the cavity as described in equation (4). $\beta_c$ is the bulk modulus, and $v_c$ is the specific volume in the cavity.

$$\frac{dp_c}{dt} = \frac{\beta_c}{v_0}(\dot{m}_n v_c + m_c \dot{v}_c) \tag{4}$$

To simplify the model, the derivation of the specific volume of the cavity and screw were neglected. Also, the bulk modulus in both the cavity and screw ($\beta_s, \beta_c$) are considered to be constant and equal to 8662bar. The mathematical model consists of five variables identified as screw position ($x := x_1$), drive velocity ($v := x_2$), derivative of the derive velocity ($\dot{v} := x_3$), screw pressure ($p_s := x_4$) and cavity pressure ($p_c := x_5$). By considering a five-state nonlinear equation the system can be modelled as equation (5), where *x* is the state vector, *U* is the input voltage and the desired output *y* for this system is the cavity pressure which is defined as the fifth state $x_5$ above.

$$\dot{X} = f(x) + g(x)U \tag{5}$$
$$y = p_c = x_4 = h(x) \qquad , \quad Q = \frac{\pi R^4}{8 v_s L \mu}$$

where,

$$f(x) = \begin{bmatrix} x_2 \\ x_3 \\ -2Dw_0x_3 - {w_0}^2x_2 \\ -\frac{\beta_s}{x_1}x_2 - \frac{Q\beta_s}{x_1}(x_4 - x_5) \\ \frac{Q\beta_c}{v_0}(x_4 - x_5) \end{bmatrix}, \quad g = \begin{bmatrix} 0 \\ 0 \\ k{w_0}^2 \\ 0 \\ 0 \end{bmatrix}, \quad x = \begin{bmatrix} x_1 \\ x_2 \\ x_3 \\ x_4 \\ x_5 \end{bmatrix}$$

### *2.2. Feedback linearisation methodology*

The method used here is based on single input feedback linearisation developed by (HASSAN K. KHALIL, 2002). By considering the following SISO (single input, single output) system and having the Lie derivative of *h* along the direction of the vector *f*:

$$\dot{X} = f(x) + g(x)U \tag{6}$$
$$y = p_c = x_5 = h(x) \ , \quad L_f h := \frac{\partial h(x)}{\partial x} f$$

The derivative of output ($\dot{y}$), can be written by equation (7).

$$\dot{y} = \frac{\partial h}{\partial x}(f(x) + g(x)U) \stackrel{\text{def}}{=} L_f h(x) + L_g h(x)U \tag{7}$$
$$L_g h := \frac{\partial h(x)}{\partial x} g$$

In the injection moulding model based on equation (5), $L_g h(x) = 0$. So, the derivative of the output should be further differentiated until *U* appears in the equation. In our model after four derivatives, this condition was satisfied. The relative degree of the system is 4, where the condition of $L_g L_f^{4-1} h(x) \neq 0$ was satisfied.

$$y^{(4)} = {L^4}_f h(x) + L_g L_f^{4-1} h(x)U \tag{8}$$
$$U = \frac{1}{L_g L_f^{4-1} h(x)} \left[-{L^4}_f h(x) + v\right], \quad y^{(4)} = v$$
$${L^4}_f h(x) = L_f L_f^{4-1} h(x), \quad L_g L_f h(x) = \frac{\partial L_f h}{\partial x} g$$

In our model:

$$L_g L_f^{4-1} h(x) = \frac{KB_s w_0^2}{x_1}$$
$${L^4}_f h(x) = \frac{Q^2 B_s^2}{v_0}\left(\frac{x_3}{x_1^2} - \frac{2x_2^2}{x_1^3}\right) + \left(\frac{Q^3 B_s^3 B_c}{v_0 x_1^3} + \frac{Q^2 B_s^2 B_c}{{v_0}^2 x_1^3}x_2 + \frac{Q^3 B_c^2 B_s^2}{{v_0}^2 x_1^2}x_2 + \frac{Q^3 B_c^3 B_s}{{v_0}^3 x_1}\right)\left(-x_2 - Q(x_4 - x_5)\right) +$$
$$\left(\frac{2Q^3 B_s^2 B_c}{v_0 x_1^3} + \frac{Q^3 B_c^2 B_s}{{v_0}^2 x_1^2}\right)(x_2 x_5 - x_4 x_2) - \left(\frac{Q^4 B_s^3 B_c{}^2}{{v_0}^2 x_1^2} + \frac{Q^4 B_c^3 B_s}{{v_0}^3 x_1} - \frac{Q^4 B_c{}^4}{{v_0}^4}\right)(x_4 - x_5) + \frac{Q^2 B_s B_c}{{v_0}^2 x_1^2}(x_4 x_3 - \frac{x_2^2 x_4}{x_1}) +$$
$$\frac{Q^2 B_c^2 B_s}{{v_0}^2 x_1}(x_3 - \frac{x_2^2}{x_1}) - \frac{B_s}{x_1}(-2Dw_0 x_3 - {w_0}^2 x_2 - \frac{x_2 x_3}{x_1} + \frac{2x_2 x_3}{x_1} - \frac{{x_2}^3}{{x_1}^2}) \tag{9}$$

By considering a feedback controller it can be assumed that $y^{(4)} = v = -Ke$, where system error *(e)* is equal to $y - y_d$ and $y_d$ is the desired output and thereby pressure profile. By considering a feedback controller it can be written:

$$v = y^{(4)} = y_d^{(4)} - k_1\dddot{e} - k_2\ddot{e} - k_3\dot{e} - k_4 e \underset{y^{(4)} - y_d^{(4)} = 0}{=} k_1\dddot{e} + k_2\ddot{e} + k_3\dot{e} + k_4 e = 0 \tag{10}$$

where $k_1, k_2, k_3$ and $k_4$ are the controller gains and should be estimated and adjusted so that the controller successfully tracks our desired pressure profile.

## 3. RESULTS

MATLAB R2021 Simulink was used to model the controller and the system. The Simulink model consists of three functions. The first block defines the model of the injection moulding machine where the cavity pressure is the output. The second is the feedback linearisation control strategy as explained in the methodology section and the last one creates the feedback gains and error. The schematic of the simulation model is presented in Figure 1.

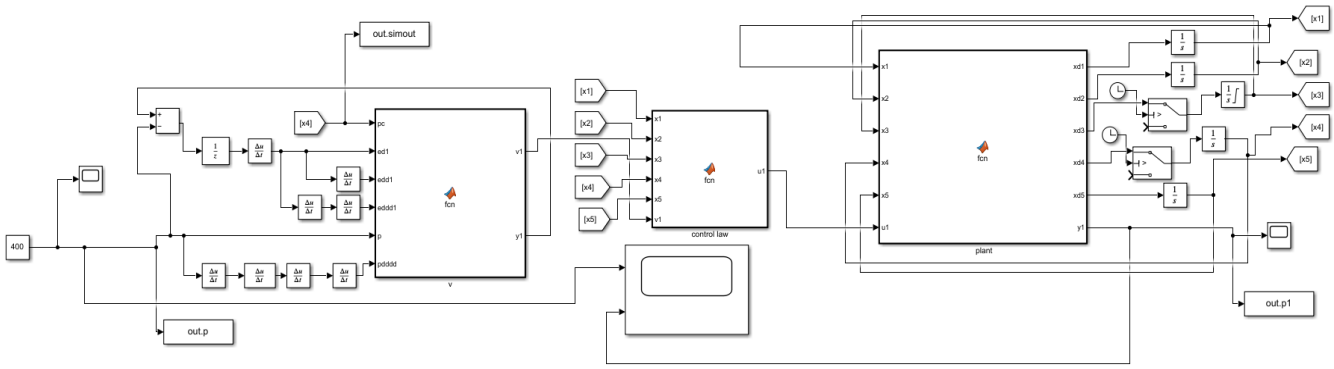


*Figure 1. Simulink simulation of the system and controller*

The performance of the controller when the cavity pressure is constant and equal to 400bar was investigated and presented in Figure 2. After almost five seconds the cavity pressure reached the desired set point of 400 bar.

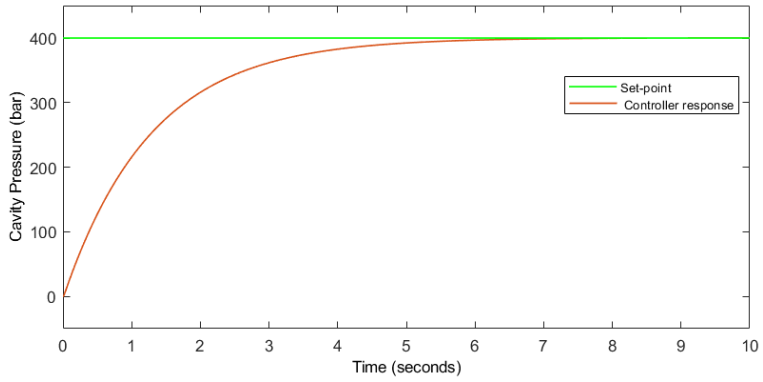


*Figure 2. Feedback linearisation response with constant cavity pressure set point*

The controller gains were chosen as $k_1 = 0.7,\ k_2 = 2,\ k_3 = 30$ and $k_4 = 2.5$.

## 4. CONCLUSION

In this paper the nonlinear mathematical model of a servo-electric injection moulding process is presented. The model contains five states named screw position, derive velocity, derivative of derive velocity, screw pressure and cavity pressure. The model was used in a feedback linearisation control approach to track a constant cavity pressure profile. The controller was designed and simulated in MATLAB R2021 Simulink.

The controller successfully tracked the cavity pressure profile while the response time was slow for the injection moulding process. The response time of the controller depends on the controller gains ( $k_1, k_2, k_3, k_4$) which should be optimised to provide the best performance. These gains can be found and optimised through machine learning algorithms.

In this research, the performance of the controller was only investigated against the constant cavity pressure profile, further research is required to evaluate the controller response with other pressure profiles and other desired outputs such as screw position and pressure. In this study the gains of the controller were selected randomly, for future work these gains should be optimised through a machine learning algorithm. Finally, the controller was designed based on the continuous model, however, injection moulding is a batch process and for better estimation, the controller should be designed based on the discrete model to have more reliable and realistic results.

## 4. REFERENCES


Chen, C. J., Wu, K. T., & Hwang, S. J. (2021). Development of a servo-hydraulic system with a self-tuning fuzzy PID controller to simulate injection molding process. *Microsystem Technologies*, *27*(4), 1217–1238. https://doi.org/10.1007/s00542-018-4171-0

Chen, J.-Y., Liu, C.-Y., & Huang, M.-S. (2019). Enhancement of Injection Molding Consistency by Adjusting Velocity/Pressure Switching Time Based on Clamping Force. *International Polymer Processing*, *34*(5), 564–572. https://doi.org/10.3139/217.3867

HASSAN K. KHALIL. (2002). Nonlinear SysteIlls Third Edition. In *Department of Electrical and Computer Engineering Michigan State University* (Vol. 122).

Jeong, B. H., Kim, N. H., & Lee, K. Y. (2015). Optimized digital proportional integral derivative controller for heating and cooling injection molding system. *Journal of Electrical Engineering and Technology*, *10*(3), 1383–1388. https://doi.org/10.5370/JEET.2015.10.3.1383

Kazmer, D. O. (2007). Injection Mold Design Engineering. In *Injection Mold Design Engineering* (pp. I–XX). München: Carl Hanser Verlag GmbH & Co. KG. https://doi.org/10.3139/9783446434196.fm

Kurt, M., Saban Kamber, O., Kaynak, Y., Atakok, G., & Girit, O. (2009). Experimental investigation of plastic injection molding: Assessment of the effects of cavity pressure and mold temperature on the quality of the final products. *Materials and Design*, *30*(8), 3217–3224. https://doi.org/10.1016/j.matdes.2009.01.004

Pannawan, A., & Sudsawat, S. (2021). Optimized parameters to tune i-pd control through firefly algorithm for heating operations of plastic injection molding. *Songklanakarin Journal of Science and Technology*, *43*(4), 1123–1130. https://doi.org/10.14456/sjst-psu.2021.147

Stemmler, S., Ay, M., Vukovic, M., Abel, D., Heinisch, J., & Hopmann, C. (2019). Cross-phase Model-based Predictive Cavity Pressure Control in Injection Molding. *2019 IEEE Conference on Control Technology and Applications (CCTA)*, 360–367. IEEE. https://doi.org/10.1109/CCTA.2019.8920461

Wu, C., & Blaabjerg, F. (2021). Advanced control of power electronic systems—an overview of methods. In F. B. T.-C. of P. E. C. and S. Blaabjerg (Ed.), *Control of Power Electronic Converters and Systems* (pp. 1–33). Elsevier. https://doi.org/10.1016/B978-0-12-819432-4.00020-2

# A DoE Investigation and Validation of the Stretch Blow Moulding Input Parameter Effects on Pressure Curve Response Measures using Simulation Data

James Grace, Queen's University Belfast

***Abstract***

The continuous development of simulation tools, achieving an ever-increasing accuracy to their real-world counterparts, has allowed the fast and efficient investigation into their properties. These simulations are used in part to make informed decisions on new processes or optimisations of current processes. An axisymmetric stretch blow moulding simulation was set up to accurately simulate the real-world stretch blow moulding process. From this easily generated simulation data a DoE is carried out to determine the effects of the inputs on the desired quality responses such as minimum thickness and pressure profile. These results are then validated through experimental trials using the Definitive Screening Design. The verification of such methods will allow for ease of investigation and optimisation of new sustainable materials which can be efficiently and effectively introduced into the current processes of manufacture.

*Key Word: Stretch Blow Moulding, Design of Experiments, Definitive Screening Design, Simulation*

## *1.INTRODUCTION*

Many papers already exist investigating the stretch blow moulding process via experimental tests, such as; investigation into constant width, simultaneous and sequential biaxial deformation of PET to determine the influence of strain rate and temperature (Menary et al., 2011). The introduction of sensory equipment to measure the pressure curve, stretch rod reaction force, and mould contact (Salomeia et al., 2012a), have allowed more in-depth analysis of the stretch blow moulding process. These additional data available from (Salomeia et al., 2012a) have enabled in depth analysis of the relationships between process inputs and process outputs, notably revealing the relationship between input parameters and blowing kinematics (Salomeia et al., 2012b). Further investigations into blowing kinematics have also enabled bubble formation manipulation and furthered deformation understanding (Cakmak et al., 1985). These blowing kinematics, developed from the input parameters to the process, have a significant impact on the final bottle quality measures such as thickness profile, strain history and subsequently the top load and burst capabilities of the blown bottle (Haddad et al., 2009).

Simulation capabilities of the stretch blow moulding process have grown, with the accuracy achievable ever increasing. This has enabled many in depth findings and process improvements as a result. Using the finite element method on the commercial software ABAQUS has been validated over a broad process window and insights presented (J. Nixon et al., 2017), the use of axisymmetric modelling when possible equates to substantial computational time savings (Menary et al., 2000). Using high speed cameras, simulation material models have been validated on their deformation and stress-strain capabilities, this process can be used to calibrate material models used in specific processes (Zimmer & Stommel, 2013). Material behaviours have been modelled for the stretch blow moulding process (Adams et al., 2000; Buckley et al., 1996; Buckley & Jones, 1995), which are the basis for the material model used for simulation in this paper.

With regard to the aforementioned investigations, there is a notable gap in research investigating the significance of the processing parameters on the measured quality indicators of the final blown container, however a few have touched on the subject through the use of free-blow trials (James Nixon et al., 2017), where the bottle is blown under processing conditions without a mould. This paper will explore the process utilising the definitive screening design (Jones & Nachtsheim, 2011), constructed using a conference matrix (Xiao et al., 2017). This design was chosen as it is an alias optimal 3-level design with comparable power to the Taguchi L32 design while using fewer design points (Jankovic et al., 2021) and capable of identifying active factors with high probability, so long

Email: James Grace
JGrace02@qub.ac.uk

as the number of active effects is less than half the number of runs with a signal-to-noise ratio above 2 (Errore et al., 2017). The design has also been previously used with success (Libbrecht et al., 2015; Mohamed et al., 2021; Tai et al., 2015). The key features of the definitive screening design are the non-aliased main factors and its required sample size of 2n+1 runs for even factors or 2n+3 runs for odd number of factors, where n is the number of factors under investigation. The design can also estimate quadratic effects. The definitive screening design has a complex aliasing structure where:

1. Main effects are non-aliased with any other effect
2. Two 2-factor interactions sharing a common term are partially aliased
3. Two 2-factor interactions with no common terms are not aliased
4. Quadratic effects are partially aliased with other quadratic effects
5. Quadratic effects and 2-factor interactions of other factors are aliased
6. Quadratic effects and 2-factor interactions involving the quadratic are not aliased

Due to the asymmetric nature of the definitive screening design, main effects determined significant cannot be determined to hold true with high certainty for similar experiments with similar ranges of factors. This reproducibility of findings can give way to generalised conclusions using such designs as a full factorial where all combination of levels are tested (Fisher, 1971).

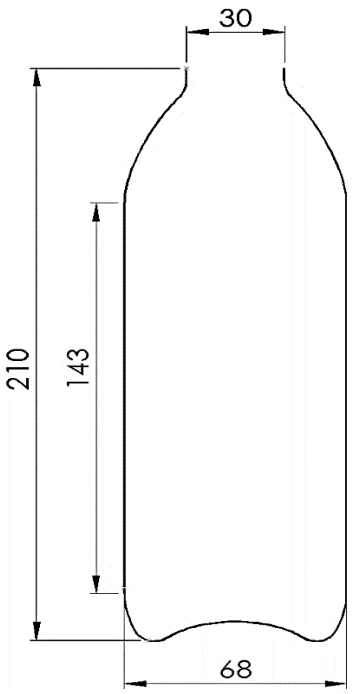

*Figure 1 Bottle profile*

Carrying out experimental runs through computer simulations yields deterministic results, therefore there is no variance to the measured response. As such, the analysis of significance can be carried out with the normal plot (Cuthbert, 1959), in which the normal curve is used as the reference distribution and significance can be determined with distance from the mean effect which is assumed zero.

Investigations into the utilisation of simulation data to efficiently model a process through design of experiments have shown success, such as Chen et al. (Chen et al., 2009), in which experimental verification of optimal processing conditions found for injection moulding through simulations results showed promising results. Guo et al. (Guo et al., 2012) also showed promising results using the central composite design for analysis of simulation data in detecting warpage defects in moulded parts. Gunasegaram et al. (Gunasegaram et al., 2009), also utilising design of experiments on simulation data which made it possible to reduce the scrappage rate by 13% for manifold casting.

### *2.Bottle Geometry and Input Ranges*

The input ranges for the design, shown in table 1, were determined to enable exploration of a wide processing window while still providing fully blown, measurable bottles as shown in figure 1. These factors are broken into subsets: temperature conditions, preblow conditions, and final blow conditions.

Temperature factors correspond to a specific temperature profile as shown in figure 2, with the temperatures ($^{o}$C) determining the height of the peaks in the temperature profile, and the offsets (position of top lamp (TPT) and position of bottom lamp (TPB)) determining the location of the peaks and determined as a ratio of distance along the top and bottom half of the bottle. The temperature profile is applied to the nodes of the preform in the ABAQUS simulation by interpolating to the specific temperature value to match the coordinates of the preform nodes.

The preblow conditions include; preblow pressure (PP) (Bar), this is the pressure used to pressurise and expand the preform; preblow timing (PT) (Seconds), the time at which the preblow pressure begins as a function of stretch rod location; preblow duration (PD) (Seconds), how long the preblow phase continues; preblow mass flow rate (PMFR) (grams/second), this is a function of the pressure and total area of the air inlet. In the simulation mass flow rate can be varied continuously unlike physical experiments where the mass flow rate is discrete and dependent on the pressure and size of inlet, this must be considered for validation.

The finalblow conditions include: finalblow pressure (FP) (Bar), the pressure used to fully blow the preform to finalise the bottle shape; finalblow duration (FD) (Seconds), how long the final phase continues and holds; finalblow mass flow rate (FMFR) (grams/ second). These processing ranges were applied to the preform shown in figure 3. The final blow stage is often set as to ensure the bottle is always fully blown.

A simple bottle design was chosen to give a foundation to the findings and conclusions not skewed by the including of geometry complexities or surface patterns. The axisymmetric nature of the bottle designs also enabled the simulations to be carried out in a relatively short period of time when compared to non-axisymmetric 3D simulations. The investigation was carried out using an ABAQUS Explicit axisymmetric simulation with element type SAX1.

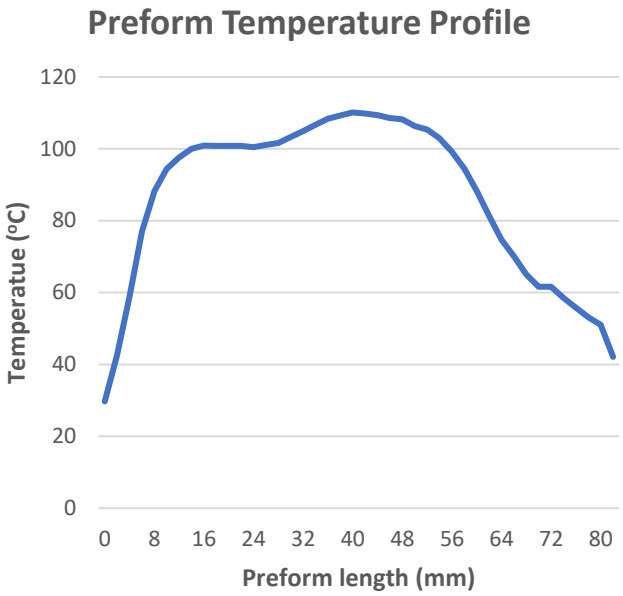


*Figure 2 Temperature profile*

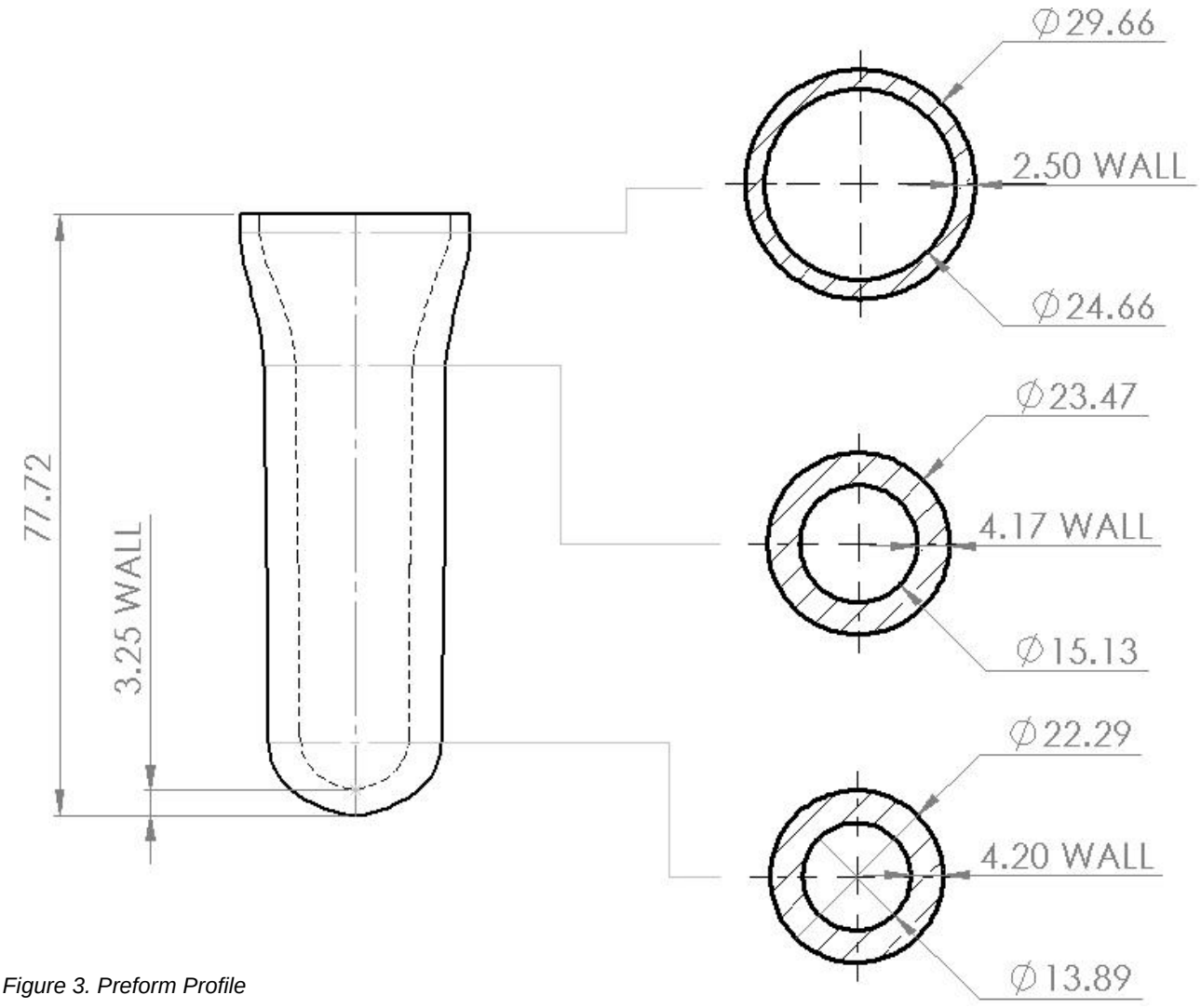


*Figure 3. Preform Profile*

### *3.Experimental* Setup

*Table 1. Input Factor Ranges*

| Factor | Low | Centre | High |
|---|---|---|---|
| Temp: Top | 100 | 105 | 110 |
| Temp: Mid | 90 | 95 | 100 |
| Temp: Bot | 90 | 95 | 100 |
| TPT | 0.25 | 0.75 | 0 |
| TPB | 0.25 | 0.75 | 1200 |
| PP | 8 | 10 | 12 |
| PT | 0 | 0.15 | 0.3 |
| PD | 0.1 | 0.15 | 0.2 |
| PMFR | 20 | 30 | 40 |
| FP | 30 | 35 | 40 |
| FD | 0.05 | 0.1 | 0.15 |
| FMFR | 900 | 1000 | 1100 |

The definitive screening design is constructed with a conference matrix, its negative, and a centre run which may be repeated, the construction is shown in equation 1, where C is the conference matrix and 0 is the centre run.

$$Design\ Structure = \begin{pmatrix} C \\ -C \\ 0 \end{pmatrix} \quad (1)$$

The conference matrix is constructed by means of equation 2, in this specific case $C_{12}$ is chosen, where $I_{n\times n}$ is an identity matrix of size 12.

$$C_n^T C_n = (n-1) I_{n\times n} \quad (2)$$

*Table 2 Definitive Screening Design Matrix*

| Order | Temp: Top | Temp: Middle | Temp: Bottom | TPT | TPB | PP | PT | PD | PMFR | FP | FD | FMFR |
|---|---|---|---|---|---|---|---|---|---|---|---|---|
| 1 | 105 | 90 | 90 | 0.75 | 0.75 | 8 | 0.00 | 0.10 | 22 | 30 | 0.05 | 900 |
| 2 | 105 | 100 | 100 | 0.25 | 0.25 | 12 | 0.30 | 0.20 | 40 | 40 | 0.15 | 1100 |
| 3 | 100 | 95 | 100 | 0.25 | 0.25 | 12 | 0.00 | 0.20 | 22 | 30 | 0.05 | 900 |
| 4 | 110 | 95 | 90 | 0.75 | 0.75 | 8 | 0.30 | 0.10 | 40 | 40 | 0.15 | 1100 |
| 5 | 100 | 90 | 95 | 0.75 | 0.75 | 12 | 0.00 | 0.20 | 40 | 30 | 0.15 | 1100 |
| 6 | 110 | 100 | 95 | 0.25 | 0.25 | 8 | 0.30 | 0.10 | 22 | 40 | 0.05 | 900 |
| 7 | 100 | 90 | 100 | 0.50 | 0.75 | 8 | 0.30 | 0.20 | 40 | 40 | 0.05 | 900 |
| 8 | 110 | 100 | 90 | 0.50 | 0.25 | 12 | 0.00 | 0.10 | 22 | 30 | 0.15 | 1100 |
| 9 | 100 | 90 | 100 | 0.25 | 0.50 | 8 | 0.30 | 0.10 | 22 | 30 | 0.15 | 1100 |
| 10 | 110 | 100 | 90 | 0.75 | 0.50 | 12 | 0.00 | 0.20 | 40 | 40 | 0.05 | 900 |
| 11 | 100 | 90 | 90 | 0.25 | 0.25 | 10 | 0.00 | 0.10 | 40 | 40 | 0.05 | 1100 |
| 12 | 110 | 100 | 100 | 0.75 | 0.75 | 10 | 0.30 | 0.20 | 22 | 30 | 0.15 | 900 |
| 13 | 100 | 100 | 100 | 0.75 | 0.75 | 12 | 0.15 | 0.10 | 22 | 40 | 0.05 | 1100 |
| 14 | 110 | 90 | 90 | 0.25 | 0.25 | 8 | 0.15 | 0.20 | 40 | 30 | 0.15 | 900 |
| 15 | 100 | 90 | 90 | 0.75 | 0.25 | 12 | 0.30 | 0.15 | 22 | 40 | 0.15 | 900 |
| 16 | 110 | 100 | 100 | 0.25 | 0.75 | 8 | 0.00 | 0.15 | 40 | 30 | 0.05 | 1100 |
| 17 | 100 | 100 | 90 | 0.75 | 0.25 | 8 | 0.30 | 0.20 | 31 | 30 | 0.05 | 1100 |
| 18 | 110 | 90 | 100 | 0.25 | 0.75 | 12 | 0.00 | 0.10 | 31 | 40 | 0.15 | 900 |
| 19 | 100 | 100 | 100 | 0.75 | 0.25 | 8 | 0.00 | 0.10 | 40 | 35 | 0.15 | 900 |
| 20 | 110 | 90 | 90 | 0.25 | 0.75 | 12 | 0.30 | 0.20 | 22 | 35 | 0.05 | 1100 |
| 21 | 100 | 100 | 90 | 0.25 | 0.75 | 12 | 0.30 | 0.10 | 40 | 30 | 0.10 | 900 |
| 22 | 110 | 90 | 100 | 0.75 | 0.25 | 8 | 0.00 | 0.20 | 22 | 40 | 0.10 | 1100 |
| 23 | 100 | 100 | 90 | 0.25 | 0.75 | 8 | 0.00 | 0.20 | 22 | 40 | 0.15 | 1000 |
| 24 | 110 | 90 | 100 | 0.75 | 0.25 | 12 | 0.30 | 0.10 | 40 | 30 | 0.05 | 1000 |
| 25 | 105 | 95 | 95 | 0.50 | 0.50 | 10 | 0.15 | 0.15 | 31 | 35 | 0.10 | 1000 |

From the simulation, the responses chosen for investigation are wall thickness, material density and the pressure curve. From these responses material distribution of the bottle can be analysed and key data points from the pressure curve can be extrapolated and analysed as seen in figure 4.

The key responses available from the pressure curve are:

- Pressure gradient
- Expansion gradient
- Finalblow gradient
- Max pressure
- Min pressure

The temperature profile, as seen in figure 2, can be estimated with the use of Bezier curves and generalised to other temperature combinations by manipulation of these Bezier curves. This method was used to estimate the temperature profiles of each run in the simulation design. Validation of the simulation will enable the use of true temperature profiles to be interpolated and used in the simulation.

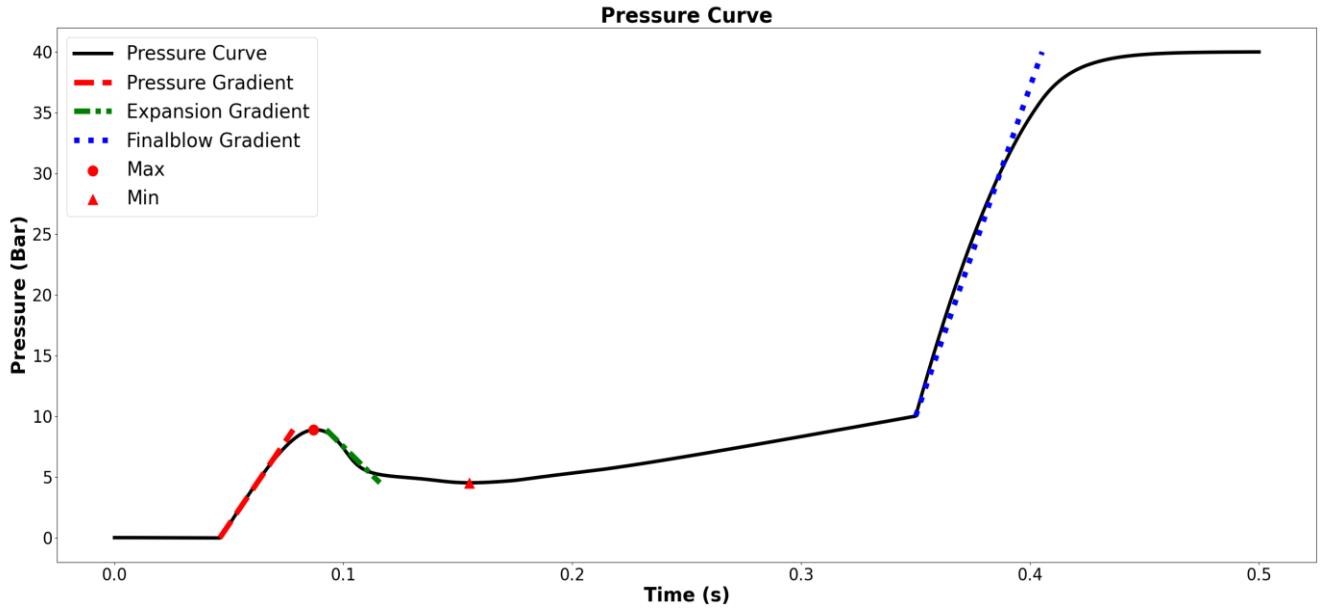


*Figure 4. Pressure Curve Key Points*

The ABAQUS simulation was set up as a simple axisymmetric case with the stretch rod and bottle mould represented as rigid bodies. The preform was meshed with a total of 80 nodes which gave an ideal accuracy for the computation time required. The material model was experimentally calibrated using free stretch blow moulding trials as seen in (Adams et al., 2000; Buckly et al., 1995; Buckly et al., 1996) As the ABAQUS simulation is deterministic in nature, each simulation need only be run once, as repeated runs will generate the same results.

### *4.Results*

The average simulation run time was 15 minutes on an Intel® Core™ i7-9700 CPU @ 3 GHz, with a maximum run time of 23 minutes and a minimum time of 9 minutes, with the variation being related to the length of the preblow delay, preblow duration and finalblow duration. Running the simulations in parallel with 5 simulations being carried out at a time yielded results for the definitive screening design in approximately 75 minutes.

As the definitive screening design was chosen, the main effects are unaliased and therefore the “pure” effects of the factors can be analysed using the average of the effects collected at low and high levels. Other interaction and quadratic effects cannot be analysed in such a manner due to the complex aliasing structure present in the definitive screening design shown in figure 7.

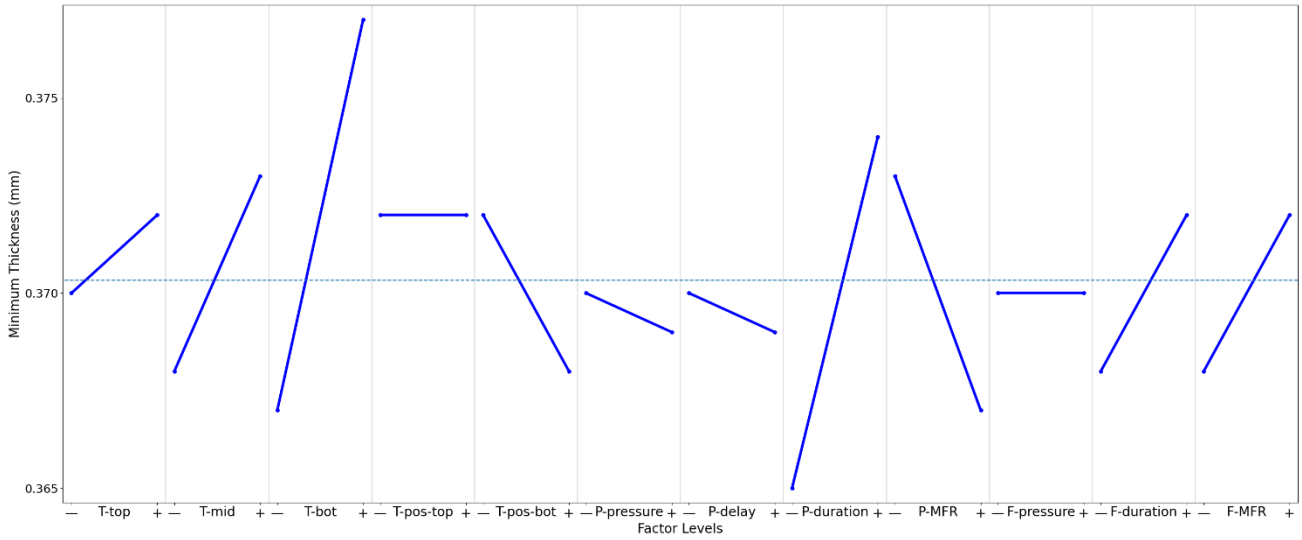


*Figure 5. Minimum Thickness Main Effects Plot*

To further determine quadratic and interaction effects through the aliasing present, a frequentist approach, such as that utilised by the popular JMP software, or by a more comprehensive Bayesian approach can be utilised to determine the model. However, only the main factors are of interest here as the process can be fully characterised using a full factorial simulation design due to the efficiency of computer simulation analysis with reduced factors.

As the main effects are unaliased, they can be simply calculated by computing the difference of the average response of each factor at the high and low levels. The results of these calculations are shown for the minimum thickness in the main effects plot, figure 5, the regression residuals followed the same pattern of explanation. As minimum thickness is a significant quality indicator in the final performance of the bottle in terms of the top load and burst pressure it was chosen for demonstration. The significant effects for all the responses tested are shown in figure 6. When compared across all responses it was found that 8 of the 12 factors tested were significant. If only one response was of interest, the number of significant factors could be reduced further.

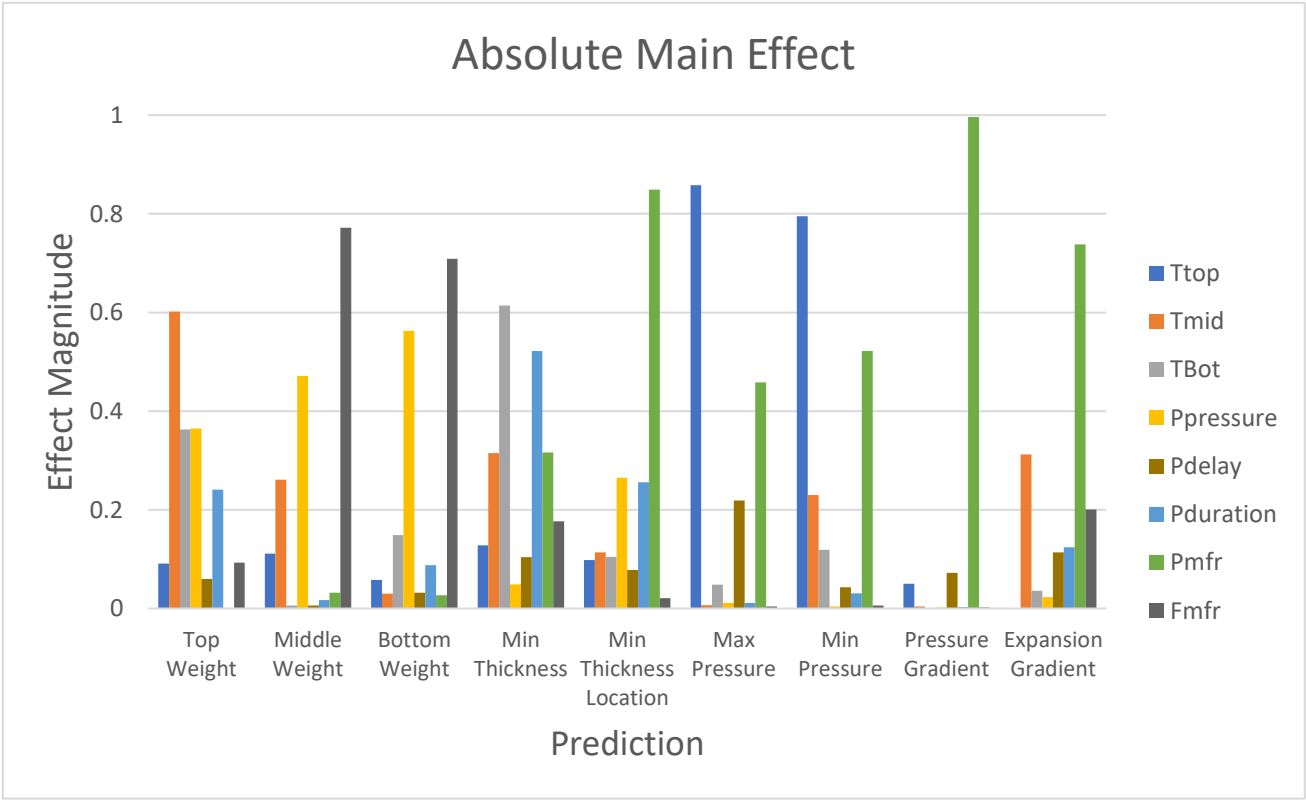


*Figure 6. Significant Effects Across All Responses*

The 8 significant factors across all responses are:

- Temperature Top
- Temperature Middle
- Temperature Bottom
- Preblow Delay
- Preblow Pressure
- Preblow Duration
- Preblow MFR
- Final MFR

The reason for some factors insignificance can be deduced from the measurements seen and an understanding of the stretch blow moulding process. In the experiment performed, the preform was relatively short in length and therefore a significant overlap in the heating cones from the IR oven lamps is present, as such the locations of the top and bottom lamp do not significantly change shape of the temperature profile relative to the magnitude of the lamp power.

As for the final pressure and final duration, understanding of the process can justify their insignificance as these parameters are used to finalise the blowing process, and therefore are always set to a level in which the bottle is fully blown, otherwise the process would fail to produce a fully moulded bottle. From the reduced factors it is now feasible to run a full factorial experiment through simulation, which has greater generalisability due to every level combination of the inputs being tested and unaliasing of the factors.

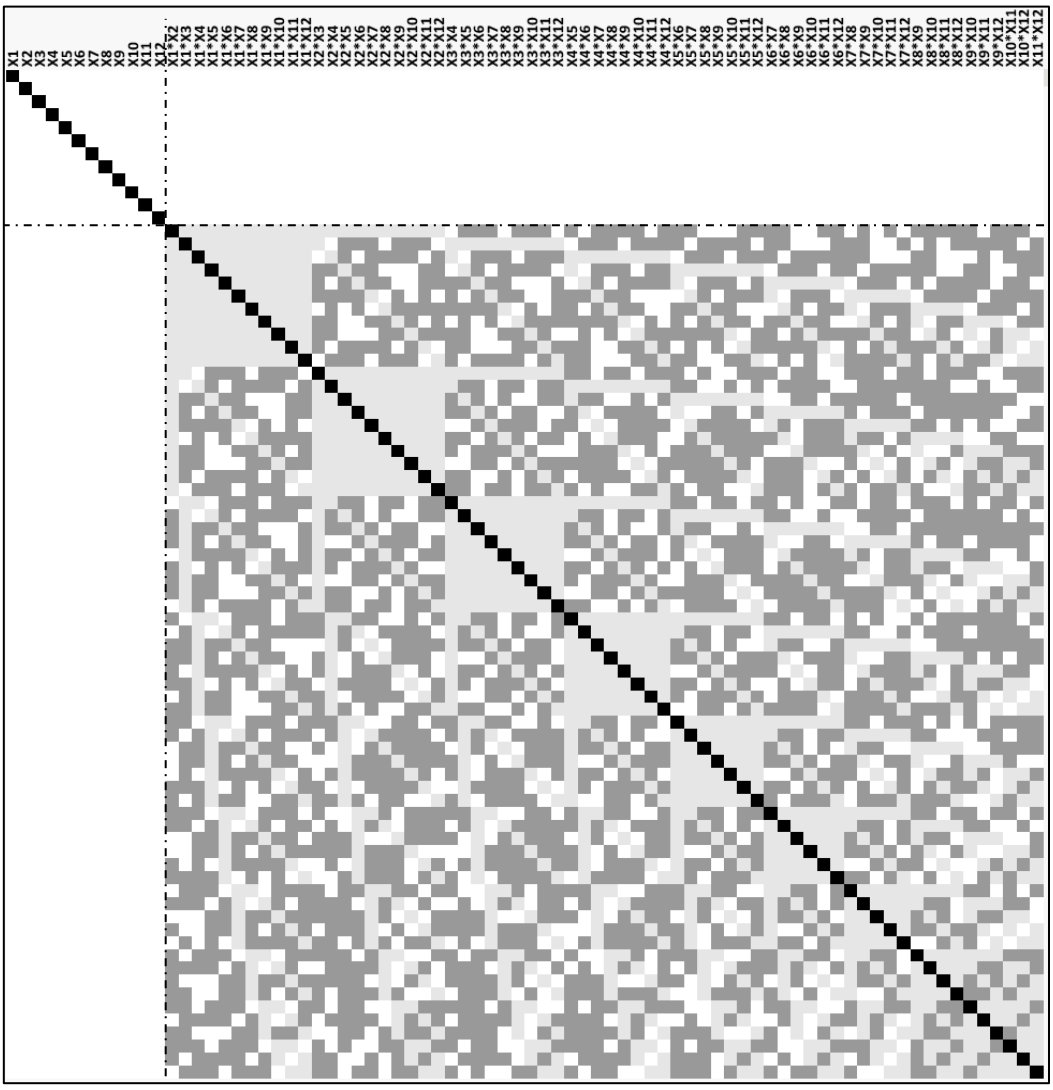


*Figure 7. 12-Factor Definitive Screening Design Aliasing Structure*

## *5.Conclusions*

In this paper the definitive screening design was successfully used to characterise reduced complexity finite element simulations of the stretch blow moulding process, making efficient use of the available data with minimal runs, identifying key relationships between the responses and input factors.

The definitive screening design is proposed as a minimal run method to validate and calibrate simulation results with experimental results in terms of model differences and differences in the raw response values collected. The then validated simulation can then be used to explore the design space through a more comprehensive space search such as a full factorial design at 2 levels or 3 levels if quadratic effects appear present from the definitive screening design.

The simulation can then be used to generate data for a data based model to explore the process in a timely manner, changing or optimising the existing process as required with little computational expense and almost instant results.

## *6.Discussion*

As this investigation will be validated using physical experiments, the exact temperature profile data will be available to be extrapolated and mapped onto the preform geometry in the simulation with relative ease. Future use cases where a simulated full factorial or space filling design will be explored, a basic model for creating synthetic temperature profiles is needed.

Further investigation into the temperature profiles would be beneficial as the temperature profile generated from the input IR heating lamps will vary depending on the spacing and length of the preform, from which at large lamp spacing and large preform length, distinct peaks in the curve can be seen, however at small lamp spacing and small preform length the lamps begin to act as one, producing a somewhat unfirm curve. Different material will also have different IR absorption rates and therefore effect the final temperature curve.

There are many areas which need care when creating the simulation setup to ensure an accurate representation of the physical process such as material behaviour, friction coefficients, mass flow rates and general blowing kinematics must be calibrated to ensure accurate conclusions are being made from such simulations. A simple axisymmetric bottle was chosen for investigation due to ease of calibration.

When carrying out experimental validation it should be noted that preform temperature cannot be set, but instead the IR lamp power and heating time determine the temperature curve. The mass flow rate and pressure are also dependent in the physical experiment as the air inlet to the preform cannot be varied enough to give exact mass flow rates desired. Instead high and low categorial levelling can be utilised, or either the pressure or mass flow rate may be held constant whilst the other is varied at desired levels.

## *7.References*


Adams, A. M., Buckley, C. P., & Jones, D. P. (2000). Biaxial hot drawing of poly(ethylene terephthalate): Measurements and modelling of strain-stiffening. *Polymer*, *41*(2), 771–786. https://doi.org/10.1016/S0032-3861(98)00834-9

Buckley, C. P., & Jones, D. C. (1995). Glass-rubber constitutive model for amorphous polymers near the glass transition. *Polymer*, *36*(17), 3301–3312. https://doi.org/10.1016/0032-3861(95)99429-X

Buckley, C. P., Jones, D. C., & Jones, D. P. (1996). Hot-drawing of poly(ethylene terephthalate) under biaxial stress: Application of a three-dimensional glass-rubber constitutive model. *Polymer*, *37*(12), 2403–2414. https://doi.org/10.1016/0032-3861(96)85352-3

Cakmak, M., White, J. L., & Spruiell, J. E. (1985). An investigation of the kinematics of stretch blow molding poly(ethylene terephthalate) bottles. *Journal of Applied Polymer Science*, *30*(9), 3679–3695. https://doi.org/10.1002/app.1985.070300913

Chen, C. P., Chuang, M. T., Hsiao, Y. H., Yang, Y. K., & Tsai, C. H. (2009). Simulation and experimental study in determining injection molding process parameters for thin-shell plastic parts via design of experiments analysis. *Expert Systems with Applications*, *36*(7), 10752–10759. https://doi.org/10.1016/j.eswa.2009.02.017

Cuthbert, D. (1959). Use of half-normal plots in interpreting factorial two-level experiments. *Technometrics*, *1*(4), 311–341.

Errore, A., Jones, B., Li, W., & Nachtsheim, C. J. (2017). Using definitive screening designs to identify active first-and second-order factor effects. *Journal of Quality Technology*, *49*(3), 244–264. https://doi.org/10.1080/00224065.2017.11917993

Fisher, R. (1971). The Design of Experiments (1935). In *Edinburgh: Oliver and Boyd*. Collier Macmillan Publishers.

Gunasegaram, D. R., Farnsworth, D. J., & Nguyen, T. T. (2009). Identification of critical factors affecting shrinkage porosity in permanent mold casting using numerical simulations based on design of experiments. *Journal of Materials Processing Technology*, *209*(3), 1209–1219. https://doi.org/10.1016/j.jmatprotec.2008.03.044

Guo, W., Hua, L., Mao, H., & Meng, Z. (2012). Prediction of warpage in plastic injection molding based on design of experiments. *Journal of Mechanical Science and Technology*, *26*(4), 1133–1139. https://doi.org/10.1007/s12206-012-0214-0

Haddad, H., Masood, S., & Erbulut, D. U. (2009). A study of blow moulding simulation and structural analysis for PET bottles. *Australian Journal of Mechanical Engineering*, *7*(1), 69–76. https://doi.org/10.1080/14484846.2009.11464580

Jankovic, A., Chaudhary, G., & Goia, F. (2021). Designing the design of experiments (DOE) – An investigation on the influence of different factorial designs on the characterization of complex systems. *Energy and Buildings*, *250*, 111298. https://doi.org/10.1016/j.enbuild.2021.111298

Jones, B., & Nachtsheim, C. J. (2011). A class of three-level designs for definitive screening in the presence of second-order effects. *Journal of Quality Technology*, *43*(1), 1–15. https://doi.org/10.1080/00224065.2011.11917841

Libbrecht, W., Deruyck, F., Poelman, H., Verberckmoes, A., Thybaut, J., De Clercq, J., & Van Der Voort, P. (2015). Optimization of soft templated mesoporous carbon synthesis using Definitive Screening Design. *Chemical Engineering Journal*, *259*, 126–134. https://doi.org/10.1016/j.cej.2014.07.113

Menary, G. H., Armstrong, C. G., Crawford, R. J., & McEvoy, J. P. (2000). Modelling of poly(ethylene terephthalate) in injection stretch-blow moulding. *Plastics, Rubber and Composites Processing and Applications*, *29*(7), 360–370. https://doi.org/10.1179/146580100101541166

Menary, G. H., Tan, C. W., Harkin-Jones, E. M. A., Armstrong, C. G., & Martin, P. J. (2011). Biaxial Deformation and Experimental Study of PET at Conditions Applicable to Stretch Blow Molding. *Society of Plastics Engineers*, 1–10. https://doi.org/10.1002/pen.22134

Mohamed, O. A., Masood, S. H., & Bhowmik, J. L. (2021). Modeling, analysis, and optimization of dimensional accuracy of FDM-fabricated parts using definitive screening design and deep learning feedforward artificial neural network. *Advances in Manufacturing*, *9*(1), 115–129. https://doi.org/10.1007/s40436-020-00336-9

Nixon, J., Menary, G. H., & Yan, S. (2017). Finite element simulations of stretch-blow moulding with experimental validation over a broad process window. *International Journal of Material Forming*, *10*(5), 793–809. https://doi.org/10.1007/s12289-016-1320-9

Nixon, James, Menary, G. H., & Yan, S. (2017). Free-stretch-blow investigation of poly(ethylene terephthalate) over a large process window. *International Journal of Material Forming*, *10*(5), 765–777. https://doi.org/10.1007/s12289-016-1318-3

Salomeia, Y. M., Menary, G. H., & Armstrong, C. G. (2012a). Experimental Investigation of Stretch Blow Molding, Part 1: Instrumentation in an Industrial Environment. *Advances in Polymer Technology*, *32*, 474–485. https://doi.org/10.1002/adv

Salomeia, Y. M., Menary, G. H., & Armstrong, C. G. (2012b). Experimental Investigation of Stretch Blow Molding, Part 2: Analysis of Process Variables, Blowing Kinematics, and Bottle Properties. *Advances in Polymer Technology*, *32*, 474–485. https://doi.org/10.1002/adv

Tai, M., Ly, A., Leung, I., & Nayar, G. (2015). Efficient high-throughput biological process characterization: Definitive screening design with the Ambr250 bioreactor system. *Biotechnology Progress*, *31*(5), 1388–1395. https://doi.org/10.1002/btpr.2142

Xiao, L., Lin, D. K. J., & Bai, F. (2017). Constructing definitive screening designs using conference matrices. *Journal of Quality Technology*, *44*(1), 2–8. https://doi.org/10.1080/00224065.2012.11917877

Zimmer, J., & Stommel, M. (2013). Method for the evaluation of stretch blow molding simulations with free blow trials. *IOP Conference Series: Materials Science and Engineering*, *48*(1). https://doi.org/10.1088/1757-899X/48/1/012004

# Chapter 5: Surface Engineering

# Jet printing of silver conducting lines using laser produced dry aerosol

Weiming Su [1], Arnoldas Sasnauskas [1], Adhiraj Sood [1], Rocco Lupoi [1], James G. Lunney [2]
[1] Department of Mechanical and Manufacturing Engineering, Trinity College Dublin, The University of Dublin, Dublin 2, Ireland
[2] School of Physics and CRANN, Trinity College Dublin, The University of Dublin, Dublin 2, Ireland

***Abstract***

Aerosol jet printing is a promising additive manufacturing technique for flexible electronics. In the wet aerosol method, a metal nanoparticle ink is aerosolised and transported to the print head. Dry aerosol jet printing, where a metal aerosol is prepared in the printing device, may offer some advantages by avoiding the need to prepare and store the nanoparticle ink, and improving the surface purity of the printed nanoparticles. Here we present a description of a novel dry aerosol jet printing method, which is based on pulsed laser ablation of a metal target in an inert gas at atmospheric pressure. The ablation vapor is condensed near the target to form a mist of nanoparticles, and thence larger nanoparticle agglomerates. The dry aerosol is transported to a print head, and aerodynamically focused into a narrow jet directed on to a moving substrate to form a fine line of weakly-bound silver nanoparticle agglomerates. The printing parameters, including the power of laser beam and the flow rates of the carrier and sheath gases, were controlled to optimize the geometry and resistivity of printed lines. For electrical applications the lines produced by both the wet and dry aerosol methods require sintering to consolidate the material and reduce the electrical resistivity. In this work, the printed samples were sintered in a furnace for 4 hr at various temperatures in the range 200–700 °C. Scanning electron microscopy was used to investigate how the microstructure evolves with increasing sintering temperature The electrical resistivity decreases monotonically with increasing sintering temperature, reaching a value of $4.2\times10^{-8}$ Ω m at 700 °C.

*Key Words: Aerosol jet printing, Pulsed laser ablation, Nanoparticles, Sintering.*

## 1. INTRODUCTION

Currently, there is an active development in new methods for the manufacture of cheap electronic devices using printing techniques (Garlapati et al., 2018), where functional materials can be directly deposited on substrates to form active and passive electronic components without using expensive photolithographic masks and stencils. Among these additive manufacturing-based printing methods, aerosol jet printing is a promising technology that allows the formation of functional elements with features sizes down to 10 μm (Seifert et al., 2015). It has been used to fabricate transistors (Hong, Kim, Mahajan, & Frisbie, 2014), solar cell elements (Mette, Richter, Hörteis, & Glunz, 2007), microheaters (Arsenov, Vlasov, Efimov, Minkov, & Ivanov, 2019), and microstructures on curved surfaces (Jabari & Toyserkani, 2016). Previous studies of this technology focused mainly on the formation of thin-film microstructures due to the strong demand for planar electronic devices. However, there is also a demand for the manufacture of very fine conductive lines, and high aspect ratio (thickness-to-width) lines in high-density circuits (Laurent, Serguei, Dupont, & Kraft, 2018; Mahajan, Frisbie, & Francis, 2013).

Aerosol jet printing technology is based on selective deposition of an aerodynamically focused nanoparticle beam onto a substrate. In conventional wet aerosol jet printing high-resolution linear structures are formed by microdroplets of an ink containing a dispersion of metal nanoparticles. To make the metal lines sufficiently conductive it is necessary to use an oven (Mahajan et al., 2013; Seifert et al., 2015) or a laser (Karnakis, Zergioti, Geremia, Theodorakos, & Zacharatos, 2014) to heat the deposited structure to evaporate impurities, such as solvent and other organic additives in ink, and to sinter metal nanoparticles together to form electrical connections. Surface impurities may hinder the consolidation of nanoparticles in the sintering process. In addition, nanoparticle segregation and solvent loss is a challenge for the storage and application of nanoparticle inks. Thus, it is expected that a dry aerosol printing method may avoid some of the complications associated with use of nanoparticle inks.

Here, we present a novel dry aerosol jet printing method based on pulsed laser ablation (PLA), which produces a solvent-free nanoparticle aerosol in an inert gas at atmospheric pressure. In the approach, a pulsed laser was used to make a vapour of the required metal in a small inert gas flow cell. The vapour condenses to form a mist

Email: Weiming Su, Rocco Lupoi, James G. Lunney
suwe@tcd.ie, lupoir@tcd.ie, jlunney@tcd.ie

of nanoparticles in the gas. The aerosol is transported to a print head, focused into a narrow jet, and printed on to a moving substrate as a fine conductive line. After printing, the printed samples were sintered in a furnace at different temperatures. The resistivity of sintered lines is discussed in relation to the microstructural evolution of the samples as a function of sintering temperature.

## 2. EXPERIMENTAL METHODS

The experimental setup for our printing method is shown in Fig. 1. The ablation cell contains a 99.95 % purity flat silver target, and 99.998 % purity argon is flowed through the cell. A 1064 nm SPI G4 Pulsed Fibre Laser delivering 200 ns pulses at 7.5 kHz with an average power of 3 W was used for ablation. The laser was scanned over the silver target at 130 mm $s^{-1}$ using a SG7110 High Speed Galvo Redpoint Scanhead. The vapour plume produced by each laser pulse is confined by the argon gas, and condensation leads to the formation of a silver nanoparticle aerosol. The aerosol is transported in the carrier gas flow to printhead where it is combined with the sheath gas, and the two flows enter a conically converging axisymmetric channel which terminates in a 300 µm diameter nozzle. The flow rates of carrier gas and sheath gas were 30 sccm and 60 sccm, respectively. An aerosol jet impinges on an $Al_2O_3$ ceramic substrate placed on a scanning stage moving at 2 mm $s^{-1}$. The distance between the nozzle and substrate was 1 mm for the samples described here. The printed samples were sintered in a muffle furnace (Carbolite Gero CWF 1200 Furnace) at various temperatures in the range 200 to 700 ℃. The morphologies of the as-printed and sintered lines were examined in a field emission-scanning electron microscope (FE-SEM, Zeiss ULTRA plus).

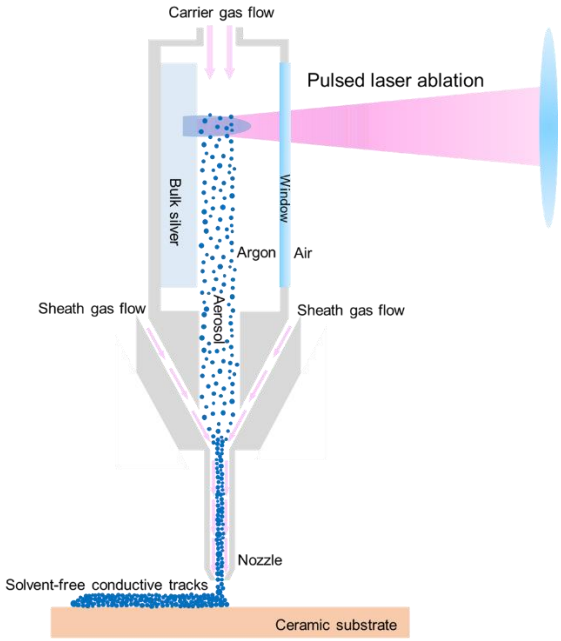


*Figure 1. Diagram of printing process on the formation of conductive tracks based upon PLA*

To measure the electrical resistivity, silver lines were printed between two silver paint pads separated by 12 mm, and the resistance of the line was measured with a multimeter. The electrical resistivity ρ of the printed and sintered lines was calculated according to the equation ρ = RA/L, where R is the resistance of the sample, A is the cross-sectional area, L is the length of the line. The cross-sectional area was determined using Profilm 3D White Light Interferometer (WLI) to measure the transverse height profile. The resistivity values presented here are the average of three measurements on the same sample under the same conditions.

## 3. RESULTS AND DISCUSSION

Figure 2(a) shows an SEM image of an as-deposited silver line. The central region of the line seems to be quite densely packed and has a transverse width of about 100 µm. On both sides of the central region there are overspray regions with a relatively sparse deposit of agglomerates in the 10 – 30 µm size range. Figure 2(b) shows the transverse height profile as measured by WLI. The agglomerates in the overspray regions are also evident in WLI height profile. For a nozzle with aerodynamic focusing the diameter $D_j$ of the carrier gas jet

leaving the nozzle is given by $D_j = D_n\sqrt{Q_a/Q_t}$, where $D_n$ is the nozzle diameter, $Q_a$ is the aerosol flow rate, $Q_s$ is the sheath gas flow rate, and $Q_t$ is the total gas flow, given by $Q_t = Q_a + Q_s$. Thus, for a $D_n$ = 300 µm, $Q_a$ = 30 sccm and $Q_s$ = 60 sccm the expected width of the deposit is 173 µm. The full width at the base of the transverse height profile is close to this value. However, the profile is more sharply peaked that would be expected from translating a uniformly distributed cylindrical aerosol jet. Most likely this is due to radial gas flow near the substrate.

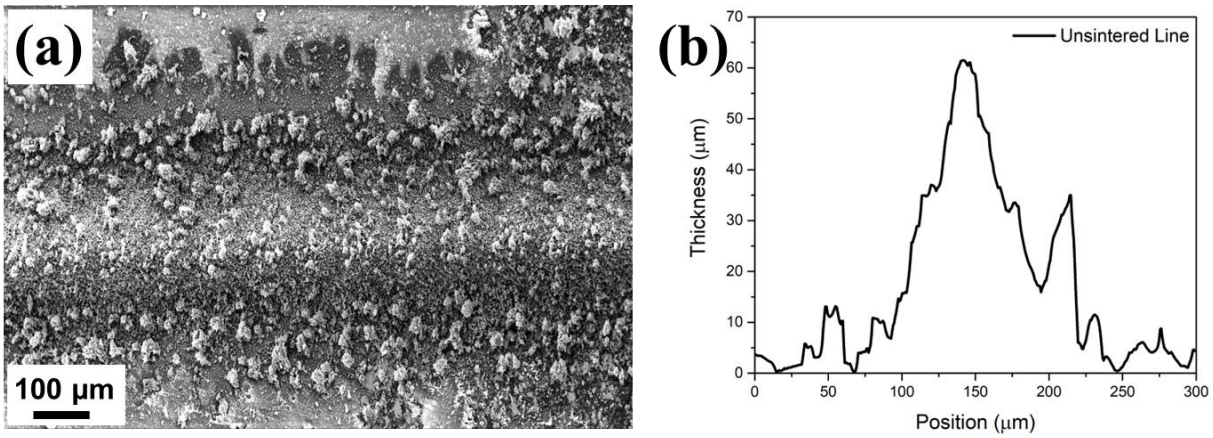


*Figure 2. (a) SEM image of the as-deposited silver line, and (b) transverse height profile as measured with WLI.*

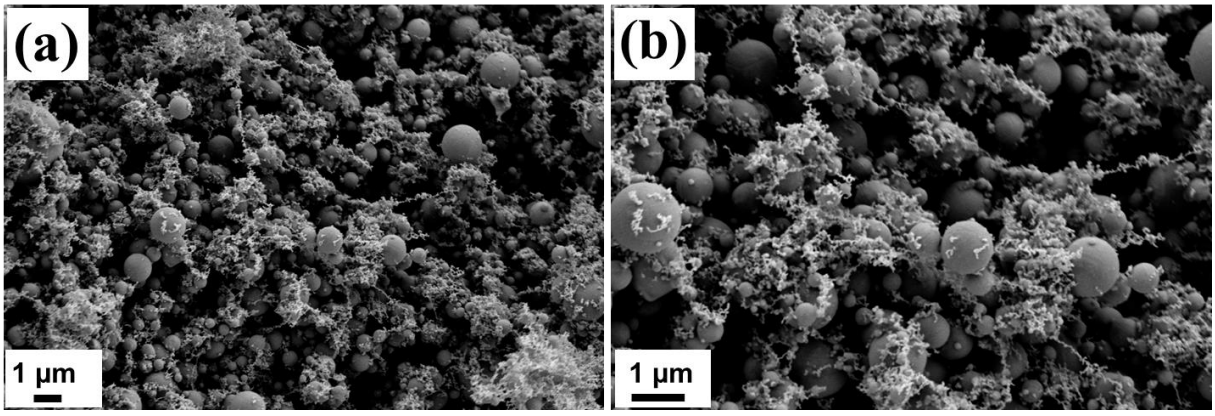


*Figure 3. SEM images of the as-deposited silver line at (a) 5000× magnification, and (b) 10000× magnification.*

Figure 3(a) and (b) show the high magnification images of the morphology of the printed line in the central region of the deposited line. Two very distinct particle morphologies are visible: (i) nanoparticle agglomerates, and (ii) highly spherical micron-sized particles. Together these two types of particles form a random 3D silver network with high porosity. The nanoparticle agglomerates are expected to arise from the condensation of the ablation plume vapour as cools while being confined by the argon gas at atmospheric pressure. The origin of the micron-sized spherical particles is less clear. They could arise from splashing of the molten silver from the ablation site, or could be due to repeated laser heating and agglomeration of the aerosol above the silver target. Further experiments are required clarify their origin.

The SEM images in Fig. 4 shows how the microstructure evolves as the sintering temperature is increased from 200 °C to 700 °C. The image in Fig. 4 (a) seems to show that the nanoparticle agglomerates have consolidated to form a network of sub-micron spherical particles. As the sintering temperature is increased up to 700 °C the material appears to become increasing dense. Clear bridging between particles is observed at 400 °C (Fig. 4(b)). At 600 ℃ and 700 ℃ a fully continuous sponge-like structure is observed. (Fig. 5(c) and (d)). The high magnification inset images also show faceting of the surface, indicating recrystallization of silver particles.

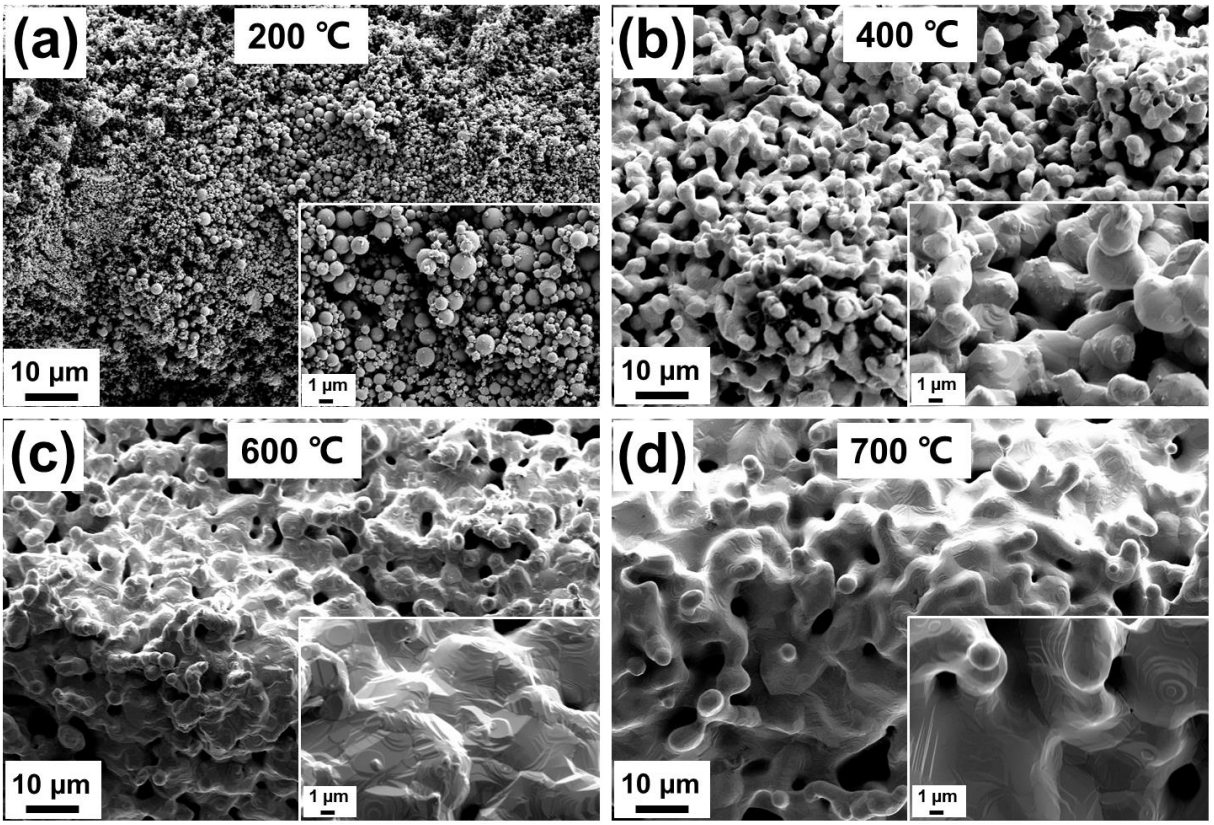


*Figure 4. SEM images of silver lines sintered at 200 ℃, 400 ℃, 600 ℃ and 700 ℃.*

Figure 5(a) shows the WLI transverse height profiles for the different sintering temperatures. There is a downward trend of the line height and cross-sectional area with increasing temperature, indicating progressive densification of the material. The height is 62 μm for a non-sintered line, but this fall to 32 μm for sintering at 700 °C. Figure 5(b) shows the dependence of the electrical as a function of sintering temperature. For sintering at 200 °C the resistivity of the silver lines was (39±6) $\times 10^{-8}$ Ω·m, compared to a value of (110±20) $\times 10^{-8}$ Ω·m for a non-sintered line. The resistivity drops to (16±1) $\times 10^{-8}$ Ω·m for sintering at 300 °C. The resistivity continues to fall as the sintering temperature is increases above 300 °C, falling to a value of (4.2±0.3) $\times 10^{-8}$ Ω·m 700 °C, which is about 2.5 times the value for bulk silver. The dependence of the electrical resistivity on sintering temperature is qualitatively consistent the temperature evolution of the microstructure described in Fig. 4, and the reduction in porosity evident in Fig. 5(a).

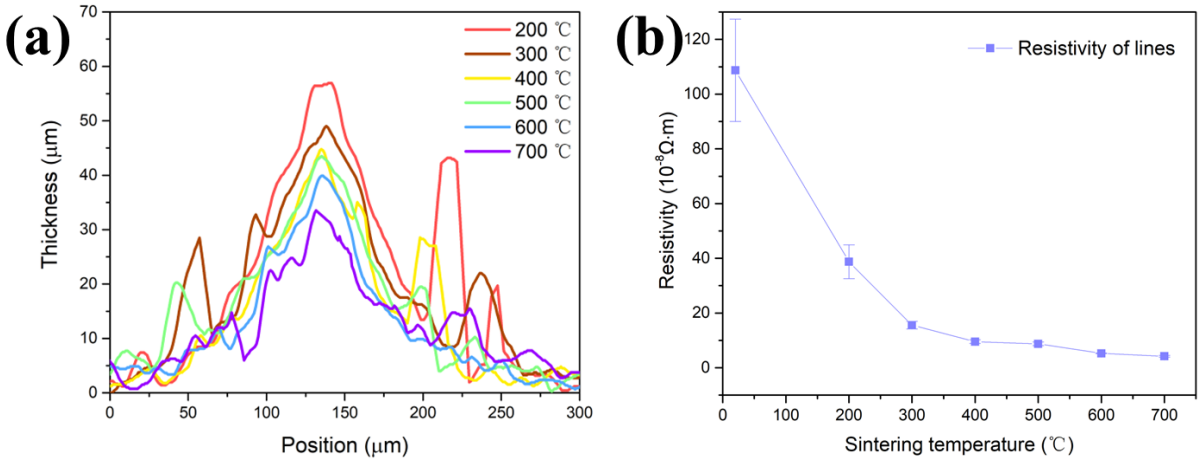


*Figure 5. Effect of sintering temperature on (a) transverse height profiles, and (b) resistivity of silver lines.*

## 4. CONCLUSION AND FUTURE WORK

A newly developed dry aerosol jet printing based upon PLA was demonstrated for direct patterning of solvent-free silver nanoparticles. This method may offer an alternative to conventional wet aerosol jet printing, and thus overcome some of the drawbacks associate with ink-based methods. Further work is required to understand the origin of the micron-sized spherical particles in the deposited line, and thus obtain a more homogeneous microstructure. Sintering at 700 °C yields a conducting line resistivity of 2.5 times that of bulk silver. While this value is sufficient for many practical applications, the sintering temperature is too high for thermally sensitive substrates, such as plastic materials. Thus, further work is required to reduce the sintering temperature to around 200 °C

## 5. REFERENCES


Arsenov, P. V., Vlasov, I. S., Efimov, A. A., Minkov, K. N., & Ivanov, V. V. (2019). Aerosol Jet Printing of Platinum Microheaters for the Application in Gas Sensors. *IOP Conference Series: Materials Science and Engineering, 473*, 012042. Retrieved from http://dx.doi.org/10.1088/1757-899X/473/1/012042. doi:10.1088/1757-899x/473/1/012042

Garlapati, S. K., Divya, M., Breitung, B., Kruk, R., Hahn, H., & Dasgupta, S. (2018). Printed Electronics Based on Inorganic Semiconductors: From Processes and Materials to Devices. *Advanced Materials, 30*(40), 1707600. Retrieved from https://onlinelibrary.wiley.com/doi/abs/10.1002/adma.201707600. doi:https://doi.org/10.1002/adma.201707600

Hong, K., Kim, S. H., Mahajan, A., & Frisbie, C. D. (2014). Aerosol Jet Printed p- and n-type Electrolyte-Gated Transistors with a Variety of Electrode Materials: Exploring Practical Routes to Printed Electronics. *ACS applied materials & interfaces, 6*(21), 18704-18711. Retrieved from https://doi.org/10.1021/am504171u. doi:10.1021/am504171u

Jabari, E., & Toyserkani, E. (2016). Aerosol-Jet printing of highly flexible and conductive graphene/silver patterns. *Materials Letters, 174*, 40-43. Retrieved from https://www.sciencedirect.com/science/article/pii/S0167577X16304049. doi:https://doi.org/10.1016/j.matlet.2016.03.082

Karnakis, D., Zergioti, I., Geremia, R., Theodorakos, I., & Zacharatos, F. (2014). Selective laser sintering of Ag nanoparticles ink for applications inflexible electronics. *Applied Surface Science*. doi:10.1016/j.apsusc.2014.10.120

Laurent, P., Serguei, S., Dupont, F., & Kraft, M. (2018). Electrical characterization of Aerosol Jet Printing (AJP) deposited conductive silver tracks on organic materials. *Microelectronic Engineering, 197*. doi:10.1016/j.mee.2018.06.002

Mahajan, A., Frisbie, C., & Francis, L. (2013). Optimization of Aerosol Jet Printing for High-Resolution, High-Aspect Ratio Silver Lines. *ACS applied materials & interfaces, 5*. doi:10.1021/am400606y

Mette, A., Richter, P. L., Hörteis, M., & Glunz, S. W. (2007). Metal aerosol jet printing for solar cell metallization. *Progress in Photovoltaics: Research and Applications, 15*(7), 621-627. Retrieved from https://onlinelibrary.wiley.com/doi/abs/10.1002/pip.759. doi:https://doi.org/10.1002/pip.759

Seifert, T., Sowade, E., Roscher, F., Wiemer, M., Gessner, T., & Baumann, R. (2015). Additive Manufacturing Technologies Compared: Morphology of Deposits of Silver Ink Using Inkjet and Aerosol Jet Printing. *Industrial & Engineering Chemistry Research, 54*, 769–779. doi:10.1021/ie503636c

# A repeatable and scalable approach for long-term surface-treated bonding of plastic microfluidic chips

Hengji Cong[1], Michael D. Gilchrist[1,2]* and Nan Zhang[1,2]*

*1: School of Mechanical & Materials Engineering, University College Dublin, Belfield, Dublin 4, Ireland*
*2: MiNAN Technologies Ltd., NovaUCD, Belfield, Dublin 4, Ireland*
** Correspondence to: nan.zhang@ucd.ie, michael.gilchrist@ucd.ie*

**ABSTRACT**

The commercialisation of laboratory research into a sustainable business is occurring more frequently in the field of microfluidic diagnostics. Among the various technological challenges during the commercialisation process, are the need to establish a flexible and repeatable approach for creating long-term hydrophilic or hydrophobic surfaces, as well as a robust process for stable chip bonding that is suitable for scale-up production of plastic microfluidic chips. The present work describes the development of a surface engineering method that combines ultrasonic spray coating followed by solvent vapor assisted thermal bonding. This two-stage process can be applied universally for hydrophilic and hydrophobic applications. A mixture solution of 1H, 1H, 2H, 2H-perfluorooctyl trichlorosilane (FOTS), cyclohexane and acetone were used to reach a hydrophobic surface of cyclic olefin copolymer (COC) chips by ultrasonic spray coating. 60 vol% cyclohexane and 40 vol% acetone were chosen as the solvent vapour to achieve efficient bonding of the COC chips. While for long-term hydrophilic treatment, OH-PEG-COOH was sprayed onto the polymethyl methacrylate (PMMA) chip surface with oxygen plasma as pre-/post-treatment and chloroform being used as the solvent vapor during bonding process. Both methods provided a deformation-free bonding with stable hydrophobicity or hydrophilicity. COC and PMMA, as two typical materials used in microfluidic devices, were employed to demonstrate the broad applicability of this workflow. Additionally, by avoiding the use of harsher and environmentally damaging chemicals, and successfully achieving a stable long-term treatment, the permanent-surface-treated bonding process provides a foundation for low-cost mass production of plastic microfluidic cartridges.

# Potentiodynamic polarization behaviour of Ni for shaping and electropolishing of micro-mould tools

Sana Zaki, Nan Zhang* and Michael D. Gilchrist*
School of Mechanical & Materials Engineering, University College Dublin, Belfield, Dublin 4, Ireland
* Correspondence to: nan.zhang@ucd.ie, michael.gilchrist@ucd.ie

***Abstract***

*The potentiodynamic polarization behaviour of nickel was examined in an electrolyte solution of nickel sulfamate to identify the etching, passivation, current limiting/polishing plateau and gas evolution regions for electropolishing and shaping of micro-mould features. Such features can be created either by means of 3D printing or direct machining and used on mould tools for mass manufacturing processes such as injection moulding. The design and precision of these micro-mould features determine the replication efficiency of the micro-injection moulding process. Demoulding of a polymeric replicate occurs at the mould tool / polymer interface and is affected by friction, adhesion and thermal stresses. Such forces can cause defects in the polymeric part in the form of cracks, burrs or distorted/fractured features. To overcome demoulding problems, the present work proposes the use of a design change, which can be achieved through electropolishing to shape and form the micro mould features by changing their draft angles and fillet radii, and thus reduce the interfacial stresses associated with demoulding. A Linear Scanning Voltammetry (LSV) was conducted with a scanning rate of 5mV/s and a positive sweeping potential of 5 to 0V with variations of temperature (°C) and magnetic agitation (rpm) to observe the polarization behaviour of Ni, which was plotted in terms of the potential (V) versus the current density (A/dm²). With an increase in temperature and magnetic agitation, higher current densities were observed up to the dynamic stability of the electrolyte. This polarization test served as a fundamental basis for electropolishing and shaping of microscale features on a Ni mould. The potentiodynamic study for Ni in the nickel sulfamate solution has been classified into three regions, namely etching, polishing and gas evolution. Changes in topography and morphology are more significant in the polishing and gas evolution region as current density is high which ensures more material removal, although the surface becomes pitted and darkened in the second of these two regimes. This potentiodynamic study serves to identify which electropolishing regime is suitable for shaping microfeatures such as linear channels or star patterns by changing draft angles and fillet radi, and by polishing the resultant surface in order to retain its high shine and low surface roughness (Sa). This ultimately should serve to reduce the occurrence of demoulding defects and should also enhance tool life and tool performance.*

*Keywords: Potentiodynamic polarization, Electropolishing and shaping, and demoulding defects*

## 1. INTRODUCTION

Micro-texturing has gained prominence in the field of research and industry. Functional properties of micro features have advanced applications i.e., micro-nano medical implants, micro lens and microfluidics(Huff, 2022; Jalili-Firoozinezhad et al., 2021; Kumar, 2019; Persaud-Sharma et al., 2012; Petsch et al., 2016). Microfabrication processes like hot embossing (Kim et al., 2022; Sequeiros et al., 2022), nano imprinting (Li et al., 2021; Nakagawa, 2022) and micro injection moulding (Li et al., 2022; Surace et al., 2021) are in high demand. Micro injection moulding involves the mass fabrication of products based on the tool life and process efficiency. Hence the quality of micro mould inserts will determine accuracy and precision of replicated feature. These micro mould tools can be manufactured by micro-milling, laser ablation, metal assisted etching and reactive ion etching. Demoulding is the ejection of polymeric replicated part from the metallic mould. The demoulding force causes friction, adhesion and thermal stresses due to contraction (Chen et al., 2021; Delaney et al., 2012; Murata et al., 2019). These adversely affects the quality of replicated parts and lowers the tool life.

In order to address the demoulding issue, a design change is suggested by shaping and forming of the edges and corners of the microfeatures. A non-contact and electrochemical method-electropolishing seems to be

Corresponding author.
Michael D. Gilchrist
*Email address:* michael.gilchrist@ucd.ie

the appropriate technique to achieve this design change. Electropolishing is the anodic dissolution of metal in an electrolytic bath which removes material based on current density gradient(Han & Fang, 2019, 2020; Karim, 2021; Kityk et al., 2021). Initial surface of metal is uneven with peak and recess areas which gets polished by micro and macro levelling at the end of EP. When the work piece is placed in the electrolytic bath layer of ions are formed at the metal and liquid side which acts as a resistive barrier and flow of ions have been explained by famous theories of acceptor ions (Matlosz et al., 1994; Park et al., 2021) and salt film formation (Grimm et al., 1992). As there is no special tool requirement and contact with the working metal, the method is suitable for machining the microfeatures without causing distortions and inducing stresses.

Other micro fabrication processes have issues of tool design, deflection, controlling the etch rates and rectilinear nature of light which makes them unsuitable for shaping and forming of micro mould features. In this research, potentiodynamic polarization behaviour of Ni was studied at various stages of etching, polishing and gas evolution to identify favourable regions for shaping and forming of microfeatures. Electropolishing has the potential to shape and form microfeatures by changing the draft angle and fillet radius of the mould tools which will ease the demoulding process. A green solution of nickel sulfamate has been used to characterize samples in electrolytic bath with varying temperature and magnetic agitation. Both temperature and agitation speed influence the material removal rate and surface quality of the micro moulds. A higher temperature accelerates the diffusion of metal ions through the resistive barrier and acceptors ions towards the metal while agitation speed ensures the fresh supply of ions and removal of by products from the workpiece (anode). In the present study, Ni samples were subjected to etching, polishing and passivation in the solution of nickel sulfamate. The topography and morphology changes were examined using 2D and 3D analysis of the features using profilometer, optical microscopy and SEM to identify favourable regions for shaping and polishing of micro tools to ease demoulding and enhance the tool life for microinjection moulding.

## *2. EXPERIMENTAL SETUP*

### *2.1 Materials and Methods*

Ni mould insert with linear micro channels was manufactured by UV LIGA and electroforming on a four inch wafer. The linear channels have varying widths of 100-200µm, height= 100µm and gap= 40-50µm. A potentiostat/galvanostat CS310 (Wuhan CorrTest Instruments Corp., Ltd., China) was used to supply voltage in a standard three electrode cell with Ni as anode, 314SS as cathode and Ag/AgCl as a reference electrode. The composition of electrolyte is based on 2M solution of nickel sulfamate ($H_4N_2NiO_6S_2$ , Ampere Galvanik Germany). A hotplate stirrer (Stuart-US152) was used to heat and provide magnetic agitation to the electrolytic solution. To insulate one side of the samples were coated with an aerosol conformal coating, which has an operating temperature of +200 °C and −70 °C. The surface reactivity of the samples was increased by giving ultrasonic bath in deionized water and acetone. The polarization cell for potentiodynamic behaviour study of Ni for shaping and polishing is shown in Fig 1.

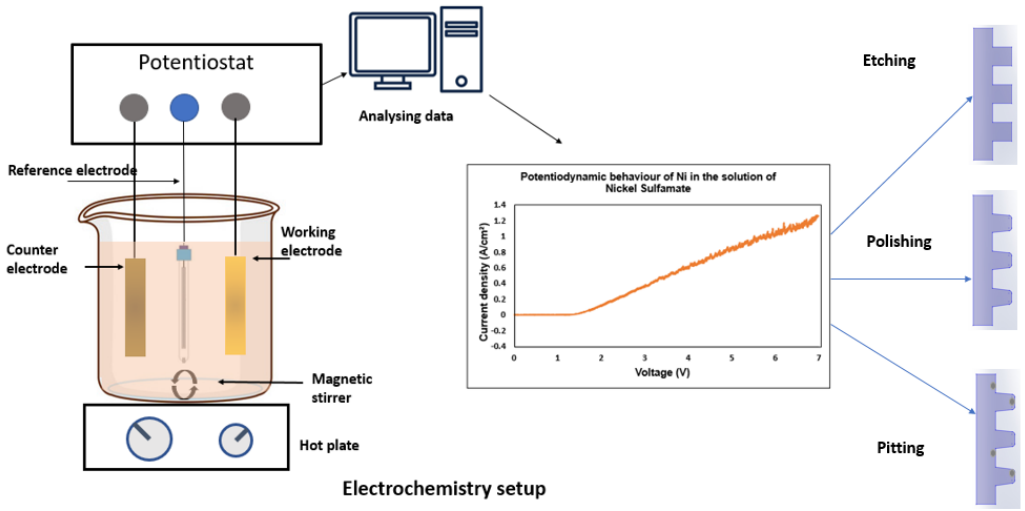


*Fig 1: A three electrode standard cell for potentiodynamic electrochemical analysis of Ni mould and resultant polarization graph.*

### *2.2 Polarization parameters*

A linear scanning voltammetry (LSV) was applied using the potentiostat/galvanostat CS310 to identify the regions of etching, polishing and gas evolution. The focus was to shape the microfeatures of Ni and improve it's surface quality. A 2M solution of nickel sulfamate with boric acid and wetting agent was prepared. A scanning speed of 10mV/s was used with a positive sweeping potential of 4 to 0V with variations in temperature (30-70°C) and agitation speed (0-600rpm) to check the trend of current density.

### *2.3 Characterisation of samples*

An optical microscope AmScope MU1000 with 10MP was used to analyze the samples at each stage of polarization. Changes in surface topography of Ni samples was characterised using a 3D profilometer (NPFLEX) which has an accuracy of 0.02µm and works on the principle of optical light interference. Several filters were applied i.e., statistic, data restore, remove tilt and Gaussian regression with long wavelength of 0.025mm. A table SEM TM 4000 was used to examine the surface morphology after each phase with voltages of 5,15 and 20kV and a magnification range of 25X to 250,000X.

## *3.RESULTS AND DISCUSSION*

The potentiodynamic polarization behaviour of Ni was classified in three regions of etching, polishing and gas evolution. This characterization study was used to analyse the changes in feature topography in the form of draft angle and fillet radi, and the surface morphology of Ni microfeatures. Moreover the effect of variations in temperature and agitation speed to influence the overall electropolishing process.

### *3.1 Effect of Temperature and Magnetic agitation*

Temperature influences the mass transport of ionic species by enhancing the diffusion rates of metal ions away and acceptor ions towards the surface. The mobility of ions changes with temperature ultimately changing the current density. Electropolishing is based on removal of material from a surface based on the gradient of current density on the protruded and recessed regions. An increase in temperature increases the localised diffusion rate and current density which enhances the material removal rate thus shaping Ni in the solution of nickel sulfamate as shown in Fig 2a.

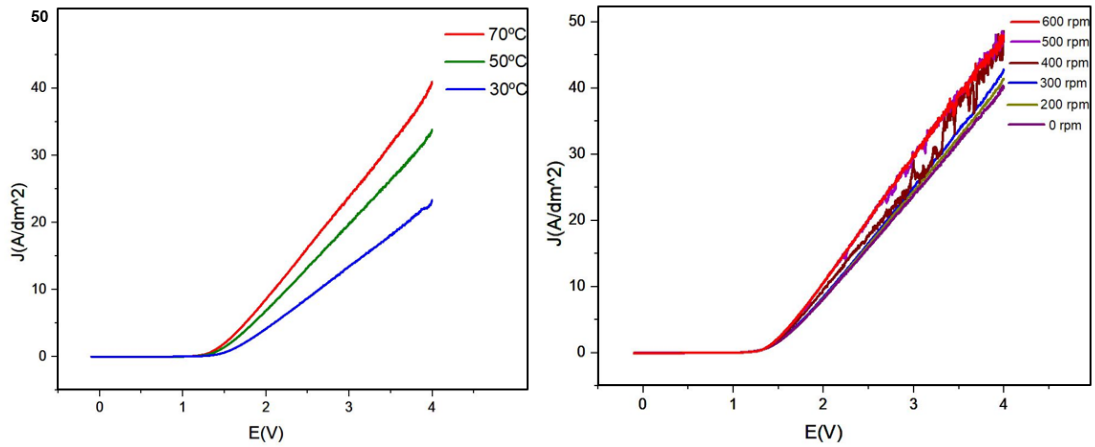


*Fig 2: Variations in temperature and agitation speed on the polarization behaviour of Ni.*

Agitation speed has an important role in the electropolishing process. It ensures the supply and movement of fresh ions in the electrolytic bath. During electropolishing metal dissolution occurs at anode and hydrogen gas evolution occurs at the cathode. The surface of anode is affected by the ion formation which is often observed in the form of bubble marks and burs. Agitation speed plays an important role in increasing the circulation rate, enables fresh supply of ions and remove the by-products. Thus an increase in agitation speed improves the surface morphology of Ni samples but moderate agitation speeds are recommended because they disturb the electrodynamic stability of solutions.

### *3.2 Etching, Polishing and Gas evolution regions*

Potentiodynamic polarization behaviour of Ni is shown in Fig 3. The characteristic curve can be classified into regions of etching, polishing and gas evolution. Electropolishing was conducted in the solution of nickel sulfamate with the parameters as shown in Table 1.

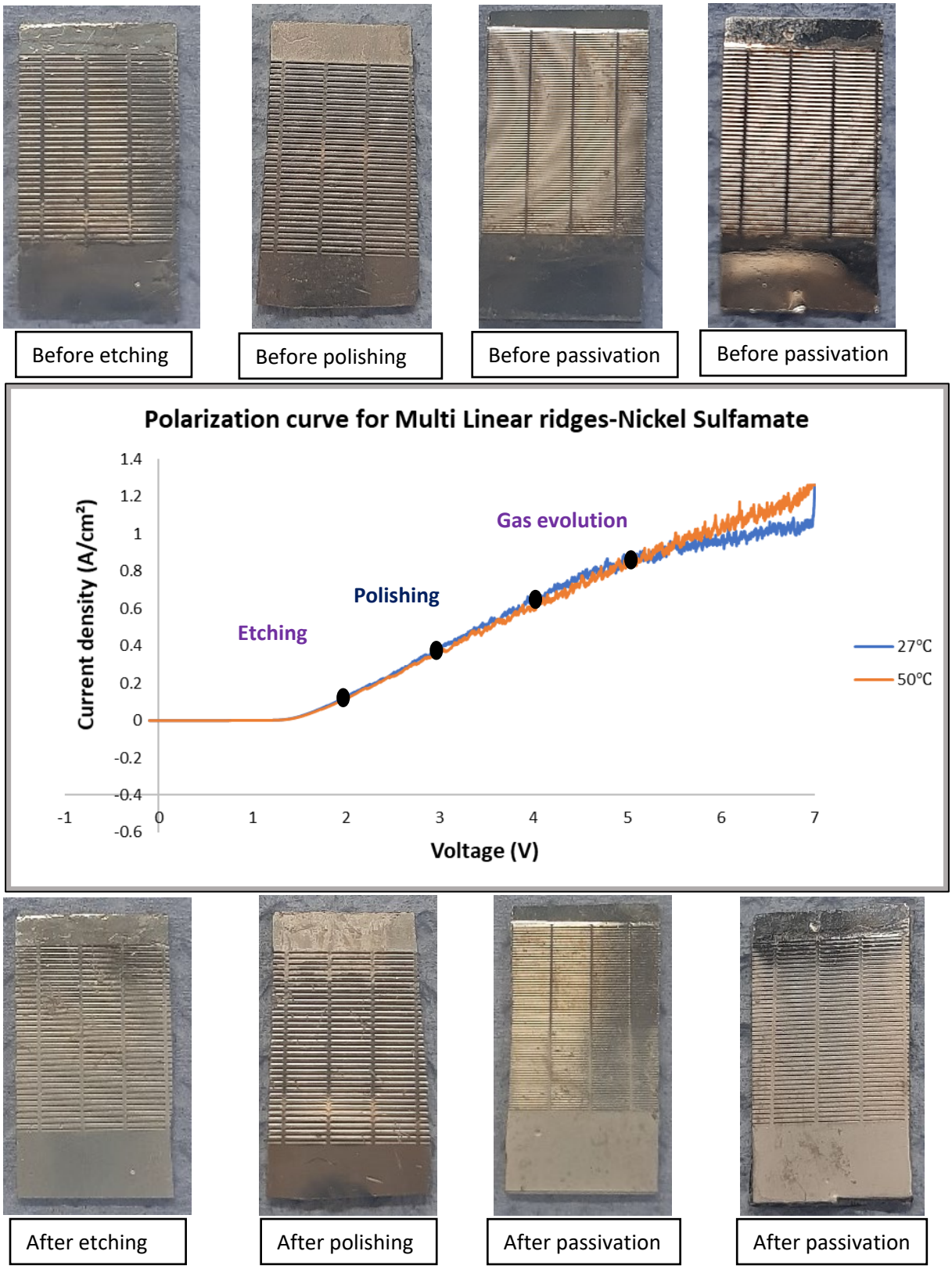


*Fig 3: Potentiodynamic behaviour of Ni at various stages of polarization curve.*

It is interesting to know the behaviour of Ni at various regions of polarization curve as the change in shaping in the form of draft angle and fillet radius and surface morphology will help to optimize the EP process. The shaping and forming of micro features is really important for design of micro mould tools as the demoulding issues of friction, adhesion and thermal stresses can be reduced. The over all aim of this study is to achieve good material removal rate and maintain surface integrity of micro tools < 50nm.

*Table 1: Parameters for electropolishing at various points of polarization curve.*

| Parameters | Voltage (V) | Temp (C) | EP time | Area (mm2) | Current (A) | Current density (A/dm2) |
|---|---|---|---|---|---|---|
| **Etching region** | | | | | | |
| S1 | 2 | 50 | 20min | 111 | 0.004 | 0.36 |
| **Electropolishing region** | | | | | | |
| S2 | 2.8 | 50 | 3min | 111 | 0.08 | 7.2 |
| **Gas evolution region** | | | | | | |
| S3 | 4 | 50 | 3min | 111 | 0.2 | 18.0 |
| S4 | 5 | 50 | 3min | 111 | 0.5 | 45 |

The changes in surface roughness is obvious at various points of the polarization curve. It is expected to be shiny and levelled in the electropolishing region where as the regions of etching leaves a rough surface due to low current density and long EP time, and gas evolution turns to pit the surface of Ni micro tools. This is indicated in Fig 4.

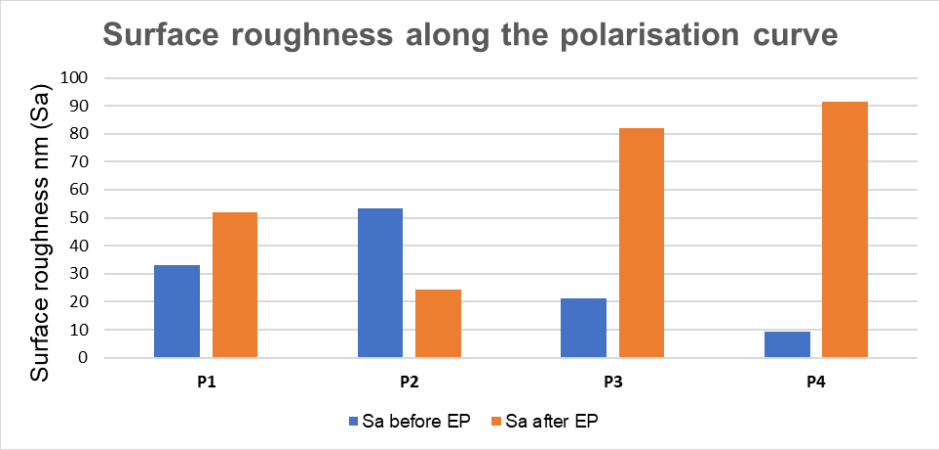


*Fig 4: Changes in surface roughness of Ni micro features at various parts of polarization curve*

**3.3 SEM analysis**

The SEM analysis is important in two aspects of feature topography and surface morphology of Ni microfeatures. Potentiodynamic behaviour of Ni at various stages of polarization have shaping effect and a change in surface quality as shown in Fig 5. The region of etching has weak current density so that surface is not much changed even after 20mins, electropolishing has a significant change in the removal of burs and embedded particles, and passivation has bad effects on the surface as pitting and marks are observed.

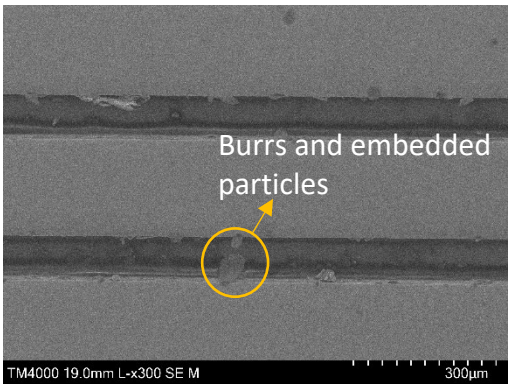


Sample before etching at 2V

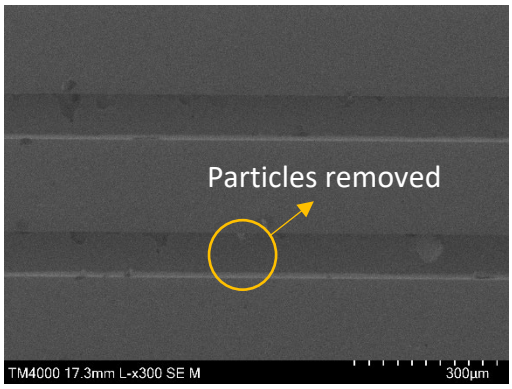


Sample after etching at 2V

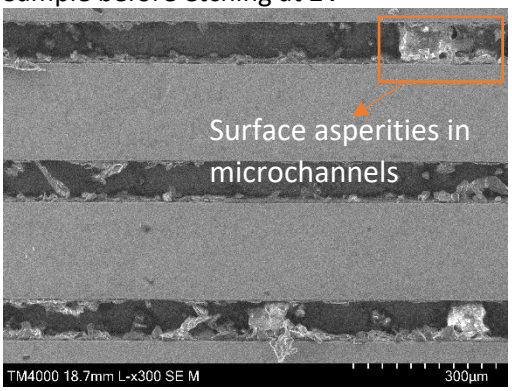


Sample before polishing at 2.8V

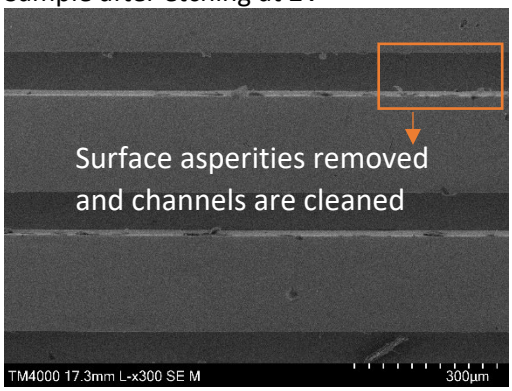


Sample after polishing at 2.8V

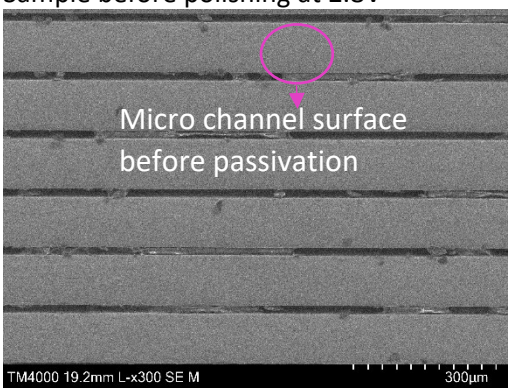


Sample before passivation at 4V

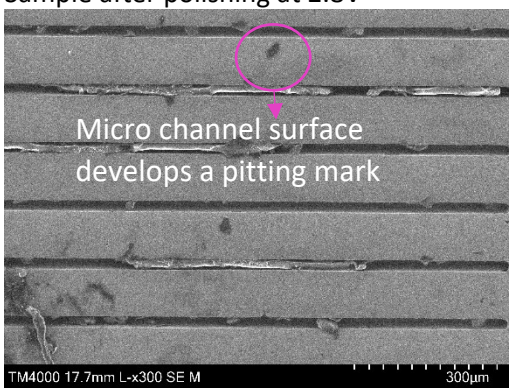


Sample after passivation at 4V

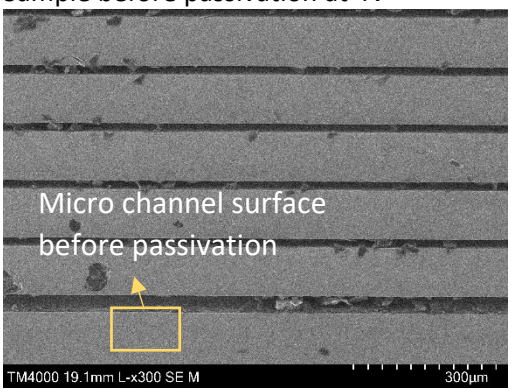


Sample before passivation at 5V

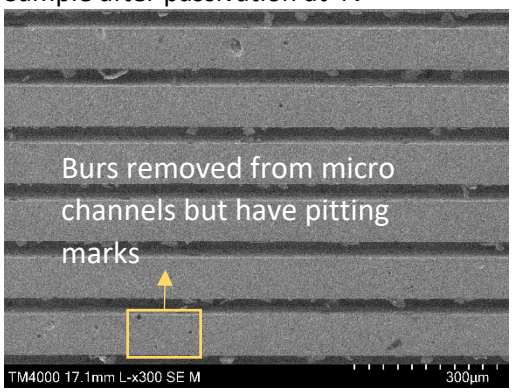


Sample after passivation at 5V

*Fig 5: Changes in feature topography and surface morphology analysed with SEM*

## 4. CONCLUSION

This study analysis the potentiodynamic behaviour of Ni microfeatures on various points of polarization curve for observing the regions favourable for shaping and polishing. The feature topography and surface morphology changes at various stages due to the change in current density. A linear scanning voltametric approach is adopted to scan the polarization behaviour and then suitable EP conditions are applied to form and shape microfeatures for reducing demoulding defects. Some of the summary points are discussed as under:

a. Potentiodynamic polarization behaviour of Ni can be classified into the regions of etching, polishing and gas evolution. The current density various in these regions, etching has the lowest value while gas evolution has the highest one.
b. Temperature influences the mass transport of ions and facilitates the diffusion through resistive barrier as per the salt layer formation and water acceptor model. An increase of temperature (30-70°C) increases the current density which favours the electropolishing process by formation, movement and settling of ions.
c. Agitation speed (0-600rpm) also has an impact on the surface of Ni microtools, It helps in the supply of newly formed ions and removes the by products of electropolishing. Thus bubble marks and burs can be avoided by adopting a moderate agitation speed between 200-300rpms. Too high agitation speeds disturbs the electrodynamic equilibrium.
d. Shaping and forming of Ni micro tools are optimum in the electropolishing region. As per previous studies and current one the microfeatures get shaped in longer EP time i.e., 15min while surface morphology gets affected with a high Sa and loss of shine. The surface quality is retained when the EP time is 3mins. This indicates that a combined pulsed approach may be favourable for shaping and polishing of microfeatures.

## Acknowledgments

We gratefully acknowledge the support of Science Foundation Ireland and I-Form (Grant 16/RC/3872).

## References

Chen, J., Yang, J., Zhou, M., & Weng, C. (2021). Self-Assembled Monolayers of Alkanethiols on Nickel Insert: Characterization of Friction and Analysis on Demolding Quality in Microinjection Molding. *Micromachines*, *12*(6), 636.

Delaney, K., Bissacco, G., & Kennedy, D. (2012). A structured review and classification of demolding issues and proven solutions. *International Polymer Processing*, *27*(1), 77-90.

Grimm, R., West, A., & Landolt, D. (1992). AC impedance study of anodically formed salt films on iron in chloride solution. *Journal of The Electrochemical Society*, *139*(6), 1622.

Han, W., & Fang, F. (2019). Fundamental aspects and recent developments in electropolishing. *International Journal of Machine Tools and Manufacture*, *139*, 1-23.

Han, W., & Fang, F. (2020). Investigation of electropolishing characteristics of tungsten in ecofriendly sodium hydroxide aqueous solution. *Advances in Manufacturing*, *8*, 265-278.

Huff, M. (2022). Process Sequence Design and Integration for Micro-and Nano-systems Manufacturing. In. Springer.

Jalili-Firoozinezhad, S., Miranda, C. C., & Cabral, J. M. (2021). Modeling the human body on microfluidic chips. *Trends in Biotechnology*, *39*(8), 838-852.

Karim, W. O. (2021). Electropolishing of pure metallic titanium in a deep eutectic solvent. *Arabian Journal of Chemistry*, *14*(1), 102906.

Kim, J., Zhang, T., Zhou, P., Guan, Q., Xu, Y., Sartori, J., Linderman, L., Mandic, V., & Cui, T. (2022). Polymer tunneling vibration sensors using hot embossing technique. *Sensors and Actuators A: Physical*, *344*, 113705.

Kityk, A., Hnatko, M., Pavlik, V., & Boča, M. (2021). Electropolishing of WCu composite in a deep eutectic solvent. *Chemical Papers*, *75*(4), 1767-1771.

Kumar, R. (2019). MEMS based cantilever biosensors for cancer detection using potential bio-markers present in VOCs: a survey. *Microsystem technologies*, *25*(9), 3253-3267.

Li, D., Zhang, Y., Liu, Y., Regi, F., Doest, M. E. B., & Tosello, G. (2022). Injection moulding of mechanical micro-manufactured structures for optically encoding plastic surfaces. *Optical Materials*, *123*, 111822.

Li, M., Chen, Y., Luo, W., & Cheng, X. (2021). Demolding force dependence on mold surface modifications in UV nanoimprint lithography. *Microelectronic Engineering*, *236*, 111470.

Matlosz, M., Magaino, S., & Landolt, D. (1994). Impedance analysis of a model mechanism for acceptor‐limited electropolishing. *Journal of The Electrochemical Society*, *141*(2), 410.

Murata, Y., Nakanishi, T., Hirai, N., Kawanishi, F., & Ibuki, H. (2019). Development of Mold for Demolding Resistance Measurement in Polymer Injection Molding. *Sens. Mater*, *31*, 3099.

Nakagawa, M. (2022). Micro-print and nano-imprint methods combining laser-drilled screen printing and ultraviolet nanoimprint lithography: a review. *Japanese Journal of Applied Physics*.

Park, K., Lee, J., Kim, Y., Yoon, S., & Yoo, B. (2021). Study of Cu Electrochemical Polishing Mechanism With Observation of Water Acceptor Diffusion. *Frontiers in Chemistry*, 928.

Persaud-Sharma, D., Munroe, N., & McGoron, A. (2012). Electro and magneto-electropolished surface micro-patterning on binary and ternary Nitinol. *Trends in biomaterials & artificial organs*, *26*(2), 74.

Petsch, S., Schuhladen, S., Dreesen, L., & Zappe, H. (2016). The engineered eyeball, a tunable imaging system using soft-matter micro-optics. *Light: Science & Applications*, *5*(7), e16068-e16068.

Sequeiros, E., Vieira, M., & Vieira, M. (2022). Micro metal powder hot embossing: influence of binder on austenitic stainless steel microparts replicability. *Powder Metallurgy*, *65*(2), 112-120.

Surace, R., Basile, V., Bellantone, V., Modica, F., & Fassi, I. (2021). Micro Injection Molding of Thin Cavities Using Stereolithography for Mold Fabrication. *Polymers*, *13*(11), 1848.

# Chapter 6: Industry 4.0 and Digital Manufacturing

# Strategies to Leverage Data in Manufacturing

Andrew Johnston, Queen's University Belfast
Syed Ehtea Samul Hossain, Queen's University Belfast
Danielle Soban, Queen's University Belfast
Alastair Long, Queen's University Belfast

***Abstract***

Manufacturing is a vital part of the global economy and is a key sector of businesses in today's world. It is also a large contributor to global energy consumption and energy-related carbon dioxide (CO2) emission. The constraint of manufacturing constantly insists that companies' goods are made cheaper, faster, or produced in increased quantities. Successful manufacturing demands that companies have high productivity while providing competitive pricing. Companies are also pressured by their governments to continually reduce their energy usage in order to minimize climate change. The pressure put on companies requires them to find new and novel ways to optimise their processes and improve their efficiencies however this can be an expensive and complex task. Data is an often overlooked vital resource that could hold the key to solving this problem. Currently within manufacturing large amounts of data are already being produced each day, however in many circumstances this data is being underutilised forgoing the ability to uncover new discoveries that provide a wealth of knowledge and give a deeper understanding of the process. This allows for more informed decisions to be made and new hypotheses to be tested that will lead to overall increases in efficiency whilst being cost effective. This paper will explore and propose different strategies to leverage data in manufacturing processes. This includes analysing the potential impact that the use of underutilised data can have on manufacturing such as an increase in efficiency, better part quality and/or improved process sustainability. Other uses for this data could include using it to analyse previous issues and identify the cause. This then enables the identification of future potential issues before they occur, allowing them to be corrected, mitigated, or avoided entirely. It will also explore and highlight some of the methods that can be used to perform data analysis that will allow for previously unknown important correlations to be discovered, tested and then verified. Finally, a strategy is presented that outlines how to go from the identification of a problem to obtaining the data, analysing the data and then using the findings to improve process efficiency and in turn sustainability.

*Data Analytics, Industry 4.0, Visual Analytics*

## 1. **INTRODUCTION**

The data revolution has started, as companies are put under increasing pressuring by the requirements of manufacturing it is vital that they find new methods of increasing process efficiency in order to thrive, the way this can be done is through the use of data. Data is a vital resource like water and fuel that can provide a wealth of key information. The amount of data is growing day by day with the International Data Corporation expecting that there will be 175 zettabytes of data worldwide by 2025 (Reinsel, Gantz, & Rydning, 2018). Currently many companies are wasting their data, this is a mistake that is hindering many key decisions on a daily basis. This paper outlines how data is currently being underutilised, methods of data analysis and a strategy that any company can adopted to make use of their data effectively to increase manufacturing efficiency and process sustainability.

## 2. DATA UNDERUTILISATION

Data is a resource that has tremendous potential to add a large amount of value to many global industries however currently the vast amount of data created today in general is being underutilised. Finding ways to usefully use this data will help improve business efficiency, decision making and will ultimately likely lead to an increase in company profitability. Some sectors that currently effectively utilise their data include the aerospace industry, the automotive industry, amazon, google and social media companies such as Facebook. The aerospace industry uses big data to determine reliability, the optimum routes for aircraft and to incorporate customer feedback effectively (Soban, Salmon, & Fahringer, 2013). Google for instance uses search data to determine the most popular websites, these will then show higher up in the search results. Social media companies use data to profile users to gain an understanding of their likes and dislikes. With this information the media presented to them when browsing will be tailored to them which encourages the user to remain on the app for a longer period and in turn view more advertisements, these advertisements are also tailored to users increasing the likelihood of purchases. Currently manufacturing companies produce large amounts of data that is currently being underutilised and has

Email: Andrew Johnston
ajohnston70@qub.ac.uk

the potential, if effectively understood, to provide beneficial insight into the processes and increase manufacturing efficiency. Before discussing how data might be utilised more effectively, it will be useful to discuss the concept of big data.

### *2.1. Big Data*

Whilst the use of large datasets has occurred since the 1970s the term 'Big Data' was coined in the 1990s, who first used the term is up for debate, but it is often associated to John Mashey as the one who made the term popular (Lohr, 2013). Big Data was first defined by Gartner as "data that contains greater variety arriving in increasing volumes and with ever-higher velocity" (Salunkhe, 2018). Big data is unstructured or semi-structured unlike the traditional data storage which is structured and stored in fixed formats or fields in a file such as company expenses or inventory (Fan, Han, & Liu, 2014). These only allow lower-level problems to be analysed and solved whereas unstructured data to gain more insight into a variety of problems. This data can take many different forms with the final aim being to analyse the data to produce useful outcomes.

### *2.2. Big Data 5Vs*

Big data is now defined by the 5 V's, these are velocity, variety, volume, veracity, and value (Ishwarappa, 2015).

- Velocity - how fast the data is received with the ideal being in real time
- Variety – the form of the data such as numerically, audio files or text
- Volume – the amount of data available
- Veracity – how accurate the data is and how much pre-processing is required
- Value – how useful the data provided can be for the desired outcome

The challenge with big data is how to effectively analyse it as this is complicated due to the large volume of information.

### *2.3 Types of Data*

Data comes in many forms (both quantitative and qualitative) which allows for many unique opportunities but that also in itself creates some challenges. This data may have link with the physical properties of the process and with other process parameters. Data can either be stored physically through print, film, magnetic and optical or it can be streamed through telephone, radio, television and the internet.

The type of information can vary drastically as well, textual data provided through written forms such as documents, newspapers, email and webpages are generally available in vast quantities as is it a common form. There are also databases which are collections of organised collections of information that is mainly to serve a specific purpose, and this can make it difficult to analyse particular parts that are necessary for analysis. Other forms of data include video and image data which can be provided by camera systems and satellites, these forms however can be difficult to combine with other forms in order to provide effective analysis and determine correlations. There is also sensor data which can provide information such as time, temperature, light and location. Deducing correlations between these different types of data can provide significant challenge but if done could reap vast rewards and discover correlations that could provide enormous benefit to the analysts (Soban, Salmon, & Fahringer, 2013).

### *2.4 Data in Manufacturing*

Many manufacturing companies contain machinery that is highly complex and as a result produce a plethora of data that in many cases is currently being underutilised. If effectively understood they could provide significant benefits such as improving part quality, reducing manufacturing downtime, increasing yield, tracking inventory among others. Within manufacturing currently data is being used for Conditional based maintenance (CBM) to predict when machine failure is likely to occur. Yam et al. used characteristics such as vibrations and temperatures to identify abnormalities that may indicate the occurrence of a functional failure (Yam, Tse, Li, & Tu, 2001). Si et al. used machine learning techniques to perform to diagnose the faults in motor pumps, rolling bearings, and rocket engines (Si, Li, & Ma, 2018). Rødseth et al. (2017) also used a neural network to predict failure by

determining if the remaining useful life of turbofan jet engines was within the next 10 engine cycles (Rødseth, Schjølberg, & Marhaug, 2017). This approach however has not been widely adopted within manufacturing and if done so could provide significant benefits to companies such as increasing efficiency and identifying unnecessary costs. By utilising data for predictive maintenance, it can decrease the planned machine downtime, unplanned machine downtime, or changeover times and typically decreases the total machine downtime by between 30% to 50% and extends the operation life by 20% to 40% (Rødseth, Schjølberg, & Marhaug, 2017). Other uses for data include within high pressure die casting, Lee et al. (2017) predicted when parts would have defects, Yarlagadda and Chiang (1999) aimed to find the optimum injection time associated with a particular melt and die temperature and Zheng et al. (2009) used it to optimize parameters for surface quality (Lee, Yoon, & Kim, 2017) (Yarlagadda & Chiang, 1999) (Zheng, Wang, Zhao, & Wu, 2009). Use of systems such as these can bring factories to the forefront of Industry 4.0.

### *2.4. Industry 4.0*

Industry 4.0 refers to the fourth Industrial Revolution (Klingenberg, Borges, & Antunes, 2022). The traditional manufacturing process is being sequentially replaced by intelligent technology like automation, Artificial Intelligence, machine learning and robotics. One of the significant features of Industry 4.0 is the goal of minimum or no level of human involvement with the process. This can be achieved by incorporating automation, artificial intelligence, machine learning, robotics within the industry or manufacturing Process (Iftikhar, Baattrup-Andersen, Nordbjerg, Bobolea, & Radu, 2019). Some examples of how industry 4.0 can be of benefit to manufacturing companies is through the use of virtual reality which could allow employees to gain an understanding of complex equipment from a safe environment where key lessons can be learnt so that these can be avoided when operating the real machine. It can also provide the benefit or reduced human interaction through automation increasing safety and by allowing for quality checks to be performed at regular stages in the manufacturing process allowing for parts to be sent back and corrected rather than having them complete each stage in the manufacturing process (Saxena, Papanikolaou, Pagone, Salonitis, & Jolly, 2020).

## *3. DATA ANALYTICS*

As shown data is a highly value resource that should be collected accurately in order have an effective impact on manufacturing. The subsequent issue presented once a viable amount of data has been collected is how a useful output is obtained from it. Data analytic techniques provide ways of interpreting large amounts of data that produce can provide useful outputs to the user.

Various analytical methods could be used to interpret this data including neural networks, K-means clustering and correlation analysis. Another potential analytic method that is currently underutilised that could provide significant insight is the field of visual analytics.

### *3.1 Neural Networks*

Neural networks are a method of artificial intelligence that is modelled on the human brain and how it processes information. They were first proposed in 1944 by Warren McCullough and Walter Pitts and have gone up and down in popularity since then but are more commonly used today due to the increase in computational power. Neural networks undertake a training process where previously obtained data is used to alter weights and bias so that for a given set of input data the correct output is achieved. Once the training process is complete the network can then be used to predict outputs for new sets of inputs. It is possible to apply this within industry so that for specific input parameters such as temperature, velocity or cycle time an output can be predicted for example if a part is likely to be a defect, this can then be investigated and corrected if needed (Fernandes de Mello & Antonelli Ponti, 2018).

### *3.2 K-means clustering*

K-means clustering is another method of machine learning. This method involves plotting the input data e.g., temperature, velocity in a graph. The datapoints are then grouped together in clusters based on similarity. From the points in these clusters a mean point is calculated, when unseen data is then tested the cluster mean closest to the point is the one the algorithm classifies it as (Watt, Borhani, & Katsaggelos, 2020). Although it can effectively

classify data this method requires subsequent verification to determine if the clusters are correct (Fernandes de Mello & Antonelli Ponti, 2018).

### *3.3. Visual Analytics*

Visual analytics utilises analysis with interactive visualisations to aid understanding, reasoning and decision making for large and complex datasets (Keim, Kohlhammer, Ellis, & Mansmann, 2010). It aims to do this by first analysing to show the important information, this can then be zoomed into and filtered to allow further analysis and has been referred to as details on demand (Keim D. , 2005). Using a combination of statistical graphics, analysis, animation, and interaction the aim is to enable users to explore and understand their data and allow them to form hypotheses by optimising the cognitive process (Maciejewski, 2011). It incorporates knowledge from multiple disciplinary fields such as data science, decision making science, cognitive perceptual science and analytical science (Franklin, et al., 2017).

The concept of using pictures to understand data has been around for centuries, such as the use of maps and graphs in the 17th century. The most cited example of statistical graphics occurred when Charles Minard mapped Napoleon's invasion of Russia (Figure 1). This map portrayed the size of the army as well as the path of Napoleon's retreat from Moscow. In addition, it also contained information on temperature and time scales to give a more in-depth insight of the event (SAS Institute Inc., n.d.). It is often referred to as the best statistical graphic ever produced.

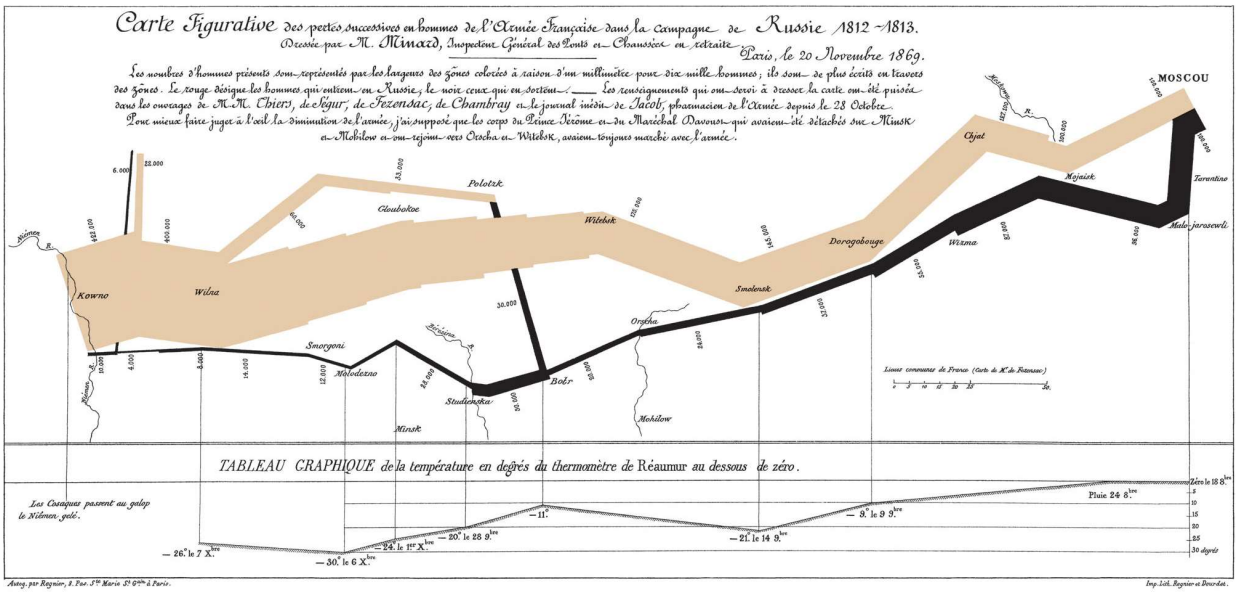


*Figure 1 - Flow Map of Napoleon's Invasion of Russia, (Flow Map of Napoleon's Invasion of Russia, n.d.)*

After the terrorist attacks on September 11th, 2001, there was a need to interpret a massive amount of diverse, complex, and rapidly changing data in real time (Zelikow, Jenkins, & May, 2004). Visual analytics was seen as an enabler that would help to protect the American people. A key deliverable that came out of this was the Illuminating the Path: The R&D agenda for visual analytics (2005) (Thomas & Cook, 2005), this document has become the definitive resource for the emerging scientific discipline of visual analytics (Soban, Thornhill, Salunkhe, & Long, 2016).

The main difference to using a visual analytics approach compared with other methods to explore the same dataset is that it allows for a deeper understanding and insight into the process for the analyst. This insight can then be used when making key decisions in numerous different circumstances. "One key goal of applied Visual Analytics in the engineering domain will be the analysis of the complexity of the production systems in correlation with the achieved output, for an efficient and effective improvement of the production environments" (Keim, et al., 2008).

One of the most significant advantages of Visual Analytics is it can handle a large amount of non-homogeneous data from multiple sources. This makes Visual Analytics a practical and versatile tool compatible with several applications. It allows for a more inherent understanding and insight into the behaviour of the process that aid the analyst. This insight is then translated into parameter strategies that are applicable across a wide variety of process circumstances.

### *3.4. Dashboards*

A dashboard is a visual tool that is designed to convey key information in a concise manner on a single screen that can be quickly interpreted by the user or "at a glance". Figure 2 shows a dashboard for a haulage company and conveys information such as how many deliveries were on time and the profit per country (Durcevic, 2021). Dashboards first appeared in the early 1990s having been of interest to researchers by providing a means of summarizing important information and visualising with graphical components such as charts, graphs, diagrams, and maps (Farmanbar & Rong, 2020). Dashboards can utilise the large power of visual perception to communicate key outcomes, but only if it is constructed in a way that effectively conveys the useful information to the user (Few, 2006).


*Figure 2 - Dashboard of haulage company*

Dashboards are used in a diverse number of fields such as in emergency rooms, manufacturing and in education to monitor and improve the performance of students within a class (Tokola, Gröger, Järvenpää, & Niemi, 2016), (Park & Jo., 2019) (Franklin, et al., 2017). Tokola et. al created three dashboards that tailored the information of each dashboard based on company hierarchy demands (Tokola, Gröger, Järvenpää, & Niemi, 2016). Dashboards are an easy and effective way to aid the decision making for users and so could benefit this project, how the information will be displayed is vital and consultation should be sought with potential users in order to optimise the layout and information displayed.

## *4. DISCUSSION*

In order to effectively use data to optimise manufacturing systems and help to increase manufacturing process efficiency and to improve manufacturing sustainability a strategy is required. A flowchart of this strategy is shown in Figure 3.

The first step of the strategy is to identify the problem you wish to address, this could be improving part quality, machine reliability etc. After this has been determined the next step is to identify the existing data that already exists and is currently being used. If data is being recorded ensure that historical records are also analysed, if this information is recorded on physical documents, it would be of benefit to enter this electronically. The key questions to ask at this stage are What is being used? Who uses it? Who owns it? Who has access to it? Who can add to it? What form is it in (handwritten, database, paper reports, electronic)?

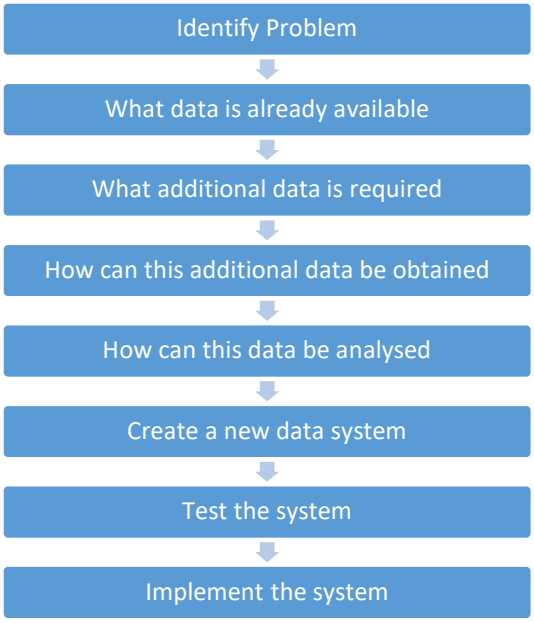


*Figure 3 - Flowchart of strategy proposed*

The next stage is to identify any additional information that would be required and determine in which areas specifically. It is important at this stage to determine why the additional data is relevant and the benefit it is likely to bring to the final conclusion. This additional information can then be obtained through various methods such as implementing a more detailed way of recording data in the future, adding more sensors to record new key variables or introducing new software that allows people to record results and observations more easily and accurately. If these are not viable then it should be discussed as to what resources are required in order to effectively record the new data.

After this it must be decided on how the data will be analysed both by which method and by who does this. Other key items to consider are who will provide the analyst with the data required and who is responsible for it? This could be done by the continuous improvement engineers for example. Once the method of analysis has been chosen the new data system must be created. This will involve using the data to discover correlations and then using those to develop hypotheses that can then be tested and validated. The use of a dashboard could be of great benefit here as it allows various key decision makers to have the data readily available without the prerequisite of requiring a deep understanding of the analysis techniques.

Now the system has been created the system must be tested, case studies can be performed to ensure that it is performing accurately and to validate any hypotheses. If the hypothesis was not correct the answer to this should be determined to aid with future analysis. User feedback should be considered at this stage as it is vital that people recording the information are accepting of the new system that is being implemented, this allows for any oversights to be caught as well allowing the system to grow. Once the system has been tested it should be updated to eliminate any errors.

Finally, once the testing stage has been completed the system should be implemented, this can be on a smaller scale to begin with for example one machine and then gradually implement across the entire factory so that the users become familiar with and accepting of the changes within the process. At this stage someone should be responsible for the system upkeep ensuring that it is performing as required and still obtaining and using accurate information. The positive impact of the system can then be analysed to determine the magnitude of the improvements it has made.

## *5. CONCLUSION*

Data recording and utilisation is vital for the improvement of manufacturing efficiency and process sustainability. By following the strategy proposed in this paper any factory will be able to implement positive change that will allow them to embrace the future and transform their business.

## *6. REFERENCES*


Durcevic, S. (2021, February 5). *How To Make Stunning Dashboards & Take Your Decisions To The Next Level*. (Datapine) Retrieved March 8, 2022, from https://www.datapine.com/blog/how-to-make-a-dashboard-with-ease/

Fan, J., Han, F., & Liu, H. (2014). Challenges of big data analysis. *National science review*, 293-314.

Farmanbar, M., & Rong, C. (2020). Triangulum City Dashboard: An Interactive Data Analytic Platform for Visualizing Smart City Performance. *Processes, 2*(250), 250.

Fernandes de Mello, R., & Antonelli Ponti, M. (2018). *Machine Learning A Practical Approach on the Statistical Learning Theory.* São Paulo: Springer.

Few, S. (2006). *Information dashboard design: The effective visual communication of data Vol. 2.* Sebastopol, CA: O'Reilly.

*Flow Map of Napoleon's Invasion of Russia*. (n.d.). Retrieved 01 28, 2022, from https://ageofrevolution.org/200-object/flow-map-of-napoleons-invasion-of-russia/

Franklin, A., Gantela, S., Shifarraw, S., Johnson, T., Robinson, D., King, B., . . . Rubio, A. (2017). Dashboard visualizations: Supporting real-time throughput decision-making. *Journal of biomedical informatics, 71*, 211-221.

Iftikhar, N., Baattrup-Andersen, T., Nordbjerg, F. E., Bobolea, E., & Radu, P. B. (2019). Data Analytics for Smart Manufacturing: A Case Study. In DATA., (pp. 392-399).

Ishwarappa, J. A. (2015). A Brief Introduction on Big Data 5Vs Characteristics and Hadoop Technology. *Procedia Computer Science, 48*, 319-324.

Keim, D. (2005). Scaling Visual Analytics to Very Large Data Sets, Presentation. Darmstadt.

Keim, D., Andrienko, G., Fekete, J.-D., Görg, C., Kohlhammer, J., & Melançon, G. (2008). Visual analytics: Definition, process, and challenges. In *Information visualization* (pp. 154-175). Berlin, Heidelberg: Springer.

Keim, D., Kohlhammer, J., Ellis, G., & Mansmann, F. (2010). *Mastering the information age: solving problems with visual analytics.* Bad Langensalza: Eurographics Association.

Klingenberg, C. O., Borges, M. A., & Antunes, J. A. (2022). Industry 4.0: What makes it a revolution? A historical framework to understand the phenomenon. *Technology in Society, 70*, Article 102009.

Lee, J. Y., Yoon, J. S., & Kim, B.-H. (2017). A big data analytics platform for smart factories in small and medium-sized manufacturing enterprises: An empirical case study of a die casting factory. *International Journal of Precision Engineering and Manufacturing, 18*(10), 1353-1361.

Lohr, S. (2013, February 1). *The Origins of 'Big Data': An Etymological Detective Story*. Retrieved from New York Times: https://bits.blogs.nytimes.com/2013/02/01/the-origins-of-big-data-an-etymological-detective-story/?searchResultPosition=1

Maciejewski, R. (2011). Data representations, transformations, and statistics for visual reasoning. *Synthesis Lectures on Visualization, 2*(1), 1-85.

Park, Y., & Jo., I.-H. (2019). Factors that affect the success of learning analytics dashboards. *Educational Technology Research and Development*, 1-25.

Reinsel, D., Gantz, J., & Rydning, J. (2018). *Data Age 2025.* Framingham, MA: International Data Corporation (IDC).

Rødseth, H., Schjølberg, P., & Marhaug, A. (2017). Deep digital maintenance. *Adv. Manuf. , 5*, 299-310.

Salunkhe, S. (2018, March). Applications of Visual Analyticsto theHigh Pressure Die Casting Process. Belfast: Queen's University Belfast.

SAS Institute Inc. (n.d.). *Data Visualization What it is and why it matters*. Retrieved 01 28, 2022, from https://www.sas.com

Saxena, P., Papanikolaou, M., Pagone, E., Salonitis, K., & Jolly, M. (2020). Digital Manufacturing for Foundries 4.0. In *Light Metals 2020* (pp. 1019-1025). Springer, Cham.

Si, J., Li, Y., & Ma, S. (2018). Intelligent Fault Diagnosis for Industrial Big Data. *Journal of Signal Processing Systems, 90*, 1221–1233.

Soban, D. S., Salmon, J., & Fahringer, P. (2013). A visual analytics framework for strategic airlift decision making. *The Journal of Defense Modeling and Simulation, 2*(10), 131-144.

Soban, D., Thornhill, D., Salunkhe, S., & Long, A. (2016). Visual analytics as an enabler for manufacturing process decision-making. *Procedia Cirp, 56*, 209-214.

Thomas, J. J., & Cook, K. A. (2005). Illuminating the Path: The R&D Agenda for Visual Analytics. *National Visualization and Analytics Center.*

Tokola, H., Gröger, C., Järvenpää, E., & Niemi, E. (2016). Designing Manufacturing Dashboards on the Basis of a Key Performance Indicator Survey. *Procedia CIRP, 57*, 619-624.

Watt, J., Borhani, R., & Katsaggelos, A. (2020). *Machine Learning Refined: Foundations, Algorithms, and Applications (2nd ed.).* Cambridge: Cambridge University Press.

Yam, R. C., Tse, P. W., Li, L., & Tu, P. (2001). Intelligent Predictive Decision Support System for Condition-Based. *Int. J. Adv. Manuf. Technol., 17*(5), 383-391.

Yarlagadda, P. K., & Chiang, E. C. (1999). A neural network system for the prediction of process parameters in pressure die casting. *Journal of Materials Processing Technology, 89*(90), 583–590.

Zelikow, P., Jenkins, B. D., & May, E. R. (2004). *The 9/11 Commission Report.* New York: W.W. Norton & Company.

Zheng, J., Wang, Q., Zhao, P., & Wu, C. (2009). Optimization of high-pressure die-casting process parameters using artificial neural network. *The International Journal of Advanced Manufacturing Technology, 44*(7), 667-674.

# Current State of the Art in IoT/AI in Status Monitoring in CNC Precision Machining

Darren W. Fitzgerald School of Mechanical, Electrical & Process Engineering, Munster Technological University, Cork
Dr. Patrick Delassus, School of Engineering, Atlantic Technological University, Galway
Dr. Olga Lyashevska, School of Science and Computing, Atlantic Technological University, Galway
Dr. Carine Gachon, School of Engineering, Atlantic Technological University, Galway

***Abstract***

This paper will present a review of the current trends and approaches currently applied to monitor the manufacturing process of precision components, using CNC Machine Centres. With the advancement of Artificial Intelligence/Internet of Things Development Boards, it has become easier to not only gather data, but process data as Machining activities are being completed. Data generation has been traditionally completed by external hardware like data loggers, needing additional PCs to carry out specific analysis (Tool Force, Acoustic analysis, Vision Systems for Tool wear), but with the availability of higher powered, microcomputers, much of this analysis can be integrated into a standalone system, that can be interrogated with via wireless means, allowing for greater integration in the machining environment. These microcomputers are also capable of high-level automated analysis, allowing shorter lead time to identify an issue or discrepancy, which can affect the quality of the part. This paper will address the current approaches and potential opportunities for future systems, which can also use Artificial Intelligence (AI) approaches, in the immerging change of Industrial Revolution, from Industry 4.0 to 5.0, where the relationship between Machine and Human will be harmonious and seamless in decision making and understanding of the relevant processes.

*Key Words: Machining, IoT, Industry 5.0, CNC.*

## 1. INTRODUCTION

Maintaining Tooling Performance has remained one of the key challenges for Modern Manufacturing Facilities. The cost associated with underperforming Tooling can be substantial, especially for volume production. Some of the areas that are also associated are cost of poor quality, rework, scrap, downtime and cost of subsequent tooling (Y. Zhou, B.Sun, W. Sun, 2020). There are some activities that can extend the life of the tool, by altering Feeds/Speeds/Dept of Cut, use of Cutting fluid that an experienced CNC Engineer can identify. In absence of the seasoned Engineer, a machine may continue machining parts, which are of below quality standards. To understand this, there has been substantial work carried out to understand potential failure modes. Status Monitoring systems have been used to identify the force applied during cutting, acoustic sound while cutting, power applied via the spindle, temperature relationship between cutting tool and part, type of chip formed. Traditional Status Monitoring Systems comprise of a sensor, data collector and a processing system to retrieve and analyse these signals. Once the relevant process parameter has been identified, a relevant sensor or probe can be selected. Depending on this Selection, the signal created, either Analog or Digital must be processed. This can be done via specific software or controllers. Once the data has been generated, a correlation between said tooling condition can be used to project the status of the cutting tool, or using previous examples of poor tooling, could be used to determine the remaining Tool life (Y.F. Yang, Y.L. Guo, Z.P. Huang, N. Chen, L. Li, Y.F. Jiang, N. He, 2019). This Information can be pivotal, in ensuring the quality of the Manufactured part.

## 2. THEOERTICAL BACKGRUND

### *2.1 Machine Centres*

A machine centre can be described as an automated system that can preform task that can be carried out on traditional machines, but with significantly greater repeatability and accuracy. A basic example of this is a traditional Milling machine fitted with encoders and servo motors to actuate the movements of the Spindle or table. In this instance, the feature is machined using programmable language to generate the cutting paths and utilisation of the correct parameters, like feeds/speeds. Uses of Machine Centres (both Lathe and Milling), have been established as the most reliable ways to bring near net products, to their final required tolerance, especially

Email: Darren W. Fitzgerald
Darren.Fitzgerald@mtu.ie

for Orthopaedic application in the medical device sector, or where Precision is required as a Critical to Quality Attribute (CTQ) Despite the upsurgence in the use of Additive Manufacturing processes, including Selective Laser Sintering and 3D Printing. Subtractive Machining, via Machine Centres, has maintained its place as the most suitable manufacturing processes, for volume production.

### *2.2 Parameters for Machining*

During the cutting process, there are 3 key areas that have been established as parameters that can yield effective data in interpreting the performance of the cutting process. These are Force, vibration, and acoustic emissions. For Milling processes, the forces and vibrations can be extracted to their respective axis (X, Y, and Z). Each of these can be affected by the process setup parameters. These include Feed Rate, described as the velocity at which the tool cuts into the material and Cutting Speed, the rate at which the spindle turns to achieve the required cut. (RapidDirect, 2022). Any slight alterations to these specifications could have a direct effect on the temperature developed between the tool and the material, power needed for the spindle to turn and compensate for, damage to tool tip if Built Up Edge (BUE) occurs. These initial parameters are dictated by the manufacturer's recommendations but with most tooling, may need to be adjusted when used on a particular machine. The improper selection of toolholder, collets vs heat shrink, spindle concentricity may need to be considered, defining a machine specific constraint that needs to be taken into account.

## 3. PRE INDISTRY 4.0

### *3.1 Traditional Practices in Machining*

In the workshops of yore, experience was the most reliable methods to ensure the machining process was running as optimal as it could. This was based of several tacit approaches, including the Machining Engineer listening to how the material was being cut, the types of chips being generated, visually inspecting both the surface finish of the part and the tooling tip itself. This approach required several years of training and exposure to develop the ear and understanding to make a call on whether the tooling or setup was incorrect. This was the early correlation between cutting conditions and chatter being present in the final workpiece. As this was based purely on instinct, it was a verification that was non transferable and hard to teach new employees. (Rathod, Kulkarni, & Kumbhar, 2019)

Other activities include the removal of the tool and checked by eye. The Machinist would check for any damage on the flank of the cutter and, if needed, sharpen the tool. This was also a skill that required years of experience to develop and hard to maintain repeatability, due to human nature. This was aided with the use of Shadow Projectors and other Metrology Equipment that could establish a standard to compare the tooling to, but still needed the machine to be down to remove the tool for inspection. With the use of Shadow Projectors, the Tool could be compared to a known "Good" Standard. (J. Downey, D. O'Sullivan, M. Nejmen, S. Bombinski, P.O'Leary, R Raghavendra, K, Jemielniak, 2016)

### *3.2 Sensors & Data Loggers*

With the development and greater availability of PCs in the workshop, it was natural that the Machine Centre would be linked to a PC to capture real time data. Many case studies have been carried out using this approach, with the use of Data Loggers to record information from Sensors applied to system. Sensor selection transitioned from a sensor that would be used to investigate forces during a particular activity, up to gathering continuous data while machining. During this time, several types of sensors were used to understand the forces and vibrations. Strain gauges were used to identify any flexing that may occur in the system. Dynamometers later followed, a device based on piezoelectric technology, can be used to determine the forces generated in any of the 3 axis of the Machine Centre that can detect any deflection. The setup for a Dynamometer doesn't lend itself for all milling products, which inhibits its use for prolonged and extended companies of production runs. (Kistler, 2022) Other sensors were then selected, smaller sized elements that could be applied directly to the machine structure. Downey et al, explained the use of such sensors, which yielded successful results and backed up when compared to known good data. The machine structure was drilled to incorporate the sensor, to facilitate the sensor while the machine was running. These sensors were then connected to a Data Logger. (J. Downey et al, 2016).

### *3.3 Tool Conditional Monitoring*

There are 4 established approaches to traditional Tool Monitoring. These include both Online or Offline (i.e., either in process or out of process) and Direct and Indirect. With the advances of Co-ordinate Measuring Machines (CMM), machined parts have become easier to verify, to heavily regulated tolerances outlined for Medical Device Requirements. This Indirect, offline approach can give greater feedback about the Machine Centre Performance, but requires separate equipment, with the part removed from the machine. The approach identified in many cases of the direction of TCMs is to create an Online system that can facilitate both Direct and Indirect features. This would allow process features, such as speeds, feeds, force, vibration, and acoustics, as well as surface finish and texture to estimate and determine the Tooling condition. Any notable changes in these parameters can identify potential tool wear and underperformance, which may lead to out of tolerance parts (Mohanraj, Shankar, Rajasekar, Sakthivel, & Pramanik, 2020). Traditional TCMs identify these signals, but still need processing to describe the actual extent of said tooling. Many CNC Controllers now have software solutions, specifically for Chatter and Feed Control, in the form of Adaptive Chatter Control (ACC) and Adaptive Feed Control (AFC). This relies on the Engineer to set a maximum feed rate for the specific material and applies more power to overcome the challenge (Heidenhain, 2013).

## 4. AGE OF IOT/INDUSTRY 4.0

### *4.1 Advancements in Sensors*

With advancements in technology, the quality of sensors and ability to record finer and finer data has heralded greater information that can be captured within the machine while it is running. The technology used within the sensor became smaller and easier to incorporate into the system. In many cases, no altering to the machine structure was needed, removing the potential to damage the integrity of the system. This, with the increased readily availability has made it easier to capture high quality data, which can be used to determine the remaining life of a tool or whether to intervein before product quality is being affected. Pimenov et al describes two approaches used in modern Status Monitoring, Direct and Indirect. Direct Sensors include accelerometers for force and acoustic sensors for Acoustic Emissions, while Indirect Sensors can use alternative machining metrics, like power consumption or spindle compensation, which can be processed via designed algorithms to determine the surface finish of a product. (D. Pimenov et al, 2022). Due to the hazardous nature within the CNC Machine Centre, sensors have been designed to withstand these conditions. One key area of concern is the use of coolant, which is a requirement of some materials for prolonged tooling life.

### *4.2 Microcontrollers*

From the review of papers, it is clear that Microcontrollers have taken the place of traditional Data Loggers in recent years. A Microcontroller can be described as a board that can be programmed to run a script of code and when connected to external hardware, can be used to carry out specific functions. An example of a Microcontroller includes Arduino Uno and Raspberry Pi Pico. Due to their small size, connectivity to a wide variety of sensors, ability to collect data for extended periods and low power consumption, it has more of a presence in research activities in machining. (Y. Guven et al, 2017). These boards can gather Direct Data from spindle Vibration (N. Rathod et al, 2019) and to use an off-the-shelf accelerometer to determine vibration of a cutter during both roughing and finishing passes. (V Jain et al, 2020). Both case studies used inexpensive boards and sensors to create a Status Monitoring System that yielded data comparable to that from stand alone Data Loggers. These boards require minimal training to use, as the programming language is based on C++, while using the dedicated Arduino Integrated Development Environment (IDE) is user friendly and intuitive. The IDE can also be used to show the data while it is running, ensuring live data can be reviewed and captured. (Arduino, 2022). An additional benefit of the use of Arduino and comparable microcontrollers is the open-source nature of their design, which has been seen to make the transition from prototype to final designed system far shorter. This is beneficial when developing a specific board layout, with selection of off-the-shelf parts easier.

Limitations have been identified with certain Arduino Boards, with Uno having 14 I/O Pins, which would be inhibited for use with a 3 Axis machine. Arduino Mega, having 54 I/O pins and the ATMega2560 chip, which is more suited for heavier processing. Research has shown that these boards can collect data, but have limited

functionality when working with the data, as the processing power is just not available with these 8-bit boards. In some applications, these drawbacks have been addressed, with the ability to install Hardware Attached on Top (HAT) boards, that when incorporated, allows greater communication between the system and user, including Wi-Fi connectivity and use of wireless sensors.

### *4.3 Application of Single Board Computers*

A continuation of Microcontrollers is the use of Microcomputers, alternatively known as Single Board Computers (SBC). As the name describes, it is a single board, that is capable of running an operating system, similar to a PC, with the added functionality of General Input/Output Pins (GPIO), that can be used to integrate variety of sensors and visual indicators. These SBC can be used to not only collect data, but also carry out work on the data. An example of this is the Raspberry Pi line of boards. These are Linux based systems and can be programmed via Python. (The Raspberry Pi Foundation, 2022). Being a larger footprint compared to Arduino, the Pi is far more capable of complex processing. An example of this is the use of a Raspberry Pi Model 4 for Machine Inspection. It is noted that due to the processing capabilities and utilisation of Python Programming, data can be collected and sent directly to the cloud for processing. This approach developed a live database of information for the Machine Centre, as well as live monitoring, with the use of a Camera to create a Vision Inspection System. (Y. Saif et al , 2022).

Many manufacturers of these board adopt the Open-Source approach, which means that the original specifications and design files, along with the original kernel coding is available to the wider public. This allows the boards to be integrated in prototypes, while also allows the design team to make specific alterations or add greater functionality, specific to their application. Many of these SBC's run Linux, or variated distros, due to the similar nature of Open-Source Coding. An example of this is shown in the use of a Beagleboard Black along with an Analog Device Accelorometer. The Sensor was fitted to the spindle to record the vibration of the spindle. Data was collected and used for the creation of a robust Status Monitoring System, designed to capture Low Frequency parameters (Temperature) and High Frequency parameters (Vibration of Spindle). Traditional DAQ systems were compared to newer methods of embedded computers and the cost implications of acquiring expensive systems. It is shown that by adopting an SBC, over a specific of-the-shelf data logger, it overcame the extensive cost of implementing a traditional sensing system. (R. Lynn, et al, 2018)

### *4.4 Applications of Machine Learning*

Machine Learning has played a key role in Status Monitoring of Machine Centres. Machine Learning can be described as a process of using existing data to create an algorithm that can make a call on whether a pass criterion has been met or not. Several Papers outline the use of Supervised and Unsupervised Learning. In these cases, labelled data is fed into the algorithm that can be used to train the system. (Dataversity, 2022). Machine Learning has been used successfully in Machine Monitoring, with applications of Artificial Neural Network (ANN) used to understand and process data directly from the machine. ANN is an approach to establish artificial Intelligence by mimicking the human brain, via the use of node, bias elements and weighting elements. This is shown by Mohan Krishna et al, when an accelerometer was applied to the spindle of a Machine Centre and the use of a Microcontroller to collect said data. Data was generated to show the vibrations for both worn and known good tools. These sample data was then fed into the ANN system, based in MATLAB. The system provided successful results, yielding 95% effectiveness, when determining if the measured tooling is worn. (Mohan & Kannadaguli, IoT based CNC machine condition monitoring system using machine learning techniques, 2020). This system was later improved by the inclusion of Long Short-Term Memory (LSTM) and increasing the number of Hidden Layers in the Neural Network. This advancement falls under the Deep Learning approach to learning and establishing how the data can be interpreted. By updating the initial approach, to LSTM, the effectiveness of the system increased to 99.7%. (Mohan & Patil, 2021).

These case studies show how data can be collected via a microcontroller, which would feed into a Machine Learning program developed on MATLAB. Another application of Machine Learning is the use of a Microcomputer to not only collect the data, but also carry out some of the processing for the data gathered. Woodruff et al, uses a Linux based SBC to carry out Fast Fourier Transforms (FFT), locally, rather than offline

on an independent PC. This was achieved by the use of open-source libraries that allowed the full potential of the SBC to compute this data.

## 5. POST INDUSTRY 4.0/ INDUSTRY 5.0

Industry 4.0 has provided a means of measuring far more metric within a machine that was previously thought possible. The use of smart sensors and microcontrollers facilitated the creation of novel and robust systems that could successfully gather and process data, outlining time sensitive characteristic. It is anticipated that a new age of understanding is currently transitioning, in the form of Industry 5.0. This phase will bring in transformations that will result in machines working side by side humans, with equal responsibility (Demir, Döven, & Sezen, 2019). The evolution to Industry 5.0 highlights greater level of smart sensors and higher level of intelligence in our systems, including elements of Artificial Intelligence, Machine Learning and bridging the gap between user and machine. This approach will allow for greater range of communication and decision making between the process at hand and the sensors that monitor key process characteristics. It is envisaged that Industry 5.0 will continue the Smart Manufacturing approach from Industry 4.0, with a greater connection and higher level of responsibility between Human and Machine. Over the last 5 years, there has been significant advances on Sensor Technology, Processing Capabilities and availability of off-the-shelf systems to facilitate this development. (Liang, Liu, & Wang, 2020). This goes hand in hand with Machine Learning, where the Machine is given the opportunity to grow its knowledge, by using continuous Data to build on its understanding of the given application (Khan & Al-Badi, 2020). Artificial Intelligence has been utilised in TCMs for Data Manipulation and extrapolation. Various Models have been utilised, including Support Vector Machine, Artificial Neural Network and Fuzzy logic to name a few (Mohanraj, Shankar, Rajasekar, Sakthivel, & Pramanik, 2020).

## 6. CONCLUSION

It has been noted that there have been significant strides in our understanding of Machining and the ability to capture the correct data, at the correct time, during the 4$^{th}$ Industrial revolution. This freedom has allowed potential failures, eminent damage and failing quality to be identified, well in advance or before potentially reaching the customer/patient. In Traditional Status Monitoring systems, they still require the need for human interaction to make relevant adjustments to the machining parameters, but it is clear that Machine Centres will be able to take advantage of the new industrial age of 5.0. The evolution of Microcomputers to Microcontrollers, to SBC's specifically designed for Artificial intelligence applications will ensure that Status Monitoring will be at the forefront of the harmonious relationship between machine and human. Advances in Technology and the philosophy of Open Source has shown what can be achieved and allows a greater understanding and flexibility when developing systems for a specific Engineering Problem and easier to transition from a Mechanical problem to a smart electronic solution. The ability to complete Artificial Intelligence tasks on SBC's is becoming more and more available to both researchers and Engineers alike, with user friendly and intuitive interfaces, ensuring that engineering disciplines are ready for the transition to the next generation of understanding the equipment interacted with.

## 7. REFERENCES


Arduino. (2022, 06 27). *https://docs.arduino.cc/software/ide-v1/tutorials/arduino-ide-v1-basics*. Retrieved from Arduino Integrated Development Environment (IDE) v1: https://docs.arduino.cc/software/ide-v1/tutorials/arduino-ide-v1-basics

D. Pimenov, M. Gupta, L. da Silva, M Kiran, N. Khanna, G. Krolczyk. (2022). Application of measurement systems in tool condition monitoring of. *Measurement*.

Dataversity. (2022, February 4). *A Brief History of Deep Learning*. Retrieved from https://www.dataversity.net/brief-history-deep-learning/#

Demir, K. A., Döven, G., & Sezen, B. (2019). Industry 5.0 and Human-Robot Co-working. *Procedia Computer Science Vol 158*, 688-695.

Heidenhain. (2013). *Dynamic Efficiency – Working Efficiently and with Process Reliability*. Retrieved from Heidenhain: https://www.heidenhain.de/de_EN/products/cnc-controls/dynamic-efficiency/. [Accessed 23 November 2020].

J. Downey, D. O'Sullivan, M. Nejmen, S. Bombinski, P.O'Leary, R Raghavendra, K, Jemielniak. (2016). Real Time Monitoring of the CNC Process in a Production Environment- the Data Collection & Analysis Phase. *Procedia CIRP Vol 41*, 920-926.

Khan, A. I., & Al-Badi, A. (2020). Open Source Machine Learning Frameworks for Industrial Internet of Things. *Procedia Computer Science, Vol. 170*, 571-577.

Kistler. (2022, May 06). *Dynamometers for measurement technology test solutions: wide application range and easy handling*. Retrieved from https://www.kistler.com/en/solutions/research-and-development-testing/dynamometers-for-test-and-measurement/#:~:text=Our%20dynamometers%20are%20used%20for,based%20on%20piezoelectric%20measurement%20technology.

Liang, X., Liu, Z., & Wang, B. (2020). Multi-pattern failure modes and wear mechanisms of WC-Co tools in dry turning Ti–6Al–4V. *Ceramics International, Vol. 46*, 24512-24525.

Mohan, K., & Kannadaguli, P. (2020). IoT based CNC machine condition monitoring system using machine learning techniques. *9th International Conference on Communication Systems and Network Technologies* (pp. 61-65). Gwalior: IEEE.

Mohan, K., & Patil, M. M. (2021). CNC Machine Condition Monitoring System Using LSTM Based Deep Learning Techniques. *19th OITS International Conference on Information Technology, OCIT 2021* (pp. 42-47). Bhubaneswar: OCIT.

Mohanraj, T., Shankar, S., Rajasekar, R., Sakthivel, N., & Pramanik, A. (2020). Tool condition monitoring techniques in milling process-a review. *Journal of Materials Research and Technology, Vol 9, Issue 1*, 1032 - 1042.

N. Rathod,V. Kulkarni, C. Kumbhar. (2019). Status monitoring system for vertical milling center machine. *5th International Conference on Computing, Communication, Control and Automation.* Pune: ICCUBEA 2019.

R. Lynn, E. W. (2018). Embedded fog computing for high-frequency MTConnect data analytics. *Manufacturing Letters 15*, 135-138.

RapidDirect. (2022, May 08). *Difference Between Feed Rate and Cutting Speed in CNC Machining*. Retrieved from RapidDirect.com: https://www.rapiddirect.com/blog/difference-between-feed-rate-and-cutting-speed/

Rathod, N., Kulkarni, V. A., & Kumbhar, C. (2019). Status monitoring system for vertical milling center machine. *5th International Conference on Computing, Communication, Control and Automation, .* Pune: ICCUBEA .

The Raspberry Pi Foundation. (2022, Mar 29). *Raspberry Pi 4: Your tiny, dual-display, desktop computer*. Retrieved from https://www.raspberrypi.com/products/raspberry-pi-4-model-b/

V Jain, S. P. (2020). , Vibration monitoring of ball nose end mill tool during milling of sculptured surfaces using MUP6050. *Materials Today: Proceedings 27*, 2477 - 2486.

Y. Guven, E. Cosgun, S. Kocaoglu, H. Gezici, E. Yilmazar. (2017). Understanding the Concept of Microcontroller Based Systems To Choose The Best Hardware For Applications. *Research Inventy: International Journal of Engineering And Science*, 38 - 44.

Y. Saif, Y. Yusof, K. Latif, A. Kadir, M. Ahmad, A. Adam, N. Hatem . (2022). Development of a smart system based on STEP-NC for machine vision inspection with IoT environmental. *The International Journal of Advanced Manufacturing Technology*, 4055 - 4072.

Y. Zhou, B.Sun, W. Sun. (2020). A tool condition monitoring method based on two-layer angle kernel extreme learning machine and binary differential evolution for milling. *Measurement, Vol. 166*.

Y.F. Yang, Y.L. Guo, Z.P. Huang, N. Chen, L. Li, Y.F. Jiang, N. He. (2019). Research on the milling tool wear and life prediction by establishing an integrated predictive model. *Measurement , vol. 145*, 178 - 189.

# A low-code proposal for a rule-based engine integration in a Digital Thread Platform context

Ivan Guevara, University of Limerick, Limerick (Ireland) and Confirm Centre
Hafiz Ahmad Awais Chaudhary, University of Limerick, Limerick (Ireland) and Confirm Centre
Tiziana Margaria, University of Limerick, Limerick (Ireland), Lero and Confirm Centres

***Abstract***

Cross-functional integration of components in a Smart Manufacturing environment is a challenging task as we need to orchestrate the several layers composing the entire system to deliver a fully cohesive solution between the different actuators. Examples are IoT connectivity and analytics, data workflow integration, AI/ML capabilities, communication between different processes, and more.

In the Internet of Things (IoT) era, devices and systems generate enormous amounts of real-time data, and demand real-time analytics in an uninterrupted manner. The typical solution, a cloud-centred architecture providing an analytics service, cannot guarantee real-time responsiveness because of unpredictable workloads and network congestion. Recently, edge computing has been proposed as a solution to reduce latency in critical systems. For computation processing and analytics on edge, the challenges include handling the heterogeneity of devices and data, and achieving processing on the edge in order to reduce the amount of data transmitted over the network. Time series compression and aggregation techniques and event or rule-based data filtering are two key approaches that can be applied to control data on the edge side. However, such solutions are complex to develop, application and domain oriented, and they only address the specific IoT scenario, without any flexibility or reusability.

Model-driven design, on the other hand, allows us to build software solutions using high-level abstractions (the models), enabling developers and maintenance to focus on the problem rather than the code. This approach has multiple advantages over the traditional code development, such as: non-programmers can be in the centre of the development process, build prototypes is less time consuming, reuse a wealth of predefined components (in our case SIBs, Service-Independent Building blocks) and the availability of user-friendly tools to lower the learning curve.

In this paper, we introduce a low-code, model-driven solution to interact with a rule-based engine, eKuiper, in the context of a Digital Thread Platform. The engine is used to deliver a fully automated solution for scheduling tasks that retrieve data from the Edge, allowing us to create a continuous flow of information. In our architecture, the integration happens by adding an External Native DSL to the Digital Thread platform, comprising a family of SIBs. These SIBs are the essential modelling capabilities in the architecture's modelling layer. They provide users with capabilities to connect, control and organise devices and components, and develop custom workflows in a simple drag and drop manner. We use the DIME integrated modelling environment as the basis for our platform.

*Key Words: Smart Manufacturing, Internet of Things, Edge Analytics, Model-Driven development, XMDD, DIME*

## 1. INTRODUCTION

The development of smart manufacturing ecosystems presents one of the most challenging engineering problems these days. It requires the orchestration of the different actuators involved, dealing with heterogeneous protocols (MQTT, Zigbee, Modbus TCP, SNMP, etc), diverse types of architectures (single node or distributed environments, local, online or in the cloud), and latency of edge devices. In software engineering terms, it also requires abiding by the "good principles" of software development during the entire lifecycle: creating good documentation, achieving clean code, modularity, good separation of concerns, and generating high-level abstractions to enable more understandable functionality, etc. All these requirements pose great challenges to the development team, due to the inherent complexity of the system itself, the possibility of having boilerplate or legacy code that needs to be understood and amended, and even people with lack of necessary skills that are nevertheless required to fully build a system with these characteristics. Edge computing and IoT components also bring an integration challenge, as they are highly heterogeneous and present diverse ways to solve various kinds

Email: Ivan Guevara
Ivan.guevara@ul.ie

of problems. Solving the data integration problem for both needs to be simplified. We adopt the open-source framework EdgeX to address this heterogeneity and the corresponding integration problem. EdgeX Foundry (EdgeX Foundry, 2017) is a scalable and flexible software framework that facilitates the interoperability between devices and applications at the IoT Edge level. It acts as a middleware between the cloud and enterprise applications on one side, and the devices and "things" on the other side, providing a uniform way to define communication pipelines (EdgeX Team, 2017). EdgeX supports several popular programming languages (Go, C++, Java) and provides several GitHub repositories where adopters can find examples already implemented, for ease of learning.

It also provides as a supporting service, a rule-based engine named eKuiper (LFEdge Team, 2022), as an open-source package. This service acts as a daemon (i.e., a service running in the background), creating a two-sided communication channel with our IoT infrastructure, where users can configure and deploy custom SQL-like rules that will interact with the Edge devices. eKuiper consists of three main components: *Source*, communicating with the data sources, *SQL*, expressing the transformation rules, and *Sink*, communicating with the actuators or dashboards. Together, they provide stream data acquisition from different communication protocols, business-oriented data filtration and transformation, and facilitate the introduction of analytics or ML capabilities in the system, as eKuiper automatically handles the needed protocols. Despite these benefits, eKuiper users still deal with

1) having to produce by hand code, which is prone to errors,
2) a steep learning curve to fully understand the procedures involved and
3) a state-of-the-art technology where is difficult to find people specially trained for it. In contrast, building the same system application using models brings advantages over the conventional direct code approach.

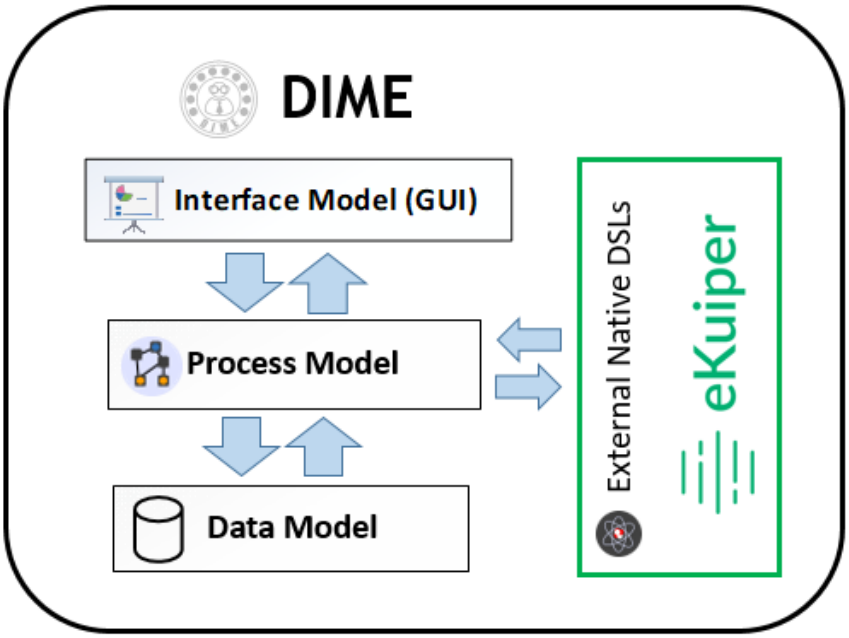


*Figure 1. eKuiper MDD extension/integration in the context of the DIME models*

In this context, we propose a low-code solution to enable a rapid and efficient development of applications involving IoT, EdgeX and eKuiper using the DIME Domain-oriented Integrated Modelling Environment (Boßelmann et al., 2016). DIME empowers prototype-driven application development following the One Thing Approach (Margaria et al., 2009) and enables an eXtreme Model-Driven Design collaboration between domain experts and programmers (Margaria et al., 2012), giving application experts (potential non-programmers) a significant role in the process. Our low-code solution integrates both platforms (see Fig. 1) by means of the DIME extension through an External Native DSL for eKuiper (on the right). This way, the rich facilities provided by the EdgeX framework, in this specific case those offered by the eKuiper rule engine, become part of the DIME ecosystem, recreating a m2m communication Digital Thread in a low-code fashion. The arising DIME workflows deliver fully working and deployable (web) applications that may include eKuiper and EdgeX services. Their

models and sub-models, as well as the single functionalities, are capable of being orchestrated into easier to understand and more robust solutions. This is possible with limited effort because DIME already supports in the same low-code model driven fashion the integration with several databases and analytics environments, as well as a complete web application development framework, where such models are transformed to code, deployed, and run. This way, users can build and deploy a cohesive platform without having to deal with complex cross-platform integrations. We take advantage of DIME's flexible capability to extend its behaviour by adding a new palette of external native SIBs for eKuiper, implemented using Java code. Once it is available, we define our convenient API to interact with the Edge.

Considering the three challenges posed by a traditional code-based bespoke eKuiper adoption, there is no need to deal with complex logic functionality or to understand and repurpose boilerplate code (1), as in our architecture we rely on reusable Service Independent Building blocks (SIBs). They are executable and reusable modelling components previously defined and implemented by experts, and the application development amounts to composing the entire workflow process using such provided SIBs, and then generating the code automatically from that workflow and the SIBs that occur in it. This also lowers the learning curve (2), as the user of our system does not need to master the technical details nor implementation of the eKuiper platform, and thus we also avoid the shortage of trained experts (3).

The paper is organized as follows: Section 2 covers related work in the application domain as well as some examples of our technology of choice. Section 3 explains in detail our API and DSL setup, the architecture developed to support the functionalities enabled and the integration work we did for the paper. Section 4 describes a use case that uses the DSL we developed, and Section 5 concerns our conclusions.

## 2. RELATED WORK

Considering previous *state-of-the-art solutions developed with DIME*, several works and case studies show the potential of this approach and how it can simplify the integration of complex heterogeneous components and then the application development. In the smart manufacturing context, in terms of integration of heterogeneous domains and technologies. Margaria et al. (2019) shows a remote control of a UR3 robot through a web-based application connecting to an IP address. A domain-specific language (DSL) corresponding to the operations in the UR3 is added to DIME, then its SIBs are used in the workflow of the Web application to control the robotic arm. Margaria et al. (2021a) shows how to extract the digital twin of this composite system (robot and controller). Chaudhary et al. (2021) shows use cases for integration of the platform to support R and REST services. R is a programming language for statistical computing and graphical visualization of the outcomes. It provides statistical capabilities (linear, nonlinear, statistical tests, timeseries analysis, classification etc.), one of its strengths is the ease to produce well-designed publication-quality plots with mathematical symbols and formulas (Team R.C, 2013). Representational State Transfer (REST), in the other hand, is an architectural style for service-oriented computing, very popular as a simple way of exposing service interfaces, especially in comparison with earlier protocols such as the complex and heavyweight SOAP/WS-* and similar RPC-inspired protocols (Pautasso et al., 2013).

In terms of *manufacturing case studies*, John et al. (2021) showed an application of DIME and EdgeX as advanced middleware platforms for secure predictive maintenance. Considering work on *monitoring systems*, Yunhao Teng et al. (2021) presents a real-time environmental monitoring system where a Kuiper-Kubernetes tool in the Edge is used for data processing and forwarding. The authors implemented an architecture using as a main board an Arduino Uno, a DHT11 sensor for capturing humidity and temperature, and a MQ-2 gas sensor to collect combustible gas data. The system analysis shows the architecture reduces the package losses by about 62% in comparison to a cloud architecture. Prabhu et al. (2022) also present a real use case scenario in the context of *telehealth*, allowing to monitor the blood pressure using eKuiper. In this case, the Edge IoT architecture uses a Biomedical Sensor, an Arduino, an Edge Gateway to handle the data, and EdgeX Foundry to provide a homogeneous response to the different actuators. The rule-based engine constantly polls the data from the device, being previously set up with rules that alert whether the pressure drops below a certain threshold. In that case eKuiper interacts with a SNMP server that sends a notification email.

This integration of eKuiper in DIME is a contribution to the construction of the Digital Thread Platform described in Margaria et al. (2021b), that aims to include heterogeneous technologies within a DIME-based low-code platform for application development in order to facilitate a seamless and rapid development of end-to-end applications that include functionalities stemming from different domains. Currently, the platform also includes a persistence layer with MongoDB and ElephantSQL, analytics in R and using cloud-based services (AWS), IoT capabilities using MQTT directly and through EdgeX, and the already mentioned robotics and REST capabilities.

## 3. METHODOLOGY

For the integration of eKuiper we introduce *virtualization* through the Service-Independent Building blocks (SIBs) mechanism of DIME. SIBs are high-level abstractions of components that hide their implementation details, and lift the technical vocabulary used in the system design and implementation to the domain specific language of the domain experts. This reduces the technical complexity of definition, design, and implementation of use cases, focussing the design on the specific step of the problem this SIB aims to solve. Domain-specific collections of SIBs that integrate external tools or platforms are called here *External Native DSLs* (domain specific languages). Having access through a collection of DSLs to pre-tested blocks of code whose execution can be fully automated helps user-defined processes and applications to be less prone to errors, as they rely at each step on a solution that is already pre-implemented and pre-tested. This significantly speeds up the development of larger components and applications.

We sketch next the integration process (Sect. 3.1), then delve into EdgeX (Sect. 3.3) and the analytics on the Edge (Sect. 3.3) and through eKuiper (Sect 3.4).

### *3.1. The Integration process*

To achieve a proper integration of external resources and capabilities, application and DSL designers need to tackle together the following steps:

1) use case definition,
2) define (if new) or identify (if existing) the SIBs palette,
3) for the missing SIBs, define which functions and methods are needed, if it is going to be directly implemented in code
4) define the application logic inside the SIB, if it is going to be implemented by means of a process,
5) test the SIB functionality,
6) include the SIB in the application workflow.

As in the traditional software development lifecycle, once the use case is defined (Step1), we define in general terms the SIBs needed in our system (Step 2).

A SIB declaration (Step 3) has a very user-friendly syntax, as shown in Fig. 2 for six EdgeX basic operations concerning device setup and management. A SIB declaration consists essentially of its signature, which is easy to read and produce: it has the same structure and elements as a function/method declaration. It starts with the SIB name, then it specifies the full path to the Java package where the class is located (the functionality itself) and the name of the method to call it. Then it lists the input parameters and the outgoing branches, i.e., the different continuation paths the function can take (in Fig. 2, they are mostly failure/success, but in general there can be many outgoing branches) and the (optional) outputs associated with each branch.

Once the SIB is properly declared, in Step 4 we define the functions and methods that implement it in Java code. A Java SIB body takes advantages of all the services and functionality provided by the Eclipse IDE and the OpenJDK 11, which include performance improvements and functional programming approaches that are useful for simplifying syntactic sugar. Alternatively, a complex SIB can itself be implemented by a process (Step 4 too) and contain business logic and other SIBs.

In Step 5, once a SIB has both a declaration and an implementation, it is thoroughly tested in order to make sure it fulfils the expected behaviour. We recommend using unit testing and integration tests for the expected use and

the most common kinds of incorrect use: trying to emulate a typical use case it will be expected to work with is effective to find potential issues and resolve them.

Finally, in Step 6 the functionality is ready to be provisioned into the DIME development environment (loading the SIB, or the palette to which it belongs), and then used in applications by dragging and dropping its symbol from the list of SIBs available in our platform. Fig. 2 shows the SIB declarations for 6 of the SIBs implemented to enable EdgeX's palette in DIME.

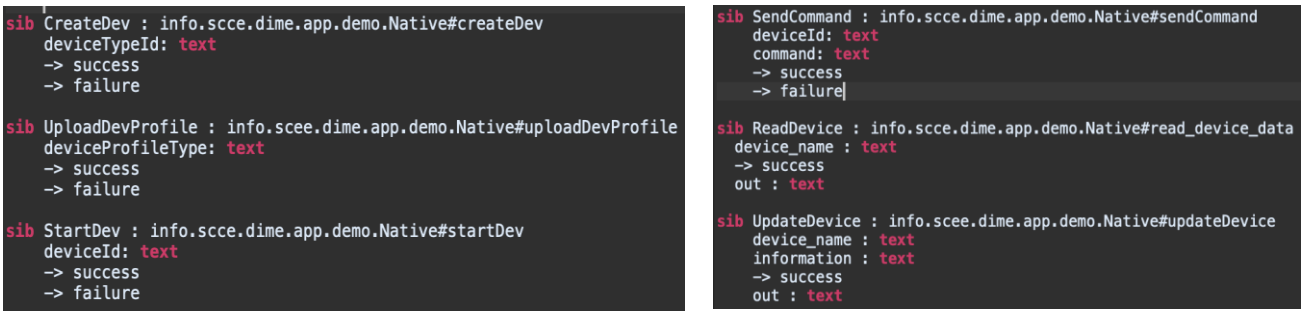


*Figure 2. SIBs declaration in the context of the EdgeX framework: a simple EdgeX DSL.*

### *3.2. EdgeX APIs and DIME*

As the EdgeX Foundry framework acts as a middleware between the IoT Edge and the application, it facilitates this interaction with simpler data structures to get the information from the IoT devices. As shown in John et al. (2021), this abstraction was taken to the next level by creating a high-level abstraction layer to support EdgeX functionality and interact in with IoT devices through a REST API.

A first version of the DIME high-level EdgeX palette contained SIBs for managing devices and data and for security management. In that work, our DLS was based on EdgeX Foundry 1.3 (Hanoi). When a new API (v2.0) was released, we migrated our DSL to the new EdgeX Foundry v2.2 (Kamakura) for forward compatibility and to be able to address and integrate as many devices as possible using our platform. The current EdgeX DSL is therefore up to date.

### *3.3. Computing on the Edge and Data Analytics*

Edge Analytics could be defined as "receive and interpret data from Edge computing". Specifically, based on the information collected from the sensors, we establish a decision-making process and take actions based on those decisions. Edge Analytics can span several levels of complexity, from a simple SQL query to retrieve a few rows of data to complex heterogeneous machine learning systems to leverage a PdM system (predictive maintenance). There are currently two main approaches to accomplish Edge analytics:

a) run the analytics service in each device/sensor, or
b) deliver data from sensors to an analytics service in the cloud.

According to Shi et. al (2016), the first option has an advantage over the second one for three main reasons:

1) Computing tasks in the cloud are efficient, but it faces a bottleneck in the speed of data, i.e., the bandwidth to transport the data towards the network.
2) Everything is becoming part of the Edge IoT environment, leading to a massive production of data for which the conventional cloud computing approach is not efficient enough.
3) Security: as the edge devices are becoming data consumers, it makes sense to process data in edge devices (e.g., mobile phones) instead of uploading raw data to cloud services for subsequent processing.

In the context of our Digital Thread framework, analytics capabilities are embedded in the EdgeX component eKuiper (Team et al., 2022). As shown in the architecture of Fig. 3, eKuiper is a rule-based engine that works by collecting data from a cross-service bus message created by EdgeX. Using SQL-like queries as rules, it brings the information from the sources and sends it to other services (sinks) through several protocols such as HTTP, REST, or MQTT. The core functionality rests on a SQL processor that manages the data streams at runtime and directs their transformation and the routing of the outcome to the sinks.

eKuiper provides great capabilities to deal with data, but it has a few issues, such as a steep learning curve (as adopters still need to be familiar with software architectures, various programming languages and REST services) and cross-system integration, as adopters need to include eKuiper (or its services) as part of a backend system. Instead of creating a side-project to integrate our desired functionalities directly with eKuiper, on a bespoke basis, we decided to integrate the EdgeX eKuiper Rule Engine as part of our DIME ecosystem. To do so, we created a palette of fully reusable and application independent SIBs that take care of the configuration and interaction with the Analytics system in a generic fashion. This approach leverages the EdgeX and other components already developed in other contexts, giving us the chance to create a fully integrated Edge Analytics ecosystem effortlessly.

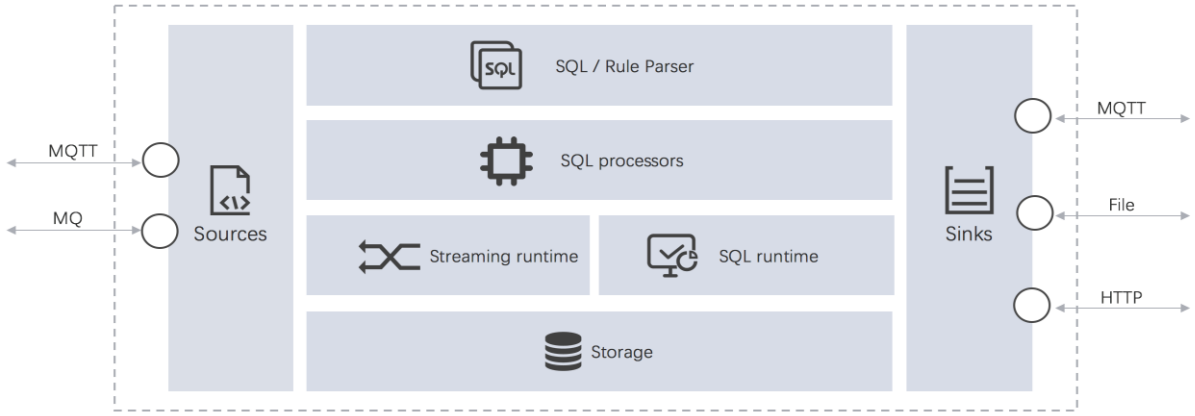


*Figure 3. Architecture for the EdgeX EKuiper Rule Engine (LFEdge Team et al., 2022)*

### *3.4. Towards model-driven edge analytics with eKuiper*

As eKuiper is a rule-based system poised to enable analytics in the EdgeX Foundry framework, it provides many functionalities to handle data from the Edge. However, it still depends on boilerplate code that an adopter needs to understand. Due to the complexity of the system itself, it also lacks the simplicity of an easy setup of the environment.

In the context of the Digital Thread Platform realised with DIME, its XMDD paradigm gives us several benefits. The integration via SIBs, as per steps 2 to 6 described in Sect 3.1, leads to the eKuiper DSL of Fig. 4, which shows the SIBs created to automate the eKuiper set-up and use workflow.

- The set-up process begins with the *CreateStream SIB*, which creates a stream to start using the rule-based system. A stream is the fundamental component of this workflow, as it indicates from which device the data comes.
- Once the stream is created, we can define the analytics rules to be applied to the stream's data. For this we use our *CreateRule SIB*, where a rule is defined by SQL-like code and a sink, i.e., the place/channel to which the data will be sent after being transformed.

These are the two essential SIBs, but for comfort of the user we also created several additional "utility" SIBs:

- *DescribeStream* and *DescribeRule* to know the status of the Streams and Rules, and
- *ShowStreams* and *ShowRules* to show the available Streams and Rules, with which we can interact.

This clarifies what we mean in Step 2 with the definition of the collection of SIBs, which is de facto the design of the specific DSL. By experience, there are a few core SIBs, but the palette grows when considering the point of view of users who in this case need, e.g., to find out information about availability of streams and which rules are already defined.

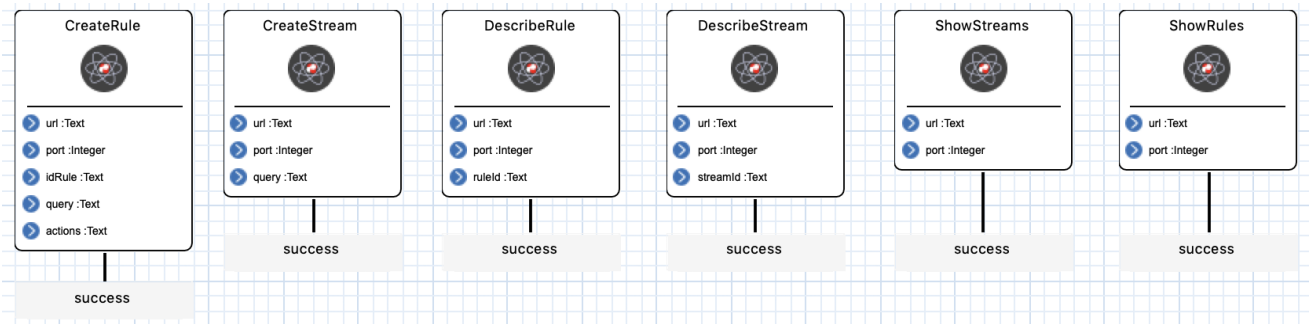


*Figure 4. SIB Library created to abstract and virtualize the logic building blocks from the EdgeX eKuiper Rule Engine*

Finally, we provide a *high-level interface* to execute queries over the system. In this interface we still need to define the properties and a query, but this DIME level is more manageable and easier to understand than the regular, code-based approach.

## 4. RESULTS AND DISCUSSION

With the eKuiper DSL in place, the DIME version of the Edge Analytics application system has the simple workflow shown in Fig. 5, with a more straightforward way to connect the different functionalities and carry out the different tasks, such as creating a device or starting a rule to perform analytics on the edge. Also, here we rely on the model-driven approach: defining the different properties of each SIB and connecting them along the control flow and data flow puts the focus on the problem instead of in the implementation details, and more readily involves domain experts as contributors to our solution. The current application addresses a simple use case:

1) we create a given *Device* (with an internal reference to it),
2) start it,
3) create a stream to communicate with the EdgeX bus message,
4) create a rule,
5) show the available rules,
6) and finally the available streams.

In spite of its simplicity, this application is complete and serves as template for adoption and blueprint for further evolution. The definitions of the SIBs happen through their declaration: it is easy to understand and change by any person with no technical knowledge of software development, as the SIBs declarations and use are very intuitive to follow. Due to the formal nature of these models, they are also a vehicle to formal verification and in perspective automated synthesis techniques, e.g., along the lines of Steffen et al. (1996).

There is still much more functionality to be addressed in EdgeX and eKuiper, but this is beyond the scope of this paper. The integrations to the EdgeX and eKuiper DSLs will happen organically over time, following the requirements of the additional use cases. We expect the additions to be carried out mostly by adopters of the Digital Thread platform, and not by ourselves. Our concern here is to show the simplicity and elegance of this set up in DIME, as a combination of SIB DSL and workflows. In parallel we are working on refining and testing this approach on productive environments.

In terms of limitations, we do not consider for now distributed environments where EdgeX is running in several locations that work in parallel and attend several requests at the same time.

Also, we concentrate for now on the "gold path." i.e., defining and testing the correct behaviour of an application. Runtime exceptions are not (yet) caught and returned to the user for review, as well as queries are not yet simplified.

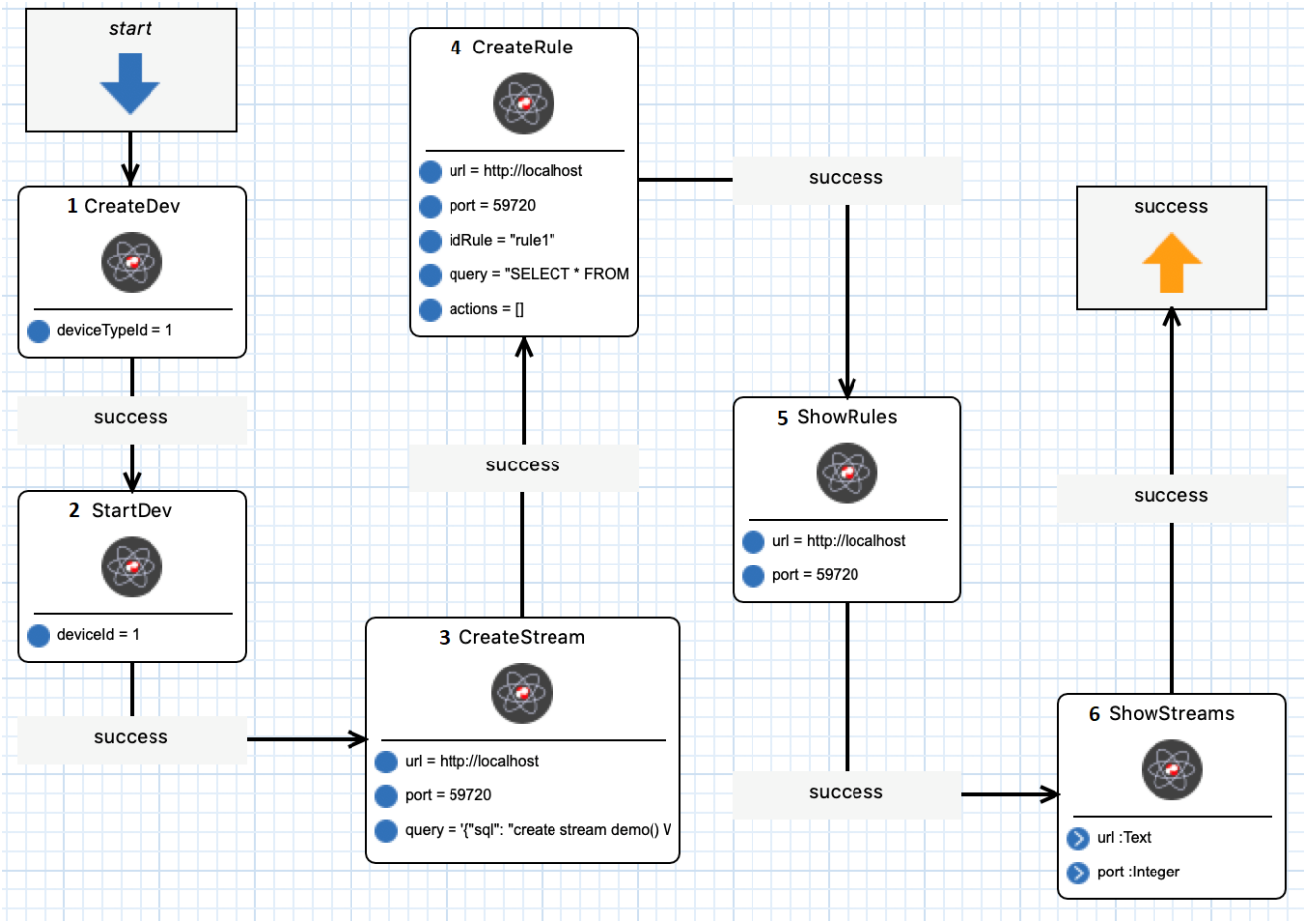


*Figure 5. DIME workflow showing the workflow for the set-up and use of eKuiper rule-based analytics.*

We rely for the rule definition language on SQL queries (this is the original eKuiper language of choice) and on the expertise of those who define them, as well as their understanding for structuring a JSON object. With the DIME approach one could consider a further abstraction layer that frees the user form the need to now SQL and JSON, through another DSL that lifts those functionalities to a more intuitive language/schema followed by transformation to SQL/JSON. This is similar to the approach taken in (Steffen, 2022) for the DSL-driven integration of highly parameterized HTTP services and REST services as a hierarchy of DSLs at different levels of abstraction and virtualization.

We intend to tackle these still pending issues in the future, in order to make the model-driven programming environment more appealing to expert users who are not programmers. So far, we consider our contribution to constitute a considerable progress in delivering a more user-friendly solution to the academic community and to our industry partners.

## 5. CONCLUSION

This paper establishes a major step towards an edge analytics low-code solution for Smart Manufacturing environments. This happens in the context of the Digital Thread Platform for smart advanced manufacturing currently under development, and through the adoption and extension of the DIME no-code/low-code platform. This technology choice privileges domain-specific abstractions that empower people with non-technical or non-programming expertise to create, deploy and run fully functional analytics solutions, virtualizing the underlying technologies, and thus making them opaque to the application designers that reuse the SIBs as pre-defined, pre-

tested building blocks. We showed this on the basis of the eKuiper Rule Engine, that is part of the EdgeX ecosystem. The effect is to democratise the development cycle and tackle down the high learning curve that is otherwise required in order to manage all these layers of knowledge. We believe this move can have a significant impact on the ability of manufacturing experts to use advanced analytics and, more in general, integration and interoperability platforms that they would not be able to program, manage and evolve with the current need of heterogeneous coding and architectural expertise.

The platform still needs some refinement (testing in productive environments and improvement of user experience), but we have a fairly complete palette of Service-Independent Building blocks (SIBs) to encapsulate the behaviour of each step and provide a high-level abstraction to the users. All they need to do is understand the SIBs and their parameters, and then orchestrate them in an appropriate way using our Digital Thread platform. Our case study targets the usage of the EdgeX Foundry framework and its advanced services like the eKuiper Rule Based engine for analytics, and leverages a more straightforward way to use it, having to deal much less with configuration files and boiler-plate code.

## ACKNOWLEDGMENTS

This work was supported by the Science Foundation Ireland grants 13/RC/2094 (Lero, the Irish Software Research Centre) and 16/RC/3918 (Confirm, the Smart Manufacturing Research Centre).

## 6. REFERENCES

Boßelmann, S., Frohme, M., Kopetzki, D., Lybecait, M., Naujokat, S., Neubauer, J., . Steffen, B. (2016, 2016). DIME: a programming-less modeling environment for web applications. doi: https://doi.org/10.1007/978-3-319-47169-3_60

Chaudhary, H. A. A., & Margaria, T. (2021). Integrating external services in DIME. doi: https://doi.org/10.1007/978-3-030-89159-6_3

EdgeX Foundry, Homepage (2017). Retrieved from https://www.edgexfoundry.org.

EdgeX Team, (2017). Retrieved from https://www.edgexfoundry.org/software/platform/

John, J., Ghosal, A., Margaria, T., & Pesch, D. (2021, 2021). DSLs and Middleware Platforms in a Model-Driven Development Approach for Secure Predictive Maintenance Systems in Smart Factories. doi: https://doi.org/10.1007/978-3-030-89159-6_10

LFEdge Team. (2022). Retrieved from https://www.lfedge.org/

Margaria, T., Chaudhary, H. A. A., Guevara, I., Ryan, S., & Schieweck, A. (2021). The interoperability challenge: building a model-driven digital thread platform for CPS. doi: https://doi.org/10.1007/978-3-030-89159-6_25

Margaria, T., & Schieweck, A. (2019,). The digital thread in industry 4.0. doi: https://doi.org/10.1007/978-3-030-34968-4_1

Margaria, T., & Schieweck, A. (2021). Towards Engineering Digital Twins by Active Behaviour Mining. In E.-R. Olderog, B. Steffen, & W. Yi (Eds.), Model Checking, Synthesis, and Learning (10.1007/978-3-030-91384-7_8pp. 138-163). Cham: Springer International Publishing. doi: https://doi.org/10.1007/978-3-030-91384-7_8

Margaria, T., & Steffen, B. (2009). Business process modeling in the jABC: the one-thing approach. In Handbook of research on business process modeling (https://doi.org/10.4018/978-1-60566-288-6.ch001pp. 1-26): IGI Global.

Margaria, T., & Steffen, B. (2012). Service-orientation: conquering complexity with XMDD. In Conquering complexity (https://doi.org/10.1007/978-1-4471-2297-5_10pp. 217-236): Springer.

Pautasso, C., Wilde, E., & Alarcon, R. (2013). REST: advanced research topics and practical applications (https://doi.org/10.1007/978-1-4614-9299-3): Springer.

Prabhu, M., & Hanumanthaiah, A. (2022, 2022). Edge Computing-Enabled Healthcare Framework to Provide Telehealth Services (https://doi.org/10.1109/WiSPNET54241.2022.9767142)

Shi, W., Cao, J., Zhang, Q., Li, Y., & Xu, L. (2016). Edge computing: Vision and challenges. IEEE internet of things journal, 3(5), 637-646. doi: https://doi.org/10.1109/JIOT.2016.2579198

Steffen, B. (2022). DSL-driven Integration of HTTP Services in DIME. BSc Thesis, Fakultät für Informatik, TU Dortmund, Dortmund Germany, February 2022.

Steffen, B., Margaria, T. & Claßen, A. (1996) Heterogeneous analysis and verification for distributed systems. SOFTWARE: Concepts and Tools 17 (1), pp 13–25, Springer Verlag.

Team, E. (2022). EdgeX rule engine tutorial. Retrieved from https://github.com/lf-edge/ekuiper/blob/master/docs/en_US/edgex/edgex_rule_engine_tutorial.md

Team, R. C. (2013). R: A language and environment for statistical computing. Retrieved from https://www.R-project.org.

Teng, Y., Cui, J., & Jiang, W. (2021, 2021). Research on application of edge computing in real-time environmental monitoring system. Retrieved from: https://iopscience.iop.org/article/10.1088/1742-6596/2010/1/012157/meta

# Implementation of Industry 4.0 Technologies & Practices in SMEs.

A. McNabb, CP Cases, Queen's University Belfast
J. Butterfield, Queen's University Belfast
P. Martin, Queen's University Belfast
M. Nolepa, CP Cases
P. Ross, CP Cases

***Abstract***

This paper presents two case studies based on the implementation of digital technology in a manufacturing SME. Because of the financial barriers SMEs face when exploring commercially available solutions, the aim of these projects is to explore the viability of developing solutions using low-cost hardware and open-source software, such that SMEs can utilise digital technology without the need for high-risk financial investment.

The first case study presents a project to use open-source simulation software to generate quantitative data from a series of proposed assembly line changes, to evaluate the impact of each. The chosen solution, JaamSim, proved to be industry-capable, informing changes that reduced process time by 15%. Training, however, was based on online resources rather than direct vendor support.

The second case study presents a project to convert analogue data into digital data, in this case a gas meter connected to a rotational moulding machine. The solution was built using a Raspberry Pi Single Board Computer and the programming language Python. Developing this solution required specialised skills in computer vision and programming, which introduces a different, but manageable, barrier for SMEs.

While the presented projects achieved their objectives using low-cost hardware and open-source software, they present manufacturers with a different barrier: the need to develop digital skills internally. While this has proved to be a significant barrier for SMEs in the past, it is argued that the emerging workforce is closing this skills gap more quickly than the financial gap between SMEs and large manufacturers is closing. Investing in the development of these skills should be seen as a lower-risk and more sustainable than investing in commercially available digital solutions.

*Key Words: Industry 4.0, SME, Discrete Event Modelling, Image Recognition, Raspberry Pi, Open-source*

## *1. INTRODUCTION*

In 2017 the UK's Department for Business, Energy & Industrial Strategy released the *Made Smarter Review*, an extensive investigation into the potential benefits to UK manufacturers of adopting digital technology (broadly referred to as Industry 4.0), and barriers that prevent widespread adoption. The review, led by a team of industry leaders, found significant potential for benefits such as increased productivity, increased quality, and reduced downtime, through manufacturers' adoption of Industrial Digital Technologies (IDTs). These benefits are claimed to lead directly to wider societal benefits such as reduced costs, higher wages, and improved sustainability, all contributing to a more competitive economy.

The Review identified five key IDTs likely to drive these benefits in the UK: additive manufacturing, Artificial Intelligence (AI) & data analytics, robotics, the Industrial Internet of Things (IIOT), and Virtual Reality (VR). It was argued that significant government investment would be required to build awareness of these technologies amongst manufacturers, and to upskill the workforce so that they can be properly utilised once adopted. Without such investment, manufacturers are unlikely to build the necessary confidence in IDTs, and adoption will remain slow, with the UK likely to remain on the coat tails of its G7 counterparts when it comes to productivity per worker.

Email: Alex McNabb
alex.mcnabb@qub.ac.uk

The Review cites lack of adoption amongst Small and Medium-sized Enterprises (SMEs) as a key contributor to the UK's below average exploitation of IDTs. In 2021, SMEs – registered companies with at least one and less than 250 employees – accounted for 98.6% of registered manufacturing companies (with at least one employee) in the UK. As such, supply chains rely heavily on SMEs, creating a knock-on effect from the weak links through the rest of the chain. There are multiple barriers identified by the Review specific to SMEs that are challenging to address at a national level. Most of these stem from the lower level of expendable resource – both human and financial – that an SME has available to dedicate to activities such as market research, research partnerships, and new technology investment. Manufacturing SMEs typically operate on finer margins than larger manufacturers. This drastically increases the level of risk associated with these activities, which would otherwise be effective methods of building digital awareness and skills. It is clear that reliable and cost-effective methods for adopting digital technology in manufacturing SMEs are needed.

## *2. LITERATURE REVIEW*

Since the Made Smarter Review in 2017, several independent academic studies have confirmed that the key barriers that SMEs face are cost and awareness. A 2020 study surveyed 271 UK-based SME manufacturers and found that, while 61% of respondents planned to invest in some form of digital technology within five years, most struggled to fund implementation (Masood & Sonntag, 2020), citing that common routes such as consultancy are not accessible to most SMEs, and internal resources tend to lack awareness of digital technology. Reasons given for lack of awareness include the limited impact of activities such as workshops and support schemes, and the overwhelming scope of technologies under the bracket 'Industry 4.0'.

The disparity in financial resources for digitalisation between SMEs and large manufacturers (>250 employees) is highlighted in Cotrino, Sebastián, & González-Gaya's 2020 study. Their analysis found that in all reviewed cases, the large manufacturer's digital investment plan exceeded the total turnover of the SME. The study proposes an SME-oriented digitalisation road map whose key differentiator is a task-based approach rather than team-based, due to the fact that SMEs tend to dedicate responsibility to fewer or single human resources for each process or area of the business. This means digital technology is implemented to solve particular problems, rather than to completely restructure the business, which focuses the scope of digitalisation making it more approachable.

Powell, Morgan & Howe's 2021 study supports the problem-focused approach by presenting three case studies of SMEs using digital technology to address specific needs. In particular, one case study used Discrete Event Modelling (DEM) and VR to simulate potential changes to existing processes, allowing 'what if' scenarios to be evaluated quantitatively before implementation. This approach further de-risked the investment by simulating a variety of possible changes each with different levels of investment, allowing a comprehensive business case to be written.

Another approach to de-risking digitalisation is presented by the Advanced Manufacturing Research Centre (AMRC) in their 2018 white paper 'Digitalisation of Legacy Machine Tools', where low-cost electronic hardware such as Single Board Computers (SBCs) and microprocessors are used to install sensors on a 1956 lathe, and collect the data digitally to enable machine health monitoring. This approach resulted in a system costing less than £400 compared to an equivalent commercially available system costing approximately £20,000. The limitation of this study, however, is that SMEs lack the time and skills to explore and develop such systems, particularly since they are bespoke for the machine in question.

The outstanding question that the presented literature does not address is how an SME manufacturer can implement digital technology using internal resources, rather than solutions developed by third parties such as academics and research centres. Using the findings presented above regarding low-cost electronic hardware and simulation software, this paper intends to address the following aim.

**Aim**: to determine whether low-cost technology can be used internally to facilitate the adoption of Industry 4.0 in SME manufacturers.

## *3. METHODS*

This paper presents two exemplar digitalisation projects at CP Cases, a manufacturing SME in the protective casing industry (Figure 1). The objective of each project was determined during a Value Stream Mapping (VSM) process, whereby diagrams were drawn to depict the flow of material and information throughout a process to locate sources of waste and opportunities for digitalisation.

*Figure 1. CP Cases' Amazon Case with machined foam insert.*

The first opportunity was in an assembly line for rotational moulded cases, where current throughput needed to increase to meet forecasted customer demands. The VSM highlighted that a high proportion of process time came from movement of material between stations, rather than value-adding processes. It was proposed that DEM be used to quantitatively assess the impact of several potential changes before implementation, to ensure that the level of investment was proportional to the benefits. To avoid dependence on expensive software (with its relatively high licensing costs and dependencies on specialised, costly training and support) or third parties, open-source software was explored. The objective of this project was:

**Objective 1**: use open-source simulation software to provide quantitative process data to inform assembly line changes.

The second opportunity was in the rotational moulding machine, which runs on gas and has a dedicated gas meter. With sustainability and rising gas prices becoming significant factors in manufacturers' decision making, it is important to track gas usage so that costs can be controlled, and sustainability activities can be evaluated. Since this gas meter is analogue, it was proposed that low-cost electronic hardware be used to capture images of the meter, then computer vision used to convert the images into digital data. This would enable better cost control and process understanding, and the framework developed could be applied to other analogue data sources. The objective of this project was:

**Objective 2**: use low-cost hardware and open-source computer vision software to digitise gas usage data.

## *4. RESULTS*

### *4.1. CASE STUDY 1: DISCRETE EVENT MODELLING*

In order to meet an increased demand for particular rotationally moulded products, CP Cases aimed to reduce the process time for the assembly of moulded cases with relatively high order quantities. To do so, a series of potential changes to the existing assembly lines were proposed, including altering the order of operations, and installing a

conveyor system to streamline material flow. The proposed solutions varied in terms of their required investment and their level of disruption during implementation.

Rather than running costly pilots for each proposed change, the use of Discrete Event Modelling software was explored. DEM (which falls within Made Smarter's AI & Data Analytics IDT category) is a category of simulation software that represents real processes as an virtual objects going through a series of sequential operations occurring along a timeline. Each logical operation represents a step in the real process, and can be represented logically as two timestamps representing the start and end of the operation, and if applicable a change in state to the object. For example, to represent a part going through a heat treatment cycle in an oven, the DEM would 'hold' an object from time $t_1$ to time $t_2$, where $t_2 - t_1$ is the length of time the real part spends in the oven. The DEM could then change the object's *HeatTreated* state to *True*, if such a state would have logical permutations in future operations.

Commercial DEM solutions proved to be prohibitively expensive, for example the popular choice AnyLogic was quoted at approximately £18,000 for a license and £3,000 annually for maintenance. Such an investment would have added risk rather than de-risking the process of digitalisation. Studies by Lang et al. (2021) and Dagkakis & Heavey (2017) highlight the viability of some open-source DEM software as genuine alternatives to commercially available software, and both conclude that the software JaamSim has the capabilities necessary to meet the needs of industrial users.

The common drawbacks of open-source versus commercial software include the lack of a refined User Interface (UI) which can act as a barrier for newcomers, and lack of support in terms of maintenance, troubleshooting and updates. These are particularly prohibitive for company-wide deployments that operations would rely on. The papers, however, highlighted that JaamSim does not suffer these drawbacks. Rather, JaamSim comes with an intuitive drag-and-drop UI (Figure 2), an active support community that includes the developers, and monthly updates. Furthermore, the logical blocks that represent operations in JaamSim (known as servers) are able to have custom logical behaviours assigned to them, such that logic specific to the company's processes can be modelled. This is especially useful when modelling manual parts of a process, which tend to be less repeatable than automated parts.

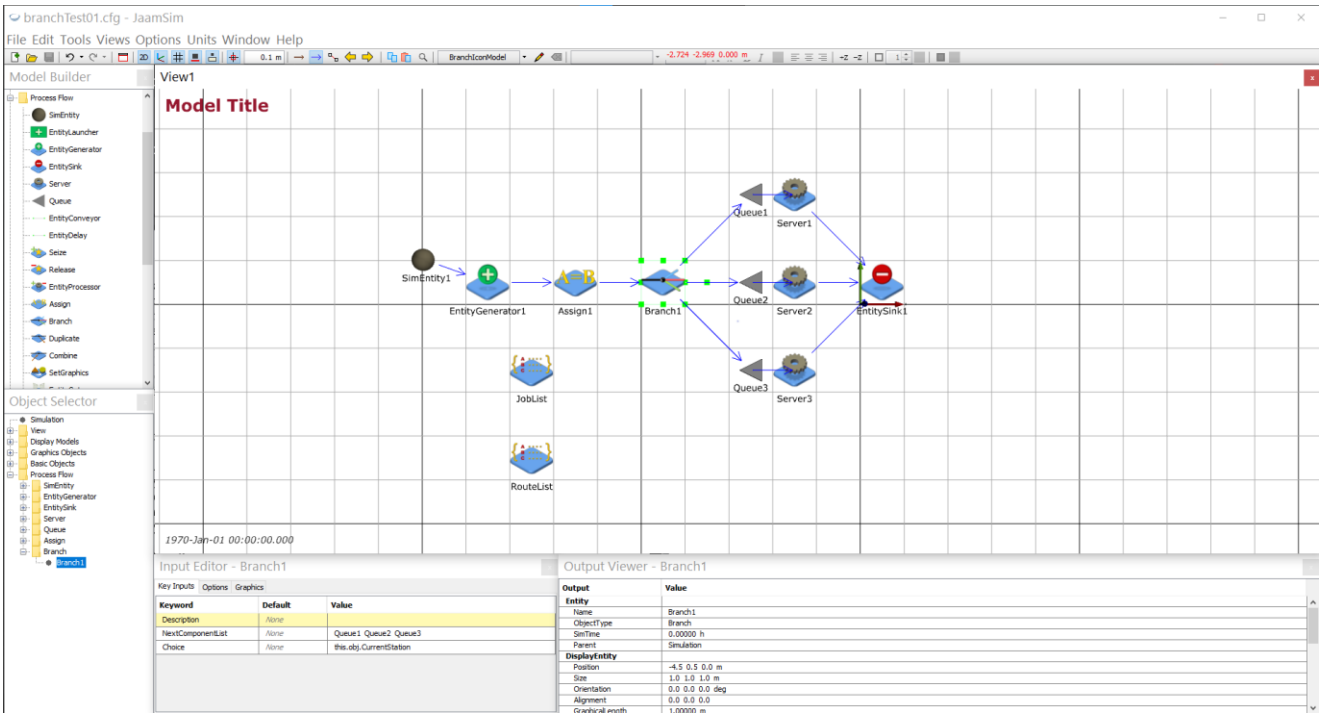


*Figure 2. JaamSim's drag-and-drop UI.*

To represent the assembly line in question the following high-level logic was implemented in JaamSim:

- Individual cases would be represented as objects flowing through the order of operations (known in JaamSim as entities).
    - A new entity would be generated at a rate equal to the cycle time of rotational moulding process.
- Each operation would be represented by a server that holds the entity for a time pulled from a given normal distribution.
    - Operators would be represented as a 'resource', where servers can not progress with their operation without a resource being free.
    - Each server relied on a different resource. This represented different operators being assigned to different stages of the assembly process.

After simulating the model for a given period of time, JaamSim is able to output statistics for each entity, server and resource. This includes the utilisation of each resource, the number of entities to complete their order of operations, and the average time taken for an entity to complete its order of operations. For each proposed change, these statistics were extracted. By comparing the statistics for each proposal, alongside its estimated cost and disruption, it was determined that in fact the conveyor system would offer only a marginally higher efficiency increase than a change to the order of operations that minimised the amount of travel time for each entity. This conclusion allowed the change of operations to be implemented at minimal cost, which reduced average cycle time per unit by approximately 15%.

This project proved the viability of using open-source simulation software to inform key operational decisions without the need for third party support. A requirement, however, is that the company has the skills internally to learn to use the software, and also the process knowledge to accurately model the process in question.

### *4.2. CASE STUDY 2: DIGITISATION OF ANALOGUE DATA*

Rising gas prices and sustainability awareness shift focus onto processes that require large amounts of consumable resource. Rotational moulding is a polymer moulding process that melts polymer in a metal mould by heating it in a gas-powered oven. Since CP Cases operate a rotational moulding machine on a daily basis, they aimed to track its gas consumption so that any measures to reduce energy costs could be accurately evaluated. The outstanding issue, as with the majority of legacy machinery, was that the gas meter that displays gas usage is analogue, so no data was stored digitally, meaning past data could not be recalled. Ideally, gas usage data would be available on a minute-by-minute basis such that gas usage rates could be mapped against specific points in the day. Trends could then be identified such as whether usage rate varies throughout the day or with particular moulds. Given the safety implications of adapting / disrupting gas supply equipment, a passive approach to converting an analogue digital display to a digital form was preferred.

The solution to this issue was to periodically capture an image of the gas meter, use image recognition to extract the numbers on the meter as digital data, and plot the data against time to visualise behaviour. Again adopting a low-cost approach, the technology used and the purpose of each are listed in

Table 1.

*Table 1. Technology used to digitise analogue data.*

| Technology | Description | Price | Purpose |
|---|---|---|---|
| Raspberry PiCamera | 8 megapixel camera | £24.90 (thepihut.com) | Capture the image |
| Raspberry Pi Model 4B | Single board computer | £35.50 (thepihut.com) | Run Python image recognition script, Run services to store and visualise data |
| OpenCV (opencv.org) | Python library | Open-source | Image processing |

| | | | |
|---|---|---|---|
| PyTesseract (pypi.org/project/pytesseract) | Python library | Open-source | Text recognition |
| InfluxDB (influxdata.com) | Time series database software | Open-source | Store each reading alongside timestamp |
| Grafana (grafana.com) | Data visualisation software | Open-source | Display datasets on a graph against time |

The Raspberry Pi 4B is an example of an SBC – a complete set of computer hardware built onto a single circuit with the approximate footprint of a bank card (Figure 3). SBCs typically run a Linux operating system which, like a typical Windows or MacOS system, can run apps, services and connect to the internet via a local network. In this application the SBC is connected to a camera from which it receives images it can then process, however other hardware can connect to SBCs such as sensors or input devices. Their low cost and portability make SBCs a valuable asset for the low-cost approach.


*Figure 3. Raspberry Pi model 4B with power and ethernet connections.*

The high-level process used in the Python script to extract data from images such as in Figure 4 was:

- Detect the area containing the numbers of interest.
  - Detect all pixels above a given ‘redness’ threshold.
  - Form a rectangle from the detected red pixels.
  - Given knowledge above the location of the area of interest relative to the red rectangle, crop the area of interest.
- Recognise numbers in the area of interest.
  - Convert the image to greyscale.
  - Use the open-source OpenCV library’s *Canny* function to highlight edges.
  - Fill in any closed edges. If the edge is within another edge (for example the inner ring of a 0), fill it in inverted.
  - Use the open-source PyTesseract function to detect the numbers remaining in the image.
- Send the data and its associated timestamp to InfluxDB

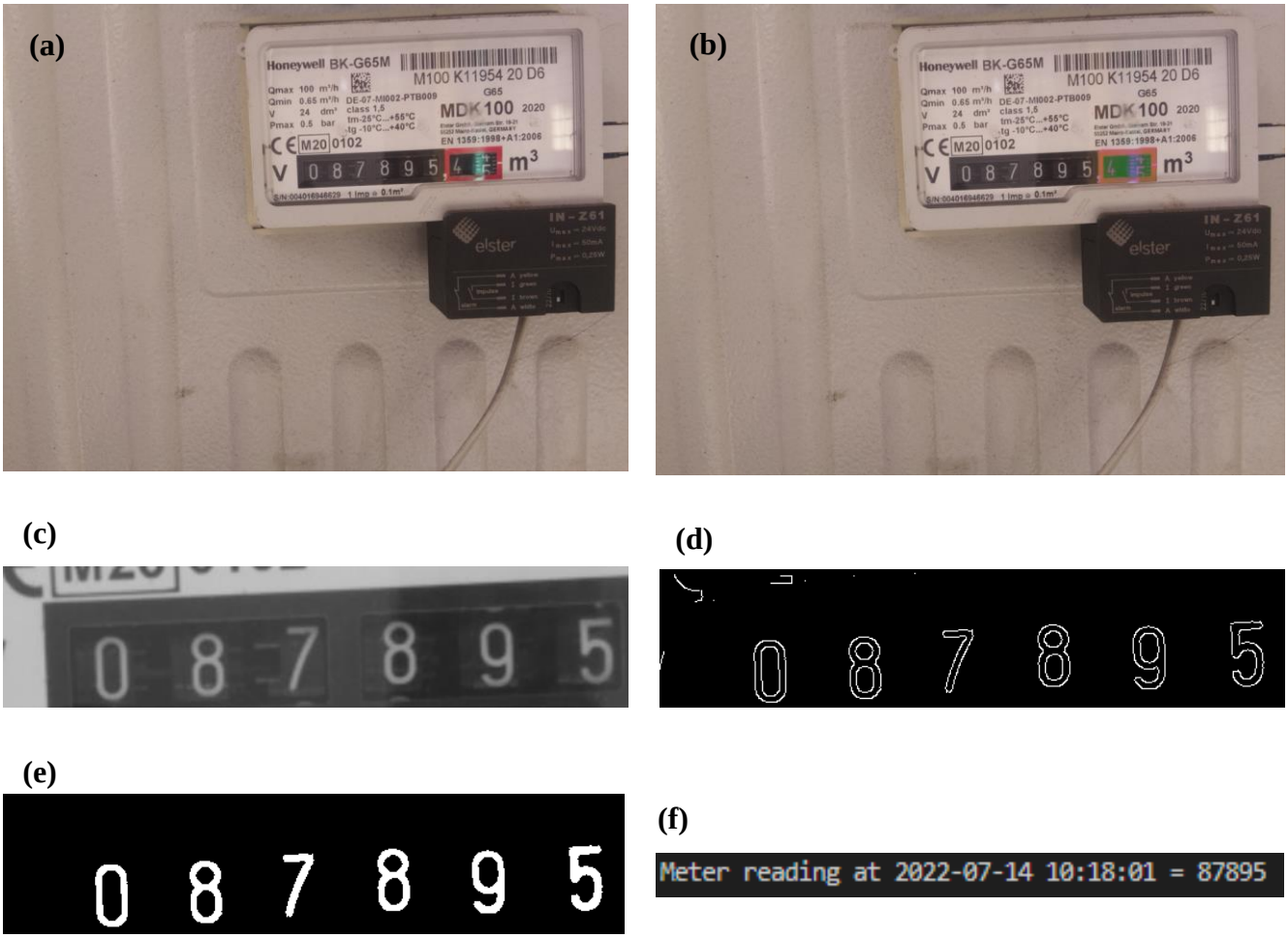


*Figure 4. (a) Raw image. (b) Red datum area highlighted. (c) Area of interest cropped. (d) Edges detected. (e) Closed edges filled in. (f) Numbers recognised.*

The outcome of this system is the continuous monitoring of gas consumption that can be mapped directly to known events, such as specific moulds entering the oven. This offers two immediate benefits. Firstly, gas usage can be tied to specific works orders, allowing accurate consumable costs to be attributed, which the sales team may choose to use as input to the quoting process. Secondly, any changes made to the rotational moulding process can be evaluated in terms of their impact on gas consumption. For example, increasing oven temperature to shorten cycle times may also significantly increase gas consumption to the point where savings are diminished. Alternatively, alterations made to the machine, such as replacing oven chamber seals, can be evaluated against their reduction in gas consumption, and accurate ROI can be calculated.

The framework built for this application can be scaled to similar applications, such as analogue water and electricity meters, as well as analogue dials on tanks and canisters. The ability to gather digital data, and subsequently analyse past behaviour, is an important step in making data-driven decisions. In a similar conclusion to Case Study 1, this project proves the viability of low-cost hardware and open-source software, however skills in software development are required to achieve this without third party support. Specifically, intermediate proficiency with an object-oriented programming language such as Python proved valuable, though this was achievable with learning resources available online.

## *5. DISCUSSION*

The aim of this paper was to explore the viability of low-cost and open-source solutions for adopting digital technology in manufacturing SMEs. Digital technology has the potential to reduce costs, improve quality, and improve productivity, however most commercially available solutions are cost prohibitive for all but large manufacturers. By presenting two exemplar projects implementing low-cost digital solutions at CP Cases, this

paper proves the viability of this approach, as long as the company has the digital skills internally to utilise key building blocks such as Python (or another programming language), Single Board Computers, and open-source software.

Case Study 1 presented an implementation of open-source Discrete Event Modelling software JaamSim, which proved to be capable of meeting industrial requirements, and is well-supported by developers such that is can be relied on by manufacturers. By using open-source software, the manufacturer does not need to invest in commercial solutions, nor require support from third parties who have access to such a solution. The barrier instead is the need for digital skills to be developed internally, since open-source software typically includes less guidance and support that commercial software. The skills needed in this project were a basic understanding of programming and simulation, as well as a high level of familiarity with the manufacturing process being modelled.

Case study 2 presented a framework built from low-cost electronic hardware and open-source software that enabled the digitisation of valuable analogue data. This project addresses a common issue amongst manufacturers where legacy assets do not inherently have the capability to interface with digital systems. The key building blocks of this project were Single Board Computers, Python, and open-source IIOT software. The limitation of this approach, again, is the need for internal digital skills, which in this case are an intermediate understanding of programming, and a basic understanding computer vision and the Linux operating system.

The requirement for digital skills is the primary barrier preventing the low-cost, open-source approach from being implemented in manufacturing SMEs, since it is widely reported that the lack of these skills remains a significant barrier. It is likely, however, that addressing this skills gap is more achievable than addressing the financial gap between SMEs and large manufacturers. Particularly with the high levels of digital skills in the emerging workforce, and the abundance of accessible online learning resources addressing topics like programming, this gap is easier to close now than it has been before.

## *6. CONCLUSIONS*

- Digital technologies can be implemented at low-cost (the order of £100s) by developing systems from low-cost and open-source building blocks.
- Open-source simulation software (e.g. JaamSim) can be used to generate quantitative data about assembly line changes to improve operational efficiencies.
- Raspberry Pi and Python can digitise analogue data using open-source computer vision software.
- The low-cost approach requires skills and understanding of programming (e.g. Python), Single Board Computers, open-source software, and networking.
- Increasing levels of digitalisation within the manufacturing domain means that levels of IT/Computer base literacy need to improve among manufacturing engineers.

## *7. REFERENCES*

UK Department for Business, Energy & Industrial Strategy (2017). *Made Smarter Review.* Retrieved from: https://www.gov.uk/government/publications/made-smarter-review

UK Department for Business, Energy & Industrial Strategy (2021). *Number of business enterprises in the manufacturing sector in the United Kingdom in 2021, by enterprise size.* [Graph]. In *Statista.* Retrieved July 28, 2022, from https://www.statista.com/statistics/677081/uk-manufacturing-businesses-by-size/

Masood, T., & Sonntag, P. (2020). Industry 4.0: Adoption challenges and benefits for SMEs. *Computers in Industry, 121.* Retrieved from: https://doi.org/10.1016/j.compind.2020.103261

Cotrino, A., Sebastián, M. A., & González-Gaya, C. (2020). Industry 4.0 Roadmap: Implementation for Small and Medium-Sized Enterprises. *Applied Sciences, 10(23).* Retrieved from: http://dx.doi.org/10.3390/app10238566

Powell, D., Morgan, R., & Howe, G. (2021). Lean First … then Digitalize: A Standard Approach for Industry 4.0 Implementation in SMEs. In A. Dolgui et al. (Eds.): APMS 2021, IFIP AICT 631, pp. 31-39.

Lockwood, A. J., Hill, G., Moldoveanu, M., Coles, R., & Scott, R. (2018). *Digitalisation of Legacy Machine Tools.* Retrieved from: https://www.amrc.co.uk/pages/publications

Lang, S., Reggelin, T., Müller, M., & Nahhas, A. (2021). Open-source discrete-even simulation software for applications in production and logistics: An alternative to commercial tools? *Procedia Computer Science, 180, pp. 978-987.*

Dagkakis, G., & Heavey, C. (2016). A review of open source discrete event simulation software for operations research. *Journal of Simulation*. 10(3). pp. 193-206. doi: 10.1057/jos.2015.9.

JaamSim [Computer software]. (2022). Retrieved from: jaamsim.com

ThePiHut. (2022). *Raspberry Pi Camera Module V2.1.* Retrieved from: https://thepihut.com/products/raspberry-pi-camera-module

ThePiHut. (2022). *Raspberry Pi 4 Model B.* Retrieved from: https://thepihut.com/products/raspberry-pi-4-model-b

OpenCV [Computer software]. (2022). Retrieved from: opencv.org

PyTesseract [Computer software]. (2022). Retrieved from: https://pypi.org/project/pytesseract/

InfluxDB [Computer software]. (2022). Retrieved from: influxdata.com

Grafana [Computer software]. (2022). Retrieved from: grafana.com

# Chapter 7: Machine Tool, Automation and Manufacturing System Design

# Implementation and Optimization of a Robotic Welding System

Fionn Foley, Chris O'Donoghue, Joseph Walsh

School of Science, Technology, Engineering and Mathematics, Munster Technological University, Clash, Tralee, Co. Kerry, Ireland, V92 CX88

e-mail: fionn.foley@mtu.ie

***Abstract*— This paper describes the research, development, and optimisation of a robotic welding system at a leading Irish AgriTech company. The project required the development of robotic welding fixtures using best design principles and generation of associated weld programs to enable the automated welding of several products in the production system of the company. This study provides complete fixtures in line with customer requirements using Autodesk Inventor CAD software. By following an integrated methodology which links the industry standard approach to fixture design with product development tools including QFD, Pugh charts, and DFMEA, a defined structure to this process is provided, while ensuring transferability throughout industry. It was found that the generation of an industry ready robotic welding program using Panasonic DTPS software was aided by following a prescribed methodology. This complex process was streamlined by applying the defined coordinated approach enabling the gradual knowledge growth necessary to complete an industry ready robotic program. The study clearly demonstrates that moving from traditional manufacturing methods to robotization is possible for an SME. The benefits for enterprises seeking to replace mechanical manufacturing processes by adopting robotic welding systems and consequently capitalizing on the potentials of this robotic technology are evident.**

***Index Terms*— Robotic Welding, Fixture Design, Industry 4.0, Internet of Things, Robotic Programming, Robotics, AgriTech***

## I. Introduction

Rapid advancement in intelligent manufacturing systems has forced many enterprises to implement modern manufacturing systems in efforts to maintain global market expansion. Those willing to change are reaping the product and organisational benefits of this evolution and expanding their knowledge of the production system. Industries are now expected to have communication and intelligent capabilities throughout manufacturing, engineering, material usage, supply chain and, life cycle management [1]. The benefits are reflected in increased productivity, improved quality, efficiency, and mass customization [2]. The emergence of the Internet of Things (IoT) and Industry 4.0 have revolutionized industrial capabilities. With Industry 4.0 the presence of these intelligent systems connected through internet of things (IoT) can provide interaction in smart factories [2]. Production systems are evolving into cyber-physical-production-systems (CPPS) and machines are now becoming smart machining centres [3]. The physical being machines and sensors and the cyber being, data storage and mining. For welding technology, Industry 4.0 can be characterised as the interaction of components, intelligent welding robots, and CPPS supported welding systems with networked product quality [4]. Welding and joining have been recognised as key enabling technologies for EU manufacturing, with almost thirteen million jobs in high tech manufacturing, it is essential for enterprises to embrace the full potential of these modern systems [5]. The implementation and optimisation of a robotic welding system at this manufacturing site highlights a considerable engineering knowledge gap which may be evident throughout the Irish AgriTech industry. This knowledge gap ensures the transformation from existing manual manufacturing methods to intelligent manufacturing systems remains a major challenge. This is a challenge shared not only in the AgriTech industry but across many enterprises seeking to adopt these systems.

Ireland has a rapidly developing economy with the AgriTech sector seeing exponential growth. Maintaining a competitive advantage within this industry requires efficient production and high-quality standards due to high labour costs. Additionally, sourcing suitably qualified welders is an ongoing challenge for industry and therefore, a gradual transition from manual arc welding to robotic welding on this product was planned. It was envisaged that robotization of the key manufacturing steps on selected products can enable superior quality, higher productivity and provide a safer working environment for its employees.

The implementation of robotic welding system is dependent on the availability of accurately designed fixtures and a high level of programming experience. These fixtures ensure locational accuracy of the workpiece while the weld program is run. Core functionality musty include elimination of movement, and sufficient torch access to each weld seam, while providing a straightforward loading and unloading system for the operator. The fixture design process can be complex, time consuming and costly, and typically heavily dependent on system and product knowledge built over many years. When acquiring this technology, the company did not have significant robotic system knowledge, with many of the existing manual fixtures developed by skilled operators to suit their specific needs. While a limited number of fixtures have been developed using CAD onsite, none have been developed following a defined approach and therefore any proposed methodology must be easily followed from the industry partners perspective to enable successful implementation. In addition to these challenges, the development of robotic weld programs is a highly specialised task and can be associated with a considerable proportion of the overall system implementation costs [6]. In fact, studies have shown these costs can be as high as

63% of total costs [6]. These programs typically require a skilled programmer or extensive operator training with limited alternatives found outside of manufacturer specific training programs, which are extremely costly. These limited training options and specific skills requirements can dilute the benefits of the robotic systems for many SMEs, highlighting the need to provide structured guidelines allowing the development of skills and process understanding through each of the individual programming stages. While novel developments in these subject areas may provide some suitable solutions, the complexities involved in implementing these solutions would in fact broaden the knowledge deficit and not serve as a useful purpose for this enterprise or similar SMEs who remain the focus of this study.

## II. METHODS

The costs associated with fixture design can be as high as 20% of the total costs of the manufacturing systems [7]. Up to 40% of all rejected parts linked to dimensioning errors can be attributed to poor fixturing design. Significant cost savings can be achieved by reducing design costs and increasing the accuracy of fixturing [8]. These figures clearly highlight fixtures as key components in modern manufacturing systems [7]. In automated welding, a fixture is required to rapidly, accurately, and securely, position the workpiece during the welding operation. Automated fixture design while extremely efficient is complex, and often relies on the use of established fixtures to finally deliver a conceptual solution. The reliance on industrial experience is highlighted in many of the design processes studied, signifying the need for a clearly defined process which provides a pathway for inexperienced designers. Following a defined process with links to the new product development process can reduce fixture implementation costs and time by up to 75% [9].

The advantages of robotic welding systems are clear, many smaller production systems have struggled to adopt Off-line programming (OLP) due to the prohibitive cost of software implementation and the requirement for either a skilled programmer or extensive operator training. Over 63% of the total costs of ownership of an industrial robot are associated with training employees or external programmers. OLP methods may vary, but the programming methodology must follow a number of core steps to generate a complete program [10]. Automatic path generation is novel but has not yet provided a sufficient fit for all requirements. Tag generation, trajectory planning, and process planning are highlighted as tedious steps and research indicates little if any generic guidance is offered. The efficient generation of robotic welding programs can be aided by a transparent methodology linking the specific software and system used with programming methods extensively adopted in industry. These issues can be supplemented by the development of a structured OLP methodology guiding SMEs through the individual programming process stages.

### A. *Fixture Design*

Developing a fixture in line with the methods documented in published literature can substantially reduce these costs and lead times. The four main stages of the design process are, setup planning, fixture planning, fixture unit design and design verification. Collaborative discussions with the industry partner provided a clear understanding of the design goals in terms of suitable materials, selected suppliers, and manufacturing methods and additionally provided alignment with other documented product design procedures observed in literature. The creation of the core requirements utilising the structured Quality Function Deployment (QFD) design tool can provide the designer with a methodical starting point while ensuring the needs of the SME remained a priority. Once concepts have been generated using the Autodesk Inventor CAD software package, the use of structured screening tools and methods including Pugh charts can enhance fixture unit design. Additionally, these can provide a clear steppingstone between the fixture planning and unit design stages. Fixture verification using the Design failure mode and effect analysis (DFMEA) enables a structured design verification throughout the process, and this broadly adopted method can be of additional support to verification methods using tools such as Autodesk Inventor and Desk Top Programming & Simulation System (DTPS). In addition to this, location accuracy and accessibility verification can be conducted on physical samples once the fixture has been manufactured.

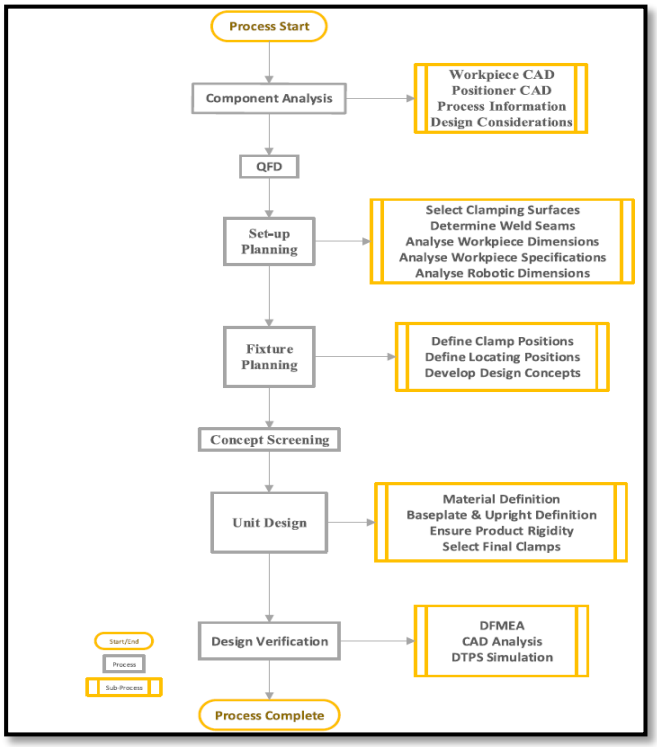


*Figure 1 Fixture Design Methodology*

### B. *Robotic Programming*

The methodology highlighted in Figure 1 provides a structure that can enable SMEs to efficiently develop a robotic weld program in line with accepted industry methods and published literature. The main programming steps are transferred into specific tasks which remain aligned with guidelines provided by the welding system supplier through each of the online training sessions and programming manuals. Positional and procedural tags are universally recognised in robotic programming and the addition of numerical weld points identifying each weld seam during the trajectory planning stage, is an accepted robotic welding process step. These were developed in conjunction with the SME through the many review meetings and are an adaption

of the existing manual welding steps. Collision avoidance is an iterative process and can be run complete once the program has been developed to a sufficient level. However, the touch sense functionality which is handled in the process planning and calibration section is only relevant to robotic welding systems utilising this type of calibration method. The complexity involved in programming a robotic welding system can be significantly reduced by closely following the high-level steps as outlined in the proposed methodology. These headings provide defined start points for the unskilled programmer and provide a structured pathway to develop the weld program. This methodology provides a combination of extensively used industry methods while remaining focused on the knowledge deficit amongst many SMEs.

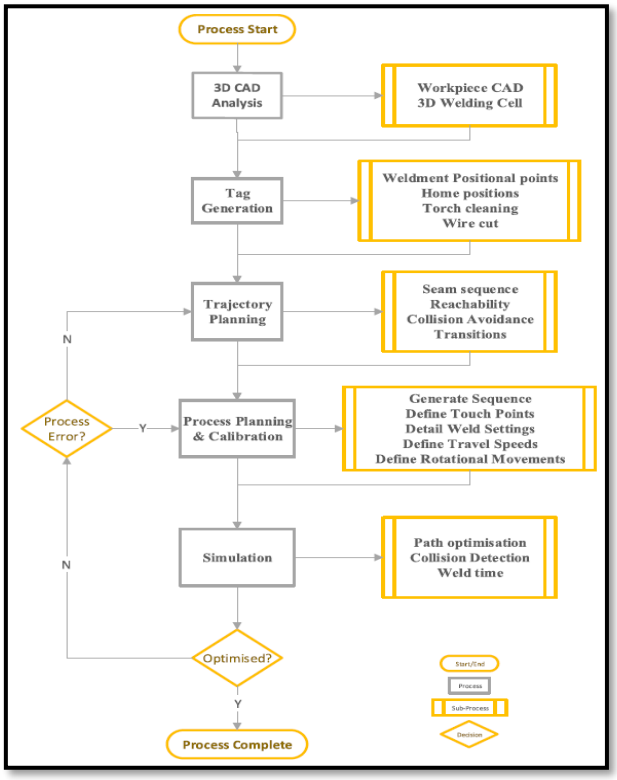


*Figure 2 Robotic Programming Methodology*

## III. Results and Analyses

### A. *Fixture Design*

By using the methodology outlined, it was possible to develop a deep and structured understanding of each critical component of the robotic welding system. Once the QFD was complete the system requirements were clearly identified, and several individual concepts were then developed. These concepts were then analysed, assessed, and ranked using Pugh charts with a final version detailed and developed in line with manufacturing requirements. The final fixtures were then validated remotely using a DFMEA, Autodesk Inventor, and DTPS simulations to ensure robotic access for all identified weld seams was possible prior to final assembly.

*Component analyses*

The first step in the design process requires the team to analyse the core aspects of the required work package. The workpiece CAD geometry provides a start point where detailed information of the size and shapes can be reviewed. High level design considerations such as existing fixtures and concepts as well as customer requests are all a fundamental part of this step. Additional considerations here include the process type, weld locations and any forces or movements that may be encountered during the welding process

*QFD*

These rankings can provide guidance throughout the design process and can be kept in alignment with the DFMEA process. From the completed QFD, the rankings highlight the following specifications as essential for the successful design of the robotic welding fixtures.

1. Ease of location and accuracy (Six Degrees Of Freedom)
2. Torch/robotic clearance
3. Low material cost (Raw Material)
4. Fixture size (HxWxD)
5. Manufacturing Complexity/cost
6. Fixture rigidity

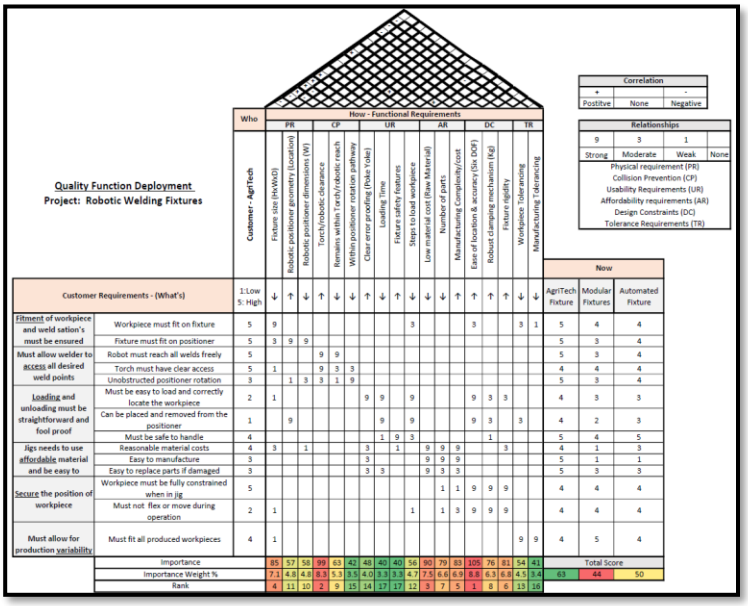


*Figure 3 Fixture Design QFD*

*Setup Planning*

During this phase it is essential to analyse the workpiece dimensions and properties, highlight potential clamping surfaces and understand the relevant robotic dimensions. Many of these dimensions link directly to the QFD specifications which provides design guidance for the team which in turn significantly reduces the time spent analysing each area once again.

*Fixture Planning*

Fixture planning involves the development of conceptual fixtures based on the requirements highlighted through both the QFD and setup planning. Once the initial system analysis has taken place it is possible for the designer to develop simple conceptual sketches or if sufficiently skilled the designer can choose to create basic CAD models. Suitable workpiece surfaces are studied, and specific points are selected as potential clamping solutions. Details of numerous clamps are analysed and imported

into 3D format for ease of manipulation and interpretation. These models provide a clear graphical overview of the workpiece, and it can be used to guide a design team through each individual concept. While fasteners may be intended in the final design, details of these items are not specified or refined at this point. Additionally, material definition can take place, while ensuring individual and customer requirements during this step. Once several solutions are generated it is then possible to use concept screening charts to select a preferred solution while observing the functional requirements as developed and prioritised in the QFD.

*Concept Screening*

Each fixture concept outlined in the fixture planning stage was input into this matrix where the pros and cons were itemised and allocated to each of the concepts. The mechanical criteria ratings follow the key functionality as outlined in the published literature and compiled in the QFD in Figure 3. All concepts were rated against each another in their ability to meet the design criteria.

**Robotic Fixture Concept Pugh Chart**

| Design Criteria | A: Concept V01 | B: Concept V02 | C: Concept V03 | D: Concept V04 | E: Concept V05 | F: Concept V06 |
|---|---|---|---|---|---|---|
| Fixture size (HxWxD) | +1 | +1 | 0 | 0 | 0 | 0 |
| Robotic positioner geometry (Location) | -1 | 0 | +1 | +1 | +1 | +1 |
| Robotic positioner dimensions (W) | -1 | -1 | +1 | +1 | +1 | +1 |
| Torch/robotic clearance | -1 | -1 | 0 | 0 | +1 | +1 |
| Within Torch/robotic reach | 0 | 0 | 0 | 0 | 0 | 0 |
| Within positioner rotation pathway | 0 | 0 | 0 | 0 | 0 | 0 |
| Clear placement error proofing (Poke Yoke) | 0 | 0 | 0 | 0 | 0 | +1 |
| Loading Time | -1 | -1 | -1 | -1 | +1 | +1 |
| Fixture safety features | -1 | -1 | -1 | -1 | +1 | +1 |
| Steps to load workpiece (4) | 0 | 0 | 0 | 0 | +1 | +1 |
| Low material cost (Raw Material 41 Kg) | +1 | +1 | -1 | -1 | -1 | +1 |
| Number of parts (17) | 0 | 0 | -1 | -1 | -1 | +1 |
| Manufacturing Complexity | -1 | -1 | -1 | -1 | +1 | +1 |
| Ease of location (Six DOF) | -1 | -1 | -1 | -1 | +1 | +1 |
| Robust clamping mechanism ( 550Kg) | 0 | 0 | 0 | 0 | +1 | +1 |
| Fixture rigitidy | +1 | -1 | -1 | -1 | +1 | +1 |
| Workpiece Tolerancing | -1 | 0 | 0 | 0 | +1 | +1 |
| Manufacturing Tolerancing | -1 | 0 | -1 | -1 | +1 | +1 |
| Sum + | 3 | 2 | 2 | 2 | 12 | 15 |
| Sum 0 | 6 | 9 | 8 | 8 | 4 | 3 |
| Sum - | -10 | -8 | -9 | -9 | -2 | 0 |
| Net Score | -7 | -6 | -7 | -7 | 10 | 15 |
| Rank | 4 | 3 | 4 | 4 | 2 | 1 |

*Figure 4 Concept Screening Method*

*Detailed Unit Design*

With a final concept selected it is then possible to refine each component and generate a final assembly. The main components including the baseplate, sides, supports and clamps must be fully defined. This design must ensure the assembly can achieve sufficient clamping forces, rigidity and absorb any workpiece tolerance. While the SME do not perform final dimensional checks on the manufactured components or assemblies it was advised through design review to ensure all fixture tolerances are kept to less than 1mm. Fully detailed 2D engineering drawings for each component were presented to the SME, here only the main design considerations are listed.

**Fixture Design Considerations**

| Overall Assembly | Headstock Legs Fixture | Hinge Fixture |
|---|---|---|
| Rigid base part | Yes (6mm & 30° bend) | Yes (8mm & 30° bend) |
| Base part with fixturing features | Yes (8.5 x 20.5mm slots) | Yes (8.5 x 20.5mm slots) |
| Absorb workpiece functional tolerance | Yes >1mm throughout | Yes >1mm throughout |
| Overall part count minimized | Yes | Yes |
| Minimum use of separate fastners | All M10 x 35 | All M10 x 35 |
| Weld access | Yes (1.5mm recess for plug weld) | Yes (1.5mm recess for plug weld) |
| Parts with end-to-end symmetry | All main uprights | All main uprights |
| Straight-line motions of assembly | Yes (90° angles only) | Yes (90° angles only) |
| Chamfers to facilitate insertion and self-alignment | Yes (2x2mm chamfer) | Yes (2x2mm chamfer) |

*Figure 5 Final fixture design considerations*

*DFMEA*

The DFMEA is utilised here to identify the main failure modes associated with the Fixtures. As highlighted in literature it considers the effects of each failure, the potential causes of the failure and the estimated frequency of the occurrence of those failures. Finally, the DFMEA provides a risk priority number which enables the indexing of each identified failure and guides the required corrective action to ensure the issues are not present in advance of final production. The top ten items from this DFMEA are highlighted below. With each identification number linking the requirements captured in the QFD. The applied methodology analyses each requirement and the associated component or feature to develop a systematic analysis of the fixture designs and build a comprehensive DFMEA.

**ROBOTIC WELDING FIXTURE DFMEA**

| Number | Item id Number | Function Description | Potential Failure Mode | Potential Effect(s) of Failure | Severity | Potential Cause(s) of Failure | Prevention Method (prevention of cause of failue) | Occurrence | Detection Method (D) (detection of potential failure mode) | Detection | RPN | Recommended Actions | Responsible Person(s) | Corrective Actions Taken |
|---|---|---|---|---|---|---|---|---|---|---|---|---|---|---|
| 1 | 9 | Must not flex or move during operation | Constraint requirements are not fulfilled | Workpiece not secure in fixture | 7 | Fixture Flex - baseplate ridity not sufficient | P: Material & Dimensions selected based on datasheets, experience and testing. | 7 | D: Assembly trials | 3 | 147 | Add 30° bend to increase baseplate rigidity | Fionn Foley | Bend added |
| 2 | 8 | Workpiece must be fully constrained when in fixture | Constraint requirements are not fulfilled | Workpiece not secure in fixture | 7 | Fixture Dowel - locating slot incorrect location and/or incorrect dimension | P: Material & Dimensions selected based on datasheets, experience and testing. P: Review of workpiece &dowel interface via 3D model | 6 | D: Verification of Cad data for fit D: Assembly trials | 2 | 84 | | | None Required to Date |
| 3 | 8 | Workpiece must be fully constrained when in fixture | Constraint requirements are not fulfilled | Workpiece not secure in fixture | 7 | Clamp force - insufficient | P: Clamp selected based on datasheets, experience and testing. | 4 | D: Clamping trials | 3 | 84 | | | None Required to Date |
| 4 | 9 | Must not flex or move during operation | Constraint requirements are not fulfilled | Workpiece not secure in fixture | 7 | Fixture Flex - upright supports not sufficient | P: Material & Dimensions selected based on datasheets, experience and testing. | 6 | D: Clamping trials | 2 | 84 | Upright support dimensions to be increased | Fionn Foley | Redesign Complete |
| 5 | 10 | Must fit all produced workpieces | Tolerance requirements are not fulfilled | Installation in fixture not possible/difficult | 8 | fixture tolerance not aligned with workpiece tolerance | P: Design based on workpiece and customer requirements P: Open tolerances >1mm | 5 | D: Verification of Cad data for fit D: Assembly trials | 2 | 80 | | | None Required to Date |
| 6 | 7 | Must be safe to handle | Operator safety requirements are not fulfilled | Installation in fixture not possible/difficult | 9 | Fixture fillets - not sufficient | P: Design based on safety requirements P: Review of fixture safety features via 3D model | 4 | D: Verification of Cad data for safety | 2 | 72 | Increase Fixture fillets to 10 mm | Fionn Foley | ;Fixture fillets increased to 10 mm |
| 7 | 7 | Must be safe to handle | Operator safety requirements are not fulfilled | Installation in fixture not possible/difficult | 9 | Clamping method - not safe | P: Design based on safety requirements P: Review of fixture safety features via 3D model | 4 | D: Verification of Cad data for safety D: Assembly trials | 2 | 72 | | | None Required to Date |
| 8 | 8 | Workpiece must be fully constrained when in fixture | Constraint requirements are not fulfilled | Workpiece not secure in fixture | 7 | Clamp position - incorrect location and/or incorrect dimension | P: Design based on workpiece requirements P: Review of workpiece &dowel interface via 3D model | 4 | D: Verification of Cad data of clamp D: Assembly trials | 2 | 56 | | | None Required to Date |
| 9 | 8 | Workpiece must be fully constrained when in fixture | Constraint requirements are not fulfilled | Workpiece not secure in fixture | 7 | Clamp supports - incorrect location and/or incorrect dimension | P: Material & Dimensions selected based on datasheets, experience and testing. | 4 | D: Verification of Cad data for fit D: Assembly trials | 2 | 56 | | | None Required to Date |
| 10 | 8 | Workpiece must be fully constrained when in fixture | Constraint requirements are not fulfilled | Workpiece not secure in fixture | 7 | Clamp supports - insufficient strength | P: Clamp selected based on datasheets, experience and testing. | 4 | D: Clamping trials | 2 | 56 | | | None Required to Date |

*Figure 6 Robotic Fixture DFMEA Top 10*

*DTPS Simulation*

The final verification steps outlined in the methodology required the analysis of the fixtures and the loaded workpiece within the DTPS environment. Further details of this software and its significance are detailed at length in section 4.2. The use of this software provides a link between the designer and programmer and emphasises the importance of cross functional collaboration between the many teams operating in a modern engineering environment. The accessibility of each seam must be analysed and if any restrictions are evident a design update will be required. Similarly, collision avoidance must be ensured, and the complete fixture design can be carefully analysed with each clamp in its closed position. This provides a clear representation of the physical outline of the complete fixture and enables a thorough assessment of the suitability of the final fixture design. This step is tightly bound to the unit design phase and indeed many of the functional requirements should have already been clearly understood by the designer prior to reaching this ultimate step. However, design errors are certainly a reality, and this study is linked to inexperienced design teams, therefore the simulations are imperative.

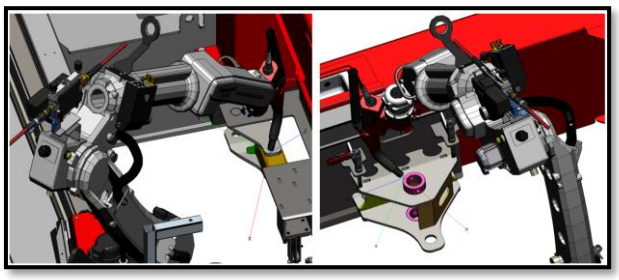

*Figure 7 Validation of fixtures within the DTPS environment*

## B. Robotic Programming

DTPS software was used in conjunction with Panasonic robotic manipulators and Panasonic Tawers weld controllers for off-line path generation and simulation [3]. The gradual development of the required knowledge was possible following the programming methodology developed. Tag generation ensures the positional data of the workpiece is accurate within DTPS and provides the opportunity to generate assistant tags such as home positions, approach points, and retreat points. The structured identification of each weld seam was handled in trajectory planning with a numerical seam sequence generated and revised. The process planning and calibration stages define the weld poses and transitions in combination with outlining the preliminary weld settings and travel speeds. The calibration points used to ensure accuracy were also programmed here as the specific system utilised Touch Sensing. The results obtained by following this methodology were of the industry required standard and once the programs were transferred to the SME they were immediately utilised for onsite testing.

### *DTPS 3D Environment*

An overview of the robotic cell as it appears in the DTPS environment is depicted in Figure 8. Major components within this cell are highlighted in the diagram including the Tawers Global Controller G3, Panasonic TM-2000WGH3 robot, VWP-R500 FE welding torch, Thielmann BRG 2000 mechanical cleaning unit with inbuilt wire cutter, VWK 7/1 water cooling unit, Panasonic AUR01060 teach pendant, BICORE BINZEL xFUME fume extraction system and Leuze light screen enabling emergency stop functionality.

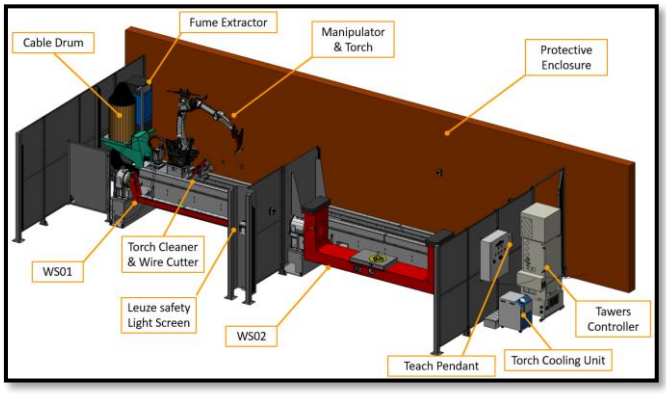


*Figure 8 Robotic Welding Cell Within the DTPS Environment*

### *Tag Generation*

Tag generation is the process of extracting the positional data and reference planes of the workpiece and aligning them within the software. This ensures the workpiece geometry is aligned with the intended position during the weld process, enabling the required accuracy to be met. Assistant tag points can also be programmed here, including cleaning, and cutting procedures, home positions, approach points, and retreat points. These procedures and points can be called at any time throughout the specific weld program. Once the workpiece assembly has been imported into the DTPS environment, the axis centre point requires a transfer to align it with the selected robotic axis position.

### *Trajectory Planning*

This step requires the programmer to analyse and identify each weld seam on the workpiece and create a high-level plan which can then provide the required steps to create a detailed weld program. Each potential configuration of the workpiece must be carefully considered to prevent collisions and minimise transitions [9]. A commonly adopted practice is to assign the weld seams and touch points a numerical value for ease of identification during post processing analysis and validation [10]. These numerical values are assigned in sequential order providing a structured workflow from one seam to the next. This enables the programmer to easily arrange the most suitable transitions and pathways between each seam. The seam identification was also highlighted as an essential step in the fixture design process. This step must be reconsidered as the workpieces are now constrained within the finished fixtures and therefore, the process must carefully identify any seams with a low clearance or challenging access.

### *Process Planning and Calibration*

Process planning involves the development and detailing of each sequence step required to generate an optimised weld program. These steps include the approach and touch points, weld settings, travel speeds and the final trajectory plot. Once the weld sequence and poses are plotted, the calibration data which in the SMEs system are touch points, can be added to the program following the selected sequence. Process planning can be time consuming and challenging, requiring a general understanding of the many commands and calls available within the DTPS system. While the provided methodology certainly delivers a high-level guide to the requirements of the process planning step, it is not designed with the intention of enabling the programmer to develop a complete weld program without specific DTPS system training

### *Simulation*

The last step involved in generating a robotic program is simulation. Here the programme can be verified using the DTPS software, which significantly reduces the downtime of a robotic system while ensuring collision and limits are avoided. Within the DTPS environment this task is straightforward as it provides the ability to simulate each individual step or the entire program. Using the specific collision detection application within DTPS it is possible to check for any collisions within the entire weld cell. If the collision detection simulation passes, the programmer can then move on to analysing each axis while the program is running. This provides a clear overview of the joint angles throughout the program and can highlight any areas where the desired limits are breached. The last step in the simulation environment provides a clear overview of the cycle time including, Arc ON time, Arc ON rate, welding length, number of seams, and wire length. This can provide a clear understanding of the impact each variable may have on the finalised cycle time

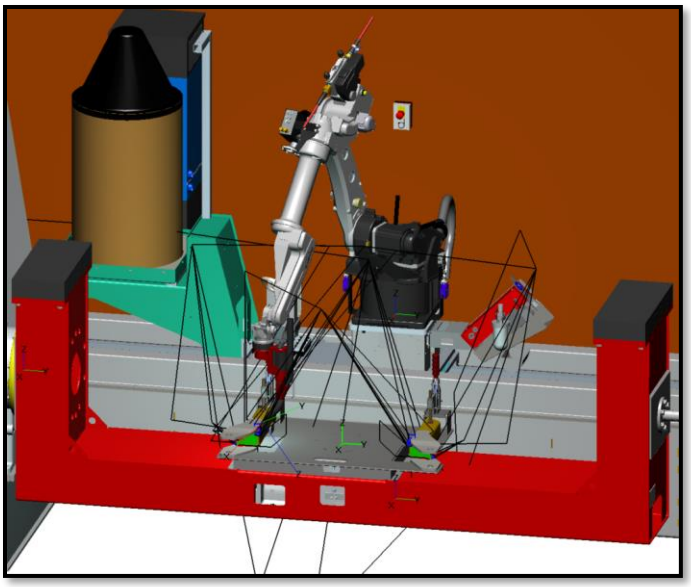

*Figure 9 The final weld path as shown by the various trajectory lines*

## IV. Conclusion

The implementation and optimisation of a robotic welding system has been successful using the integrated methodologies developed throughout this study. The structured design and optimisation of two robotic welding fixtures and the generation of associated robotic welding programs has been complete.

1. It was shown that the development of robotic welding fixtures was significantly enhanced following the outlined methodology which links an industry standard approach to fixture design with product development tools which provide a defined structure to the design process. The application of these tools including QFD Pugh charts and DFMEA provides a link between many phases in the design process and as they are universally accepted tools, transferability of this methodology throughout industry was ensured.
2. The generation of an industry ready robotic welding programs was developed in line with the methodology detailed. This coordinated approach ensured this process was streamlined and development of the required programs was structured to enable the gradual knowledge growth necessary to complete this complex process.

In previous studies the methodologies used to develop fixtures displayed several significant gaps with many of these providing little guidance on knowledge development or general structure. Here, the integration of industry recognised product development tools removed the reliance on extensive prior knowledge and provides structure, enabling the designer to make informed decisions on key requirements, material screening and design changes throughout the development process. Similarly, by following the proposed programming methodology a gradual development of the required skillset is possible. This methodology has effectively guided the development of two industry ready robotic welding programs which are currently undergoing online tests to ensure optimisation of each step.

## V. References


[1] B. Alexandros, P. Nikos, M. Babis, A. Dimitris and M. Gregoris, "Enabling condition-based maintenance decisions with proactive event-driven computing," *Computers in industry*, vol. 100, pp. 173-183, 2018.

[2] W. H. T. Luo, Y. Ye, C. Zhang and Y. Wei, "A hybrid predictive maintenance approach for CNC machine tool driven by Digital Twin," *Robotics and Computer Integrated Manufacturing*, vol. 65, 2020.

[3] H. Kagermann, W. Wahlster and J. Helbig, "Recommendations for implementing the strategic initiative INDUSTRIE 4.0: Final report of the Industrie 4.0 Working Group," Acatech, Frankfurt, 2013.

[4] B. Wang, S. J. Hu, L. Sun and T. Freiheit, "Intelligent welding system technologies: State-of-the-art review and perspectives," *Journal of Manufacturing Systems*, vol. 56, pp. 373-391, 2020.

[5] Weld 4.0, "Weld 4.0: European welder report on existiing curriculum and digitisation needs," HighSkillz, Bremen, 2017.

[6] Z. Pan, J. Polden, N. Larkin, S. V. Duin and J. Norrish, "Recent progress on programming methods for industrial robots," *Robotics and Computer-Integrated Manufacturing*, vol. 28, no. 2, pp. 87-94, 2012.

[7] S. Gothwal and T. Raj, "Different aspects in design and development of flexible fixtures: review and future directions," *International Journal of Services and Operations Management*, vol. 26, no. 3, 2017.

[8] I. Boyle, Y. Rong and D. C. Brown, "A review and analysis of current computer-aided fixture design approaches," *Robotics and Computer-Integrated Manufacturing*, vol. 27, no. 1, pp. 1-12, 2011.

[9] R. D. Khatu, B. T. Patil, D. K. Bhise and H. B. Vaishnav, "Design of a fixture for wire-cut EDM: A generic approach," *Materials Today: Proceedings*, 2021.

[10] H. K. Banga, P. Kalra, R. Kumar, S. Singh and C. I. Pruncu, "Optimization of the cycle time of robotics resistance spot welding for automotive applications," *The journal of Advanced Manufacturing and processing*, vol. 3, p. 10084, 2021.

# A Task and Action Planning Framework for Human Robot Collaborative Workstations

Cemalettin Ozturk[1, 5], David Gutierrez Perez[1], Amine Lamine[1], George Evangelou[2], Nikos Dimitropoulos[2], George Michalos[2], Sotiris Makris[2], Michele Garraffa[3], and Spyros Kouka[4]
1 Collins Aerospace, Cork City, Ireland
[2] Laboratory for Manufacturing Systems and Automation (LMS) Department of Mechanical Engineering and Aeronautics University of Patras, Patras 26504, Greece
[3] University College Cork, Cork City, Ireland
[4] Intrasoft International S.A, Athens, Greece
[5] Munster Technological University, Cork, Ireland

***Abstract***

Over the last years both Research and Industry have tried to address the requirement for flexible production by introducing technologies that allow humans and robots to coexist and share production tasks. The focus has been to ensure the safety of humans while interacting with robots. In this paper, we present a Task and Action Planning Software (TAPS) module that is responsible for the sequencing and orchestration of the actions performed by both human operators and robotic resources, at both work center and factory level. Its main goal is to optimize task and order executions respectively based on a set of evaluation criteria and to provide assembly plans that maximize the assembly line's throughput capabilities. Thus, available resources are to be utilized efficiently and productively.

*Key Words: robotics, planning and scheduling, optimization, constraint programming, artificial intelligence*

## 1. INTRODUCTION AND BACKGROUNDHEADING

Enhancing human robot collaboration is a contemporary topic of human-machine interaction domain and covers similar challenges and opportunities as well. As being very accurate and fast in their operations, robots are in general less costly than hu-man in manufacturing. However, they have lack of adaptability of new prod-ucts/conditions as well as performing tasks requires special capabilities and creativity still makes human the driving factory of this collaboration. This can be achieved by drifting away from stationary, mindless robotic agents and replacing them with space-aware, mobile and multiple-capabilities robots: Human-Robot Collaborative (HRC) workcells [1]. The main challenges when designing HRC workcells arises from the integration of human factor requirements (e.g. posture, strength, fatigue and cog-nition), robot requirements (e.g. joints position, movement sensors signals by the ro-bot), Human-Robot Interaction (HRI) requirements (e.g. force or feedback force) and assembly requirements. The latter represents the manufacturing goals such as the completion time and overall quality, expressed by the evaluation metrics of consid-ered course of actions [2], [3]. Following the above analysis, it is concluded that there is an increasing need in or-chestrator agents that steer the actions of all resources, combining them in a holistic HRC production system. Thus, planning and scheduling of manufacturing activities is the major task for factory decision makers. In this manner we see a trend in recent publications in the domain to exploit mathematical (i.e., mixed integer programming) and artificial intelligence (particularly constraint programming) methods [4], [5], [6], [7], [8], [9], [10] and [11]. To the best of our knowledge, the constraint programming-based factory level planning module integrated with cell level planning module pre-sented in this paper is bridging the gap in the literature for effectively solving holistic decision problems in HRC production systems.

In Section 2, the architecture of the proposed architecture as well as its software implementation is presented, while in Section 3, our conclusions and ideas for future work are being shared.

## 2. FRAMEWORK ARCHITECTURE

The architecture of the developed framework is focused around 4 individual modules:

Email: Cemalettin Ozturk
cemalettin.ozturk@mtu.ie

**Task and Action Planning Software (TAPS):** This module comprises of two sub-modules: i) Factory level sub-module, and ii) Cell level sub-module.
**Graphical User Interface (GUI):** The interface responsible for providing a de-tailed view on work cell information, scheduling settings, search parameters and evaluation criteria.
**Knowledge Repository (KR):** The database containing all useful work cell information. Knowledge Repository contains the knowledge data model that represents the required information. Data models related to the presented functionalities are the factory cells, the manufacturing resources and the factory and product orders. A description of the shop floor, manufacturing resources and shop floor orders is provided hereafter.

Factory Cells
Each factory is composed of shop floor model which are composed of assembly lines. Each assembly line has cells and each cell has several manufacturing resources. For each cell, the current job as well as the available Robot Docking Stations, are part of the data model.
Manufacturing Resources
All manufacturing resources that are available in the system are described in the data model. A manufacturing resource can be a robot such as a stationary robot, a mobile robot or an overhead robot. Operators and their capabilities are also de-scribed.
The products and their subassemblies are described in the KR data model. Further information is included such as the geometry, weight of each product.

Orders
The KR data model describes the manufacturing tasks using classes such as the order, job, and task model. The orders are also connected with products. An order is composed of jobs which are assigned to specific stations and each job is composed of tasks which are assigned to specific resources. The tasks include precedence con-strains for the order in which they will be executed.
A factory level order can be broken down in several Cell Level Orders, which are comprised of product orders. Each product order references specific cell products that can be produced by specific cells. Figure 1 below shows the relations between these entities.

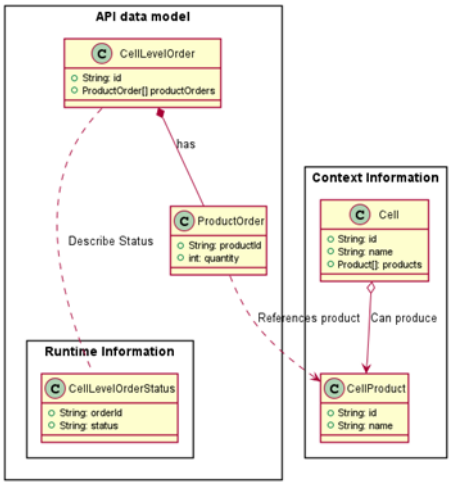

*Figure 1. POM and KR related data models UML*

**Production Orchestration Module (POM):** The role of the production orchestration module in the task and action planning framework is to integrate the factory and cell level planning interactions. In particular the factory level planner notifies POM when new orders are available. Then POM requests the next unprocessed order from the factory level planning module and asks the cell level planner to create an optimal task plan for the appropriate cell that will execute the order. Finally, when the task plan is executed successfully and the order is completed the POM notifies the factory level planner for the status of the order execution.

More information on execution of factory and cell level planning modules will be provided in the Sections 2.1 and 2.2.

### *2.1. Factory Level Planning Module*

Factory level planning module is responsible for propagating the tactical level master schedules to the operational level shop floor decisions. It takes the customer order and capacity information as input, and generates the schedule of these orders in which to be used as the input for cell level planning module. As such the execution of the planning module highly depends on the manufacturing setting; we develop tailored decision models for individual use cases. In this section, we present a constraint programming formulation for one of them: assembling heavy payloads and finding the best sequence of customer orders subject to operational constraints. Due to page limit, we refer readers to [5] for further details of constraint programming technology. In the following, we provide the notation required for formulating the problem.

Parameters:
$J$: set of jobs to be scheduled, including a dummy job $j_0$
$P$: set of positions in the schedule
$duration_j$ : duration of the job $j \in J$
$duedate_j$: due date of the job $j \in J$
$p_j$ : priority of the job $j \in J$
$width_j, length_j$ : width and length of the job $j \in J$

Variables
$nextJob_j$: predecessor of job $j \in J$, $nextJob_j \in J$
$nextJobWidth_j, nextJobLength_j$: width and length of the immediate predecessor of job $j \in J$.
$nextJobWidth_j, nextJobLength_j \in \mathrm{Z}^+$
$setup_j, changeLength_j$: binary variable indicating whether the width or the length of the job $j \in J$ is different than the immediate predecessor job. $setup_j, changeLength_j \in \{0,1\}$
$sequence_i$: indicates the job in position $i \in P$, $sequence_i \in J$
$position_j$ : indicates the position of job $j \in J$in the schedule, $position_j \in P$
$priorityDelta_{ij}$: binary variable indicates that whether consecutive jobs $i, j \in J$ are ordered based on predefined priority values, $p_i, p_j$. $priorityDelta_{ij} \in \{0,1\}$

Constraint Programming formulation of the factory level planning sub-module in a specific use case is presented as in the following:

$$\min \sum_{j \in J} \sum_{j' \in \pi : j' \le j} \left| duration_{j'} - duedate_j \right| \quad (1)$$

$$\min \sum_{j \in J} setup_j \quad (2)$$

$$\min \sum_{i,\, j \in J} priorityDelta_{ij} \quad (3)$$

$$\min \sum_{j \in J} changeLength_j \quad (4)$$

Subject to:

$$\pi = circuit\left(nextJob, J \cup j_0\right) \quad (5)$$

$$nextJobWidth_j = width_{nextJob_j} \quad \forall j \in J \quad (6.1)$$

$$nextJobLength_j = length_{nextJob_j} \quad \forall j \in J \quad (6.2)$$

$$width_j \neq nextJobWidth_j \Rightarrow setup_j = 1 \quad \forall j \in J \quad (7.1)$$

$$width_j = nextJobWidth_j \Rightarrow setup_j = 0 \quad \forall j \in J \quad (7.2)$$

$$length_j \neq nextJobLength_j \Rightarrow lengthChange_j = 1 \quad \forall j \in J \quad (8.1)$$

$$length_j = nextJobLength_j \Rightarrow lengthChange_j = 0 \quad \forall j \in J \quad (8.2)$$

$$sequence_1 = j_0 \quad (9.1)$$

$$sequence_j = nextJob_{sequence_{j-1}} \quad \forall j \in P - \{1\} \quad (9.2)$$

$$position_{sequence_j} = j \qquad \forall j \in J \quad (9.3)$$

$$\left(p_i > p_j\right) \wedge \left(position_i < position_j\right) \Rightarrow priorityDelta_{ij} = 1 \quad \forall j \in J \quad (10.1)$$

$$\left(p_i < p_j\right) \wedge \left(position_i > position_j\right) \Rightarrow priorityDelta_{ij} = 1 \quad \forall j \in J \quad (10.2)$$

$$\left(p_i \geq p_j\right) \wedge \left(position_i \geq position_j\right) \Rightarrow priorityDelta_{ij} = 0 \quad \forall j \in J \quad (10.3)$$

$$\left(p_i < p_j\right) \wedge \left(position_i < position_j\right) \Rightarrow priorityDelta_{ij} = 0 \quad \forall j \in J \quad (10.4)$$

Objective function (1) minimizes the deviation from the due date and the completion of the individual job, heavy payload. Note that while delay in the completion time causes losing customer goodwill, producing earlier equally causes inventory holding cost. Objective function (2) is minimizing the number of setups due to changing position of fixers. The third objective function (3) minimizes the discrepancy be-tween priorities of hangers produced consecutively and tries to ensure heavy payload with higher priority number is produced before than the lower one. And the last objective function minimizes the change of length of hangers produced consecutively. Constraint (5) is a global constraint [14] makes sure that all jobs are processed by ensuring a Hamiltonian Circuit on the graph of set of jobs where jobs represent the nodes using circuit global constraint [15]. Length and width of the job in sequence is taken from the job in the Hamiltonian Circuit through element global constraint [16] as a channelling constraint [17] through equations (6.1) and (6.2). Setup constraints (7.1) & (7.2) and length change constraints (8.1) & (8.2) depict that corresponding binary variables (i.e., changeover) needed if and only if the width (or length) of the current hanger is different than the previous one. Constraints (9.1) and (9.2) channel the sequence variable and its position in the permutation variable together with position variable (9.3). Finally constraints (10.1)—(10.2) channels the model priority violations (the higher the priority of the job *i*, the lower is the value of $p_i$).

Above constraint programming model is implemented in JAVA environment, solved by using open-source solver Google OR-Tools [18] and gives the best sequence of jobs optimizing the objective function described above. Due to confidentiality of the data used for prototyping the proposed model, in this paper we only present the conceptualisation of the developed framework.

### *2.2. Cell Level Planning Module*

The algorithm behind the generation of alternative task plans originates from concepts such as iterative deepening search and heuristic functions. Its main foundation lays on the selective search of the solution space, instead of using exhaustive meth-od. As the number of tasks, resources and possible assignments increases, the solution space becomes excessively large, which, consequently, vastly increases the computational and memory requirements of the exhaustive search method. It is important to note, that the referred solution space is the set containing all possible task-resource assignment sequences that lead to feasible action plans. To solve this, our algorithm splits the plan generation in sub-plans and only tries to complete the best one each time. By viewing the task-to-resource assignments as tree-nodes, the algorithm iteratively creates random, yet valid, groups of such nodes, noted as branches. It then extends, or ‘reproduces’, the optimal branch, of the currently generated. The selection of the fittest branch is performed by estimating the utility value of each one, first calculating its node sequence utility value and then adding the average utility value of some of its random extensions, or ‘samples’. A branch’s sample is a random sequence of nodes that completes said branch, as they together form a sequence of nodes, or task plan, containing all required assembly tasks.

As a starting point, the assembly procedure needs to be decomposed in a Work-load and Resources (WAR) model. After examining the sequence of operations required to gather, use and assemble all parts into the final product, POM must organize them in groups and denote any precedence constraints between them. A precedence constraint is a rule that restricts the execution of an operation, if one or more other operations have to be executed a priori. For example, screwing a lock mechanism on a panel requires that both the panel and the lock mechanism are positioned correctly on the workbench and a screw is already in the corresponding hole.

After successfully forming all information, TAPS can view most important data in a more user-friendly manner, utilizing the ‘Workload Information’ tab on the GUI. The planner first inquires data concerning the assembly information and resources, and then utilizes the user defined inputs, such as search characteristics and evaluation

criteria settings. Its goal is to create a sequence of task-to-resource assignments, depending on given information that aims to complete all tasks in an intelligent manner, while maximizing the plan's performance to the required thresholds and parameters.

By viewing the task-to-resource assignments as tree-nodes, the algorithm iteratively creates random, yet valid, groups of such nodes, noted as branches. It then ex-tends, or 'reproduces', the optimal branch, of the currently generated.

The aforementioned utility values of branches and their respective samples are calculated using custom created evaluation criteria. These are Java classes that, given an arbitrary set of nodes, either branches or samples, collect the properties of the tasks and resources involved and produce a score calculation of each respective metric.

Determining assembly goals like the decrease of cycle time (flow time), walking distance and increase of human safety and ergonomics, a list of criteria developed. After the generation of each plan according to the workshop information and user defined parameters, the operator can view all details concerning the plan metrics (Fig. 2).

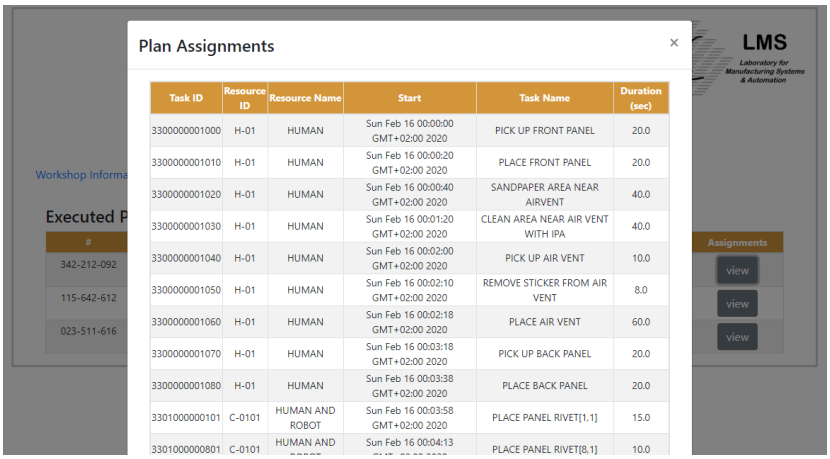


| Task ID | Resource ID | Resource Name | Start | Task Name | Duration (sec) |
|---|---|---|---|---|---|
| 3300000001000 | H-01 | HUMAN | Sun Feb 16 00:00:00 GMT+02:00 2020 | PICK UP FRONT PANEL | 20.0 |
| 3300000001010 | H-01 | HUMAN | Sun Feb 16 00:00:20 GMT+02:00 2020 | PLACE FRONT PANEL | 20.0 |
| 3300000001020 | H-01 | HUMAN | Sun Feb 16 00:00:40 GMT+02:00 2020 | SANDPAPER AREA NEAR AIRVENT | 40.0 |
| 3300000001030 | H-01 | HUMAN | Sun Feb 16 00:01:20 GMT+02:00 2020 | CLEAN AREA NEAR AIR VENT WITH IPA | 40.0 |
| 3300000001040 | H-01 | HUMAN | Sun Feb 16 00:02:00 GMT+02:00 2020 | PICK UP AIR VENT | 10.0 |
| 3300000001050 | H-01 | HUMAN | Sun Feb 16 00:02:10 GMT+02:00 2020 | REMOVE STICKER FROM AIR VENT | 8.0 |
| 3300000001060 | H-01 | HUMAN | Sun Feb 16 00:02:18 GMT+02:00 2020 | PLACE AIR VENT | 60.0 |
| 3300000001070 | H-01 | HUMAN | Sun Feb 16 00:03:18 GMT+02:00 2020 | PICK UP BACK PANEL | 20.0 |
| 3300000001080 | H-01 | HUMAN | Sun Feb 16 00:03:38 GMT+02:00 2020 | PLACE BACK PANEL | 20.0 |
| 3301000000101 | C-0101 | HUMAN AND ROBOT | Sun Feb 16 00:03:58 GMT+02:00 2020 | PLACE PANEL RIVET[1,1] | 15.0 |
| 3301000000801 | C-0101 | HUMAN AND | Sun Feb 16 00:04:13 | PLACE PANEL RIVET[8,1] | 10.0 |

Figure 2. Outlook on the assignments and task sequence of a generated plan.

## 3. CONCLUSION

Nowadays, manufacturing industry is in a transition to integrate artificial intelligence and data analytics methods into their conventional business processes to automate and improve manufacturing practices further by establishing connectivity of shop floor components via internet of things. Connected devices, autonomous machines and robots are the main enablers of this transition however, yet none of the as crucial as human workers for the productivity. In this paper we propose a novel task and action planning framework to exploit data generated from human robot collaborative stations facilitating efficient collaboration through various artificial intelligent methods and empower both human operators and robots.

As next steps, the application of the solution to real industrial field will follow. Also, authors will enhance both factory and cell level sub-modules with multi-criteria. Finally, performance comparison with similar methods from the literature will be provided.

**Acknowledgements**

This research has been supported by the European project "SHERLOCK Seamless and safe humancantered robotic applications for novel collaborative workshops" (Grand Agreement: 820689) (www.sherlock-project.eu) funded by the European Commission [12].

## 4. REFERENCES

Please list all references in this section in alphabetical order. Please adhere to the APA 6th Edition referencing style. Examples are shown below.

1. Tsarouchi, P., Makris, S., & Chryssolouris, G.: Human–robot interaction review and challenges on task planning and

programming. *International Journal of Computer Integrated Manufacturing*, 29(8), 916-931. (2016)
2. Pini, F., Ansaloni, M., & Leali, F.: Evaluation of operator relief for an effective design of HRC workcells. In 2016 *IEEE 21st international conference on emerging technologies and factory automation* (ETFA) (pp. 1-6). IEEE. (2016).
3. Tsarouchi, P., Makris, S., & Chryssolouris, G.: Human–robot interaction review and chal-lenges on task planning and programming. *International Journal of Computer Integrated Manufacturing*, 29(8), 916-931. (2016)
4. Ozturk, C., Ornek A.: "Optimisation and Constraint Based Heuristic Methods for Advanced Planning and Scheduling Systems", *International Journal of Industrial Engineering*, 23(1), 26-48 (2016).
5. Bogner, K., Pferschy, U., Untenberger, R., Zeiner, H.: "Optimised scheduling in human-robot collaboration – a use case in the assembly of printed circuit boards", *International Journal of Production Research*, Volume 56, No:16, pp. 5522-5540, (2018)
6. N. Kousi, S. Koukas, G. Michalos, S. Makris:"Scheduling of smart intra – factory material supply operations using mobile robots", *International Journal of Production Research*, Volume 57, Issue 3, pg. 801-814, (2018)
7. Nikolakis, N., Sipsas, K., Tsarouchi, P., Makris, S: "On a shared human-robot task scheduling and online re-scheduling" *Procedia CIRP*, Volume 78, Pages 237-242, (2018)
8. Kolakowska, E., Smith, S., F. Kristiansen, M.: "Constraint optimization model of a schedul-ing problem for a robotic arm in automatic systems". *Robotics and Autonomous Systems*, Vol.62, No:2. (2014)
9. Mossige, M.,Gotlieb, A., Meling, H.:" Deploying Constraint Programming for Testing ABB's Painting Robots. *AI Magazine*", Vol 38 No 2: Summer 2017 , pp.94-96 (2017)
10. Behrens, J., Lange, R., Mansouri, M. :"A Constraint Programming Approach to Simultaneous Task Allocation and Motion Scheduling for Industrial Dual-Arm Manipulation Tasks". *International Conference on Robotics and Automation* (ICRA) / [ed] Howard, A; Althoefer, K; Arai, F; Arrichiello, F; Caputo, B; Castellanos, J; Hauser, K; Isler, V Kim, J; Liu, H; Oh, P; Santos, V; Scaramuzza, D; Ude, A; Voyles, R; Yamane, K; Okamura, A, IEEE , p. 8705-8711 (2019).
11. Booth, K., Tran, T., Nejat, G., Beck, J.: "Mixed-Integer and Constraint Programming Techniques for Mobile Robot Task Planning". *IEEE Robotics and Automation Letters*, Vol. 1, Issue: 1, pp. 500-507 (2016)
12. SHERLOCK homepage, https://www.sherlock-project.eu/home, last accessed 2021/03/08
13. Rossi F., Beek P., & Walsh T. (2006). Introduction. In F. Rossi, P. van Beek & T. Walsh, (Ed.*). Handbook of Constraint Programming* (3-10). Amsterdam: Elsevier Science.
14. Global constraint, https://www.sciencedirect.com/topics/computer-science/global-constraint, last accessed 2021/03/08
15. Circuit Global constraint, https://sofdem.github.io/gccat/gccat/Ccircuit.html, last accessed 2021/03/08.
16. Element Global constraint, https://sofdem.github.io/gccat/gccat/Celement.html, last accessed 2021/03/08.
17. Channeling constraint https://web.imt-atlantique.fr/x-info/sdemasse/gccat/Kchannelling_constraint.html, last accessed 2021/03/08.
18. Google OR-Tools, https://developers.google.com/optimization , last accessed 2021/03/08.

# Development and construction of an automated harvesting arm for the efficient cultivation of duckweed

Abin Abraham Oommen[1], Neil E. Coughlan[2], Marcel A.K. Jansen[2], Alan P. Morrison[1]
[1] Electrical & Electronic Engineering, School of Engineering & Architecture, University College Cork.
[2]School of Biological, Earth and Environmental Sciences, University College Cork.

***Abstract***

Duckweed is a small floating aquatic plant that grows on the water's surface. It reproduces vegetatively via clonal growth and can quickly produce large amounts of biomass, doubling in size in as little as two days. Duckweed has a high protein content (25-35% of dry mass) and can be used to feed animals such as swine, poultry, and fish. In addition, duckweed cultivation can remove phosphates, ammonia, and nitrates from high-nutrient wastewater and aid the improvement of water quality while cultivating valuable biomass. Currently, duckweed tends to be harvested by hand from indoor and outdoor growth systems, which is time-consuming and labor-intensive. The present study describes the design and operation of a semi-automated system to harvest duckweed from a 500-liter indoor vertically stacked cultivation system. The harvesting system consists of a mechanical arm designed to gather approximately 40% of the duckweed surface cover, with the remaining 60% used to promote continued growth. Accordingly, the automated harvesting arm enables consistent duckweed harvesting while maintaining a stable area for further development. The developed robotic arm avoids regular labor-intensive human intervention, ensures the collection of specified mass amounts, and provides the clearance of a defined surface area to prevent overcrowding of the duckweed.

The harvesting system uses an Arduino microcontroller to control the motion of the duckweed collection arm powered by two servo motors. A load cell unit measures the harvested duckweed mass and displays this on an LCD screen. The individual arm parts were designed using SolidWorks software. The automated harvester uses the load cell to weigh the harvested duckweed upon collection. The mass of harvested duckweed is currently used to control the cycles of the harvesting arm. Once the mass exceeds a combined threshold value, then harvesting ceases. Proper duckweed harvesting prevents overgrowth and provides the duckweed with enough surface area to grow further. Future design iterations will incorporate optical feedback from the water surface to estimate the coverage area and decide upon harvesting cycles. This paper elaborates on the automated harvesting system's design, manufacture, and implementation.

***Keywords:*** duckweed cultivation, harvesting arm, process automation, microcontroller, load cell.

## 1. INTRODUCTION

A robotic arm was designed to harvest 40% of the duckweed surface cover in 3-4 cycles from a modulated stacked tank system to ensure continued duckweed growth. The main components of this system are: the robotic arm, which is mainly made of acrylonitrile butadiene styrene (ABS) and stainless steel, an Arduino microcontroller, 2 servo motors, one for the base movement of the arm, and the second motor for the movement of the end-effector/net-structure, a load cell to measure the mass of the duckweed harvested, and an LCD for displaying the measured mass. Timing for each harvesting event is controlled using the mass of the duckweed harvested. During the harvest, very little water (if any) should be taken out with duckweed because the same water is recirculated between the various tanks, stimulating the growth of the duckweed. The duckweed should be harvested using an automated arm and deposited into a receptacle. The movement of the arm is controlled using the motors. The mass of the harvested duckweed in the container is measured using a load cell arrangement connected to the controller. The measured weight of the harvested duckweed is displayed on the LCD screen. The amount of duckweed harvested controls the delay between harvesting cycles. That is, if the measured mass from the harvesting event is greater than the threshold of 0.17 kg, then the harvesting delay will be less than two days, whereas if the mass is less than the threshold value, then the delay will be for two days which ensures that there is a good amount of growth, with proper harvesting.

The process described above is for harvesting duckweed from a single tank. The robotic arm must be replicated to implement autonomous harvesting across all levels of the stacked system. This automated operation ensures fewer human interventions and reduces the required person-hours.

## 2. LITERATURE REVIEW

Duckweed is an aquatic plant that grows on the surface of the water and can be used to feed animals, poultry, and fish because of its high starch (10% -36% under specific conditions) and protein content (25-35%)(Cheng & Stomp, 2009; Ge *et al*., 2012; Körner *et al.*, 2003). Duckweed can absorb a large amount of nitrogen (ammonium or nitrate) and phosphorus. Swine wastewater produced in industries is sometimes released directly to waterbodies which is harmful to aquatic life. A practical method to solve this is to use

the duckweed to absorb the harmful nutrients. Thus, preventing the discharge into waterways. Recycling the nutrients which require the effective harvesting of the duckweed. It is also essential that duckweed covers the entire surface of the required water bodies to maximize nutrient absorption (Xu & Shen, 2011).

Duckweed can quickly absorb nutrients required for its rapid growth and is easy but labor-intensive to harvest. It is also efficient in impeding algal growth on the liquid. Experiments have shown that duckweed biomass has a considerable amount of starch content that can be used to produce methanol as a sustainable biofuel without prior thermal-chemical treatment. The process of methanol production is cheaper compared to other methods. The wastewater produced as a by-product from livestock or industries such as food processing, etc., can be used for the growth of the duckweed, thus preventing competition for fertilizers required for soil-based crops. Growth rates for duckweed depend on nutrient concentration and environmental conditions. Lemna minor is considered one of the top eight species of duckweed for the efficiency of its phytoremediation performance(Cheng & Stomp, 2009; Ge *et al*., 2012; Körner *et al.,* 2003; Xu *et al.,* 2012).

Duckweed naturally grows on slow currents, polluted waters, saline water, and eutrophic bodies(*Wst.1997.0207*, n.d.). The ideal pH range is 4.5-7.5. Anything more than a pH of ten will not support duckweed growth. The dense layer on the surface results in low oxygen content in water, minimizes interaction with wind and reduces evaporation. Harvested duckweed can be gathered and used for biofuel production, as a source of protein, or as fertilizers and compost for crops (*Wst.1997.0207*, n.d.).

Duckweed has a high ability to phytoremediate wastewater. Studies show that the growth rate does not directly depend on the actual light intensity, but light helps increase the protein content in the duckweed. Thus, there is a need to balance the cost of using high-intensity lights for duckweed farming in indoor conditions with yield benefits (Walsh *et al*., 2021). Water depth is another parameter that helps enhance the duckweed's growth and helps improve the absorption of nutrients (Zhao *et al.,* 2014). The Plant Ecophysiology group at the School of BEES team assesses the operational parameters of their indoor duckweed systems to optimize flow rates, water depths, and LED lighting regimes. For them, an automated harvesting arm represents the next step to developing these systems for industrial applications.

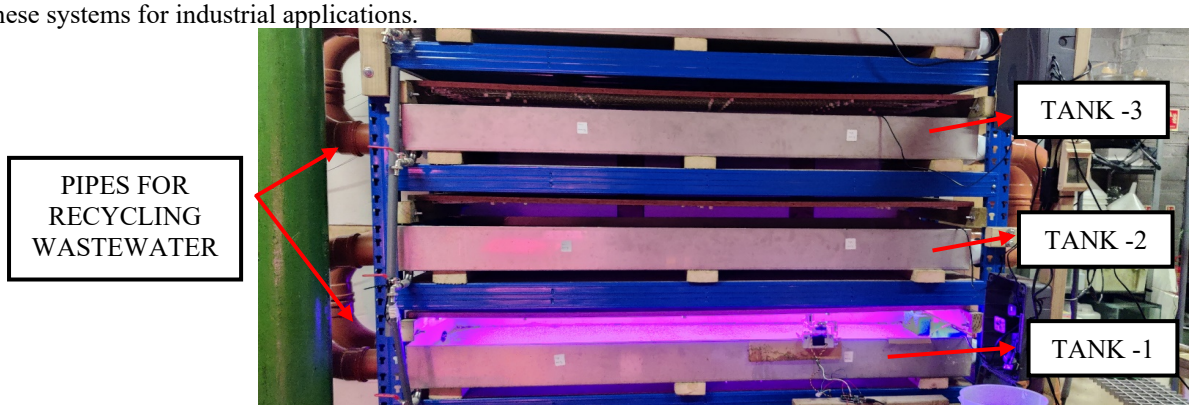


*Figure 1. Duckweed harvesting system at BEES lab UCC with each tank used for the growth of duckweed with led illumination and recycling wastewater*

Figure 1 shows the duckweed cultivation set up at the School of Biological, Earth, and Environmental Sciences (BEES) UCC. The wastewater is circulating continuously, ensuring that all the duckweed gets enough nutrients required for growth.

## 3. METHODOLOGY

The design requirement is to harvest duckweed from the tank's surface, equivalent to 40% of the surface area. The tank in which the duckweed is cultivated is shown in Figure 1. The duckweed with the wastewater has the natural tendency to flow towards the right based on the tank and recycling wastewater system. The harvesting arm moves in the opposite direction of the water flow, which helps in the better collection of the duckweed. The first servo motor moves the entire arm and removes the duckweed from the receptacle. The first servo motor is responsible for the movement within the tank, rotates the whole arm to the required destination, and returns the arm to the home position. The second servo motor makes the end effector contact the duckweed surface and drop the duckweed from its surface to the receptacle. The absolute control of the end-effector/net structure is with the second servo motor. A single harvesting cycle will not remove 40% of the surface area required for harvesting. It is necessary to complete 2-3 cycles to achieve the 40% target, thus providing the space for the continued growth of the duckweed. The harvesting logic is based on the number of days controlled using a load cell connected to the Arduino, which ensures a suitable delay is reached based on the amount harvested.

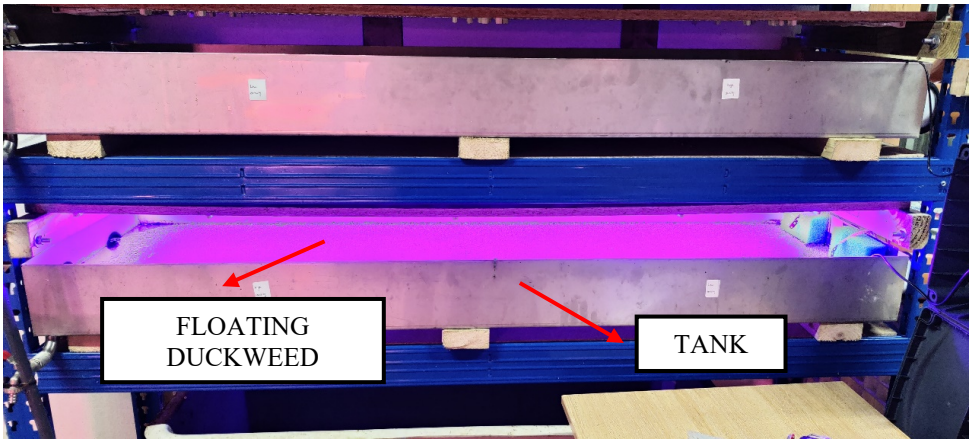


Figure 2. The harvesting arm is specifically designed for harvesting duckweed from this particular tank

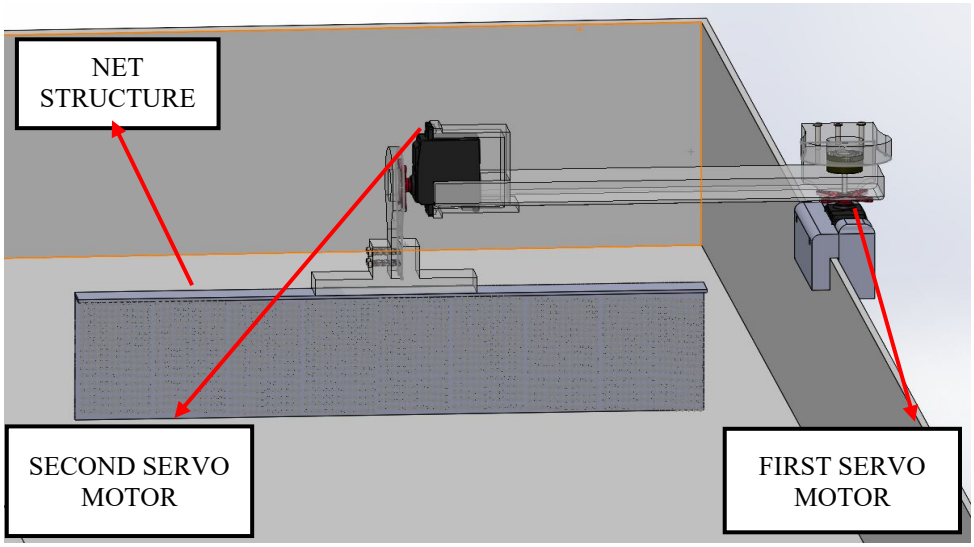


*Figure 3. Isometric view of the tank and automated arm designed using SolidWorks*

The duckweed harvested using the net structure is collected in a container. Mass cannot be measured directly from the arm because of the sticking nature of the duckweed. After each cycle, only a partial amount of the duckweed is collected in the container. Hence the mass of the duckweed in the container is measured using a load cell connected to Arduino. After each cycle, the mass of the deposited duckweed is calculated.

### *3.1 IMPLEMENTATION*

The algorithm controlling the harvesting arm

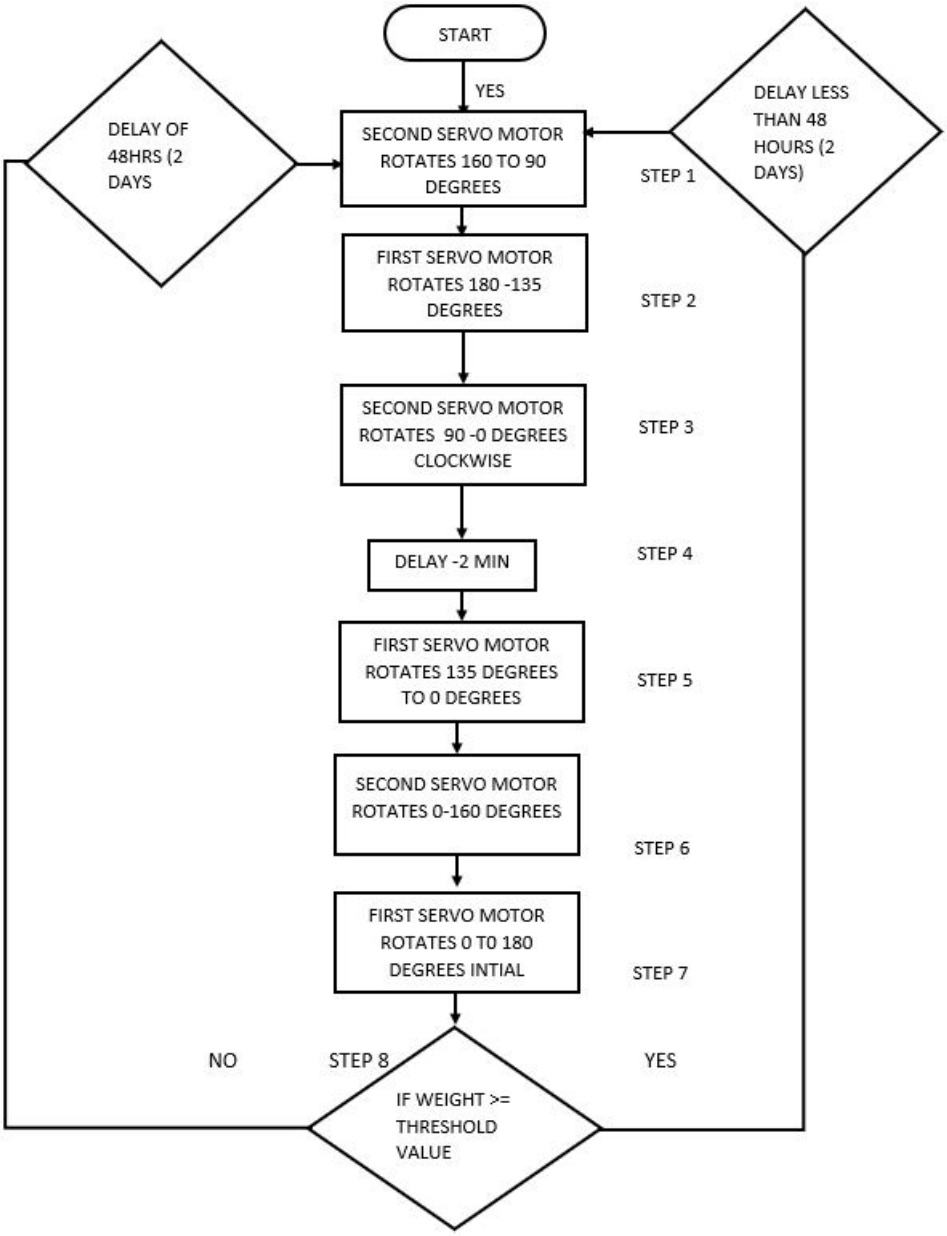


*Figure 4. Flow Chart of an algorithm for controlling the harvesting arm*

Step 1. End-effector/net structure to contact with duckweed surface– In Step 6, the net structure is at 160 degrees which was the last position of the servo, then rotates to 90 degrees, returning to the initial step and continuing with Step 1 based on the number of cycles. Step 5 and 6 is responsible for taking the arm to the home position.

Step 2. Rotating the arm to capture the duckweed - The net structure/end-effector is already in the water, as shown with the net structure's initial position perpendicular to the tank surface. The base rotates from 180 degrees to 135 degrees in an anticlockwise direction. The first servo motor is used for this purpose. This step helps in capturing the duckweed to the net structures.

Step 3. Lift the net structure from water - The end effector/ net structure rotates 90 degrees to 0 degrees clockwise. The second servo motor ensures this operation. The end effector side is again parallel to the water to make it available to move out of the tank. Step 1 and 2 ensures the duckweed is collected to the surface of the net structure.

Step 4. Drain the water from the end effector/net structure- A delay after Step 3 of approximately two minutes is given to ensure that the collected duckweed is free from the water media. The net structure has several holes that help drain the water from the harvested duckweed. One of the essential design criteria includes reducing the amount of water media taken out of the tank.

Step 5. Moving the arm outside the tank – After Step 1, the base servo rotates from 135 degrees to 0 degrees in the anticlockwise direction, from inside the tank to outside the tank. Using the first servo motor, the harvesting arm moves outside the tank.

Step 6. Empty the net contents into the receptacle- The end effector/net structure rotates 160 degrees in the anticlockwise direction to remove the duckweed collected using the second servo motor.

Step 7. Rotate the arm to the initial position - The base rotates 180 degrees clockwise using the first servo motor. It takes back to the initial place covered earlier by the servo. Movement of the arm from the receptacle back to the home position.

Step 8. Measuring the mass of the duckweed- The captured duckweed in the receptacle is weighed using a load cell and displayed on an LCD screen. Once a cycle of three iterations is completed, the mass measurement is compared to the threshold value, deciding the delay required for the following cycle, thus varying the time at which the duckweed is harvested.

The testing was conducted in four stages for the harvesting arm, and the final stage was conducted at the School of BEES laboratory, as shown in Figure 5.

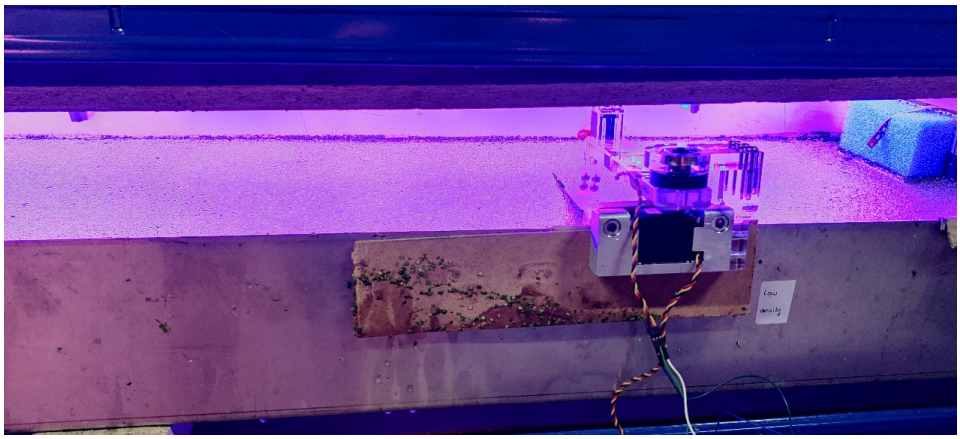

*Figure 5. The harvesting arm is clamped onto the tank as part of the prototype testing phase.*

Figure 5 shows that the arm is clamped to the tank, which can be tightened. The net structure is dipped in the water with duckweed which is considered the first step of the algorithm. Further, the Arduino controller is connected to both the servo motors. The testing of the harvesting was conducted, and the following improvements were made.

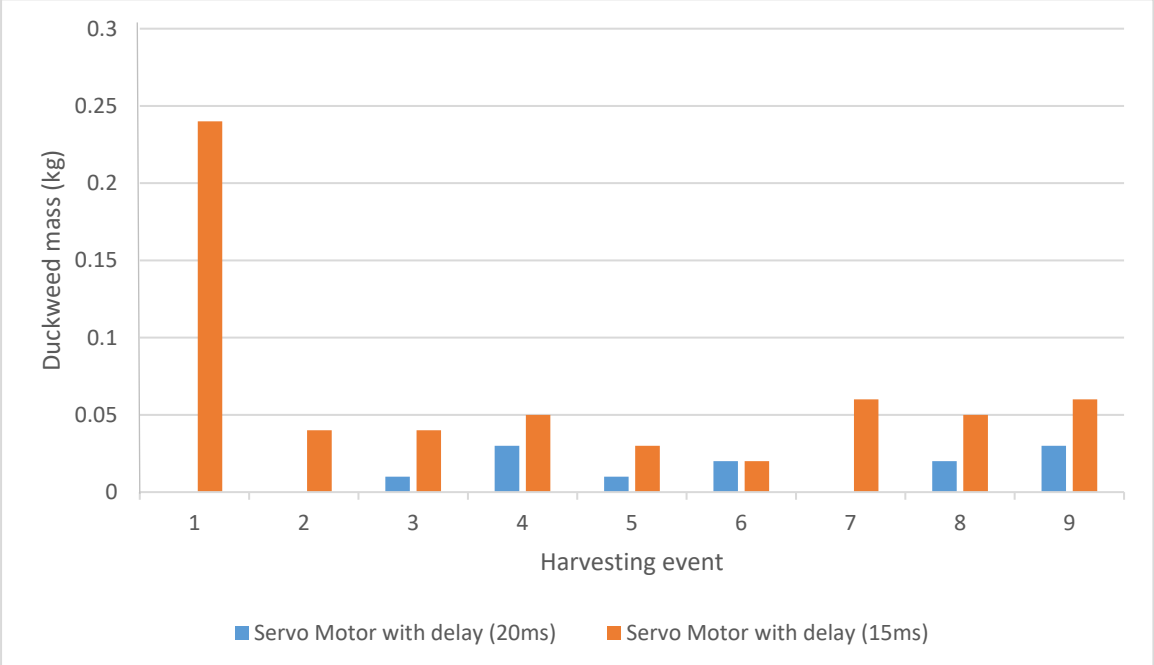

- The first three steps of the algorithm or code involved capturing the duckweed. A delay is provided in the Arduino code, which is the waiting time for the servo to reach the position. By default, the value is 20ms, which is then varied (15ms) to get the maximum rotation speed with the required accuracy, resulting in better performance. Based on the testing shown in figure 6, the rotation speed was increased by reducing the delay to collect more duckweed effectively. Slow rotation can result in pushing the duckweed in the opposite direction. Hence the speed of rotation was varied.

- Step 6 in the algorithm or code is where the second servo rotates and drops the duckweed in the receptacle. Now the rotation speed is increased with the help of delay time 5ms by default 20ms which is the waiting time of the servo to reach a particular position, rotation speed which is vital for the process, controlled using delay in milliseconds. Thus, improving the overall performance of the harvesting arm using the Arduino code.
- Delay, the algorithm's third step, as an initial requirement, is necessary to ensure water media is not taken outside the tank. For this purpose, a delay of One minute was changed to two minutes to drain most of the water content in the tank itself without taking it outside.

The mass measurement setup included the load cell for measuring the mass of the duckweed. The output of the load cell is in less voltage range. Hence, an amplifier (HX711) connects to the Arduino board. The testing connection is set up as per the details given in Table 2. The setup is shown in Figure 7.

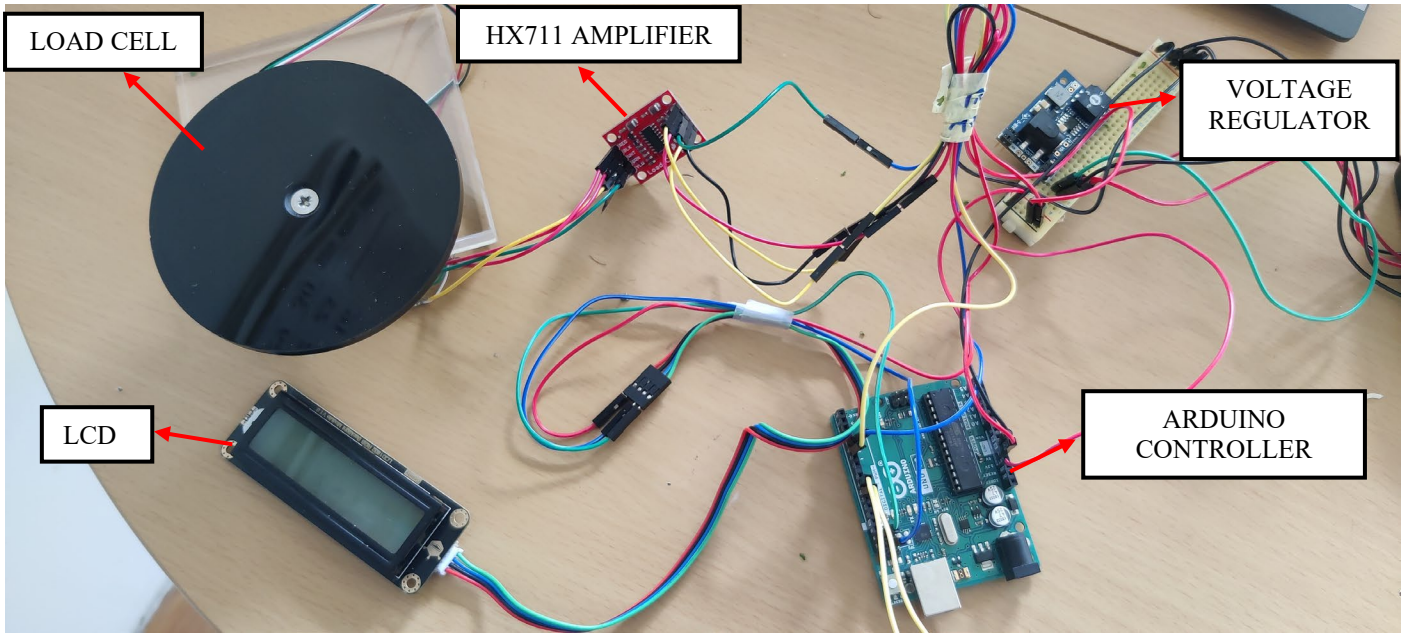


*Figure 7. Load cell connection to the Arduino with an HX711 amplifier for mass measurement and LCD for the mass display*

## 4. RESULTS

Factors that helped to improve duckweed harvesting are given below.

1. Duckweed sticks to any surface and is difficult to remove once the water gets drained. The net structure was changed to a thin stainless-steel material to capture most of the duckweed, reducing the duckweed's sticking property.
2. The positioning of the harvesting arm and the clamping is adjusted to perform better during the harvesting event.
3. The initial selection of motor was not suitable for operation. HS-5645MG servo motors are currently used that provide more than the required torque and help in the smooth operation
4. The accuracy of the motor is checked and changed initially during the prototype test using a DPC-11 servo programmer. Further, based on the requirement in each algorithm step, the Arduino code was modified to achieve the best result.
5. As shown in figure 8, the initial study shows that the rotation speed is directly proportional to the amount of duckweed collected by the harvesting arm. The rotation rate for each step in the algorithm is ideally 20 seconds. Reducing that to 5 sec can result in a faster rotation pace with the required accuracy and performance.

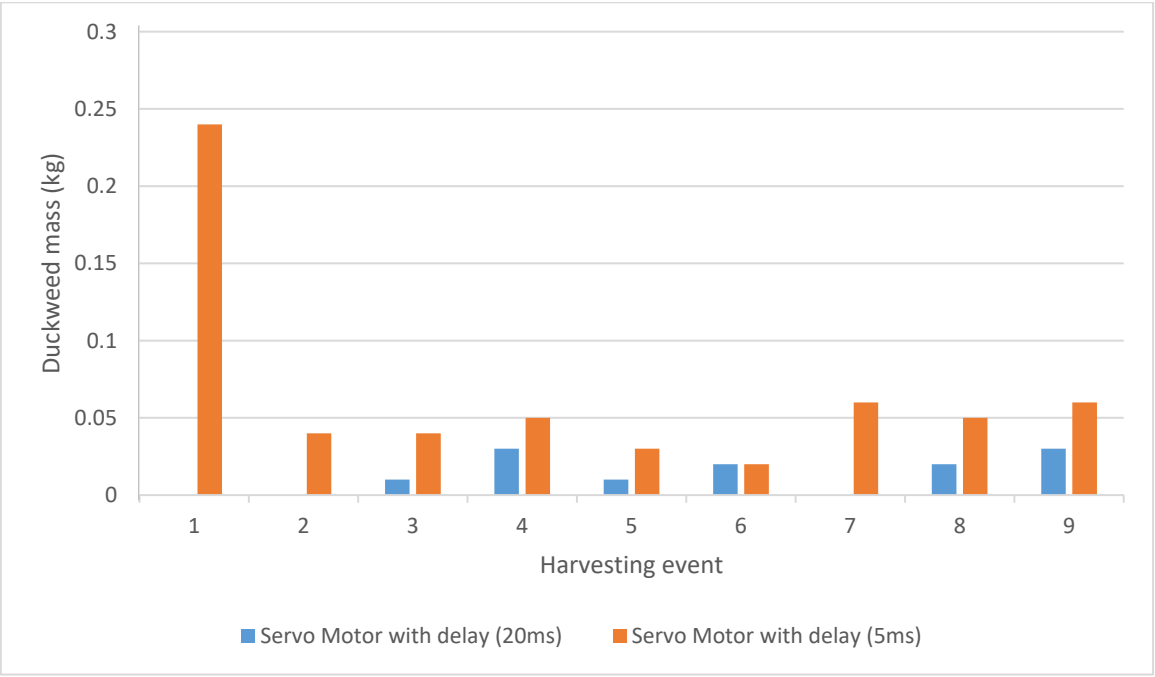


*Figure 8. Comparison of the duckweed harvest before and after delay time changes for dropping duckweed to the receptacle*

6. A voltage regulator was added for an accurate, current supply for the servomotors, improving the duckweed harvest accuracy.

As shown in figure 8, the mass collected before the changes is less than 50 grams with a target of 170 grams. Table 1 shows the harvesting arm's consistency and performance after improving the abovementioned factors. The mass of duckweed collected has improved with a median value of 130 grams.
The consistency of the harvesting arm is measured further and shown in the table. It gives the amount of duckweed collected from each harvesting event for the first time with the tank filled with duckweed to the maximum amount, conducted nearly seven times, thus clarifying the arm's harvesting capabilities. The harvesting target is about 40 percent which is 0.17 kg or 170 grams. With present design and logic, it can achieve a value close to 130 grams ( median value).
Harvesting close to 130 gm results in harvesting every 1 day since it is not exceeding more than 170 gm.

*Table 1. Mass of duckweed harvested (kg) for the first time with a fully covered duckweed tank surface*

| HARVESTING CYCLE NO. | MASS OF DUCKWEED HARVESTED (kg) |
|---|---|
| 1 | 0.13 |
| 2 | 0.10 |
| 3 | 0.12 |
| 4 | 0.15 |
| 5 | 0.11 |
| 6 | 0.14 |
| 7 | 0.15 |

The graph shows the amount of duckweed harvested in 9 harvesting events, each consisting of 3 cycles. Along the x-axis is the number of harvesting events. Along the y-axis is duckweed mass in kg. The graph clearly shows that the first harvest is critically essential and contributes the maximum amount to the harvesting. Each harvesting cycle is expected to harvest nearly 40 percent, which is 0.17kg or 170 gm( target mass). Based on the initial prototype model and logic, the amount collected is less than the target amount. The basic logic is that if the amount harvested is less than 40 percent, harvesting happens after 24 hours. If the duckweed harvest is more than 40 percent, then harvest occurs after 48 hours. The variability in the amount of duckweed harvested is mainly because of the following reasons.

- Sticking nature of the duckweed - Duckweed tends to stick to most of the surface, including the net structure of the harvesting arm. The technique used is to collect more duckweed over less surface area. So, duckweed overlaps and helps to drop the entire net structure's content into the receptacle. If the duckweed collected has a single layer on the net structure, then the amount of mass collected will be significantly less.

- Variation in duckweed growth- If the duckweed is harvested at regular intervals. It can provide the necessary surface area for growth. And fast growth of duckweed can result in a better collection of duckweed.

Figure 9 shows that the first harvest is the most critical and the amount of duckweed harvested continuously for a day. The mass was collected during each harvest with a delay of 2 minutes instead of 48 hours. If the mass exceeds the target mass, the delay is 5 seconds instead of 24 hours. The delay time is varied for testing purposes. It was clear that the first harvest was higher than the other, and the variation is mainly because the harvesting was done continuously in a day.

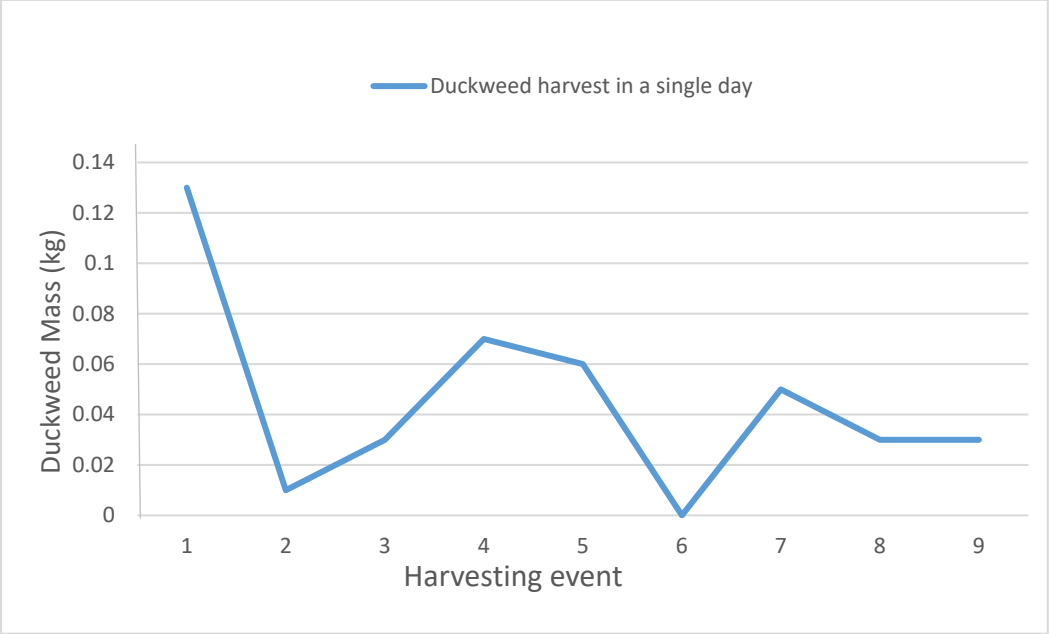


*Figure 9. Mass of duckweed collected continuously in a single day*

## 5. DISCUSSION

The design started with understanding the physical requirements, such as the area to be harvested, space available for the arm to be placed, etc. Then essential solid works tools were used to create a mechanical model that would suit the harvesting application, which had many challenges since the only input for the arm's design is the tank's dimension. So, the dimensions of many parts needed to be assumed and visualized based on the tank dimensions. There were many limitations, including the space available for the arm because it needed to be placed between the stacked tanks. The developed model was built to overcome all these challenges. Once the solid works model was built, which gave an idea of the arm's mass, including the entire component and duckweed. Testing with mass helped formulate the torque requirement and the selection of a particular dc motor for the harvesting arm. Moment and rotation were the first visualized, which helped derive the design and algorithm.

Problems faced include the actual torque requirement of the arm, the resistance of the water when the component is in contact, the out-of-box range of rotation for the motor not matching with the specification, large part of the mass concentration on the base servo motor shaft, and the sticking nature of duckweed.

The key accomplishments include developing a robust mechanical design in solid works following modifications during the various stages of prototype testing, selecting, and testing the motor for the harvesting arm, and transforming the programming in the servo. Comprehensive component testing was completed and underpinned the manufactured model, motor, and Arduino integration. Furthermore, improvements were made to increase the overall efficiency of the duckweed harvesting process. A mass-based measurement system using the load cell and LCD has also been developed. Integrating the measured mass with the harvesting algorithm allows refined control of the days of harvesting cycles. Integration is done on the Arduino controller side.

The tested and designed harvesting arm can achieve the initial objective of 170 grams (40 percent). It also provides options to control the harvest if the mass is less or more than the target mass using an Arduino controller, making it suitable for the application. Further gives an option to add optical techniques to the system. Exact growth accuracy could be monitored with optical techniques. However, the system won't benefit significantly compared to the current tested technique because the controller allows adjusting the harvesting event based on mass collected during each harvesting event that is used as feedback for

the next event. Thus, providing maximum flexibility using the current technique for the harvesting application. The automated harvesting arm thus helps avoid human intervention and regular duckweed harvesting, reducing the man-hours required for the entire duckweed collection process. This system can be replicated for different tanks with minimal cost, making it suitable for the application. If there are Hundreds of tanks, the time for harvest and man-hours saved could be enormous. The automated arm thus helps control the harvesting cycles, preventing overgrowth and eliminating the workforce.

## 6. REFERENCES


Cheng, J. J., & Stomp, A. M. (2009). Growing duckweed to recover nutrients from wastewaters and for production of fuel ethanol and animal feed. *Clean - Soil, Air, Water*, *37*(1), 17–26. https://doi.org/10.1002/clen.200800210

Ge, X., Zhang, N., Phillips, G. C., & Xu, J. (2012). Growing Lemna minor in agricultural wastewater and converting the duckweed biomass to ethanol. *Bioresource Technology*, *124*, 485–488. https://doi.org/10.1016/j.biortech.2012.08.050

Körner, S., Vermaat, J. E., & Veenstra, S. (2003). The Capacity of Duckweed to Treat Wastewater. *Journal of Environmental Quality*, *32*(5), 1583–1590. https://doi.org/10.2134/jeq2003.1583

Walsh, É., Kuehnhold, H., O'Brien, S., Coughlan, N. E., & Jansen, M. A. K. (2021). Light intensity alters the phytoremediation potential of Lemna minor. *Environmental Science and Pollution Research*, *28*(13). https://doi.org/10.1007/s11356-020-11792-y

*wst.1997.0207*. (n.d.).

Xu, J., & Shen, G. (2011). Growing duckweed in swine wastewater for nutrient recovery and biomass production. *Bioresource Technology*, *102*(2). https://doi.org/10.1016/j.biortech.2010.09.003

Xu, J., Zhao, H., Stomp, A. M., & Cheng, J. J. (2012). The production of duckweed as a source of biofuels. In *Biofuels* (Vol. 3, Issue 5). https://doi.org/10.4155/bfs.12.31

Zhao, Y., Fang, Y., Jin, Y., Huang, J., Bao, S., He, Z., Wang, F., & Zhao, H. (2014). Effects of operation parameters on nutrient removal from wastewater and high-protein biomass production in a duckweed-based (Lemma aequinoctialis) pilot-scale system. *Water Science and Technology*, *70*(7). https://doi.org/10.2166/wst.2014.334

# Reconfiguration of quality inspection approach to the food processing industry

Chengsi Lin, Muhamad Arfauz A Rahman, and Paul G. Maropoulos,
*School of Mechanical and Aerospace Engineering, Queen's University Belfast*

***Abstract***

On the production line, the inspection process is crucial to shorten the product's production cycle and improve productivity and quality. In the era of continuous advancement of the industrial revolution, enterprises face many difficulties and challenges in developing the world's equipment manufacturing industry, especially in terms of technology and economy. To this end, an automatic inspection system based on a charge-coupled devices (CCD) camera and laser scanner is proposed to replace the previously time-consuming and error-prone manual inspection schemes. As an important part of the production process, the inspection system has great potential for improvement. To build the system more rationally, the work first investigates the current manufacturing manual inspection process, exploring alternatives to the current manual inspection process in manufacturing. The inspection system is then designed according to the selected sandwich automated production line. CCD cameras and image processing modules are used to inspect the coverage of sandwich fillings, while the three-dimension (3D) scanner is used to measure whether the height of the fillings meets the standard. To verify the system's viability, the design used Siemens software Process Simulate to simulate a production line designed with Solidworks. By recording the time of each stage and comparing the results of the two simulations, the automatic inspection of each production cycle is reduced by about 6s compared to manual inspection. The improved production line requires only one mobile worker to inspect and modify image processing programs. A cylinder and jacking frame are also installed underneath the inspection system, which can quickly push out unqualified products. The simulation results of the production line met expectations, and the feasibility of the system will be further verified later by the construction of a virtual production environment.

*Quality, Inspection system, CCD camera, 3D scanner, manufacturing industry.*

## 1. INTRODUCTION

With the advent of the era of the Fourth Industrial Revolution, many enterprises and manufacturers are facing great opportunities and challenges. On the one hand, the increase in demand gives enterprises more excellent prospects for development. On the other hand, the competitive pressure enterprises face has also significantly increased. The most priority issue for enterprises and manufacturers is how to speed up production, ensure production quality, and save costs.

Traditional industrial production lines are composed of many technical tools and processing methods. It is used to complete a series of operations such as assembly, processing, testing, and analysis of products. After investigation, it was found that workers generally inspect the products with their naked eyes or other testing tools. This test method is not only time-consuming, but often, its test accuracy cannot be guaranteed. Therefore, the inspection system on the production line has become a link that needs improvement. And to respond more quickly to market changes, reduce the number of steps in the engineering and manufacturing stages, reduce part and product costs, and reduce the time to market for products, many enterprises have begun to establish global communication networks to advance digital manufacturing. Virtual environments can quickly obtain high-precision and real-time 3D simulations to evaluate and optimise manufacturing processes (Wang, 2009).

This research proposed using CAD software to reconstruct the inspection system on the production line, design an automatic inspection system, and preliminarily verify its feasibility through simulation. A complete production line will be built using a virtual environment later in the experiment, further optimising the designed system and demonstrating its feasibility and optimisation quality.

Email: Chengsi Lin
clin08@qub.ac.uk

## 2. LITERATURE REVIEW

### *2.1. Inspection process*

Generally, the inspection process is divided into physical properties, quantitative measurement, and intelligent product quality testing (Liu et al., 2016). Quantitative measurements include inspection morphological characteristics such as product size, shape, and colour. Qualitative testing is mainly aimed at some images that are difficult to capture, separating the product to be inspected from the background of the image.

### *2.2. Manual inspection methods*

Manual inspection methods typically involve one or more workers testing products using their naked eye or other measuring tools. As shown in Table 1, the accuracy of manual inspection and judgment depends on many factors, and the efficiency and accuracy of manual inspection is lower than that of automated inspection (See et al., 2017). Therefore, many manual inspection links are gradually replaced by automated inspection systems.

*Table 1. Factors impacting inspection performance (See et al., 2017)*

| Task | Individual | Environmental | Organisational | Social |
|---|---|---|---|---|
| Defect rate | Defect rate | Lighting | Feedback | Pressure |
| Defect type | Age | Noise | Training | Isolation |
| Defect salience | Visual Acuity | Temperature | Retraining | Consultation |
| Defect location | Intelligence | Shift Duration | Instructions | Communications |
| Complexity | Aptitude | Time of day | Incentives | |
| Standards | Personality | Vigilance | Job Rotation | |
| Overlays automation | Time in job | Workplace design | Feedforward Information | |
| Multiple inspections | Experience | | Management support | |
| Pacing | Visual lobe | | | |
| | Scanning strategy | | | |
| | Biases | | | |

### *2.3. Common automated inspection system design schemes*

In the past decade, mechanical, ultrasonic, and electrical methods have been gradually replaced by non-contact optical vision inspection (Hanh & Hieu, 2021). For quantitative inspection systems, the most used device is an RGB camera with laser inspection capabilities. The simplest and fastest inspection method is to examine the grayscale and RGB pixel values, match them in the form of a pixel matrix, find out the ratio of the original area length to the number of pixels, and set thresholds and compare (Khan et al., 2005). And Barth et al. (2007) place the camera in a static position and viewing angle perpendicular to the conveyor measuring area to build an automated inspection system that measures the length of the heat shrink tubing, the layout of the system is shown in Figure 1. The camera operates in continuous mode and averages continuous measurements of the tube length. The measurement results are evaluated based on the given target length and tolerance.

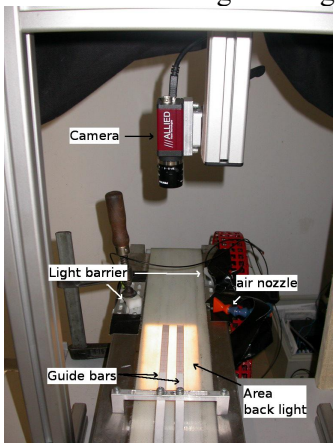


*Figure 1. Automated inspection system for measuring the length of heat shrink tubing (Barth et al.，2007)*

In recent research, new processing methods such as projection, filtering, and computer-based intelligent learning have replaced template matching and image subtraction, especially in qualitative measurements. The most popular sensors in image acquisition analysis are Charge-Coupled Devices (CCD) and frame grabbers (Kumar &Kannan, 2010). In addition, semiconductor is also widely used in visual inspection progress. Rahman et al. (2019) optimised the semiconductor inspection scheme's parameters and determined the setting range of the parameter values, avoiding excessive exclusion and significantly improving productivity. While in terms of deep learning, the development of artificial intelligence is also gradually being applied to production systems. Future research will also increasingly develop automated inspection systems based on the computer learning to define product grades based on the traits inspected by the algorithms written.

### *2.4. 3D Scanner*

3D scanning is a cutting-edge metrology method that enables the digital reconstruction of surface shapes with high precision and accuracy (Wang et al., 2021). Most current 3D scanners are simulated time-of-flight (TOF) scanners, which are programmed in C++, rendered in 3D graphics using Direct 3D 11.0, and vector algebraic calculations using the DirectMath library (Kot et al., 2021). Due to the maturity of 3D scanner products, many designers are also considering using 3D scanners as inspection instruments. 3D scanners directly capture 3D information about objects by relying on sensors that rely on artificial light or pattern projection, making it easier to reshape models and analyse their structural defects in the computer (Khries, 2021). Han et al. (2018) integrates industrial robots and stripe-based 3D scanners that take advantage of their high speed and ability to measure free surfaces, performing phase measurement profile measurements based on the repeatability of the robot's motion. This provides a precedent for 3D scanners for product inspection.

### *2.5. Digital manufacturing*

Weerabahu et al. (2021) proposed that the Concept of Industry 4.0 in manufacturing or digital manufacturing supply chains can be designated as a network of integrated collaborative systems that respond in real-time to meet the conditions and needs of a dynamic supply network from product design to logistics processes. And virtual manufacturing environments offer more options. Virtual manufacturing systems are used for a variety of purposes such as designing shop floor layouts, estimating control strategies, scheduling, testing control procedures, simulating in-plant operations, etc., to meet human-machine collaborative solutions, effectively interact with proposed designs early in the development cycle, and avoid costly tool replacements during the development cycle (Hanwu et al., 1996).

## 3. METHODOLOGY

### *3.1. Original production line*

Further advanced by the authors' previous research (Lin et al., 2022). Select a semi-automated sandwich production line for improvement. As shown in Figure 2, The workflow of the original production line is to let the robot arrange the bread from the feeding mechanism to the conveyor belt in turn, and then the conveyor belt transports the bread to the first inspection link, and the machine confirms whether the position angle and size of the bread are uniform. Then, the filling machine coats the bread occasionally, and the staff needs to confirm the amount of bread covered and whether the filling completely covers the entire bread. After manual inspection, the machine covers the unpainted bread on the stuffed bread and then cuts it in half and folds it diagonally. Finally, the robot moves the sandwich to a packaging mechanism for packaging and storage. The inspection part of the production line is carried out by two workers with their eyes, using their experience to determine whether the products on the production line meet the quality requirements. This inspection method is relatively crude, leading to more non-compliant products, and the production efficiency of the product will not match the current market demand. The research will reconstruct an automated inspection system on this production line.

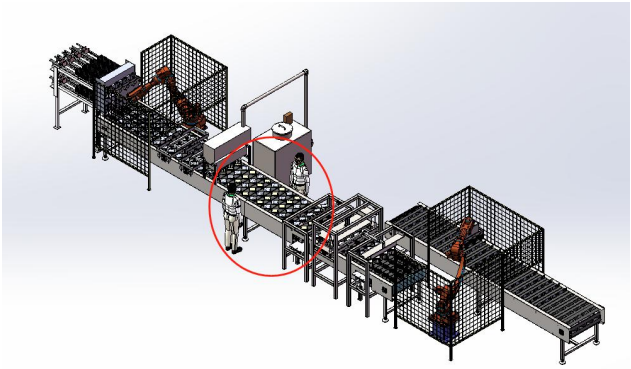

*Figure 2. The original sandwich production line*

### *3.2. Design of automated inspection systems*

*3.2.1. design of filling coverage and thickness inspection system*

Based on an understanding of the sandwich production process, it can be concluded that the sandwich line inspection process is mainly to check whether the quality of the filling (assumed to be cream in this research) meets the label. And it can be divided into two aspects: the coverage and the thickness of the filling, which is the same as the inspection method of the human eye. As shown in figure 3, the coverage inspection section mainly comprises CCD cameras and image processing modules. The photoelectric sensor is triggered when the sandwiches arrived below the CCD camera. The sensor feeds the signal back to the CCD camera, which will take a clear picture of the sandwich and upload it to the image processing module. The image processing module uses a processor to perform high-speed calculations to de-denoise, marginalise and enhance the picture, and compares the coverage of the filling with the surface of the bread to measure the percentage of the filling coverage. The addition of LED ring lights makes the resulting image sharper and easier to distinguish inspected items from the background. The system also adds an LCD controller and touch screen to realise better human-computer interaction, which can obtain real-time feedback and quickly adjust the inspection program. The product will be transferred to the filling thickness inspection system when the filling coverage test is complete. The 3D scanner will perform a comprehensive scan of the products on the production line, and the computer uses CAD software to quickly reconstruct and analyse the model, measure the thickness of the filling, and mark the sandwiches that do not meet the standard.

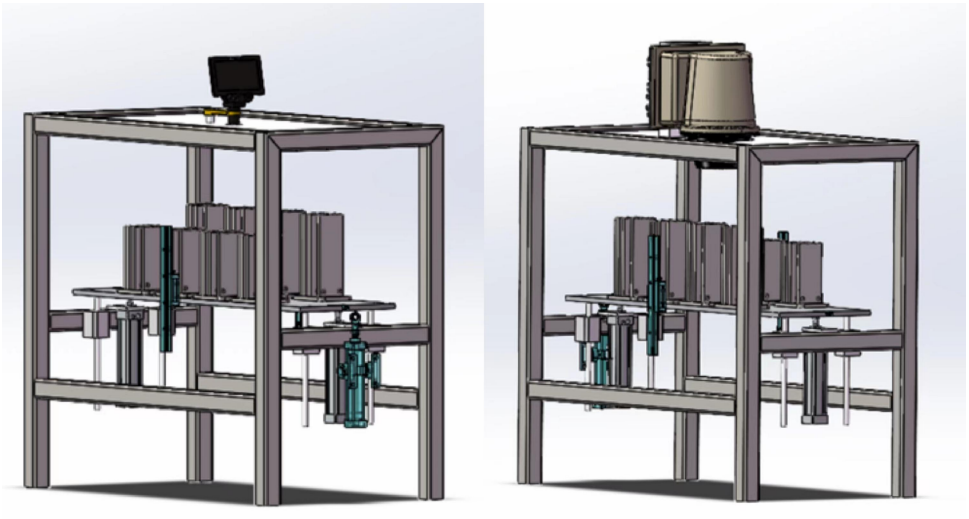

*Figure 3. Filling coverage and thickness inspection system*

*3.2.2. Recording and rejection of defective products*

The system position located under the conveyor belt is also equipped with a cylinder and a jacking frame, if a defective product is inspected, the PLC count is triggered to calculate the location of residues in the inspection system accurately, and the control system PLC will send a high-level signal to the solenoid valve, the cylinder that receives the signal can be pushed out, and the top frame can be raised to achieve the purpose of pushing out

the defective products. At the same time, historical alarm information will also be stored and generate data reports.

### *3.3. Assembling and simulation of the production line*

Assemble the designed inspection system onto the original production line and remove the workers (see Figure 4). The CAD file is converted into a COJT modular file and imported into the Siemens software Tecnomatix Process Simulate for position adjustment and reassembly. As shown in Figure 5, each module of the production line is designed according to its workflow, and each link's motion trajectory is optimised. The efficiency of the automated inspection system is preliminarily verified by comparing the production cycle of the original and optimised production lines.

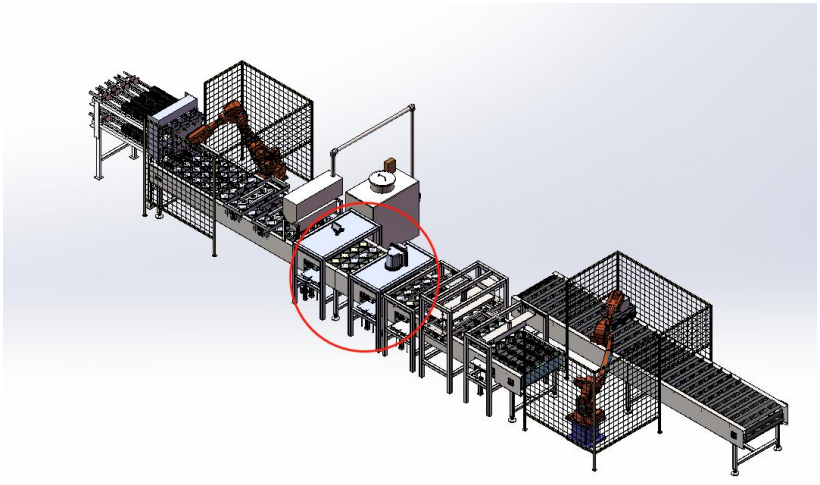

*Figure 4. The optimised auto production line*

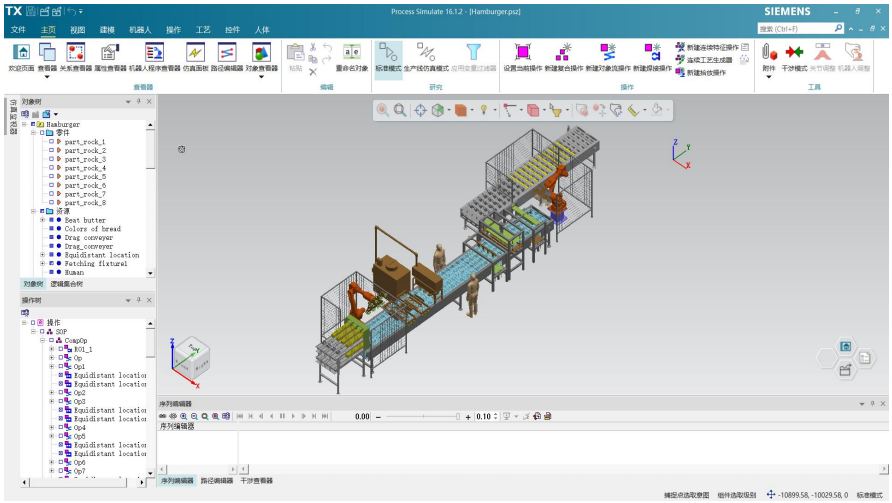

*Figure 5. Simulation of the production line*

### *3.4. Build a virtual manufacturing environment*

In future tests, it is planned to introduce the production line into virtual reality glasses to build a virtual manufacturing environment. Then, using the virtual environment, the efficiency and accuracy of the automated inspection are further compared and optimised.

## 4. RESULTS AND DISCUSSION

### *4.1. Cycle time*

As shown in Table 2, by recording the cycle time of the production line to simulate production, it can be clearly seen that the inspection time of the new inspection system is 6 seconds faster than the original manual inspection. If a defective product is found during the production process, the time to launch the defective

product is about 2 seconds, the total cycle time will be 56-58 seconds. This means that the optimised line can save 2-6 seconds per cycle, which significantly improves the production efficiency of sandwiches that need to be mass-produced.

*Table 2. Compare simulation runs without and with the automated inspection*

| STEP | RUN | TIME (WITHOUT AUTOMATED INSPECTION) | TIME (WITH AUTOMATED INSPECTION) |
|---|---|---|---|
| 1 | The robot places the bread on the production line | 6s | 6s |
| 2 | The machine confirms that the position angle and size of the bread are uniforms | 6s | 6s |
| 3 | The filling machine coat the bread | 6s | 6s |
| 4 | Inspection | 14s | 8s |
| 5 | The machine covers the unpainted bread over the stuffed bread | 8s | 8s |
| 6 | The robot cuts the sandwich in half | 6s | 6s |
| 7 | The machine folds the sandwich, and then the robot transports it to the packaging and storage area | 14s | 14s |
| | Total | 60s | 54s |

### *4.2. Inspection accuracy*

Since the shape of the sandwich bread during the inspection phase is square, and the side length of each loaf of bread is 121±0.5 mm. The addition of the image processing module can segment the image according to the threshold, distinguish the inspected object from the background, and use the resolution to calculate the surface area of the inspected object by using the resolution of the processed image information. And the sandwich filling thickness standard set by the production line is 5mm±0.5mm, which is a smaller range, and it is difficult to make accurate judgments based on the inspection angle where the workers are located. The 3D scanner can scan a whole working area of the product and accurately capture the characteristic information of the product to complete the reconstruction, measuring whether the volume and thickness of the filling meet the standard. The error between the obtained data and the actual situation is minimal, almost reaching the nanometre level.

### *4.3. Human resources*

The original production line required two workers to inspect the products on the production line, while the inspection part of the improved production line was wholly completed by equipment. The line only requires a technician periodically or when the line alarms the system's program and to recycle defective products. In the "Industry 4.0" era, companies need to pay substantial financial and material resources to recruit and train excellent employees, and the ability of employees need to match positions to maximise work efficiency and quality results. Therefore, when machine inspection can replace manual processes, the waste of human resources can be avoided. In the long run, this can also save companies and producers a lot of money.

### *4.4. Obstacles to image processing and digital manufacturing*

When inspecting the surface coverage of a sandwich fill, if the grey value of the captured image fill is uneven with the background or the colour of the two is too close, the image processing module has a hard time distinguishing the inspected object from its background. And due to manufacturers and partners may employ different computer design systems, they cannot read each other's data, so the connection between companies and customers is challenging. Companies are hesitant to embrace the need for the level of interoperability required between many different systems. Examples of interoperability crashes are common in today's CAD systems, and the flow of information between design and manufacturing is frustrating.

## 5. CONCLUSIONS

The construction of food inspection systems is a diverse field of research. This study reconstructs a new set of automated inspection systems through the recent investigation and understanding of manual and automatic inspection systems. The system replaces traditional manual inspection methods with CCD cameras, image processing modules and 3D scanners as the primary inspection components. After preliminary verification, the inspection system can increase the cycle of the production line by 2-6 seconds. At the same time, it can ensure the accuracy of the inspection and reduce the waste of talents. The design conforms to the sandwich filling quality inspection process, is highly scalable, easy to understand and upgrade, and meets the design requirements. The level of accuracy improvement brought by the 3D scanner and the actual operability of the inspection system on the production line requires the subsequent construction of a virtual manufacturing environment and further testing and adjustment.

## 6. ACKNOWLEDGMENT

The authors are grateful to the academic and technical staff in the School of Mechanical and Aerospace Engineering, Queen's University Belfast, for providing materials support and other helpful information. Special thanks to Siemens Ltd. China software development department for providing software (process simulate) to complete the project.

## 7. REFERENCES

Barth, A., Herpers, R., & Greßnich, M. (2007, September). Real-time applicable visual quality control in industrial line production. In 2007 IEEE/ASME international conference on advanced intelligent mechatronics (pp. 1-6). IEEE.

Han, L., Cheng, X., Li, Z., Zhong, K., Shi, Y., & Jiang, H. (2018). A robot-driven 3D shape measurement system for automatic quality inspection of thermal objects on a forging production line. Sensors, 18(12), 4368.

Hanh, L. D., & Hieu, K. T. G. (2021). 3D matching by combining CAD model and computer vision for autonomous bin picking. International Journal on Interactive Design and Manufacturing (IJIDeM), 15(2), 239-247.

Hanwu, H., Youlun, X., Shuzi, Y., & Bo, W. (1996, December). Virtual manufacturing systems and environment. In Proceedings of the IEEE International Conference on Industrial Technology (ICIT'96) (pp. P13-P24). IEEE.

Hopkins, E., & Siekelova, A. (2021). Internet of Things Sensing Networks, Smart Manufacturing Big Data, and Digitized Mass Production in Sustainable Industry 4.0. Economics, Management & Financial Markets, 16(4).

Khan, U. S., Iqbal, J., & Khan, M. A. (2005, October). Automatic inspection system using machine vision. In 34th Applied Imagery and Pattern Recognition Workshop (AIPR'05) (pp. 6-pp). IEEE.

Khries, H. M. (2021). Photogrammetry versus 3D scanner: producing 3D models of museums' artifacts. Collection and Curation.

Kot, T., Bobovský, Z., Heczko, D., Vysocký, A., Virgala, I., & Prada, E. (2021). Using Virtual Scanning to Find Optimal Configuration of a 3D Scanner Turntable for Scanning of Mechanical Parts. Sensors, 21(16), 5343.

Kumar, D. P., & Kannan, K. (2010). A roadmap for designing an automated visual inspection system. Int. J. Comput. Appl, 1(19), 34-37.

Lin, C., Rahman, M. A. A., & Maropoulos, P.G. (2022). Enhancing the quality inspection process in the food manufacturing industry through automation. CODIT 22.

Liu, J., Tang, Z., Zhang, J., Chen, Q., Xu, P., & Liu, W. (2016). Visual perception-based statistical modeling of complex grain image for product quality monitoring and supervision on assembly production line. Plos one, 11(3), e0146484.

Rahman, M. A. A., Rahman, M. H., Mohamad, E., Rahman, A. A. A., Salleh, M. R., & Mo, J. P. (2019). Enhancing the automated quality inspection in manufacturing process through parameter optimisation. system, 5, 6.

See, J. E., Drury, C. G., Speed, A., Williams, A., & Khalandi, N. (2017, September). The role of visual inspection in the 21st century. In Proceedings of the Human Factors and Ergonomics Society Annual Meeting (Vol. 61, No. 1, pp. 262-266). Sage CA: Los Angeles, CA: SAGE Publications.

Wang, L. (2009). Subdivision-based digital geometry processing as a fundamental building block of digital manufacturing. International Journal of Production Research, 47(3), 687-702.

Wang, R., Law, A. C., Garcia, D., Yang, S., & Kong, Z. (2021). Development of structured light 3D-scanner with high spatial resolution and its applications for additive manufacturing quality assurance. The International Journal of Advanced Manufacturing Technology, 117(3), 845-862.

Weerabahu, W. S. K., Samaranayake, P., Nakandala, D., & Hurriyet, H. (2021, December). Enabling Factors of Digital Manufacturing Supply Chains: A Systematic Literature Review. In 2021 IEEE International Conference on Industrial Engineering and Engineering Management (IEEM) (pp. 118-123). IEEE.

# Object pose and centroid analysis for automated material handling.

Dylan Do Couto, Queen's University Belfast
Joseph Butterfield, Queen's University Belfast
Adrian Murphy, Queen's University Belfast
Karen Rafferty, Queen's University Belfast
Joseph Coleman, Combilift

***Abstract***

Continual advancements of automation made in manufacturing and logistic industries have led to a greater demand of sub systems that provide essential data. An increasing trend in the SOA that reflects this is the development and implementation of 3D vision system. Examples of these 3D vision systems can be found in pick and place stations in automated assembly lines and other structured environments. The limitation of these systems is the dependence on explicit knowledge of the target Object Of Interest (OOI). Typically, these systems depend on CAD files of the OOI to determine the object pose or centre of mass to direct a manipulator to interact with it. In the case of manufacturing processes that have taken a gradual approach to automation, this level of data may not be available. Furthermore, in some applications, such as automated forklifts for logistics, a fixed camera setup for a vision system is not possible which leads to a larger variance in the captured data retrieved for these 3D vision systems.

Current development of 3D vision systems capable of operating in these types of environments, known as unstructured environments, have shown reproducible and repeatable object detection and isolation. This step of isolation allows for further development of these 3D vision systems to encompass the analysis of key properties of the OOI such as the objects volumetric distribution to determine suitability for interaction. In this study, we propose a method of determining these key properties from data retrieved from unstructured environments. This includes the implementation of the SOA in object detection and isolation to retrieve the OOI from an unstructured environment. With the OOI isolated from the unstructured environment, the object is then segmented into detectable planes. This analysis provides the essential data that allows for a close approximation of how the OOIs its mass is distributed. Experimentation is ongoing for this study, with preliminary findings showing promising results.

*Key Words: Automation, 3D Vision, Machine Vision.*

## 1. INTRODUCTION

Machine vision is an established field in automation engineering that has directly benefited manufacturing and logistics such as the autonomous grasping of complex objects (Le et al., 2021). In recent years, advancements in this field have been focused on analysing an Object Of Interests (OOIs) structure and position in 3D space through pose estimation, either for planned interactions with the OOI or with determining an objects placement and trajectory for Autonomously Guided Vehicles (Ahmad et al., 2021; Le et al., 2021; Louedec et al., 2020; Monica et al., 2020; O' Mahony et al., 2019; Z. Song et al., 2019; Wenzel et al., 2021). The State Of the Art (SOA) approach to this is to develop a catalogue of object types and classifying the OOI within this catalogue to determine a close estimation of the OOIs pose (Z. Song et al., 2019), (Muzahid et al., 2020; W. Song et al., 2021; Wang et al., 2019). For autonomous operations that involve interacting with the OOI, a more precise approximation of the OOIs pose and stability is required, in the SOA this requires a database of 3D models of the exact OOI structure and dimensions, which is then superimposed on captured data of the OOI to determine its pose based on a form of complex template matching, known as key point matching (Chowdhary, 2019; Liu et al., 2021; Pan et al., 2021).

The constraint of this approach is the dependency on machine learning techniques, such as Convolutional Neural Networks (CNN). To develop these systems a large database of training and testing data of comparable OOIs is required. Collecting this data for a diverse set of OOIs is a substantial obstacle in developing 3D vision systems for autonomous applications. Alternatively, for structured systems that consist of OOIs with a consistent and rigid structure, such as an unorganised bin picking station, a 3D model of the OOI can be generated with for the application of template matching algorithms (Asmaria et al., 2019; Park et al., 2019; Vock et al., 2019). However, for more complex systems where the OOIs experience large diversity in structure and format, such as multi-body

Email: Primary Author Name
Primary Author Email address

OOIs that can be found in logistic application as shown in fig. 1, the process of modelling a 3D CAD file for template matching is not a viable option. Machine learning approaches have been successful in the classification of complex objects in these cases (Vock et al., 2019), however the variance in condition of the OOI structures makes the determination of the OOIs properties such as pose and centre of volume impractical for machine learning methods (Park et al., 2019). For application in autonomous material handling, the determination of an OOIs centre of volume is a key property that the SOA has not yet presented a sufficient method of determination for complex OOIs. It is important to note that this property is referred to as centre of "volume" and not centre of "mass" as there is no indication that a consistent density can be determined from the 3D OOI data. This property is generalized to the term "centroid" for the remainder of this study.

*Figure 1:multibody OOI.*

To address the determination of complex OOIs, particularly to assess the centre of volume of the OOI for planned autonomous material handling interactions, a method is proposed in this study that does not rely on conventional methods of machine learning. Instead, this study proposes a morphological approach to determine the properties of OOI point clouds based on the structure and distribution of point data. This approach, if implemented correctly, will be able to determine the centre of volume of a wide range of complex objects without the need of generating specific CAD models or capturing comparable data. However, to achieve this goal a mathematical model must be developed that can accurately and repeatably determine the centre of volume for a wide variety of complex objects.

## 2. METHODOLOGY

To achieve the goals of this study, determining a complex objects centroid position, a concise methodology was developed. This methodology relies of serval concepts that are present in SOA, which have been examined and explored in detail. The first of these concepts is the isolation of the OOI from the environment it is captured in.

### *Isolation*

Isolation is a necessary step to analysing an OOI and its properties to ensure that only the data relevant to OOI is considered. Several methods of OOI isolation can be found in the SOA literature, in Muzahid et al (Muzahid et al., 2020) a method is presented that classifies and isolates OOIs using an improved variation of a CNN approach, described as a malorientation volumetric deep neural network (MV-DNN). The benefit of using a machine learning approach such as this is the proficiency of systems at classifying data, such as determining points that pertain to the OOI. The constraint of this system however is the dependency of a 3D model of the OOI required for the classification process. Monica et al (Monica et al., 2020) presents an alternative method that does not depend on 3D models or any prior knowledge of the OOI, instead using a combination of morphology principles,

plane and edge detection, integrated with a genetic algorithm, a non-neural network machine learning process. In comparison to Muzahid et al, this method determines the OOI with no explicit prior knowledge of the OOI other than an approximate position and non-dimensioned physical distributors. Implementing the method presented in Monica et al allows for the isolation and segmentation of data from unstructured environments. This allows for further analysis of the OOI for the goals of this study.

***Plane segmentation***

To further segment and classify the data a 3D plane segmentation method was explored. Similar to the isolation process discussed previously, machine learning can be applied to determine what planes are present in the OOI data using a Random Sampling Consensus method (RANSAC)(Ghahremani et al., 2021). This method of machine learning will analyse the structure of points in the data set to determine their relation to one another and classify the points present based on which estimated plane they belong to. To implement this process the segment_plane method available with the python 3D analysis tool, Open3D, was used. This implementation of the RANSAC algorithm allows for finite tuning of the process through the sample number of points considered (*ransac_n*), the maximum distance between points and an estimated plane (*distance_threshold*) and the number of times an estimated plane is sampled for verification (*num_iterations*).

***Single Body Centroid***

To analyse the centre of volume OOI as a single object, a histogram approach is taken for each axis. Consider the conventional centre of mass equation Eq. 1 that considers any number of bodies of mass denoted as $m_i$, for I bodies, placed a distance of $x_i$ from an arbitrary origin respectively, relatively to a joint mass of the OOI denoted at $M$. The result of this equation is the centroid position, $X$, of the joint body OOI relative to the axis that was used to determine distances $x_i$.

*Equation 1*

$$X = \lim_{\Delta m \to 0} \frac{\sum_{i=1}^{N} \Delta m_i x_i}{M} = \frac{\int_0^M x \, dm}{M}$$

In the case of point cloud data, there is no way to determine the mass of point data. Instead, if we consider the volumetric distribution of the points, using the number of points present in each body to represent the unit of volume replacing the variables $m_i$ and $M$ with $v_i$ and $V$ respectively, we can determine the centroid of a multi body OOI. To determine the centroid position in 3D space, the volumetric distribution equation is applied for each axis of distance measurement from the world origin, Eq. 2.

*Equation 2*

$$X = \frac{\int_0^V x \, dv}{V} \qquad Y = \frac{\int_0^V Y \, dv}{V} \qquad Z = \frac{\int_0^V z \, dv}{V}$$

This method can be applied further to more precise OOIs such as single body complex OOIs. By applying a histogram approach to point grouping as a solution to the integral equation, the volumetric distribution of points with respect to each axis (Fig. 2) can be determined. To apply this histogram approach for each axis, the pixels are segmented into overlapping groups that encompass pixels within a fixed distance from the world origin, i.e., points between a distance of 100mm and 110mm from the world origin.

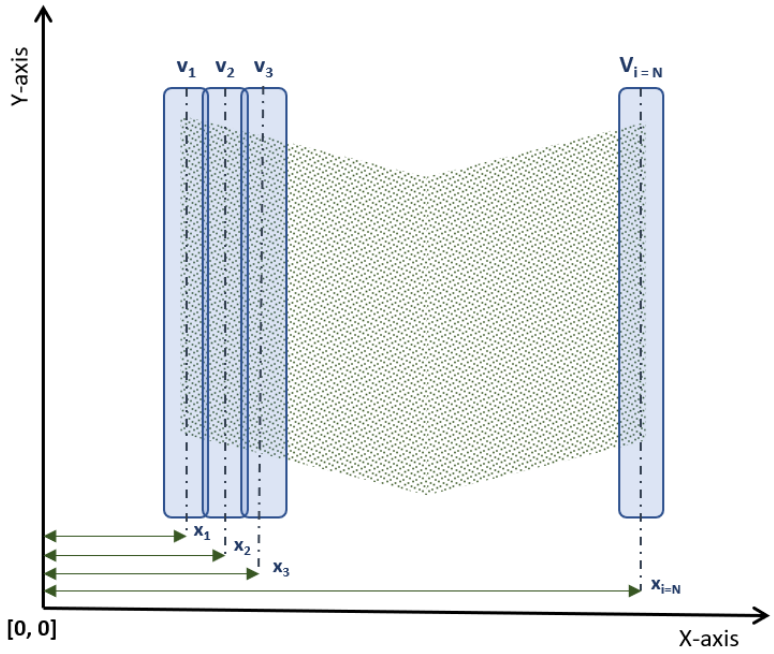


*Figure 2: Point grouping for histogram approach of centroid analysis, x-value centroid determination.*

Each of these point groups are then treated as separate mass bodies and are inserted into the original mass distribution equation presented in Eq. 1, where $v_i$ represents the number of points present in each group as shown below in Eq. *3*. This process is repeat for each axis of the 3D data frame.

*Equation 3*

$$X = \lim_{\Delta v \to 0} \frac{\sum_{i=1}^{N} \Delta v_i x_i}{M} \qquad Y = \lim_{\Delta v \to 0} \frac{\sum_{i=1}^{N} \Delta v_i y_i}{M} \qquad Z = \lim_{\Delta v \to 0} \frac{\sum_{i=1}^{N} \Delta v_i z_i}{M}$$

This process is effective in determining the *x* and *y* position of the OOIs centroid with some degree of error, however regardless of the structure of the OOI this method will perceive the OOI as a hollow shell with only the visible planes considered in the centroid equation. This leads to considerable positional error of the centroid position, particularly in the z axis. A better solution to this process is to consider each detectable plane to predict the solid structure of the OOI based on planes visible.

***Multi-body system analysis***

This method may be applied further to consider a multi-body load. Presented in Fig. *3* is an example of a typical multi body load consisting of several cardboard boxes placed on a pallet. This presented an additional challenge multiple surfaces in a complex arrangement. The method presented previously can still be applied to this case to give a general centre of volume for the combined load using Eq. *3*.

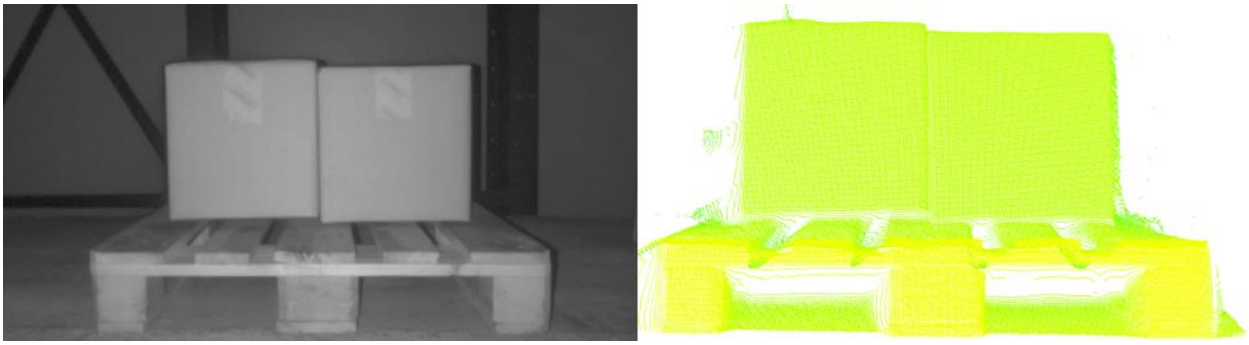

*Figure 3: Arrangement of cardboard box objects on a pallet, grayscale image (left), point cloud image (right).*

However, for more complex operations that require the consideration of each object individually to determine their stability for interaction, a different approach is required. If we consider in this case that the group of objects have been isolated from the scene together, with no further separation. Using the method presented previously as plane segmentation, the front faces of each object can be segmented from the scene for individual centroid analysis. Once a plane is isolated using the RANSAC method, a bitwise NAND operation can be used to remove the plane from further consideration for the next isolation loop. This process is simply repeated for suspected number of objects present or until the RANSAC algorithm can no longer find planes that match the desired criteria of size and point-to-point distance thresholds. For joint analysis of the volumetric distribution of the objects, the equation presented in Eq. 3 can be applied where the centroid value is used rather than point cloud histogram groupings.

## 3. PRELIMINARY RESULTS

This work is ongoing and further experimentation is required for full validation of the process, however some preliminary results were recorded. Following the principles presented in the methodology a small experiment group was created to test the centroid analysis process and provide visual evidence of the centroid being located correctly. Belo shown in Fig. 4 is one of these experiment sets where the OOI was places on a matt black pole that does not reflect the source light of the 3D camera and as a result is not present in the depth/range data, Fig 4. (centre), aiding in the isolation process. The OOI was then isolated from the background and the centroid position relative to the world reference frame provided by the capture device. This centroid position was then used to place a marker on the original input image, Fig 4 (left), to indicate where the centroid was calculated to be.

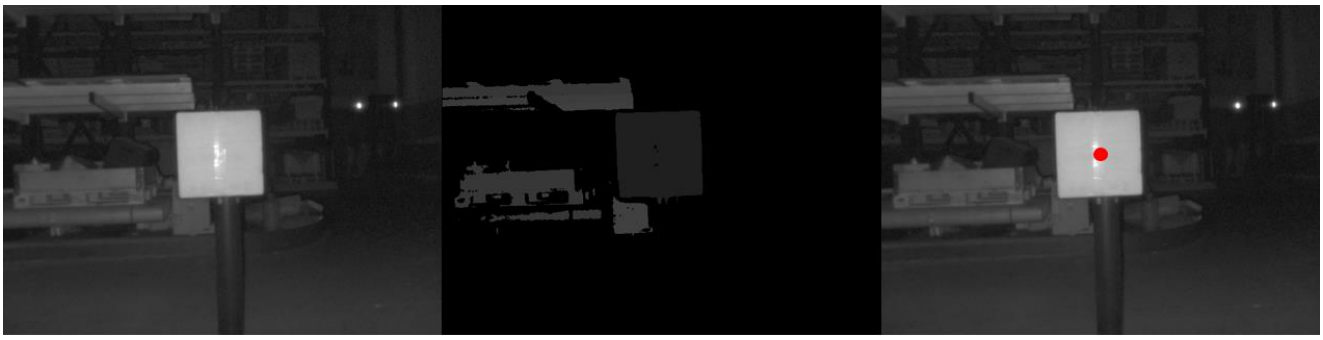

*Figure 4: OOI placed on a matt pole (left), Depth image of OOI for Point cloud analysis (centre), OOI with calculated centroid position marked (right).*

The goal of this work is to conduct further experiments that involve a precise method of determining the OOIs actual centroid position, such as the use of QR code markers as shown below in Fig. 5.

*Figure 5: Example of QR code markers to indicate plane centroid position.*

## 4. CONCLUSION

Review of the SOA literature indicates a clear gap in the analysis of the properties of unknown OOIs. Currently the literature presents methods that are proficient in the detection and isolation of OOIs. Through various machine learning techniques, the properties of known objects can be determined however there is no method present for the determination of these properties for unknown objects. In this study we have presented an experimental method of deriving one of the key properties of object analysis, the centre of volume, without the need for explicit knowledge of the object being analysed. This study is still ongoing with further development planned in the near future. The goal of this work is to present a concise real world experimentation data set of this methodology being applied, in tandem with a ground truth data set for comparison with this methodology presented to determine the proficiency of this system.

## 4. REFERENCES

Ahmad, S., Sunberg, Z. N., & Humbert, J. S. (2021). End-to-End Probabilistic Depth Perception and 3D Obstacle Avoidance using POMDP. *Journal of Intelligent & Robotic Systems*, *103*(2), 33. https://doi.org/10.1007/s10846-021-01489-w

Asmaria, T., Annur, D., Utomo, M. S., Sari, A. K., Malau, D. P., Prabowo, Y., Rahyussalim, A. J., & Amal, M. I. (2019). Validation of 3D Models using Template Matching for Implant Planning. *2019 16th International Conference on Quality in Research (QIR): International Symposium on Electrical and Computer Engineering*, 1–4. https://doi.org/10.1109/QIR.2019.8898275

Chowdhary, C. L. (2019). 3D Object Recognition System Based On Local Shape Descriptors and Depth Data Analysis. *Recent Patents on Computer Science*, *12*(1), 18–24. https://doi.org/10.2174/2213275911666180821092033

Ghahremani, M., Williams, K., Corke, F., Tiddeman, B., Liu, Y., Wang, X., & Doonan, J. H. (2021). Direct and accurate feature extraction from 3D point clouds of plants using RANSAC. *Computers and Electronics in Agriculture*, *187*, 106240. https://doi.org/10.1016/j.compag.2021.106240

Le, T.-T., Le, T.-S., Chen, Y.-R., Vidal, J., & Lin, C.-Y. (2021). 6D pose estimation with combined deep learning and 3D vision techniques for a fast and accurate object grasping. *Robotics and Autonomous Systems*, *141*, 103775. https://doi.org/10.1016/j.robot.2021.103775

Liu, A.-A., Zhou, H., Nie, W., Liu, Z., Liu, W., Xie, H., Mao, Z., Li, X., & Song, D. (2021). Hierarchical multi-view context modelling for 3D object classification and retrieval. *Information Sciences*, *547*, 984–995. https://doi.org/10.1016/j.ins.2020.09.057

Louedec, J., Li, B., & Cielniak, G. (2020). Evaluation of 3D Vision Systems for Detection of Small Objects in Agricultural Environments: *Proceedings of the 15th International Joint Conference on Computer Vision, Imaging and Computer Graphics Theory and Applications*, 682–689. https://doi.org/10.5220/0009182806820689

Monica, R., Aleotti, J., & Rizzini, D. L. (2020). Detection of Parcel Boxes for Pallet Unloading Using a 3D Time-of-Flight Industrial Sensor. *2020 Fourth IEEE International Conference on Robotic Computing (IRC)*, 314–318. https://doi.org/10.1109/IRC.2020.00057

Muzahid, A. A. M., Wan, W., Sohel, F., Khan, N. U., Cervantes Villagómez, O. D., & Ullah, H. (2020). 3D Object Classification Using a Volumetric Deep Neural Network: An Efficient Octree Guided Auxiliary Learning Approach. *IEEE Access*, *8*, 23802–23816. https://doi.org/10.1109/ACCESS.2020.2968506

O' Mahony, N., Campbell, S., Carvalho, A., Krpalkova, L., Riordan, D., & Walsh, J. (2019). 3D Vision for Precision Dairy Farming. *IFAC-PapersOnLine*, *52*(30), 312–317. https://doi.org/10.1016/j.ifacol.2019.12.555

Pan, X., Xia, Z., Song, S., Li, L. E., & Huang, G. (2021). *3D Object Detection With Pointformer*. 7463–7472. https://openaccess.thecvf.com/content/CVPR2021/html/Pan_3D_Object_Detection_With_Pointformer_CVPR_2021_paper.html

Park, K., Patten, T., Prankl, J., & Vincze, M. (2019). Multi-Task Template Matching for Object Detection, Segmentation and Pose Estimation Using Depth Images. *2019 International Conference on Robotics and Automation (ICRA)*, 7207–7213. https://doi.org/10.1109/ICRA.2019.8794448

Song, W., Liu, Z., Tian, Y., & Fong, S. (2021). Pointwise CNN for 3D Object Classification on Point Cloud. *Journal of Information Processing Systems*, *17*(4), 787–800. https://doi.org/10.3745/JIPS.02.0160

Song, Z., Tang, S., Gu, F., Shi, C., & Feng, J. (2019). DOE-based structured-light method for accurate 3D sensing. *Optics and Lasers in Engineering*, *120*, 21–30. https://doi.org/10.1016/j.optlaseng.2019.02.009

Vock, R., Dieckmann, A., Ochmann, S., & Klein, R. (2019). Fast template matching and pose estimation in 3D point clouds. *Computers & Graphics*, *79*, 36–45. https://doi.org/10.1016/j.cag.2018.12.007

Wang, C., Cheng, M., Sohel, F., Bennamoun, M., & Li, J. (2019). NormalNet: A voxel-based CNN for 3D object classification and retrieval. *Neurocomputing*, *323*, 139–147. https://doi.org/10.1016/j.neucom.2018.09.075

Wenzel, P., Schön, T., Leal-Taixé, L., & Cremers, D. (2021). Vision-Based Mobile Robotics Obstacle Avoidance With Deep Reinforcement Learning. *2021 IEEE International Conference on Robotics and Automation (ICRA)*, 14360–14366. https://doi.org/10.1109/ICRA48506.2021.9560787